April 2021
Report No. 21-017

Charles D. Baker
Governor
Karyn E. Polito
Lieutenant Governor
Jamey Tesler
MassDOT Secretary & CEO

Post-Fire Damage Inspection of Concrete Structures

Principal Investigator (s)
Dr. Simos Gerasimidis
Dr. Scott Civjan
University of Massachusetts Amherst

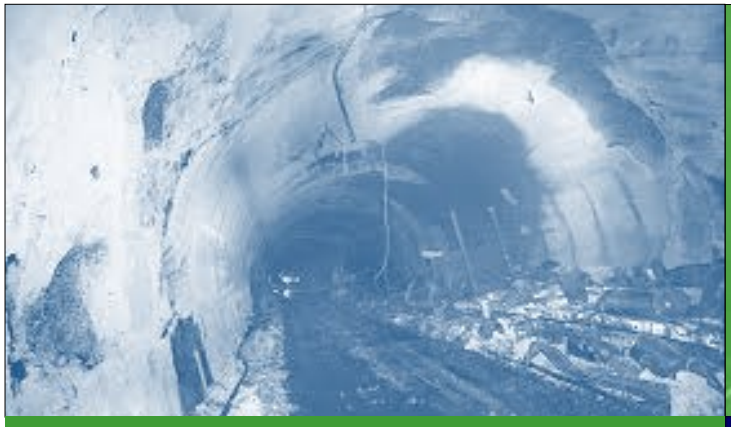

Research and Technology Transfer Section
MassDOT Office of Transportation Planning

U.S. Department of Transportation
Federal Highway Administration

Technical Report Document Page

1. Report No.	2. Government Accession No.	3. Recipient's Catalog No.
21-017	n/a	n/a

4. Title and Subtitle	5. Report Date
Post-Fire Damage Inspection of Concrete Structures: Final Report	April 2021
	6. Performing Organization Code

7. Author(s)	8. Performing Organization Report No.
Simos Gerasimidis, Scott Civjan, Nick Menz	20-017

9. Performing Organization Name and Address	10. Work Unit No. (TRAIS)
University of Massachusetts Amherst UMass Transportation Center 130 Natural Resources Way Amherst, MA 01003	11. Contract or Grant No.

12. Sponsoring Agency Name and Address	13. Type of Report and Period Covered
Massachusetts Department of Transportation Office of Transportation Planning Ten Park Plaza, Suite 4150, Boston, MA 02116	Final Report - April 2021 [January 2020 - April 2021]
	14. Sponsoring Agency Code n/a

15. Supplementary Notes
Project Champion- John Czach, MassDOT

16. Abstract
Although concrete tunnel structures can lose strength and long-term durability due to fire, literature on the remaining capacity of structures after fire events is scattered, and few published post-fire inspection protocols exist, especially for tunnel structures. This project investigates the deleterious effects of fire on concrete tunnel structures and how the extent and degree of fire damage can be assessed, with the goal of developing a rapid inspection protocol/checklist for inspectors to assess the relative safety of a tunnel structure after fire. The project includes an extensive literature review, covering published standards, technical reports, academic papers, and a survey of post-fire inspection practices at other state DOTs and transit organizations. Topics include residual mechanical properties of concrete, steel, and concrete/steel bond after fire; residual strength and stiffness of structural members after fire; existing inspection tools and methods for assessing concrete structures after fire; and repair methods for fire-damaged concrete structures. Preliminary experimental testing outcomes are presented, including setup of a new heat system; procurement of sample specimens for testing; thermal and physical testing of specimens; and evaluation of results. Finally, recommendations for a second phase of experimental testing are presented.

17. Key Word	18. Distribution Statement
concrete tunnel, post fire, capacity of structure, safety inspection	unrestricted

19. Security Classif. (of this report)	20. Security Classif. (of this page)	21. No. of Pages	22. Price
unclassified	unclassified	186	n/a

Form DOT F 1700.7 (8-72) Reproduction of completed page authorized

This page left blank intentionally.

Post-Fire Damage Inspection of Concrete Structures

Final Report

Prepared By:

Simos Gerasimidis, Ph.D.
Principal Investigator
sgerasimidis@umass.edu

Scott Civjan, Ph.D.
Co-Principal Investigator
civjan@umass.edu

Nick Menz
Graduate Researcher
nmenz@umass.edu

University of Massachusetts Amherst
130 Natural Resources Way
Amherst, MA 01003

Prepared For:
Massachusetts Department of Transportation
Office of Transportation Planning
Ten Park Plaza, Suite 4150
Boston, MA 02116

April 2021

This page left blank intentionally.

Acknowledgments

Prepared in cooperation with the Massachusetts Department of Transportation, Office of Transportation Planning, and the United States Department of Transportation, Federal Highway Administration.

Disclaimer

The contents of this report reflect the views of the authors, who are responsible for the facts and the accuracy of the data presented herein. The contents do not necessarily reflect the official view or policies of the Massachusetts Department of Transportation or the Federal Highway Administration. This report does not constitute a standard, specification, or regulation.

This page left blank intentionally.

Executive Summary

This study of post-fire damage inspection of concrete structures was undertaken as part of the Massachusetts Department of Transportation (MassDOT) Research Program. This program is funded with Federal Highway Administration (FHWA) State Planning and Research (SPR) funds. Through this program, applied research is conducted on topics of importance to the Commonwealth of Massachusetts transportation agencies.

Tunnels are a vital part of Massachusetts' transportation infrastructure, more so than ever after the completion of the Central Artery/Tunnel project. Recent fire incidents in MassDOT tunnels have revealed the need for inspection protocols to help evaluate the structural condition of tunnels after fire events, as it is well known that fire can result in the loss of strength of tunnel structures and tunnel elements. Though the decision of whether to close a tunnel may be obvious in the case of a severe fire with extensive damage, or a minor fire with no obvious damage, it may not be obvious in the case of an intermediate intensity fire. The purpose of this research is to understand how fire affects the residual strength capacity of tunnel structures and tunnel elements and to develop a post-fire inspection protocol that can be quickly and easily implemented.

This report describes the findings of Tasks 1–3 of the project. Task 1 consists of a review of existing procedures and literature on post-fire assessment of tunnels; Task 2 consists of preliminary experimental testing using a radiant heating system; and Task 3 consists of recommendations for Phase II of experimental testing. Section 1 is a brief introduction to the problem and a description of the scope of the research. Section 2 presents the results of an extensive literature review of structural codes, standards, technical reports, and academic papers on the post-fire mechanical properties of concrete, steel, and the concrete/steel bond. A great deal of research effort has been expended in the past 70 years on these subject areas, as fire can negatively affect the mechanical properties of concrete and steel. Furthermore, understanding the post-fire mechanical properties of concrete and steel is critical to predicting the residual strength and durability of structures and structural members after fire exposure. Section 3 presents existing experimental studies that have been conducted to assess the residual strength of reinforced concrete members after fire exposure. Section 4 describes common techniques for post-fire inspection of concrete structures, focusing on visual and non-destructive testing methods that can be quickly performed. These techniques can help inspectors evaluate the extent of damage and estimate the residual strength of structural members. Section 5 reviews common repair methods for fire-damaged concrete structures. Section 6 presents the results of a survey of post-fire inspection practices/protocols of other state DOTs and transit authorities, which was conducted by video conferences and email correspondence with members of these organizations. This survey revealed a general lack of standardized procedures for the post-fire inspection of tunnels in public transportation organizations across the United States. Section 7 presents the findings of preliminary experimental testing conducted at the University of Massachusetts, Amherst, which includes validating the ability of the proposed heating system for heating structural and non-structural components, and preliminary data on the effect of heating structural and non-structural tunnel elements. Section 8 presents recommendations for Phase II experimental testing.

This page left blank intentionally.

Table of Contents

Technical Report Document Page i
Acknowledgments v
Disclaimer v
Executive Summary vii
Table of Contents ix
List of Tables xi
List of Figures xiii
List of Acronyms xix
1.0 Introduction to Fire and Tunnels 1
1.1 Introduction to the Residual Condition of Structures after Fire 2
1.2 Introduction to Fire Resistance Design 3
1.3 Additional Documents on Residual Condition of Structures After Fire and Fire Resistance Design 4
2.0 Effect of Fire on Structural Materials 5
2.1 Concrete 6
2.1.1. Physical and Chemical Changes during Heating and Cooling of Concrete 6
2.1.2. Strength of Concrete at Elevated Temperatures and after Cooling Down 7
2.1.2.1 Codes and Standards 8
2.1.2.2 Experimental Studies 12
2.1.3. Stiffness of Concrete at Elevated Temperatures and after Cooling Down 15
2.1.4. Thermal Spalling of Concrete 16
2.1.5. Temperature Distribution of Concrete Exposed to Fire 21
2.1.6. Summary of Effects of Heat on Concrete 24
2.2 Steel 25
2.2.1. Structural Steel 25
2.2.2. Reinforcing Steel 30
2.2.3. Cold-Worked and Heat-Treated Steel 33
2.2.4. Prestressing Steel 35
2.2.5. Summary of the Effects of Heat on Steel 40
2.3 Residual Bond between Concrete and Steel 40
2.3.1. Summary of Effects of Heat on Residual Bond Strength between Concrete and Steel 45
3.0 Effect of Fire on Structural Members 47
3.1 Experimental Studies on Residual Strength of Structural Members 47
3.1.1. El-Hawary et al., 1996: Reinforced Concrete Beams in Flexure 47
3.1.2. Kodur et al., 2010: High-Strength Reinforced Concrete Beams in Flexure 49
3.1.3. – Federal Highway Administration (FHWA) 2007: Prestressed Concrete Box Beams in Flexure 52
3.1.4. Agrawal & Kodur, 2019: Super-High-Strength Reinforced Concrete Beams in Flexure 55
3.1.5. Choi et al., 2013: Reinforced Concrete Beams in Flexure 57
3.1.6. Summary of Effects of Fire Exposure on Residual Strength of Structural Members 61
4.0 Existing Post-Fire Inspection Methods for Concrete Structures 63
4.1 Visual Inspection Methods 63
4.1.1. Examination of Debris Materials 63
4.1.2. Concrete Color Change Due to Heat 66

4.1.3. General Visual Damage Classification 68
4.2 Onsite Non/Partially Destructive Testing Methods 69
4.2.1. Rebound Hammer 71
4.2.2. Pullout Tests 75
4.2.3. Carbonation Tests 78
4.2.4. Penetration Resistance Tests 80
4.2.5. Ultrasonic Pulse Velocity (UPV) 82
4.2.6. Other Non-Destructive Testing Methods 84
4.3 Laboratory Testing Techniques 85
4.4 Summary of Existing Inspection Methods for Fire-Damaged Structures 86
5.0 Repair Techniques for Fire-Damaged Concrete Structures 89
5.1 Evaluation/Classification of Damage 89
5.2 Common Repair Techniques 90
5.3 Case Studies in Repair of Fire-Damaged Structures 93
5.3.1. Tauern Tunnel, Austria 93
5.3.2. Full-Scale Fire Test of an Industrial Precast Hall 96
5.4 Summary of Repair Methods for Fire-Damaged Concrete Structures 99
6.0 Survey of Post-Fire Inspection Practices of Other State DOTs and Transit Authorities 101
6.1 Reaching Out to State DOTs and Transit Authorities 101
6.2 Summaries of Email Correspondence and Video Conferences with State DOTs and Transit Organizations 103
6.2.1. Summaries of Email Correspondence 103
6.2.2. Summaries of Video Conferences 105
6.3 Findings of the Survey 107
6.4 Summary of the Findings of the Survey 109
7.0 Preliminary Experimental Testing at UMass Amherst 111
7.1 Purpose 111
7.2 Heating Units and Setup 112
7.2.1. Heat Source 112
7.2.2. Insulation Requirements 115
7.3 Thermocouple Monitoring 116
7.4 Specimens for Testing 118
7.5 Initial Trials 120
7.5.1. Heating of Small Plain Concrete Specimens 120
7.5.2. Heating of Concrete Slabs 121
7.5.3. Heating of Panel Block Specimens and Aluminum Wireway 122
7.5.4. Testing of Minimally Reinforced Beam Specimens 127
7.6 Beam Tests 132
7.7 Supplemental test data 139
7.7.1. Carbontest® 139
7.7.2. Rebound Hammer Results 140
7.8 Conclusions 142
8.0 Recommendations for Phase II Experimental Program 145
9.0 Conclusions 149
10.0 References 155
11.0 Appendices 161
11.1 Appendix A: Questions for the Survey of Post-Fire Inspection Practices 161
11.2 Appendix B: Draft Post-Inspection Checklist 162

List of Tables

Table 1.1: Standards, codes, and technical reports on topics of fire and structures 4
Table 2.1: Summary of mineralogical changes in concrete due to heating 7
Table 2.2: Summary of types of fire spalling 18
Table 3.1: Details about beam specimens and results of load testing 51
Table 3.2: Strength results from load testing of beams 54
Table 3.3: Details of beam specimens and results of experimental testing 57
Table 3.4: Construction and heating details for each beam specimen 58
Table 3.5: Residual strength results of loading tests 60
Table 4.1: Degradation of selected materials at given temperatures 64
Table 6.1: Summary of surveyed organizations' experiences with tunnel fires and their post-fire inspection procedures 108

This page left blank intentionally.

List of Figures

Figure 1.1: Comparison of common design fire curves 3
Figure 2.1: Compressive strength reduction factors for concrete at elevated temperatures per *EN 1992 1-2* 9
Figure 2.2: Stress-strain curves for concrete made with siliceous aggregates at elevated temperature per *EN 1992 1-2* 9
Figure 2.3: Comparison of reduction factors for compressive strength of concrete at elevated temperature and after cooling (residual) per *EN 1994 1-2* 10
Figure 2.4: Strength reduction curves for compressive strength of concrete made with siliceous aggregates per *ACI 216.1-14* 11
Figure 2.5: Strength reduction curves for compressive strength of concrete made with calcareous/carbonate aggregates per *ACI 216.1-14* 11
Figure 2.6: Compressive strength loss of normal-strength concrete (NSC), separated by test type: residual (L), stressed (c), unstressed (R) 12
Figure 2.7: Compressive strength loss of normal-strength concrete, separated by type of aggregate: siliceous (L), calcareous/carbonate (C), lightweight (R) 13
Figure 2.8: Residual compressive strength of normal-strength and high-strength concrete with calcareous aggregates, separated by test type: residual (L), stressed (C), unstressed (R) 13
Figure 2.9: Best-fit lines (proposed models) for residual compressive strength loss of normal-strength and high-strength concrete, compared to ACI 216.1-14 curves, separated by aggregate type: siliceous (L), calcareous (C), lightweight (R) 13
Figure 2.10: Relative residual compressive strength of high-strength concrete 14
Figure 2.11: Relative modulus of elasticity of concrete from unstressed tests 15
Figure 2.12: Relative modulus of elasticity of concrete from unstressed residual tests 16
Figure 2.13: Process of thermal spalling according to pore pressure theory (a–d) 19
Figure 2.14: Illustration of combined thermal and applied stress on an axial member (a–b) 19
Figure 2.15: Progression of post cooling spalling in a cylinder: before heat exposure (L); after 120 min in ISO fire (C); 1 week after heat exposure (R) 21
Figure 2.16: Isothermal lines (Celsius) after 60 minutes of exposure to ISO 834 design fire (L); 500°C isotherms after 30, 60, and 90 minutes of exposure to ISO 834 design fire (C); heating conditions of beam (R) 22
Figure 2.17: Temperature distributions in slabs (L) and columns (R) exposed to unspecified design fire 22
Figure 2.18: Temperature distributions within slabs during ASTM E119 fires tests: carbonate aggregate concrete (top L); siliceous aggregate concrete (top R); semi-lightweight aggregate concrete (bottom) 23
Figure 2.19: Damage and temperature depth in concrete exposed to ISO 834 fire 24
Figure 2.20: Reduction factors for yield stress and elastic modulus of hot-rolled structural steel at elevated temperatures 26
Figure 2.21: Reduction factors for yield strength of S350 GD + Z steel based on experimental results; reduction factors for yield strength of hot-rolled structural steel from *EN 1993 1-2* 26
Figure 2.22: Relative residual yield strength of hot-rolled structural steel (L); relative residual ultimate strength of hot-rolled structural steel (R) 27
Figure 2.23: Residual stress-strain curves for A992 steel after heating to: 200°C (L), 500°C (R), and cooling by each method 28
Figure 2.24: Residual stress-strain curves for A992 steel after heating to: 700°C (L), 1000°C (R), and cooling by each method 29

Figure 2.25: Reduction factors for yield strength of A992 steel based on maximum temperature (L); reduction factors for ultimate strength of A992 steel based on maximum temperature (R) 29
Figure 2.26: Reduction factor for elastic modulus of A992 steel for each cooling method 30
Figure 2.27: Reduction factors for yield stress and elastic modulus of Class N hot-rolled reinforcing steel at elevated temperatures per *EN 1992 1-2* 31
Figure 2.28: Strengths of different types of reinforcing steel at elevated temperatures per *ACI 216.1-14* 31
Figure 2.29: Relative residual yield strength of hot-rolled reinforcing steel (L); relative residual ultimate strength of hot-rolled reinforcing steel (R) 32
Figure 2.30: Stress-strain curves for φ29 mm deformed carbon steel reinforcing bars after heating and cooling 33
Figure 2.31: Stress-strain curves for φ24 mm smooth carbon steel reinforcing bars after heating and cooling 33
Figure 2.32: Comparison of yield strength and elastic modulus reduction factors for hot-rolled and cold-worked reinforcing steel per *EN 1992 1-2* 34
Figure 2.33: Relative residual yield strength of heat-treated/cold-worked steel (a); relative residual ultimate strength of heat-treated/cold-worked steel (b); relative residual elastic modulus of heat-treated/cold-worked steel (c) 35
Figure 2.34: Reduction factors for yield strength and elastic modulus of different types of prestressing steel per *EN 1992 1-2* 36
Figure 2.35: Comparison of reduction factors for yield strength of prestressing wires (top L); reduction factors for ultimate strength of prestressing wires (top R); reduction factors for elastic modulus of prestressing wires (bottom) at elevated temperatures 37
Figure 2.36: Residual 0.1% proof stress of prestressing steel and yield strengths of reinforcing and heat-treated/cold-worked steel 38
Figure 2.37: Residual ultimate strength of prestressing steel, reinforcing steel, and heat-treated/cold-worked reinforcing steel 38
Figure 2.38: Relaxation of untreated cold-drawn prestressing wire due to thermal exposure 39
Figure 2.39: Schematic of the crushing and splitting of concrete with an embedded deformed rebar under tension 41
Figure 2.40: Residual bond strength of C20 (20 MPa) concrete 42
Figure 2.41: Residual bond strength of C35 (35 MPa) concrete 42
Figure 2.42: Three different locations of rebar specimen (φ16 bar) for pullout tests 43
Figure 2.43: Residual bond stress for three locations of rebar 43
Figure 2.44: Beam test specimen for assessing residual bond strength 44
Figure 2.45: Degradation coefficients for bond strength measured by beam test, concrete compressive strength, and bond strength measured by pullout test on similar concrete 44
Figure 3.1: Schematic of furnace (L) and time-temperature curve of furnace (R) 48
Figure 3.2: Ultimate load for each beam (L); load-deflection plots for each beam (R) 48
Figure 3.3: Location of thermocouples in each beam 49
Figure 3.4: Two design fires used in experiment 50
Figure 3.5: Bottom rebar temperatures during heating 50
Figure 3.6: Residual strength of reinforcing steel 52
Figure 3.7: Fascia of Ridgefield, CT, bridge after the fire 53
Figure 3.8: Cross-section of typical prestressed box beam in bridge 53
Figure 3.9: Visual condition of bottom of Beam 4, Ridgefield bridge 54
Figure 3.10: Beam cross-sections and locations of thermocouples (cross-section A, bottom L; cross-section B, bottom C; cross-section C, bottom R) 55
Figure 3.11: Air temperature inside furnace for each heating regime 56
Figure 3.12: Specimen cross-sections and locations of thermocouples, for specimens with cover of 40 mm 58

Figure 3.13: Temperature distribution in NSC beams with 40 mm cover (L); with 50 mm cover (R) 59
Figure 3.14: Temperature distribution in HSC beams with 40 mm cover (L); with 50 mm cover (R) 59
Figure 3.15: Spalling in HSC beams with 40 mm cover (top); with 50 mm cover (bottom) 60
Figure 4.1: Picture taken during Newhall Pass fire event (L); post-fire condition of tunnel (R) 65
Figure 4.2: Melted aluminum alloy on wheel of truck 65
Figure 4.3: Color change of high performance and ordinary concrete, mortar, and cement paste heated to temperatures from 100°C to 1000°C 66
Figure 4.4: Concrete specimen heated on left face (transient heat analysis) 67
Figure 4.5: Visual damage classification scheme for fire-damaged concrete 68
Figure 4.6: Damage classification scheme for post-fire inspections 69
Figure 4.7: Common inspection methods for fire-damaged structures 70
Figure 4.8: Extensive list of possible inspection methods for fire-damaged tunnel linings 70
Figure 4.9: Ratio of rebound index after heating to rebound index before heating 72
Figure 4.10: Relative residual strength of cubes from compression tests (L); relative rebound index of cubes plotted against compressive strength decay ratio (R) 73
Figure 4.11: Concrete wall partially blocked by concrete duct (L); average rebound indices measured at each line (C); recorded temperature and corresponding compressive strength decay at lines A–C on wall (R) 73
Figure 4.12: Extraction of concrete cores for compressive strength tests 74
Figure 4.13: Measured core strength of concrete vs. rebound number and compressive strength estimated by rebound number 74
Figure 4.14: Schematic showing procedure of conducting post-installed pullout test 75
Figure 4.15: Compressive strength–pullout force correlations from several studies 76
Figure 4.16: Measured pullout force vs. maximum temperature of concrete cube (L); pullout force vs. measured strength decay of the cubes (R) 77
Figure 4.17: CAPO results for concrete panels heated on only one side 77
Figure 4.18: Color range of phenolphthalein 78
Figure 4.19: Schematic of Carbontest device (L) and Carbontest device in use (R) 79
Figure 4.20: Carbontest tubes with concrete powder after addition of phenolphthalein 79
Figure 4.21: Estimated maximum temperature at carbonation front 80
Figure 4.22: Carbonation depths in buildings exposed to fire, measured 3–4 years after fires 80
Figure 4.23: Windsor Probe testing kit (probe gun, probes, depth gauge) 81
Figure 4.24: Area damaged by insertion of metal probe 81
Figure 4.25: Diagram showing principle of ultrasonic pulse velocity test 82
Figure 4.26: Transmission types used for ultrasonic pulse velocity test 83
Figure 4.27: Concrete wall heated on only one side 83
Figure 4.28: Schematic of fastest path for pulse, with X-T curve 84
Figure 4.29: Relative merits of different non-destructive testing techniques 87
Figure 5.1: Buckled reinforcing bars in underside of slab 91
Figure 5.2: Pros and cons of sprayed concrete for replacing fire-damaged concrete 91
Figure 5.3: Pullout test setup 92
Figure 5.4: Possible failure modes during the pull-off test 92
Figure 5.5: Cross-section of Tauern Tunnel before 1999 fire 94
Figure 5.6: Rebar to connect existing concrete to shotcrete layer 94
Figure 5.7: Schematic of repairs for sidewall 95
Figure 5.8: Installation of precast ceiling panels 95
Figure 5.9: Repairs of sidewall and ceiling 96
Figure 5.10: Cross-section of pretensioned roof girder (L), pretensioned roof girder after fire test (R) 97
Figure 5.11: Application of shotcrete to damaged girder 97
Figure 5.12: Midspan of girder after repair 98

Figure 5.13: Load testing setup for girder 98
Figure 6.1: Summary of reach-outs and replies 102
Figure 6.2: Summary of responses to inquiry 103
Figure 7.1: Heaters on wheel dolly assembly 112
Figure 7.2: Heating chamber configuration (top L and R); direct heating of specimen (center L and R); heating of smaller specimen between two throwaway slabs (bottom L and R) 113
Figure 7.3: Sheet metal shield (L); flat expanded metal shield (R) 114
Figure 7.4: Damage to heater elements from shield (L); from thermocouple (R) 114
Figure 7.5: Deformation of shield 115
Figure 7.6: Typical Insulation setup. Heating setup before adding any insulation (top); firebrick around heaters (bottom L); insulation around firebrick (bottom R) 116
Figure 7.7: Thermocouple readings 117
Figure 7.8: Panel as delivered 119
Figure 7.9: Panel dimensions and reinforcement 119
Figure 7.10: Specimens obtained from panel: three primary beams (L), blocks, smaller beams, and miscellaneous (R) 120
Figure 7.11: Sample test setup for heating plain concrete specimens 120
Figure 7.12 Plain concrete specimens: unheated (top); heated to surface temperatures up to 560°C (bottom) 121
Figure 7.13: Concrete slab heating setup 121
Figure 7.14: Typical map cracking pattern for slabs after heating up to 930°C 122
Figure 7.15: Slab before heating (L); whitening after heating to surface temperatures up to 930°C (R) 122
Figure 7.16: Specimens with tile side up (near) and tile side down (far) 123
Figure 7.17: Charring of grout material 123
Figure 7.18: Tile and grout removal by chipping hammer and chisel. Unheated specimen (top); specimen heated to 470ºC with clean break at grout line (bottom) 124
Figure 7.19: Appearance of aluminum wireway and wall panel tile: before heating (top L), and after one hour at: 400°C (top R); 550°C (bottom L); 750°C (bottom R) 125
Figure 7.20: Sagging of aluminum wireway after heating 125
Figure 7.21: Closeup of tile and aluminum wireway after heating 126
Figure 7.22: Removal of grout with a screwdriver after heating 126
Figure 7.23: Melting of epoxy reinforcement coating 127
Figure 7.24: Spalled minimally reinforced beam specimen after heating (L); after removal from setup (R) 128
Figure 7.25: Intact minimally reinforced beam specimen after heating 128
Figure 7.26: Heating curve temperature vs. time plots: spalled specimen (top); intact specimen (bottom) 129
Figure 7.27: Schematic of test setup for minimally reinforced beams 129
Figure 7.28: Photo of minimally reinforced beam specimens during load testing. Propagation of crack in control specimen during load application (top); after failure of heated specimen (bottom) 131
Figure 7.29: Load vs. deflection plot of minimally reinforced beam specimens 131
Figure 7.30: Interior visual inspection of heat effects of ruptured specimens: control specimen with consistent color through ruptured sections (L); specimen heated to 600°C specimen (C); closeup of specimen heated to 600°C (R) 132
Figure 7.31: Beam cross section 132
Figure 7.32: Spalling of 600°C beam specimen prior to heating (L), post heating (R) 133
Figure 7.33: Heating curve temperature vs. time plots: spalled specimen (top); intact specimen (bottom) 134
Figure 7.34: Test setup schematic for beam tests 134
Figure 7.35: Test setup photo for beam tests 135

Figure 7.36: Photo of control specimen after failure 135
Figure 7.37: Photos of 300ºC intact specimen load testing. Multiple flexural cracks in constant moment region during load application (top and middle); after failure (bottom) 136
Figure 7.38: Photos of 600°C spalled specimen load testing. Prior to loading (top); propagation of crack during load application (center L and R); after failure (bottom) 137
Figure 7.39: Load vs. deflection of tested specimens 138
Figure 7.40: Ruptured surface of 300ºC heated specimen 139
Figure 7.41: Photo of slab Carbontest tubes from: center of heated zone (L), unheated zone (R) 140
Figure 7.42: Photo of 900ºC slab rebound hammer and sample locations 140
Figure 7.43: Unheated beam rebound hammer results 141
Figure 7.44: 300°C beam rebound hammer results 141
Figure 7.45: 600°C spalled beam rebound hammer results 142
Figure 8.1: Shop drawings of typical precast, prestressed ceiling panel present in MassDOT tunnels: plan view (L); reinforcement view (R) 146
Figure 8.2: Proposed panels analogous to existing MassDOT precast, prestressing ceiling panels: plan view (L); reinforcement view (R) 147

This page left blank intentionally.

List of Acronyms

Acronym	Expansion
ACI	American Concrete Institute
ASCE	American Society of Civil Engineer
ASTM	ASTM International (formerly American Society for Testing and Materials)
CEN	European Committee for Standardization
CFRP	Carbon fiber reinforced polymer
DOT	Department of Transportation
FHWA	Federal Highway Administration
FRP	Fiber-reinforced polymer
fib	International Federation for Structural Concrete
GFRP	Glass fiber reinforced polymer
HC	Hydrocarbon fire curve
HCM	Hydrocarbon modified fire curve
ISE	Institute of Structural Engineers
RWS	Rijkswaterstaat fire curve
$f'_c/f'_{c,r}/f'_{cmo}/R^{20}_c$	Compressive strength of concrete before heating
$f'_{cT}/f'_{c,T}/f'_{cm}/R^{T}_c$	Compressive strength of concrete in the “hot” state, or after cooling
E_c	Concrete elastic modulus
f_y	Yield strength of steel before heating
f_{yT}	Yield strength of steel in the “hot” state, or after cooling
f_u	Ultimate strength of steel before heating
f_{uT}	Yield strength of steel in the “hot” state, or after cooling
$f_{p0.1}$	0.1% proof stress of steel before heating
$f_{p0.1T}$	0.1% proof stress of steel in the “hot” state, or after cooling
f_p	Yield strength of prestressing steel
f_{pT}	Yield strength of prestressing steel in the “hot” state, or after cooling
E_s	Elastic modulus of steel before heating
E_{sT}	Elastic modulus of steel in the “hot” state, or after cooling

This page left blank intentionally.

1.0 Introduction to Fire and Tunnels

This study of Post-fire Damage Inspection of Concrete Structures was undertaken as part of the Massachusetts Department of Transportation (MassDOT) Research Program. This program is funded with Federal Highway Administration (FHWA) State Planning and Research (SPR) funds. Through this program, applied research is conducted on topics of importance to the Commonwealth of Massachusetts transportation agencies.

Owing to a couple of recent tunnel fire incidents in MassDOT-owned tunnels, MassDOT has identified fire incidents as a major concern for the safe, uninterrupted operation of its tunnels. As such, a research project has been initiated to develop a post-fire inspection protocol that would allow inspectors to quickly assess the condition of a tunnel after a fire event. Post-fire inspections pose many challenges. For one, the level of damage may range from minor to severe, and the inspector must be able to identify any potential hazards or structural deficiencies. Furthermore, fire events are generally rare, and inspectors may have limited experience in performing these types of inspections. In some cases, inspectors may have only a short window of time to determine if a tunnel is safe to be reopened or risk significant economic and social ramifications.

MassDOT is not alone in its concerns about the effect of fire on its tunnel structures. Several recent and well-known tunnel fires, such as the 1996 Channel Tunnel fire and the 1999 Mont Blanc tunnel fire, have greatly accelerated the pace of structural fire research in the last couple of decades [1]. Fire can negatively affect structures in a variety of ways, such as loss in strength and stiffness of structural members, excessive deflections/distortions, and reduction in the long-term durability of the structure. The purpose of this report is to investigate how fire exposure affects the residual strength of structures and use this knowledge to inform the development of rapid inspection protocol for MassDOT's tunnels.

At present, there are two overarching topics in the field of research on fire and structures:

- Residual condition of structures after fire
- Fire resistance design

The residual condition of structures after fire is mainly concerned with the strength and serviceability loss of a structure after a fire event, as well as the long-term health of the structure. On the other hand, fire resistance can broadly be defined as the "ability of an element (not a material) of building construction to fulfill its designed function for period of time in the event of a fire" [1]. This report focuses on the topic of the residual condition of structures after fire, as this is more pertinent for a post-fire evaluation. Indicatively, the research literature between the two topics has not been balanced. Most of the research efforts have focused on fire resistance design, as it is important to design against a fire event. Published work on the residual conditions of structures after a fire is a much less-explored field, and this research project is aiming in this direction, with an emphasis on tunnel structures.

The contents of this report are as follows:

- Section 2 presents a literature review of structural codes, standards, technical reports, and academic papers on the post-fire mechanical properties of concrete, steel, and the concrete/steel bond.
- Section 3 presents existing experimental studies that have been conducted to assess the residual strength of reinforced concrete members after fire exposure.
- Section 4 describes common techniques for post-fire inspection of concrete structures, focusing on visual and non-destructive testing methods that can be quickly performed.
- Section 5 reviews common repair methods for fire-damaged concrete structures.
- Section 6 presents the results of a survey of post-fire inspection practices/protocols at other state DOTs and transit authorities, which was conducted by video conferences and email correspondence with members of these organizations.
- Section 7 presents the findings of preliminary experimental testing conducted at the University of Massachusetts, Amherst (UMass Amherst), which includes validating the ability of the proposed heating system for heating structural and non-structural components, and preliminary data on the effect of heating structural and non-structural tunnel elements.
- Lastly, Section 8 presents recommendations for Phase II experimental testing.

1.1 Introduction to the Residual Condition of Structures after Fire

The residual condition of concrete structures after fire is the focus of this report, as it has been extensively demonstrated that fire can harm the residual strength, residual serviceability, and long-term durability of concrete structures. The level of damage sustained by a structure is largely dependent on the decay in mechanical properties of concrete and steel, as their post-fire mechanical properties dictate the residual behavior of the structural members and the structure as a whole after fire. Both concrete and steel may suffer a permanent loss in strength and stiffness after a fire event, and as a result, numerous studies have been conducted on the post-fire properties of these materials. Heat exposure can also result in thermal spalling of concrete, which can reduce the effective cross-section of structural members and expose reinforcing steel. Several studies have also been conducted on the residual strength and stiffness of structural members or subassemblies that have been exposed to fire. Since in most cases, full-scale load tests of damaged structures or structural members are impractical, most post-fire inspection techniques are aimed at characterizing the residual mechanical properties of concrete and steel material after fire.

Several factors govern the level of damage that a structure sustains after a fire event. The air temperature during the fire has a significant effect, as the decay in the mechanical properties of concrete and steel are largely dependent on the maximum temperature experienced during the fire. In addition, the duration of the fire is also important, as longer fires generally result in heat penetrating deeper into the concrete, not only damaging a greater volume of concrete

but also potentially causing steel reinforcement to experience higher temperatures. Another important factor is the location of the fire during the fire event. Since concrete structures have excellent thermal insulation on account of the thermal insulation properties of concrete itself, typically only regions of the structure near the fire location will sustain damage.

To develop a post-fire inspection protocol, all the possible detrimental effects of fire exposure on the residual condition of a structure and its structural elements must be considered. The purpose of this report is to elucidate these effects and present inspection methods that can identify the types of damage that are likely to occur due to fire.

1.2 Introduction to Fire Resistance Design

Though the focus of this report is on the residual condition of structures after fire, the topic of fire resistance design is briefly summarized in this section, as some concepts overlap between the two fields of study. Fire resistance can be defined broadly as the "ability of an element (not a material) of building construction to fulfill its designed function for period of time in the event of a fire" [1]. In other words, fire resistance design is focused on the immediate safety of occupants during a fire by ensuring that a structure can withstand fires of a certain duration. The majority of research on structures and fire has focused on fire resistance design, and several codes and standards are available to assist designers in creating fire-resistant structures. Fire resistance design can be categorized by three approaches: fire testing, prescriptive methods, and performance-based methods.

Fire testing usually involves exposing a structural element or sub-assembly of a structure to high temperatures in a testing furnace while the element is subjected to a service load with its expected support conditions. The air temperature in the furnace over the course of the test is usually stipulated by design fire curves. Several design fire curves exist, such those shown in Figure 1.1 [2].

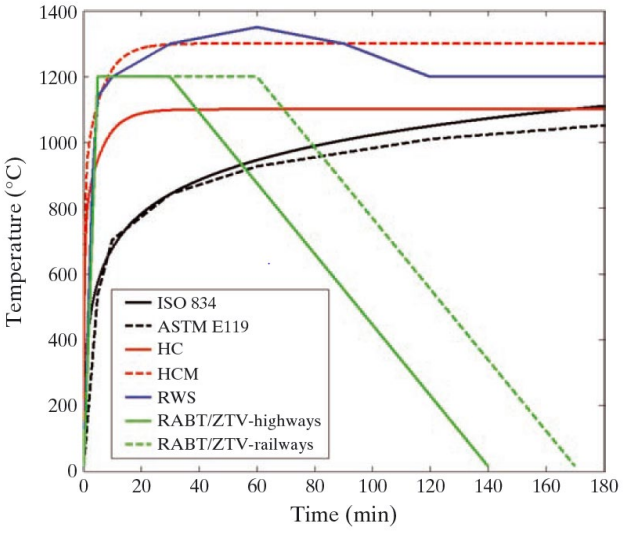

Figure 1.1: Comparison of common design fire curves

The ISO 834 and ASTM E119 fire curves are very similar and are intended for the design of typical buildings. The hydrocarbon (HC) and hydrocarbon modified (HCM) curves are intended to represent the combustion of hazardous materials such as chemicals and fuels. Lastly, the Rijkswaterstaat (RWS) and RABT/ZTV fire curves were developed specifically for the design of tunnels, as experiences with several tunnel fires showed other fire curves may not be severe enough to represent tunnel fires [2].

Prescriptive methods for fire design are much simpler and are the most widely implemented of the three methods. Examples of prescriptive methods include requirements of minimum cover to reinforcement for certain design fires, and requirements of maximum temperatures within certain elements for a design fire.

Performance-based methods have gained traction in the last few decades, and some countries have implemented these methods in their codes. These methods involve the use of engineering calculations and finite element analysis to prove that structures can meet fire design criteria specified at the beginning of the design process, such as withstanding expected fire loads without collapse [1,3].

1.3 Additional Documents on Residual Condition of Structures After Fire and Fire Resistance Design

For reference, a non-exhaustive list of standards, codes, and technical reports on the subjects of the residual condition of structures after fire and fire resistance design are shown in Table 1.1.

Table 1.1: Standards, codes, and technical reports on topics of fire and structures

Organization	Country/Region	Document Name	Document Type	Publication Date
Fire Safety Journal/CIB W14	N/A	*The Repairability of Fire-Damaged Structures*	Journal Article/Technical Report	1990
American Society of Civil Engineers (ASCE)	USA	*Structural Fire Protection*	Standard	1992
Eurocode (CEN)	EU	*EN 1992 1-2, EN 1993 1-2, EN 1994 1-2*	Building Code	2004 & 2005
Concrete Society	Britain	*Assessment, Design, and Repair of Fire-Damaged Structures*	Technical Report	2008
International Federation for Structural Concrete (*fib*)	EU	*Fire Design of Concrete Structures – Structural Behavior and Assessment*	Technical Report	2008
Institution of Structural Engineers (ISE)	Britain	*Appraisal of Existing Structures*	Technical Report	2010
American Concrete Institute (ACI)	USA	*Code Requirements for Determining Fire Resistance of Concrete and Masonry Construction Assemblies*	Building Code	2019

2.0 Effect of Fire on Structural Materials

It is well known that both concrete and steel experience decay in their mechanical properties at elevated temperatures and after cooling down from elevated temperatures, with the most significant effect being the potential reduction in strength [4,5]. Understanding the behavior of these materials is critical for the assessment of concrete tunnels after fire. Since it is impractical to perform full-scale load tests on a tunnel exposed to fire to determine its residual strength, most inspection methods are aimed at relating the properties of the structural materials to the residual strength of structural members and of the entire structure. As a result, many studies have been conducted on the properties of concrete and steel with respect to fire. The vast majority of these studies have been conducted on individual concrete and steel specimens, such as concrete cylinders and steel coupons, allowing researchers to isolate the most important factors dictating the response of these materials to thermal exposure.

The difference between "at elevated temperature" and "residual" should be distinguished here. "At elevated temperature" refers to the properties of a material when it is in the "hot" state. This is most relevant to the behavior of materials during a fire scenario. "Residual" refers to the properties of a material after it has been heated and cooled. This is most relevant to the post-fire scenario. However, the properties of materials both at elevated temperatures and after cooling will be discussed herein, as it is important to understand the differences between these two conditions for assessing a structure after fire.

To understand the results of these experimental studies, it is important to understand the main test methods that have been employed for analyzing the mechanical properties of concrete and steel at elevated temperature and after cooling down. Concrete and steel are the focus of this report, as they are the materials most commonly used in a tunnel construction. The methods are summarized as follows.

i. **Unstressed test:** Specimens are heated to a certain temperature (without the application of any load) until steady-state conditions (uniform temperature) are achieved in the specimen. The specimen is then loaded until failure while hot, typically with compression tests for concrete and tensile tests for steel. The results of these tests are most applicable for estimating the performance of structural materials that are under very low stress during a fire.
ii. **Stressed test:** Specimens are loaded to service-level stress and then heated to a certain temperature until steady-state conditions (uniform temperature) are achieved. While it is still hot, the load on the specimen is then increased until failure occurs. The results of these tests are most applicable for estimating the performance of structural materials that are under service-level stress during a fire.
iii. **Unstressed residual test:** Specimens are heated to a certain temperature (without the application of any load) until steady-state conditions (uniform temperature) are achieved in the specimen. The specimen is then cooled to ambient temperature, usually by air but sometimes by water, and then loaded until failure, typically with

compression tests for concrete and tensile tests for steel. These tests are applicable for estimating the performance of structural materials after a fire event.

iv. **Stressed residual test:** These types of tests are far rarer than the previous three. Specimens are loaded to service-level stress and then heated to a certain temperature until steady-state conditions (uniform temperature) are achieved. The specimen is then cooled to ambient temperature, usually by air but sometimes by water, and then loaded until failure, typically with compression tests for concrete and tensile tests for steel. These tests are most applicable for estimating the performance of structural materials after a fire event.

Although the unstressed residual test and the stressed residual test are most applicable for post-fire assessment situations, results from elevated temperature testing (stressed and unstressed) are included in this report as well, since some design codes present equations both at elevated temperatures and after cooling (residual).

2.1 Concrete

Concrete is the most commonly used material in modern tunnel engineering and structural engineering in general. Its performance at elevated temperatures and after cooling has been researched extensively over the last 50 to 60 years, particularly due to its use in nuclear power plants. In terms of its performance with respect to fire, concrete has two advantages: It is incombustible, and it has good thermal insulating properties on account of its low thermal diffusivity, allowing it to shield parts of the structure from fire [2]. On the other hand, concrete can experience loss of strength, loss of stiffness, and spalling due to heat exposure, reducing the residual strength and durability of a structure [1].

This section describes the physical and chemical processes and the loss of strength and stiffness that occur due to heat exposure in concrete, thermal spalling of concrete, and some studies on the temperature distribution in concrete due to fire.

2.1.1. Physical and Chemical Changes during Heating and Cooling of Concrete

When heated, concrete undergoes several largely irreversible physical and chemical processes that can damage the concrete and lead to decay of its mechanical properties [1,6]. Three main factors contribute to the decay of mechanical properties.

i. Physical and chemical changes in the cement paste.
ii. Physical and chemical changes in the aggregate.
iii. Differential thermal strains between the aggregate and the cement paste.

The critical physical and chemical changes in the aggregate and cement paste are summarized in Table 2.1. The dehydration of the cement matrix and aggregate is of particular importance, as some studies have directly linked dehydration to strength loss [7,8].

Table 2.1: Summary of mineralogical changes in concrete due to heating

Heating temperature: °C	Changes caused by heating	
	Mineralogical changes	*Strength changes*
70–80	Dissociation of ettringite	Minor loss of strength possible (<10%)
105	Loss of physically bound water in aggregate and cement matrix commences, increasing capillary porosity	
120–163	Decomposition of gypsum	
250–350	Oxidation of iron compounds causing pink/red discolouration of aggregate. Loss of bound water in cement matrix and associated degradation becomes more prominent	Significant loss of strength commences at 300°C
450–500	Dehydroxylation of portlandite. Aggregate calcines and will eventually change colour to white/grey	
573	5% increase in volume of quartz (-to-quartz transition) causing radial cracking around the quartz grains in the aggregate	Concrete not structurally useful after heating in temperatures in excess of 500–600°C
600–800	Release of carbon dioxide from carbonates may cause a considerable contraction of the concrete (with severe micro-cracking of the cement matrix)	
800–1200	Dissociation and extreme thermal stress cause complete disintegration of calcareous constituents, resulting in whitish-grey concrete colour and severe micro-cracking	
1200	Concrete starts to melt	
1300–1400	Concrete melted	

Note: Table reprinted from source [9]

Differential thermal strain between the aggregate and the cement paste occurs because cement paste physically expands until reaching it reaches temperatures up to 150°–200°C, then begins to contract at temperatures above this range, while the aggregates will continuously expand with increasing temperature. It has been noted, however, that the effects of these differential thermal strains are reduced during heating when the concrete under load, due to a phenomenon called load-induced thermal strain (transient creep), which causes the relaxation and redistribution of thermal stresses in the concrete [1]. As concrete cools down after heating, the beneficial effect of load-induced thermal strain is no longer active, and the differential thermal strains of the cement paste and aggregate can create further damage in the concrete. This explains why the strength of concrete after cooling from a certain maximum temperature is generally lower than the strength of the concrete when it is at that maximum temperature [6].

2.1.2. Strength of Concrete at Elevated Temperatures and after Cooling Down

Though concrete is incombustible and possesses excellent thermal insulating properties, it can experience a decay in its strength at elevated temperatures and after cooling down due to largely irreversible physical and chemical changes. In terms of the post-fire assessment of a structure, the loss in strength of the concrete is of particular concern [10]. Though the focus of this report is on the post-fire condition of structures, both the properties at elevated temperature and after cooling down are described, as it is important to understand the differences between these two conditions for assessing a structure after fire. Although a great amount of research has been conducted on both the strength of concrete at elevated temperatures [11,12] and the residual strength of concrete after cooling [4,13–17], the heterogenous nature of concrete makes theoretical predictions of mechanical properties in these scenarios difficult. Therefore, the majority of existing models for estimating the

strength of concrete at elevated temperatures or after cooling down are based on the results of experimental studies [4,13,17].

Due to the wide variety of concrete strengths, types, and mixtures available, identifying the main factors that affect the strength of concrete during and after thermal exposure has been a focus of several studies. A couple of factors have emerged as the most significant [4,13].

- Original concrete compressive strength
- Type of aggregate (siliceous, calcareous, etc.)

Although other factors, such as maximum aggregate size or water/cement ratio, can significantly affect the strength of concrete during and after thermal exposure, it has been shown that their effects can be seen through more general predictors such as compressive strength and are therefore generally not explicitly considered [4]. As far as the conditions to which the concrete is exposed, maximum temperature of the concrete material and loading conditions have also been shown to significantly affect the strength of concrete during and after thermal exposure. Furthermore, there are notable differences between the strength of concrete at elevated temperature and the residual strength of concrete after cooling.

2.1.2.1 Codes and Standards

Design codes and standards produced by several organizations, including CEN (Eurocode) and American Concrete Institute (ACI), feature equations and curves that describe the strength and stiffness of concrete both at elevated temperatures (in the hot state) and after cooling from elevated temperatures (residual).

For instance, *EN 1992 1-2* provides a set reduction factors that can be applied to the original compressive strength and elastic modulus of concrete to estimate the compressive strength and elastic modulus of concrete at elevated temperatures (in the hot state) [18]. The reduction factors for compressive strength are plotted in Figure 2.1. *EN 1992 1-2* distinguishes between concrete made with siliceous aggregates and that made with calcareous aggregates. The factors shown in Figure 2.1 are only intended for normal strength concrete up to strength class C50/60 (concrete with a minimum 28-day cylinder compressive strength of 50 MPa). Additional strength reduction factors based on more limited data are provided in *EN 1992 1-2* for high-strength concrete (concrete up to C90/105).

The reduction factors in Figure 2.1 show that concrete begins losing compressive strength at elevated temperatures in the range of 200°–300°C, and that concrete at temperatures of 600°–700°C will have about 50% of its original strength. Equations are also provided in *EN 1992 1-2* to transform the strength reduction factors for concrete at elevated temperatures into stress-strain curves for concrete at elevated temperatures, as shown graphically in Figure 2.2 for siliceous aggregate concrete.

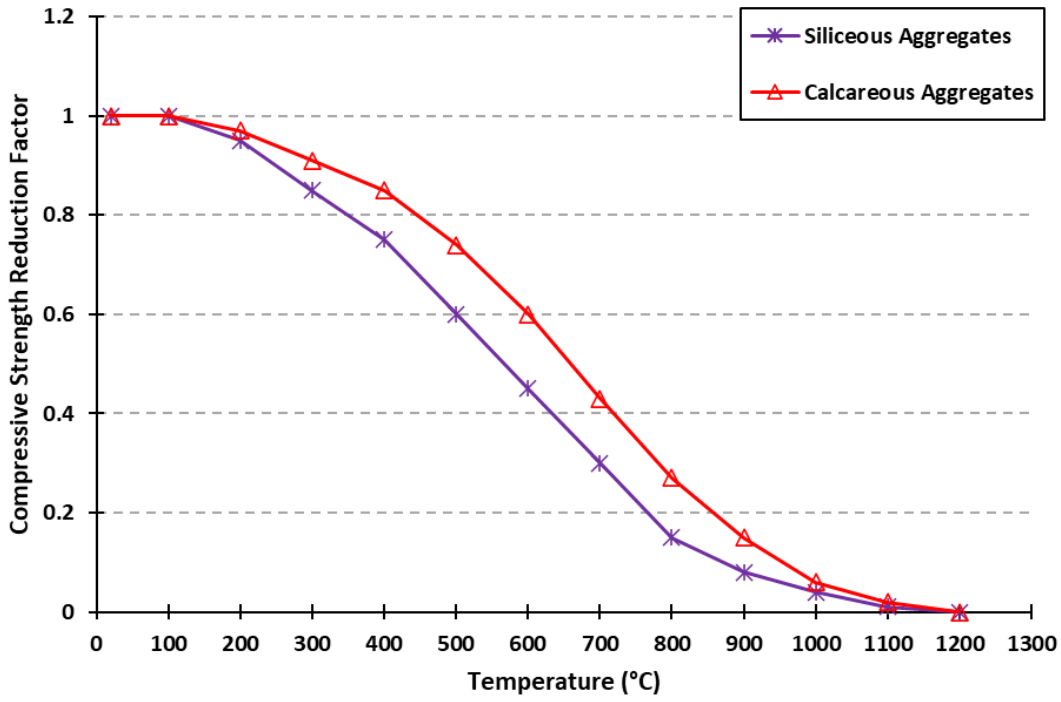

Figure 2.1: Compressive strength reduction factors for concrete at elevated temperatures per *EN 1992 1-2*

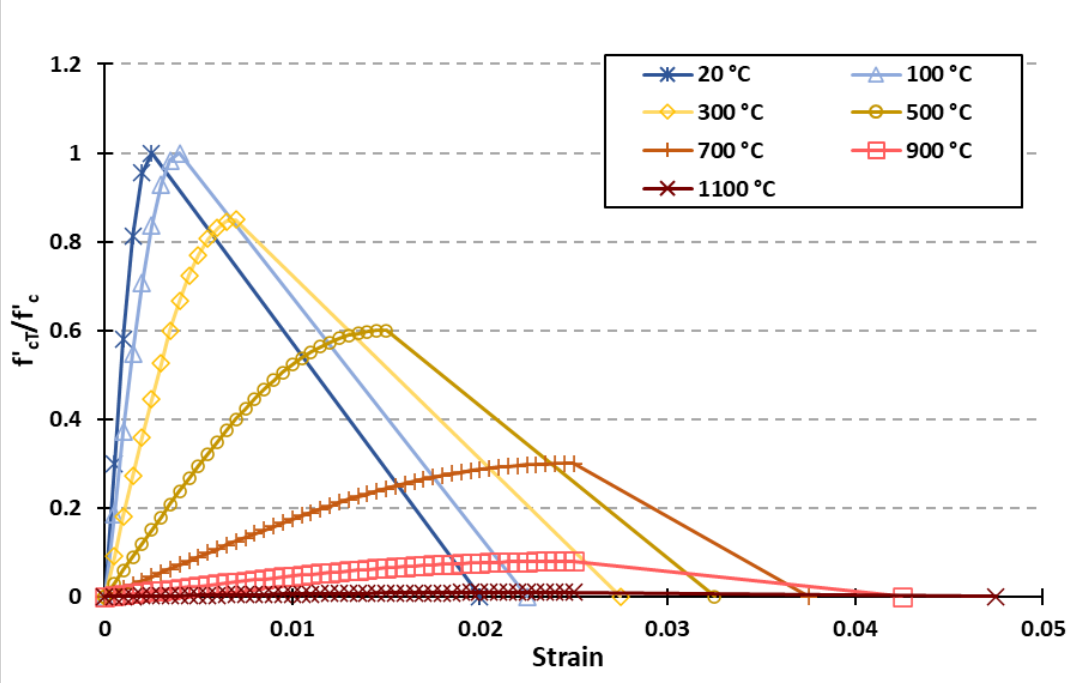

Figure 2.2: Stress-strain curves for concrete made with siliceous aggregates at elevated temperature per *EN 1992 1-2*

Though *EN 1992 1-2* does not provide any guidance or equations on assessing residual strength of concrete or concrete members, *EN 1994 1-2* does provide equations for the residual strength of concrete [19]. The difference between *EN 1992 1-2* and *EN 1994 1-2* is that the former is a code for design of concrete structures, whereas the latter is a code for design of composite steel and concrete structures. Three equations are provided in *EN 1994 1-2* that modify the reduced strength factors for concrete at elevated temperatures to give the residual strength of concrete based on the maximum temperature of exposure. The comparison of the strength curve for the residual concrete strength and concrete strength at elevated temperature is shown in Figure 2.3.

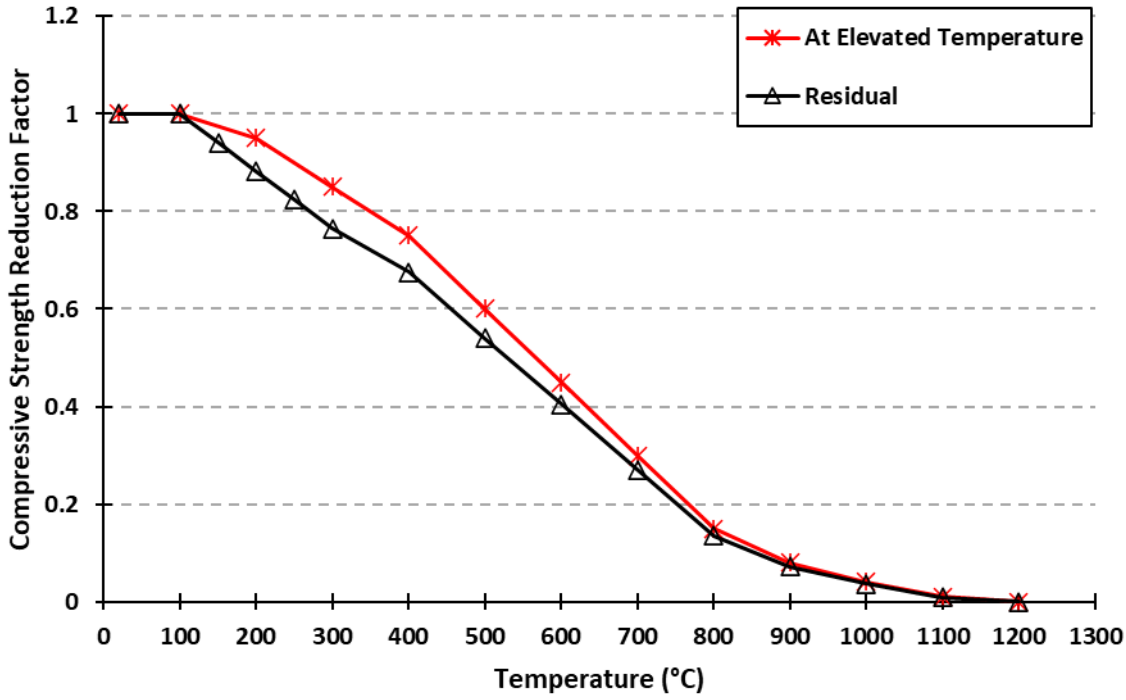

Figure 2.3: Comparison of reduction factors for compressive strength of concrete at elevated temperature and after cooling (residual) per *EN 1994 1-2*

According to *EN 1994 1-2*, the residual strength of concrete is slightly lower than that of concrete at elevated temperatures, meaning that the concrete loses additional strength as it cools down. The additional loss of strength during cooling has been attributed in part to the differential thermal strains between the aggregate and the cement paste [6].

Though Eurocode provides a wealth of information on the design of structures for fire, it is worth pointing out that the codes are based on the common materials and construction practices in Europe, which may differ significantly from those in the United States. *ACI 216.1-14* is one of the U.S. codes for fire design of concrete structures, which also contains strength reduction curves to predict the residual strength and the strength at elevated temperature of concrete. As with Eurocode, *ACI 216.1-14* also distinguishes between concrete with siliceous aggregates and concrete made with carbonate/calcareous aggregates. The strength reduction curves are shown in Figure 2.4 (siliceous aggregate) and Figure 2.5

(carbonate/calcareous aggregate) [20]. According to [4], these curves were developed based on a single study that mostly used specimens with an initial compressive strength less than 6 ksi.

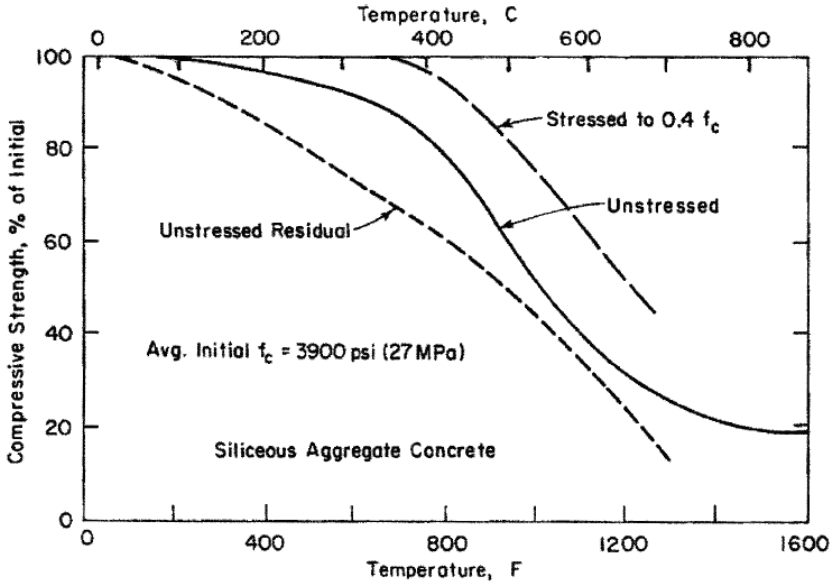

Figure 2.4: Strength reduction curves for compressive strength of concrete made with siliceous aggregates per *ACI 216.1-14*

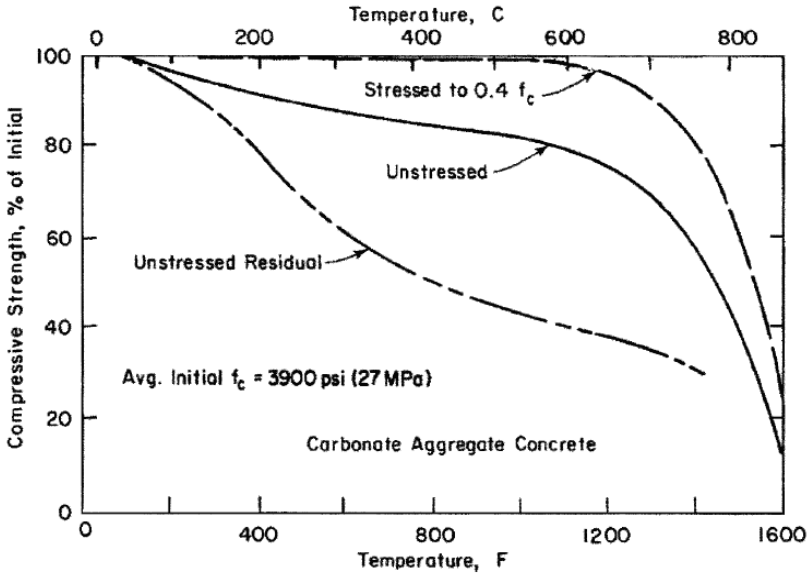

Figure 2.5: Strength reduction curves for compressive strength of concrete made with calcareous/carbonate aggregates per *ACI 216.1-14*

In terms of the behavior of concrete at elevated temperatures, one notable difference between the documents is the addition of the curve to predict the properties of concrete at elevated temperatures with applied compressive stress in *ACI 216.1-14* ("stressed to 0.4f_c"). The *ACI*

216.1-14 curves show that the presence of compressive strength has a significant benefit for the strength of the concrete when at elevated temperatures. Eurocode does not treat stressed and unstressed concrete differently in regard to temperature.

The unstressed residual strength curves from *ACI 216.1-14* show reasonable agreement with the residual strength curves from *EN 1994 1-2*. The *ACI 216.1-14* curves predict that calcareous/carbonate aggregate concretes generally have a slightly lower relative residual compressive strength than siliceous aggregate concretes up until approximately 500°C, after which siliceous aggregates have a lower compressive strength.

2.1.2.2 Experimental Studies

Though both the ACI and Eurocode design documents provide valuable information regarding the compressive strength of concrete after fire, each has a notable shortcoming: The curves in *ACI 216.1-14* were developed from the data set of a single study, and the Eurocode curves/equations are based on studies of concrete made using materials not native to North America. In an effort to study the data from a larger pool of studies that performed tests on concrete made with materials native to North America, [4] compiled nine studies and performed a meta-analysis of their data. The data points included in the study cover a variety of concrete strengths (both normal-strength and high-strength, and aggregates: calcareous, siliceous, and lightweight). In this study, concrete with a strength above 6 ksi was considered to be high strength. At the time this document was written, an Excel sheet database containing data points from 14 studies compiled by the authors of [4] can be found at the University of Notre Dame's Fire Research Group webpage (https://www3.nd.edu/~concrete/concrete-fire-database/).

A regression analysis was performed to develop best-fit lines for the compiled data. Several figures from the study are shown in Figures 2.6 to 2.9 [4], which present the data in a variety of ways, such as by splitting up by test type or by comparing to curves from *ACI 216.1-14*.

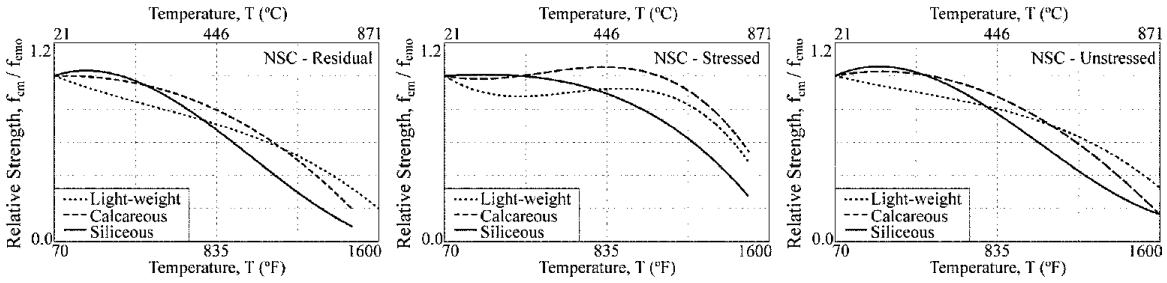

Figure 2.6: Compressive strength loss of normal-strength concrete (NSC), separated by test type: residual (L), stressed (c), unstressed (R)

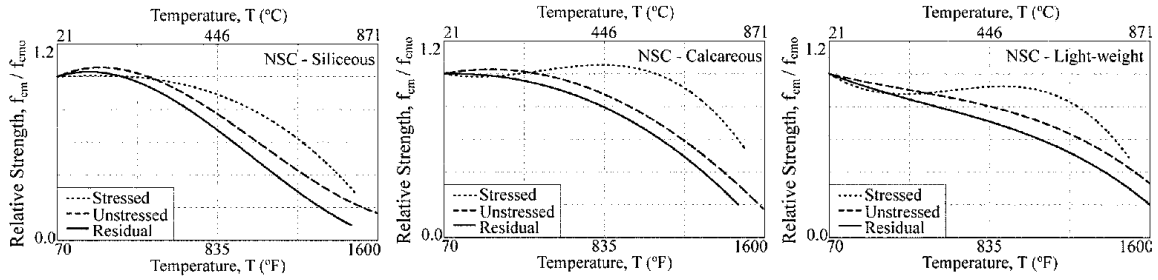

Figure 2.7: Compressive strength loss of normal-strength concrete, separated by type of aggregate: siliceous (L), calcareous/carbonate (C), lightweight (R)

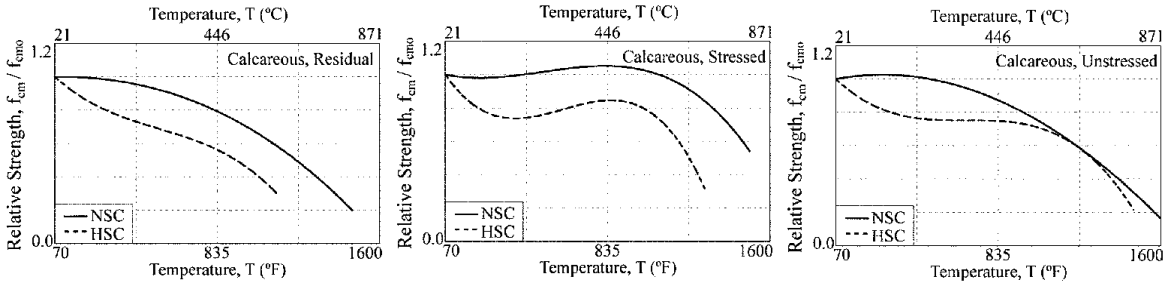

Figure 2.8: Residual compressive strength of normal-strength and high-strength concrete with calcareous aggregates, separated by test type: residual (L), stressed (C), unstressed (R)

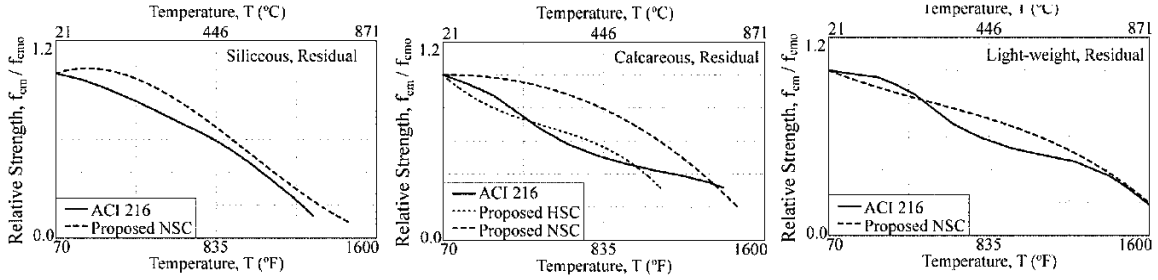

Figure 2.9: Best-fit lines (proposed models) for residual compressive strength loss of normal-strength and high-strength concrete, compared to ACI 216.1-14 curves, separated by aggregate type: siliceous (L), calcareous (C), lightweight (R)

Several important conclusions can be drawn from the data:

- The strength loss for the stressed test type was generally lowest, whereas the strength loss for the residual test type was generally greatest. The presence of compressive stress at elevated temperature generally has a beneficial effect on the strength compared to when the concrete is unstressed.
- Siliceous aggregate concretes exhibit greater strength losses for all three test types above 446°C than calcareous or lightweight aggregate concretes.
- The strength loss of high-strength concrete is almost universally greater than that of normal-strength concrete for a given temperature.

Given that high-strength concrete has been shown to behave differently than normal-strength concrete with heat exposure, some studies have focused specifically on the mechanical properties of high-strength concrete, due to heat exposure. This is especially pertinent for tunnels, since high-strength concrete is frequently used for these structures. One recent study [17] conducted a meta-analysis of data from 54 studies to characterize the residual compressive strength of high-strength concrete (greater than 6 ksi was considered to be high-strength for this study). A regression analysis was performed to find a best-fit curve for the data, and a conservative design curve was proposed that was more conservative than 90% of the data points. These curves are shown in Figure 2.10, where the black dots are individual data points, the solid line is the best-fit curve, and the dashed line is the proposed conservative design equation [17].

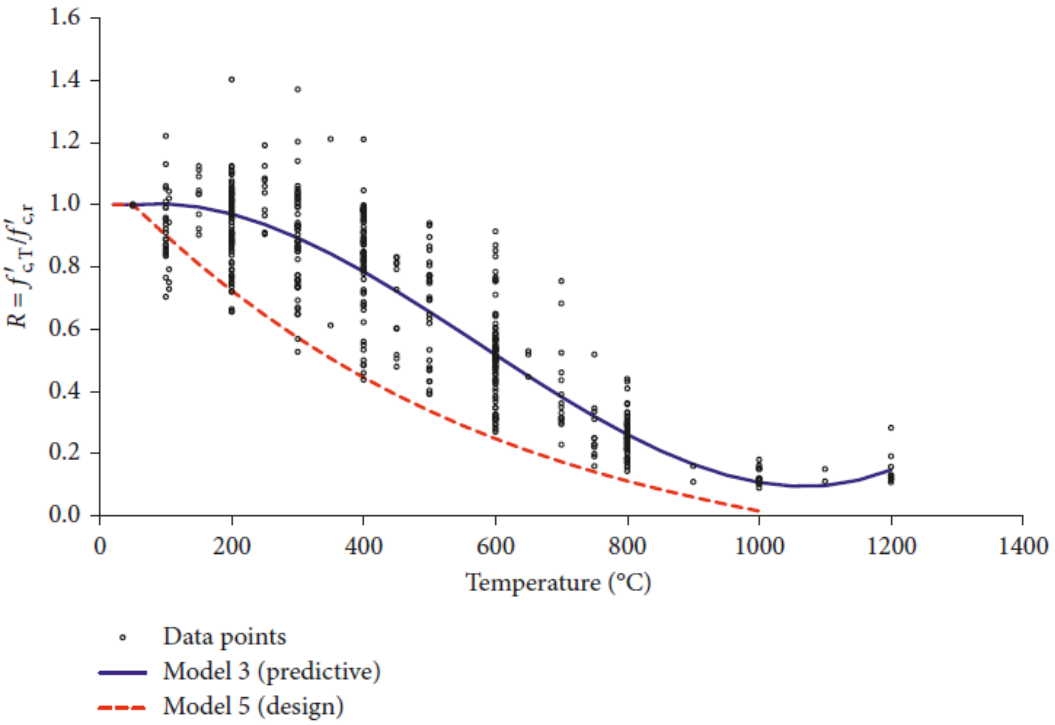

Figure note: Black dots are individual data points of each specimen; solid line is a best-fit line; dashed line is proposed conservative design curve.

Figure 2.10: Relative residual compressive strength of high-strength concrete

This meta-analysis did not distinguish between type of aggregate or concrete mixture additives. In general, comparison of Figure 2.10 with the *ACI 216.1-14* curves in Figure 2.4 and Figure 2.5 show that the high-strength concrete may have a higher residual strength for given temperatures compared to normal-strength concrete. This contrasts with the findings of [4], which stated that high-strength concrete experiences greater strength losses than normal-strength concrete, though [4] had more limited test data on high-strength concrete.

2.1.3. Stiffness of Concrete at Elevated Temperatures and after Cooling Down

Some studies have focused on the stiffness loss in concrete that can occur at elevated temperatures and after cooling down. One well-known study compiled the results of several studies, showing the relationship between modulus of elasticity and maximum temperature for various types of concrete [13]. The study only included figures for the unstressed (Figure 2.11) and unstressed residual (Figure 2.12) test types, as not enough data was available for the stressed test type.

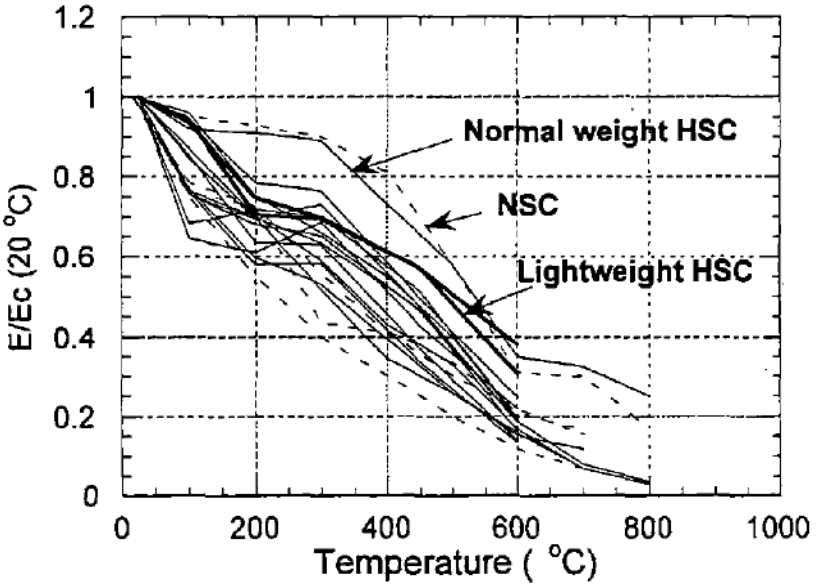

Figure note: Each line shows data from a different study.

Figure 2.11: Relative modulus of elasticity of concrete from unstressed tests

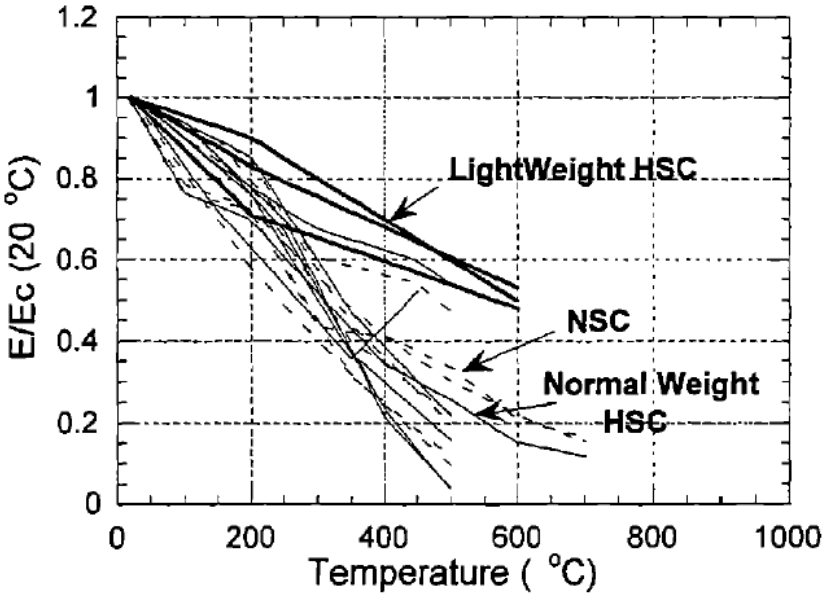

Figure note: Each line shows data from a different study.

Figure 2.12: Relative modulus of elasticity of concrete from unstressed residual tests

Overall, the relative modulus of elasticity seems to diminish at a similar or even greater rate than the relative strength as temperature increases, which is expected, given the close relationship between strength and modulus of elasticity in concrete [21].

In reviewing the literature, a couple of gaps in knowledge remain. For one, although it has been shown that the presence of compressive stress has a beneficial effect on the mechanical properties of concrete at elevated temperatures, none of the studies conducted residual strength tests on specimens that were subjected to any sort of stress during the heating and cooling phase. If this beneficial effect also occurs after concrete has cooled from elevated temperatures (residual), the curves that have been proposed for the residual strength of concrete may be overly conservative. Second, it is unclear if sustained heating at a particular steady-state temperature further damages the concrete in a significant manner. With that said, the latter point may be less important, since sustained heating at a given temperature is unlikely to occur in an actual fire event.

2.1.4. Thermal Spalling of Concrete

In addition to strength and stiffness losses, another possible deleterious effect of thermal exposure on concrete is thermal spalling, a subject which has been extensively researched [22–30]. Though the potential mechanisms were not understood until more recently, spalling of concrete in structures during fire events has been observed since the early 1900s [27]. The potential for fire spalling raises considerable structural concerns; however, these concerns differ slightly, depending on whether a scenario during a fire or a post-fire scenario is being considered. During a fire, spalling can reduce the strength of concrete members by reducing the effective cross-section of members or by exposing reinforcing steel. The former can reduce load-bearing capacity of concrete in compression, whereas the latter can expose the reinforcing steel to very high temperatures and cause loss of bond, which is particularly

concerning for flexural members [31]. Existing structural codes largely focus on the structural concerns of fire spalling during fire events, such that elements/structures can be designed to achieve the desired fire resistance rating. For instance, *EN 1992 1-2* provides recommendations to reduce the incidence of explosive spalling, such as recommendations for spalling-resistant mix designs and additives to reduce spalling [18]. In the post-fire scenario, spalling is still a major concern. If the spalling occurs during heating, reinforcing steel and deeper regions of the concrete may reach higher temperatures due to loss of the outer layers of concrete. Furthermore, spalling that occurs at any point in the process (during heating or cooling, or after cooling) can reduce the effective cross-section of structural members, potentially reducing their residual strength capacity. The occurrence of spalling also means that repairs will often be required to return the structure to its previous condition [10].

Four general types of fire spalling have been identified, each differing in nature and severity: explosive spalling, surface spalling, aggregate spalling, and corner spalling/sloughing-off. The characteristics of these types of spalling are summarized in Table 2.2, though it should be noted that these are typical characteristics, and deviations from these typical characteristics have been noted. Furthermore, other types of spalling, such as spalling that occurs in the days or weeks after a fire event, have also been observed [30].

Explosive spalling is recognized as the most severe type of fire spalling, and much of the existing research on thermal spalling has focused on explosive spalling [1]. Explosive spalling is often described as a violent form of spalling that is often accompanied by a loud explosive noise or “bang.” It can occur as a single explosion or a series of explosions that each remove a layer of concrete, with dimensions generally ranging from 100 to 300 mm in length/width, and 15 to 20 mm in depth. It typically occurs in the first 7 to 30 minutes of a fire, when the concrete is in the range of 150°–450°C [30, 31]. Explosive spalling has been observed in several well-known tunnel fires, such as the 1996 Channel Tunnel fire, the Mont Blanc Tunnel fire, and the Tauern Tunnel fire, often causing extensive damage to the concrete tunnel lining [31]. Currently, there is no consensus in the research community as to the mechanisms that drive explosive spalling. A detailed discussion of these theories is beyond the scope of this report, but the three most popular theories are described: the pore pressure theory, the thermal stress theory, and the combined pore pressure and thermal stress theory.

Table 2.2: Summary of types of fire spalling

Table I Characteristics of the different forms of spalling

Spalling	Time of occurrence (min)	Nature	Sound	Influence	Main influences
Aggregate	7–30	Splitting	Popping	Superficial	H, A, S, D, W
Corner	30–90	Non-violent	None	Can be serious	T, A, F_t, R
Surface	7–30	Violent	Cracking	Can be serious	H, W, P, F_t
Explosive	7–30	Violent	Loud bang	Serious	H, A, S, F_s, G, L, O, P, Q, R, S, W, Z

A = aggregate thermal expansion, D = aggregate thermal diffusivity, F_s = shear strength of concrete, F_t = tensile strength of concrete, G = age of concrete, H = heating rate, L = loading/restraint, O = heating profile, P = permeability, Q = section shape, R = reinforcement, S = aggregate size, T = maximum temperature, W = moisture content, Z = section size

Note: Table Reprinted from Source [1].

The pore pressure theory, or moisture clog theory, attributes explosive spalling to the presence of moisture in the concrete. According to the pore pressure theory, as concrete is heated, the temperature gradient in the concrete drives moisture from the surface of the concrete deeper into the concrete, creating three moisture zones: a dry zone at the surface, an intermediate zone with vaporized water, and moisture saturated zone (the "moisture clog") (Figure 2.13 [26]). As moisture from the intermediate zone attempts to travel deeper into the concrete, it will encounter the moisture clog, creating a zone of high pore pressure between the intermediate vapor zone and the moisture saturated zone, which can cause high tensile stresses at this interface and contribute to spalling [30,31].

The thermal stress theory states that the temperature gradients that develop in heated concrete will induce compressive stresses near the surface of the concrete, due to the restrained thermal expansion (assuming the member is axially restrained), as well as tensile stresses deeper in the concrete in the direction normal to the face of the member. This results in a triaxial stress in the concrete near the surface, as shown in Figure 2.14 [26], which can rupture the concrete along this boundary [30,31].

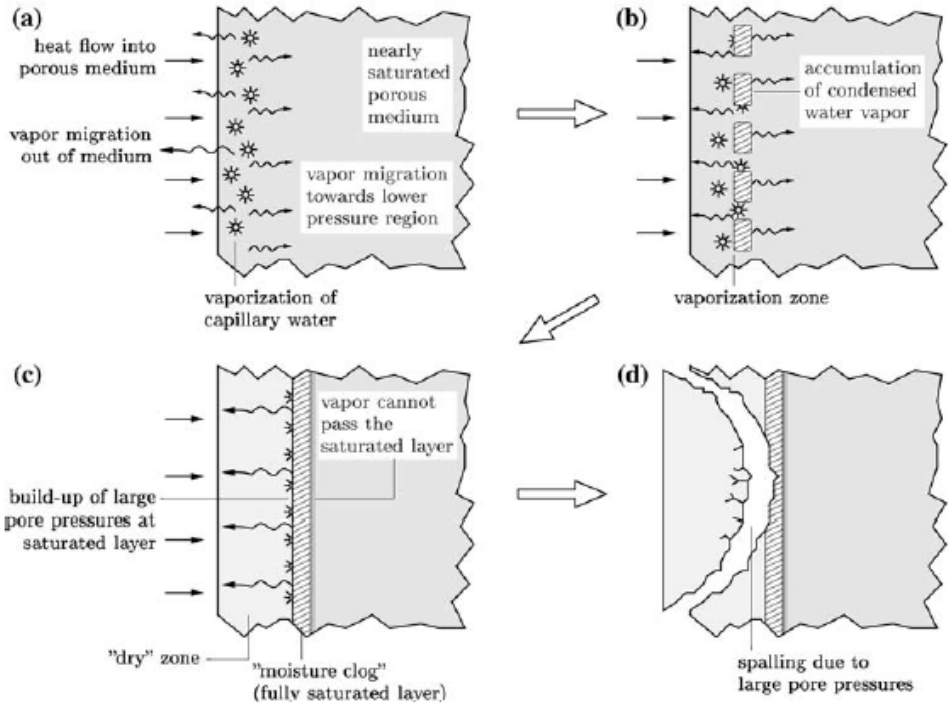

Figure 2.13: Process of thermal spalling according to pore pressure theory (a–d)

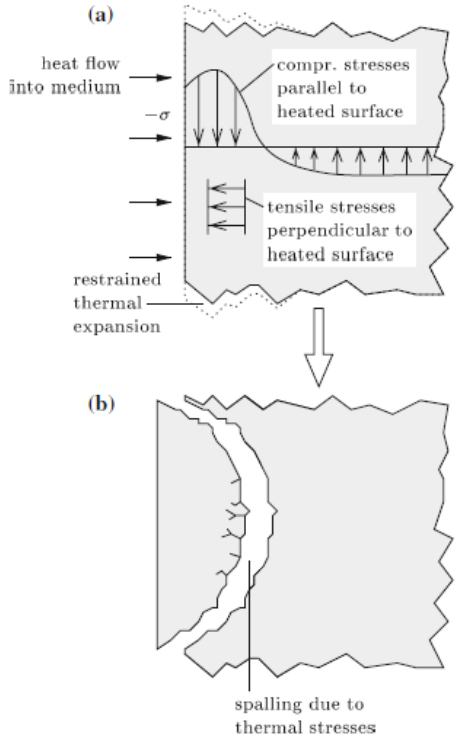

Figure 2.14: Illustration of combined thermal and applied stress on an axial member (a–b)

Lastly, the combined pore pressure and thermal stress theory simply states that the stress increases due to pore pressure and thermal stress both contribute to spalling. This theory is supported by the fact that both moisture content and applied stress have been shown to have a significant effect on the likelihood of explosive spalling [31].

The incidence of explosive spalling has been described as stochastic and is still very difficult to predict using computer models [1]. Fortunately, a wealth of experimental data has revealed the main factors which increase the likelihood of explosive spalling. High-strength concrete has a much higher likelihood for explosive spalling compared to normal-strength concrete. It is thought that the higher incidence of explosive spalling in high-strength concrete can be attributed to densifying agents such as silica fume which are often used in high-strength concrete [31]. Similarly, higher concrete density has also been linked to explosive spalling, which has been attributed to the lower permeability of these concretes which may prevent moisture from escaping as easily. Higher moisture content in concrete has also been shown to increase explosive spalling, which supports the pore pressure theory of explosive spalling. Higher heating rates have long been linked to increased chance of explosive spalling, though explosive spalling can still occur at low heating rates. Greater applied stress has also been shown to increase the chance of explosive spalling. Other factors, such as amount and pattern of reinforcing steel, and the shape of the member, can also affect the chance of explosive spalling, though the exact nature of these relationships is still not entirely known [23].

Surface spalling is considered to be a subset of explosive spalling, differentiated by its lesser severity than explosive spalling [31].

Corner spalling/sloughing-off is associated with the chemical processes that occur in heated concrete, such the reduced bond between aggregate and cement that gradually remove layers of the concrete mainly at the edges of beams and columns [10,30]. Though not a violent form of spalling, it can still have implications for the residual load-bearing capacity of structural members.

Aggregate spalling is not considered to have a major effect on the structural capacity of members. Its occurrence has been attributed to the water retained by aggregates such as flint or sandstone, which can create high vapor pressures that cause the aggregate to “burst” out of the concrete and leave a pitted surface [23,30].

Recently, post-cooling fire spalling has also been observed in concrete. Post-cooling spalling occurs in a similar manner to sloughing-off and is related to the rehydration of calcium oxide, which can cause a 44% increase in volume of the oxide. Post-cooling spalling can occur progressively over a couple of weeks after a fire, causing further damage to the structure [30]. An example of post-cooling spalling in a concrete cylinder is shown in Figure 2.15 [28]. Few studies are available regarding post-cooling spalling, and its incidence of occurrence is still unknown.

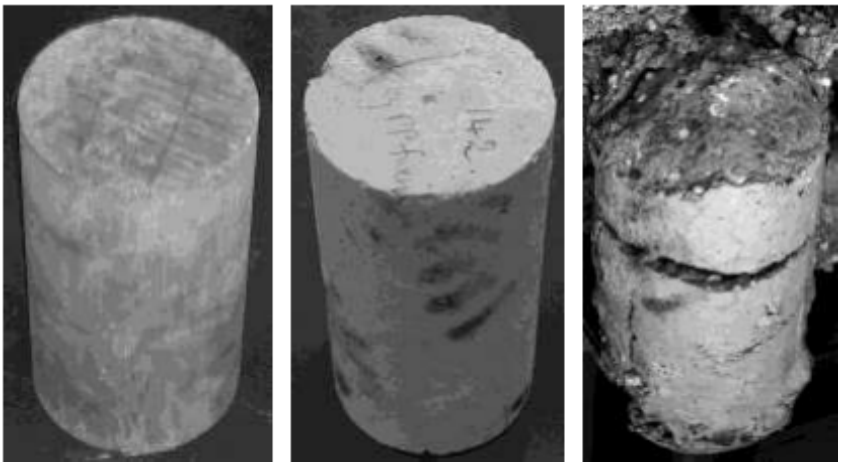

Figure 2.15: Progression of post cooling spalling in a cylinder: before heat exposure (L); after 120 min in ISO fire (C); 1 week after heat exposure (R)

2.1.5. Temperature Distribution of Concrete Exposed to Fire

To fully understand how the loss in strength and stiffness of concrete due to fire will affect a structure, it is important to recognize the insulating properties of concrete. Though the air temperatures in a fire can exceed 1000°C, the insulating properties of concrete will result in a large temperature gradient in the material, in which the outer layers have a high temperature while the inner layers remain relatively cool. Estimating the maximum temperature reached at different depths within the concrete can help estimate the extent of the damage, since relationships between maximum temperature and residual strength loss are known.

An illustrative example of a temperature distribution in a 160-mm-wide concrete beam that was exposed to the standard ISO 834 fire on three sides is shown in Figure 2.16. Shown on the left are the isothermal lines (lines of equal temperature) after 60 minutes of fire exposure, and on the right the locations of the 500°C isothermal lines after 30, 60, and 90 minutes of exposure to the ISO 834 fire [1]. For reference, the ISO 834 fire curve is shown in Figure 1.1. As another example, Figure 2.17 shows the temperature of the concrete along the depth of slabs and 380-mm-square columns exposed to an unspecified design fire. Each line shows the temperature at certain depths in the members after certain durations of exposure to the design fire [10]. *ACI 216.1-14* also provides charts for estimating the temperatures within concrete slabs subjected to the *ASTM E119* heating curve, as shown in Figure 2.18 [20]. To help visualize the depth of damage in concrete exposed to fire, another study superimposed the damage level of concrete with the temperature distribution from exposure to the ISO 834 fire, as shown in Figure 2.19 [6]. The dehydration of calcium hydroxide ($Ca(OH)_2$) and calcium silicate hydrate (C-S-H) have both been directly linked to the strength loss that occurs in concrete during and after thermal exposure.

Given the importance of estimating the distribution of maximum temperatures within the concrete during the fire, some of the inspection techniques described in Chapter 4 are aimed at this purpose.

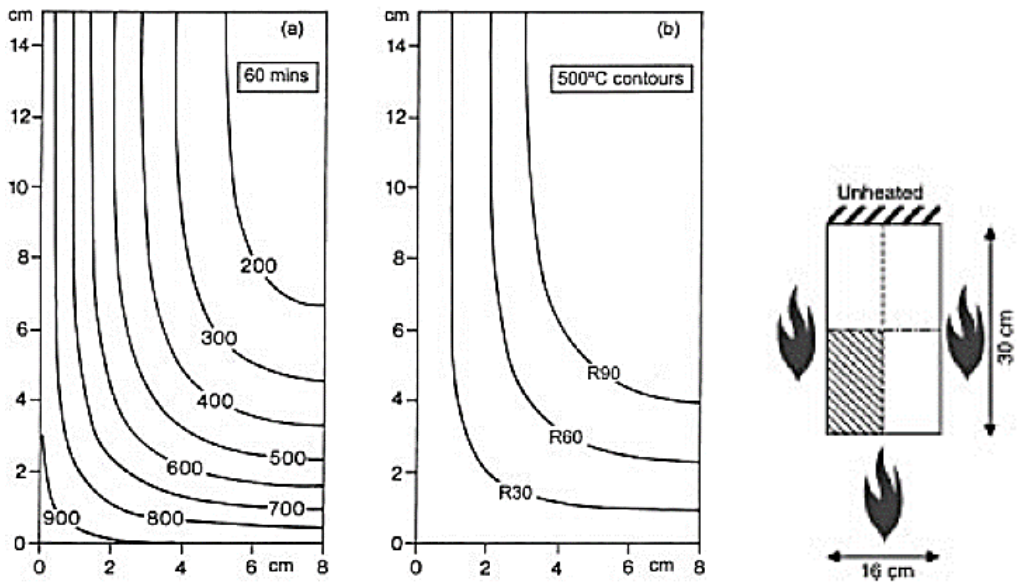

Figure 2.16: Isothermal lines (Celsius) after 60 minutes of exposure to ISO 834 design fire (L); 500°C isotherms after 30, 60, and 90 minutes of exposure to ISO 834 design fire (C); heating conditions of beam (R)

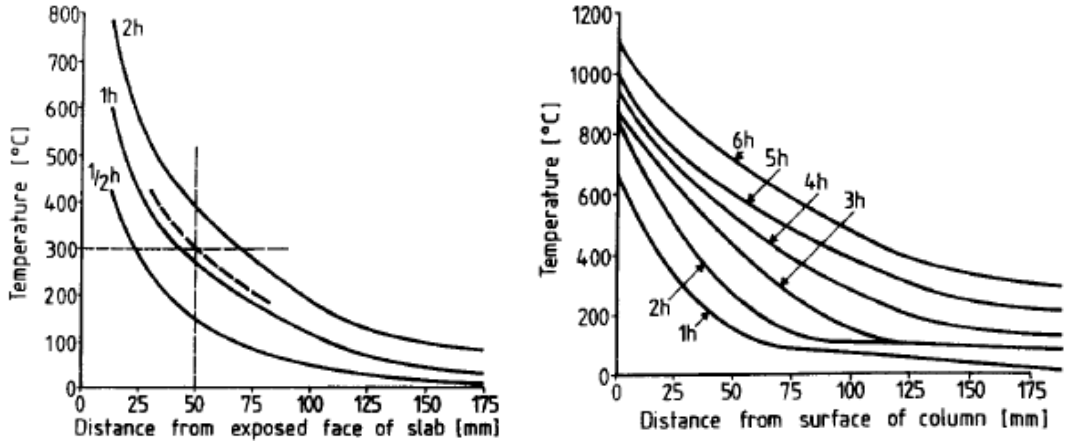

Figure 2.17: Temperature distributions in slabs (L) and columns (R) exposed to unspecified design fire

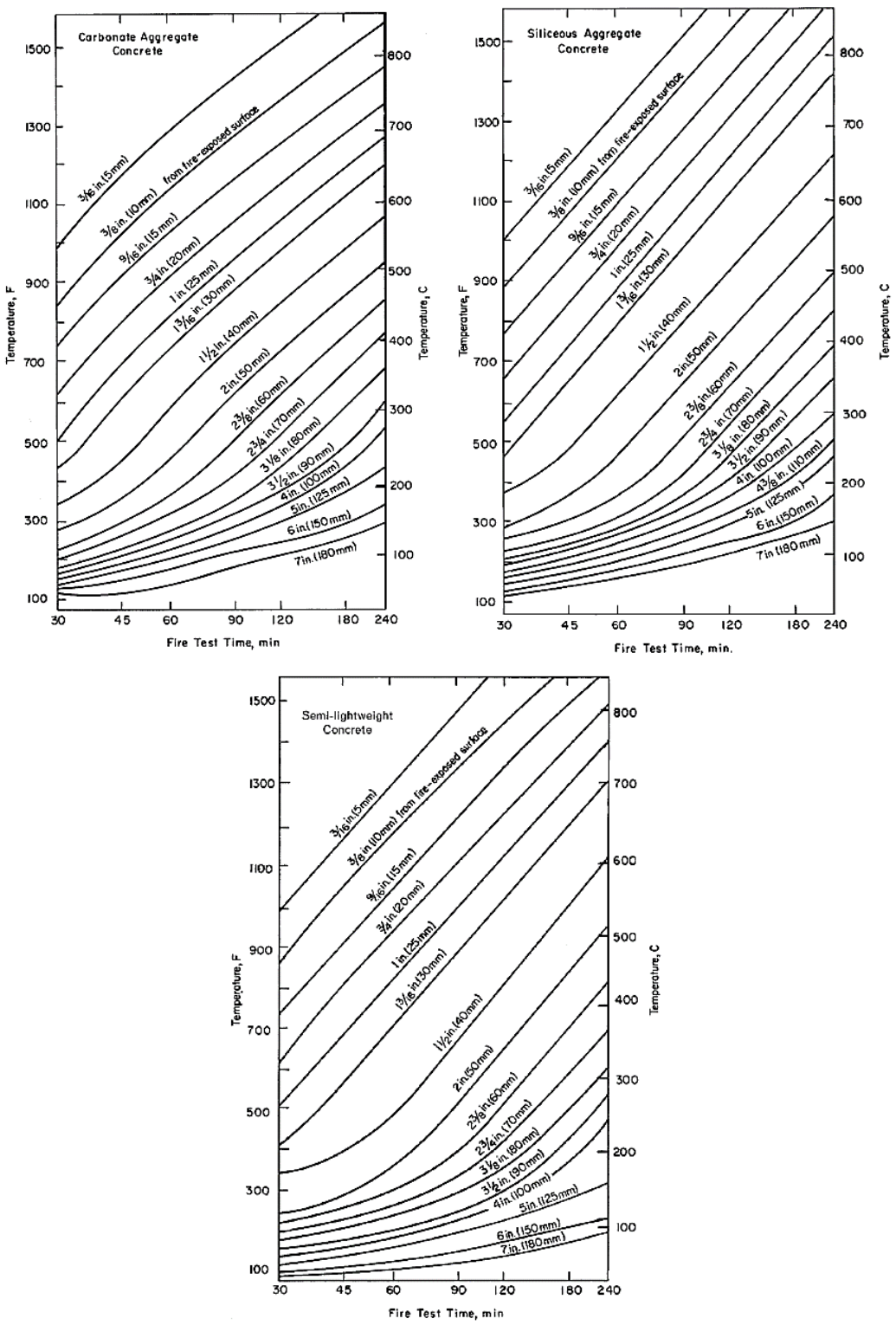

Figure 2.18: Temperature distributions within slabs during ASTM E119 fires tests: carbonate aggregate concrete (top L); siliceous aggregate concrete (top R); semi-lightweight aggregate concrete (bottom)

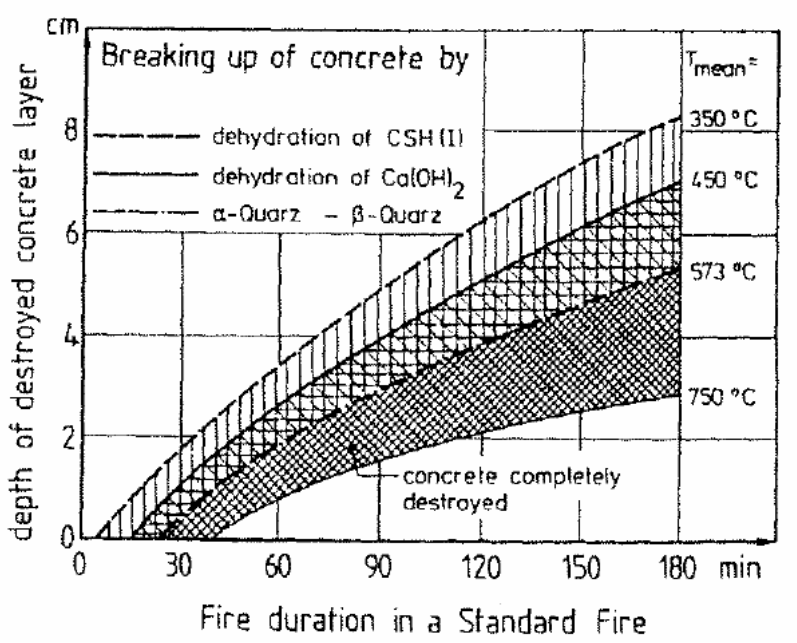

Figure 2.19: Damage and temperature depth in concrete exposed to ISO 834 fire

2.1.6. Summary of Effects of Heat on Concrete

The key points from the previous sections on concrete can be summarized as follows:

Physical and chemical transformation in concrete due to thermal exposure

- Several physical and chemical transformations occur in concrete during heating and cooling that can contribute to spalling and the decay in mechanical properties of concrete at elevated temperatures and after cooling down.

Strength and stiffness of concrete

- The strength and stiffness of concrete at elevated temperatures and after cooling down mainly depend on the maximum temperature of the concrete.
- The residual strength of concrete is generally lower than the strength of the concrete at elevated temperatures, due to damaging processes that occur during cooling.
- Aggregate type has a significant impact on the strength and stiffness of concrete at elevated temperatures and after cooling down. Siliceous aggregates are particularly affected by thermal exposure.
- The residual strength of concrete begins to decrease after reaching temperatures of 200°–300°C. After reaching 500°C, the residual strength can be 40%–60% of its original value. After reaching 800°C, the residual strength can be 10%–20% of its original value.

Concrete spalling

- Thermal spalling can affect the residual strength of members by reducing cross-sectional area and exposing rebar.
- Thermal spalling exposes the spalled surface to the heat source.
- Of the four main types of spalling, explosive spalling is most severe.

- Explosive spalling is likely caused by a combination of pore pressure buildup in the concrete material and restrained thermal dilation in the member.

Temperature distributions in concrete exposed to fire

- Due to its thermal insulating properties, concrete exposed to fire will generally only reach temperatures that affect strength and stiffness on its surface layers, while the interior layers will remain relatively unaffected.

2.2 Steel

Steel is another ubiquitous tunnel construction material that can be affected by heat exposure. Numerous studies have analyzed the mechanical properties of steel, both at elevated temperatures and after exposure to elevated temperatures, and many structural codes provide equations to describe the strength and stiffness of steel in these scenarios. Though steel is often referred to as a monolithic entity, in fact many different types of steel are used for structural purposes, each with unique mechanical properties. When discussing the effect of thermal exposure on the mechanical properties of steel, four main categories of steel are usually distinguished: hot rolled structural steel (W-shapes, angles, etc.); reinforcing steel; heat-treated/cold-worked or work-hardened steel; and prestressing steel.

Though a detailed review of metallurgical concepts is beyond the scope of this report, the changes in the mechanical properties of steel exposed to heat can generally be attributed to changes in microstructure or sometimes the chemical composition in the steel [5,32]. Furthermore, the manufacturing method for different types of steel can have a pronounced effect on both the behavior at elevated temperatures and the residual behavior. For example, reinforcing steel typically undergoes a greater degree of deformation than structural steel during the hot rolling process. As a result, the effect of heat on the stress-strain curves for each type is different [5]. Moreover, heat-treated/cold-worked steels and prestressing steels generally lose strength faster with temperature than structural or reinforcing steels as high temperatures can damage the microstructural arrangements that the heat treating and cold working processes create.

This section focuses on the residual mechanical properties of these four types of steels, but the mechanical properties at elevated temperatures are also discussed for comparison. The specific mechanical properties discussed are yield strength, ultimate strength, and stiffness.

2.2.1. Structural Steel

As mentioned previously, of the four main types of steel used in structures, hot rolled structural steel is generally least susceptible to the effects of thermal exposure, both at elevated temperatures and after cooling. First, the properties of hot rolled structural steel at elevated temperatures are discussed.

EN 1993 1-2 provides equations and curves describing the stress-strain behavior of several European grade hot-rolled structural steels at elevated temperatures. *EN 1993 1-2* gives reduction factors to be applied to the yield stress and elastic modulus of hot-rolled structural

steel at room temperature, which give the yield stress and elastic modulus of structural carbon steel at elevated temperatures up to 1200°C. The reduction factors are shown in plotted form in Figure 2.20.

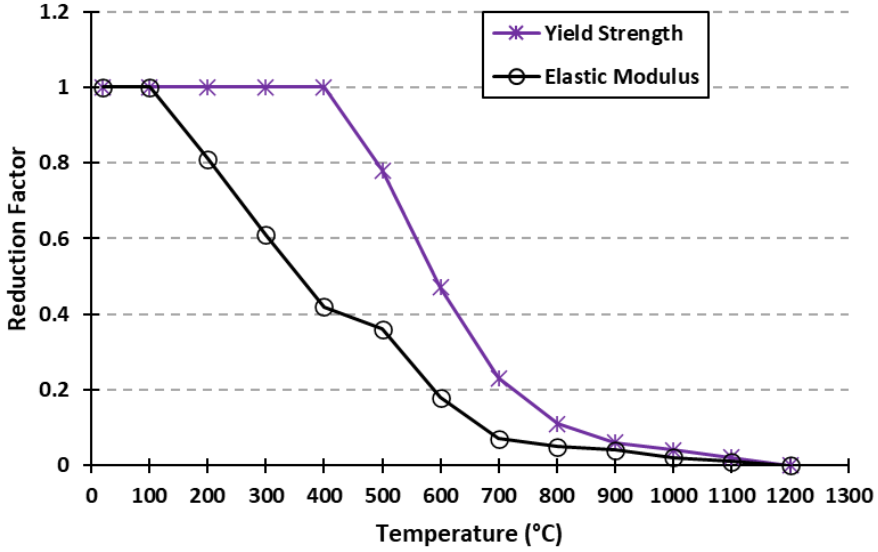

Figure 2.20: Reduction factors for yield stress and elastic modulus of hot-rolled structural steel at elevated temperatures

A 2004 study performed stressed tests, in which the specimen was subjected to loading during heating, on a European structural steel (S350GD + Z) [33]. The reduction factors for yield strength determined from these tests, along with those from *EN 1993 1-2*, are shown in Figure 2.21.

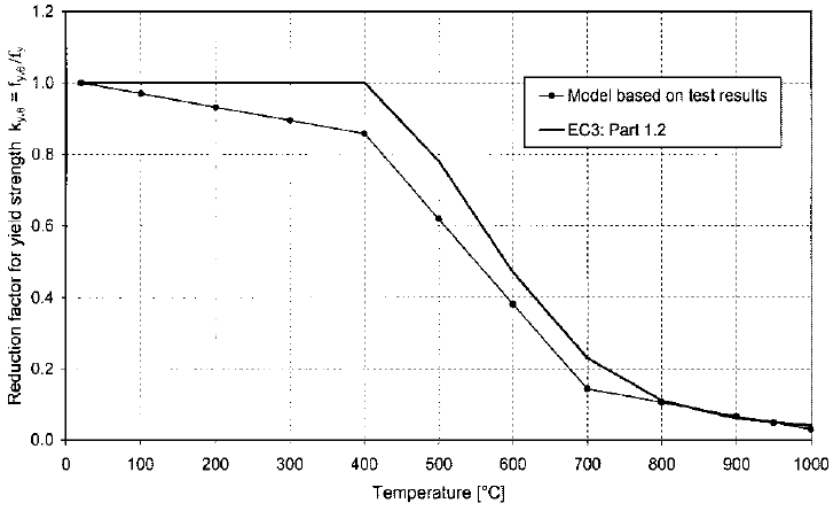

Figure note: S350 GD + Z steel based on the experimental results (lines with dots); hot-rolled structural steel from *EN 1993 1-2* (solid line).

Figure 2.21: Reduction factors for yield strength of S350 GD + Z steel based on experimental results; reduction factors for yield strength of hot-rolled structural steel from *EN 1993 1-2*

The experimental results suggest the reduction factors for *EN 1993 1-2* are unconservative for all temperatures up to 800°C. Further studies with other types of steel would be helpful to clarify the reliability of the models for structural steel at elevated temperatures in *EN 1993 1-2*.

The residual properties of hot-rolled structural steel are discussed as follows. A 2013 study [5] performed a meta-analysis of the test results across eight studies on the residual properties of structural steel (stress-strain curves, yield strength, ultimate strength, and modulus of elasticity), though it should be noted that only one of these studies used ASTM steels, which are standard in the United States. Furthermore, the majority of the tests were unstressed residual tests, though the researcher noted that the difference between results from stressed residual tests and unstressed residual tests was minor. The yield strength of steels in the eight studies ranged from 231 to 789 MPa, and most of the test specimens were coupons that were heated and then cooled by air. Figure 2.22 shows the relative residual yield strength and the relative residual ultimate strength as a function of maximum temperature from the results of the studies, with the individual data points plotted as circles and with best-fit curves (Eq. (3) and Eq. (4)) for each plot [5].

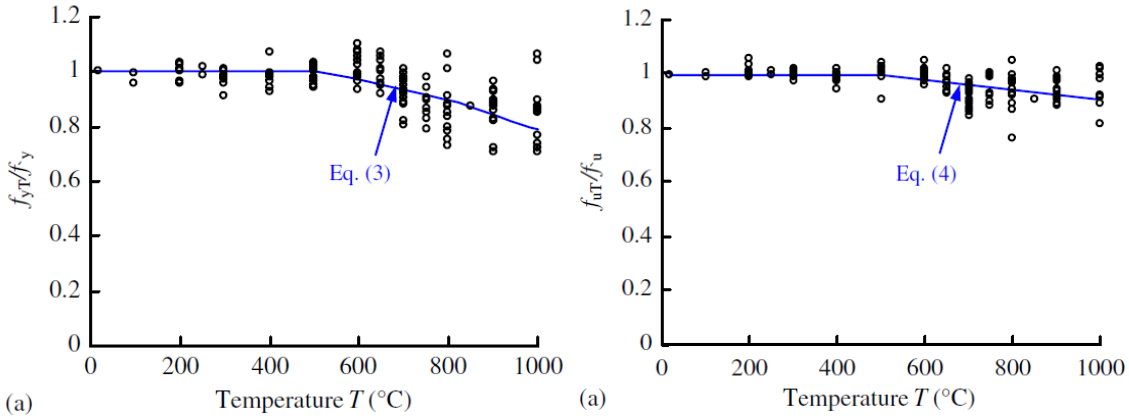

Figure 2.22: Relative residual yield strength of hot-rolled structural steel (L); relative residual ultimate strength of hot-rolled structural steel (R)

The residual ultimate strength of hot-rolled structural steel is less affected by heat than the yield strength, with only about 10% reduction after exposure to 1000°C, in comparison to about 25% reduction in yield strength after exposure to 1000°C. Comparing the residual yield strength to the yield strength at elevated temperature stipulated by *EN 1993 1-2* (Figure 2.20), it can be seen that hot-rolled structural steel regains much of the strength loss that occurs at elevated temperatures after it has cooled. For instance, *EN 1993 1-2* states a 95% reduction in the yield strength of hot-rolled structural steel at 1000°C, whereas the data from the studies in [5] show only 25% reduction in yield strength after the steel has cooled from 1000°C.

The meta-analysis included very limited data on the residual modulus of elasticity of hot-rolled structural steel, but the available data showed a maximum reduction of 10% for hot-rolled structural steel for temperatures up to 1000°C.

Since the 2013 meta-analysis mostly included studies of steels less common in the United States, it is worth taking a closer look at the study that performed tests on *ASTM A992* steel, the most commonly used steel grade for wide flanged w-shapes in the United States [34]. The study evaluated the effect of different cooling methods on the residual stress-strain properties of the coupons. After heating coupons in a furnace, three different cooling methods were employed: cooled in blanket (CIB); cooled in air (CIA); and cooled in water (CIW).

The residual stress-strain curves for the specimens heated to 200°C, 500°C, 700°C, and 1000°C and cooled by the three different methods are shown in Figure 2.23 and Figure 2.24 [34]. Overall, the cooled in blanket and cooled in air specimens exhibited similar stress-strain behavior and strength reductions, with permanent residual yield and ultimate strength losses beginning at a temperature of 700°C. For both of these cooling methods, temperature had a greater effect on the yield strength than the ultimate strength. The cooled in water method, on the other hand, gave noticeably different results at higher temperatures. In addition to the different stress-strain behavior, which can be most clearly seen in Figure 2.24, increasing temperature generally increased the strength of the steel rather than decreasing it, as was observed for the other two cooling methods. The difference in behavior has been attributed to increased hardness due to the formation of bainite and martensite, which can occur at very high cooling rates such as the cooled in water method [5].

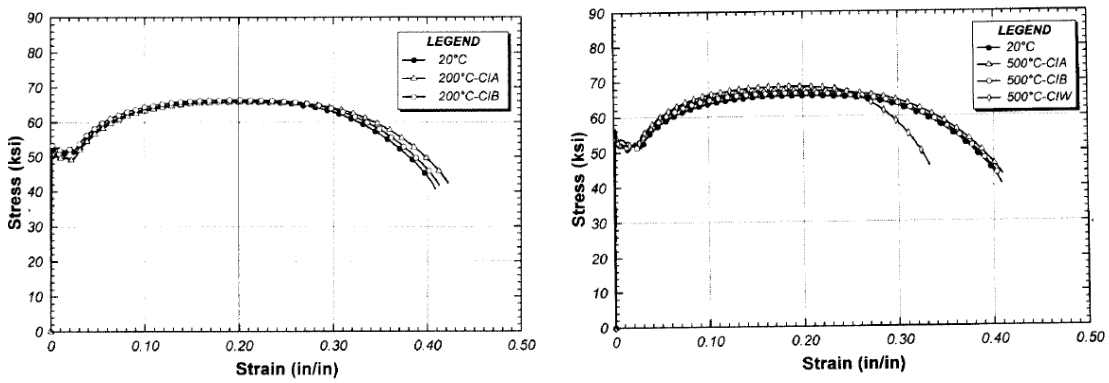

Figure 2.23: Residual stress-strain curves for A992 steel after heating to: 200°C (L), 500°C (R), and cooling by each method

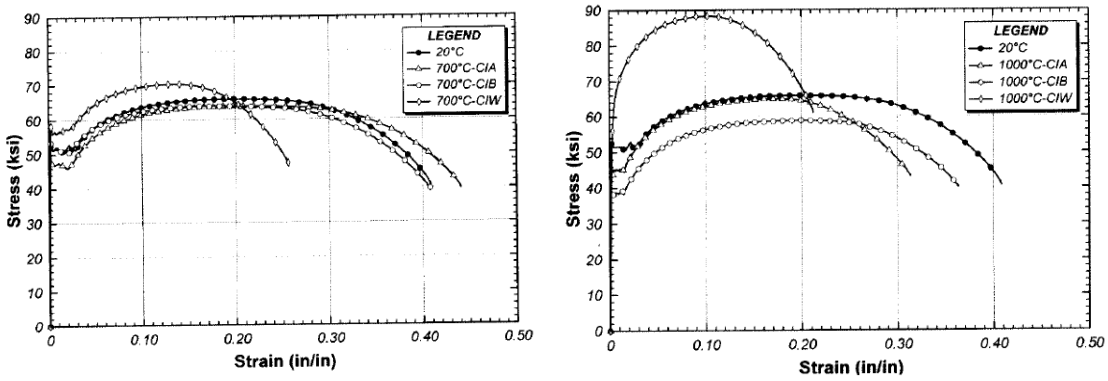

Figure 2.24: Residual stress-strain curves for A992 steel after heating to: 700°C (L), 1000°C (R), and cooling by each method

For comparing the changes in yield strength and ultimate strength for the different maximum temperatures and cooling method, Figure 2.25 shows the yield strength reduction factor and the ultimate strength reduction for the three cooling methods [34].

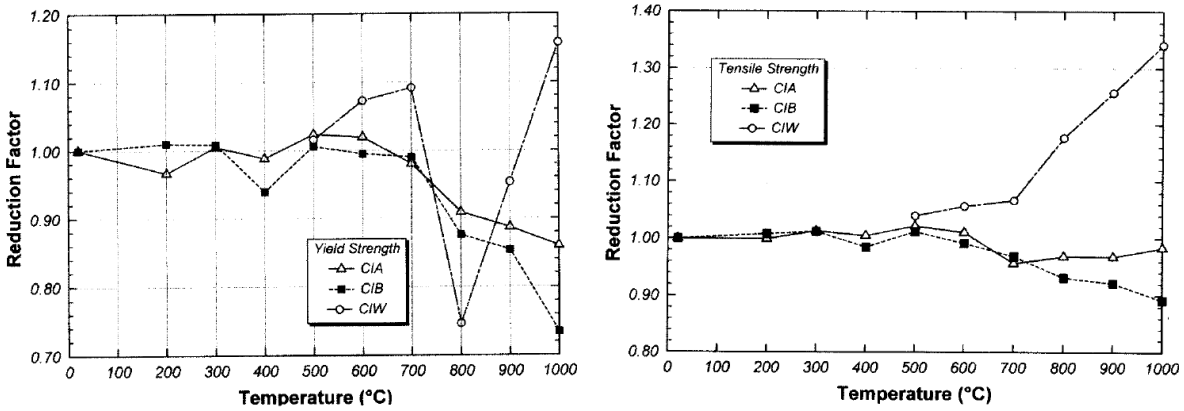

Figure 2.25: Reduction factors for yield strength of A992 steel based on maximum temperature (L); reduction factors for ultimate strength of A992 steel based on maximum temperature (R)

Lastly, the study also included data on the residual elastic modulus for each cooling method. The reduction factors for the elastic modulus for each cooling method are shown in Figure 2.26 [34]. In general, temperature exposure up to 1000°C has only a very minor effect (about +/-7%) on the elastic modulus of A992 steel.

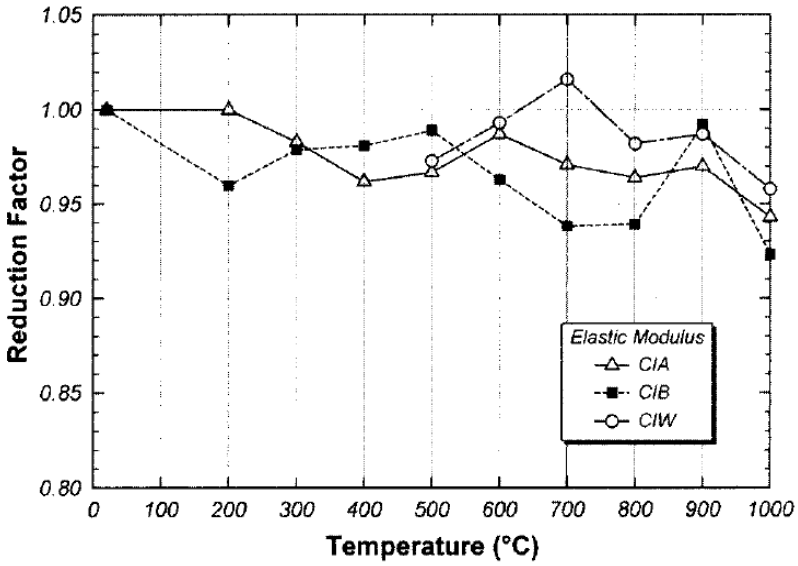

Figure 2.26: Reduction factor for elastic modulus of A992 steel for each cooling method

2.2.2. Reinforcing Steel

Given its widespread use in concrete structures, numerous studies have been conducted on the mechanical properties of reinforcing steel at elevated temperatures and after cooling down. First, the properties of reinforcing steel at elevated temperatures are discussed. Equations/curves for reinforcing steel at elevated temperatures can be found in *EN 1992 1-2* and *ACI 216.1-14*. For example, similar to the provisions for hot-rolled structural steel, *EN 1992 1-2* provides reduction factors to be applied to the yield stress and modulus of elasticity of reinforcing steel at ambient temperatures, which give the yield stress and modulus of elasticity of reinforcing steel at elevated temperatures up to 1200°C. The reduction factors given for Class N hot-rolled reinforcing steel are shown in Figure 2.27, and the code also provides equations for cold-worked reinforcing steels. *ACI 216.1-14* also contains provisions for the strength of reinforcing steel at elevated temperatures, shown in Figure 2.28 [20]. This graph also includes data for prestressing steel, which is discussed in Section 2.2.4.

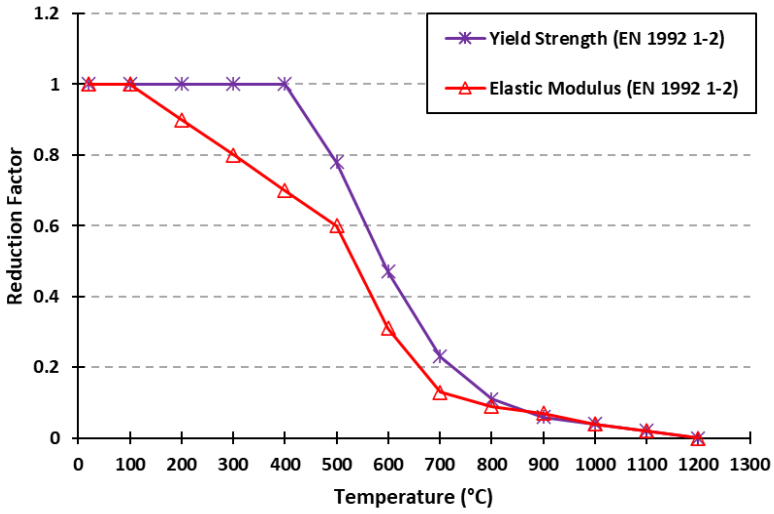

Figure 2.27: Reduction factors for yield stress and elastic modulus of Class N hot-rolled reinforcing steel at elevated temperatures per *EN 1992 1-2*

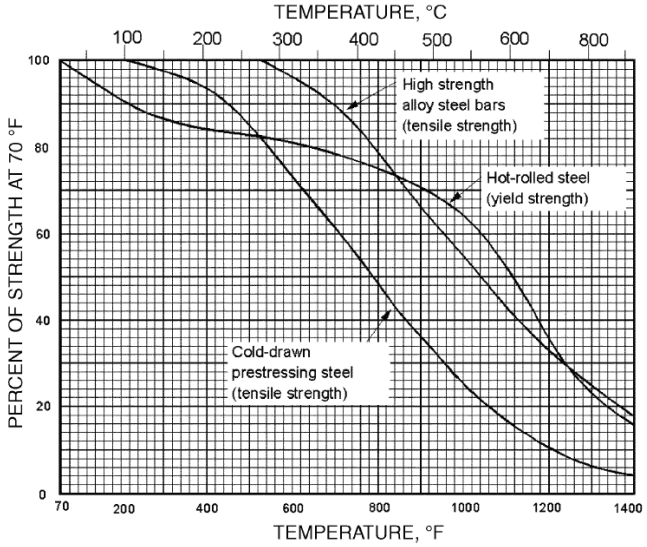

Figure 2.28: Strengths of different types of reinforcing steel at elevated temperatures per *ACI 216.1-14*

The *EN 1992 1-2* and *ACI 216.1-14* provisions for yield strength of hot-rolled reinforcing steel vary quite significantly in the range of 20°–400°C, as *EN 1992 1-2* does not show any loss of strength, whereas *ACI 216.1-14* shows a strength reduction of 14%. Beyond 400°C, the *EN 1992 1-* provisions are generally more conservative than the ACI provisions. *ACI 216.1-14* also provides a strength curve for high strength alloy steel bars.

In addition to the studies on the properties of reinforcing steel at elevated temperatures, several studies on the residual properties of reinforcing steel have been conducted [36,37,38]. The 2013 study presented in the previous section [5] also conducted a meta-analysis of studies on the residual mechanical properties of reinforcing steel, comprising test results from 18 studies. These tests were typically conducted on reinforcing bar specimens that were

heated, cooled, and tested to failure. Only data for hot-rolled reinforcing steel was included for this part of the analysis. Figure 2.29 shows the relative residual yield strength and the relative residual ultimate strength as a function of maximum temperature from the results of the studies, with the individual data points plotted as circles and with best-fit curves (Eq. (5) and Eq. (6)) for each plot [5]. The data for structural steel, which are also shown in Figure 2.22, are shown alongside the data for reinforcing steel for comparison.

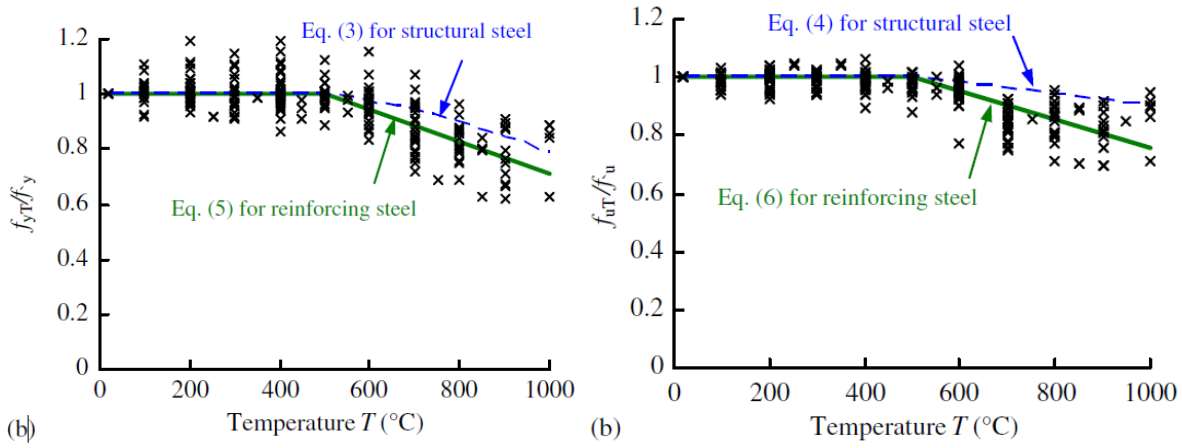

Figure 2.29: Relative residual yield strength of hot-rolled reinforcing steel (L); relative residual ultimate strength of hot-rolled reinforcing steel (R)

Overall, the residual capacity of reinforcing steel is more affected by thermal exposure than hot-rolled structural steel, which is due to the higher degree of deformation experienced by reinforcing steel than structural steel during the hot-rolling process [5]. Furthermore, as with structural steel, reinforcing steel appears to gain back much of the strength loss that occurs at elevated temperatures after it is cooled. For example, at 700°C (before cooling), the Eurocode provisions predict the steel would have 23% of its original yield strength, and *ACI 216.1-14* predicts the steel would have 34% of its original yield strength. The data from the meta-analysis indicates that the residual yield strength after cooling from 700°C would be about 90% of its original yield strength, meaning that steel regains nearly all of its strength after cooling.

Noting that the data from the meta-analysis contained data of steels from wide variety of countries, one study focused more specifically on the differences in residual properties of reinforcing bars more common in the United States (carbon steel bars) and reinforcing bars more common in Europe (quenched and self-tempered steel bars (QST)) [39]. Quenched and tempered steel is a type of heat-treated steel and therefore will be discussed in the next chapter rather than here. Figure 2.30 and Figure 2.31 shows stress-strain curves from the study for deformed carbon steel bars and smooth carbon steel bars, respectively, after heating and cooling [39]. Both types of bars experienced little change in the residual yield and ultimate strength after cooling from 550°C, which agrees with the data from the 2013 meta-analysis of reinforcing steels. After cooling from 850°C, the deformed and smooth bars experience a 20%–25% loss in residual yield strength and a 15% loss in ultimate strength.

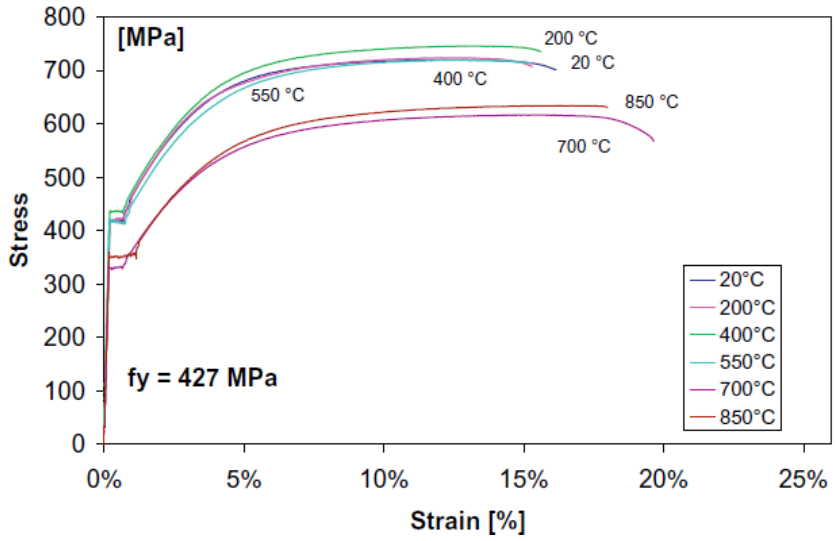

Figure 2.30: Stress-strain curves for φ29 mm deformed carbon steel reinforcing bars after heating and cooling

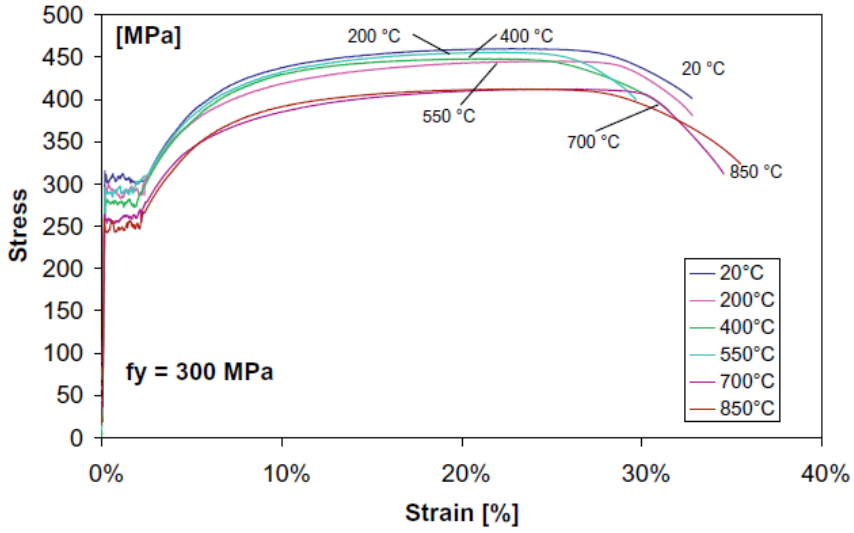

Figure 2.31: Stress-strain curves for φ24 mm smooth carbon steel reinforcing bars after heating and cooling

2.2.3. Cold-Worked and Heat-Treated Steel

It has been noted that cold-working and heat-treating processes can result in significantly different behavior at elevated temperatures and after cooling down, compared to hot-rolled steels [5].

First, the properties of cold-worked reinforcing steel at elevated temperatures are discussed. Equations/curves for cold-worked reinforcing steel at elevated temperatures can be found in *EN 1992 1-2*. Figure 2.32 shows a comparison of the reduction factors for the yield strength and elastic modulus for both hot-rolled and cold-worked reinforcing steel. Notably, the

reduction factors for both yield strength and elastic modulus are lower for cold-worked steel than for hot-rolled steel, suggesting that the former has worse mechanical properties during a fire.

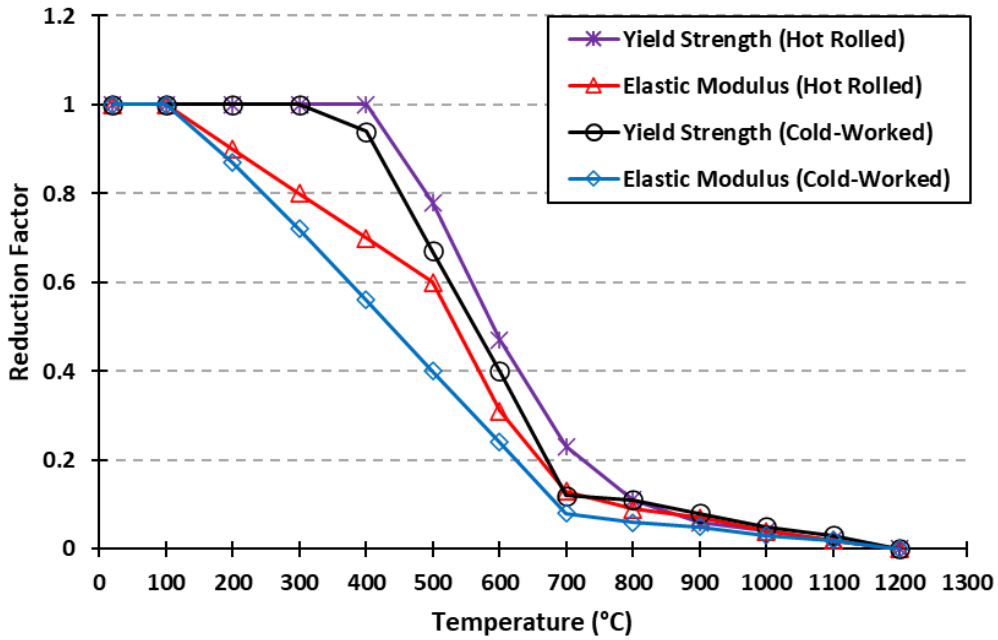

Figure 2.32: Comparison of yield strength and elastic modulus reduction factors for hot-rolled and cold-worked reinforcing steel per *EN 1992 1-2*

The residual properties of cold-worked and heat-treated steel are discussed below. The 2013 study presented in the previous two sections also conducted a meta-analysis of studies on the residual mechanical properties of heat-treated and cold-worked steel [5]. The meta-analysis grouped these two types of steel together, as they exhibited very similar residual behavior. Figure 2.33 shows the relative residual yield strength, the relative residual ultimate strength, and the relative residual elastic modulus of heat-treated and cold-worked steels from the collection of studies [5].

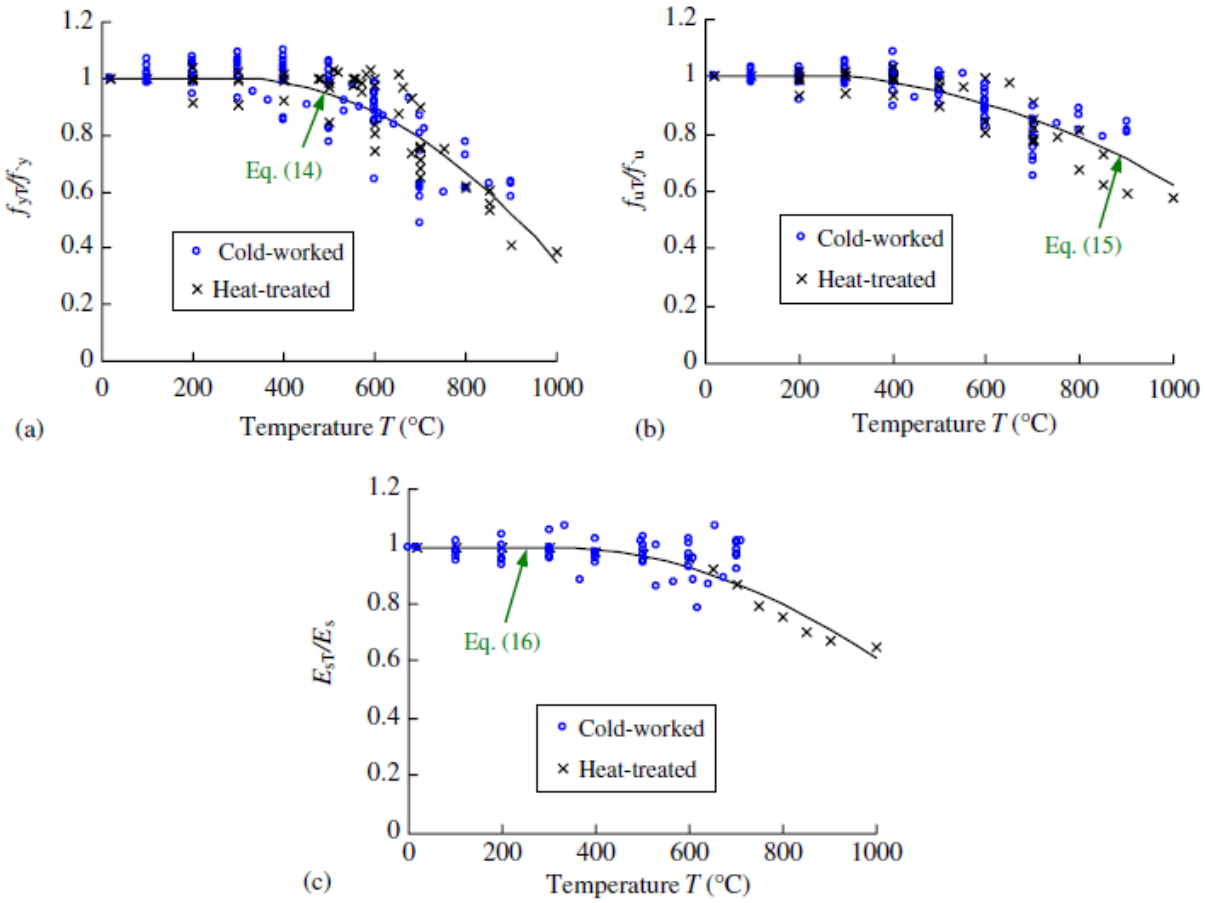

Figure 2.33: Relative residual yield strength of heat-treated/cold-worked steel (a); relative residual ultimate strength of heat-treated/cold-worked steel (b); relative residual elastic modulus of heat-treated/cold-worked steel (c)

Compared to the data for hot-rolled structural and reinforcing steel in Figure 2.29, heat-treated/cold-worked steel has markedly lower strength and ductility above 300°–400°C, where the residual properties of heat-treated and cold-worked steel begin to degrade. For example, the residual yield strength after cooling from 800°C is about 30%–35% for the heat-treated/cold-worked steels, as compared to 15%–20% for the hot-rolled structural and reinforcing steels after cooling from 800°C. Comparing with the Eurocode provisions shown in Figure 2.32, it appears that heat-treated and cold-worked steel does regain some its strength capacity after cooling down, but to a lesser extent than hot-rolled steel.

2.2.4. Prestressing Steel

Similar to the other types of steel, numerous studies and code equations are available on the mechanical properties of prestressing steel at elevated temperatures [35,37,40]. The condition of prestressing steel during and after a fire is considered to more critical than that of other types of steel, as prestressing steel can experience significant strength reductions even after exposure to temperatures in the range of 200°–400°C [41]. Three main types of prestressing steel are used in concrete structures: cold-drawn wires, strands, and high-strength bars. Cold-

drawn wires are created by drawing hot-rolled steel rods through dies while they are cold, a process which increases the strength of the steel. Many cold-drawn wires are also heat-treated after the cold drawing process. Stress-relieved wires are heated for a short time, while low-relaxation wires are heated while being held in tension. Strands are produced by wrapping several individual cold-drawn wires around a central core wire, and the types of wires used for strands include stress-relieved and low-relaxation wires. Lastly, high-strength bars are created by adding alloys to the steel and by subsequent cold working processes [32].

Equations/curves for prestressing steel at elevated temperatures can be found in *EN 1992 1-2* and *ACI 216.1-14*. *EN 1992 1-2* gives strength reduction factors for the yield strength and elastic modulus of prestressing steel at elevated temperatures, shown in Figure 2.34. *EN 1992 1-2* distinguishes between cold-worked strands and quenched and tempered bars. Figure 2.28 shows the *ACI 216.1-14* curve for the yield strength of cold-drawn prestressing steel at elevated temperatures.

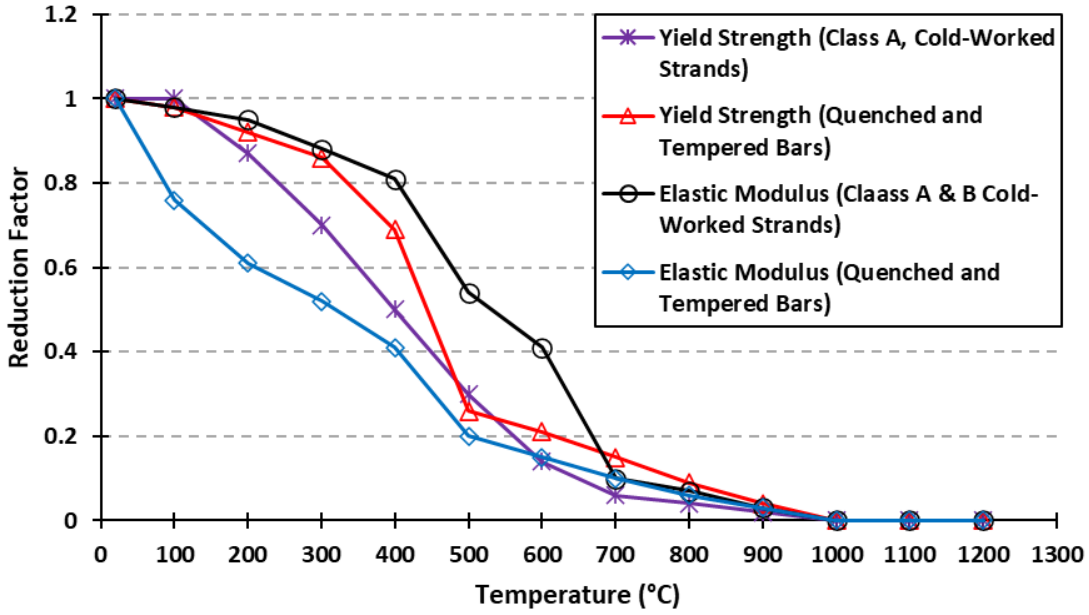

Figure 2.34: Reduction factors for yield strength and elastic modulus of different types of prestressing steel per *EN 1992 1-2*

The *EN 1992 1-2* yield strength reduction factors are generally slightly more conservative, though both sources have similar strength reduction values overall.

A 2017 study compared various models for the mechanical properties of prestressing wires at elevated temperatures, including models created based on their own data, models in Eurocode, and models proposed by other researchers [40]. Figure 2.35 shows the comparisons of various models for yield strength, ultimate strength, and elastic modulus, where the two lines in each plot labelled "prestressing wire, *x*" are the models proposed by the researchers [40]. In general, there was excellent agreement among the models from the different studies and Eurocode.

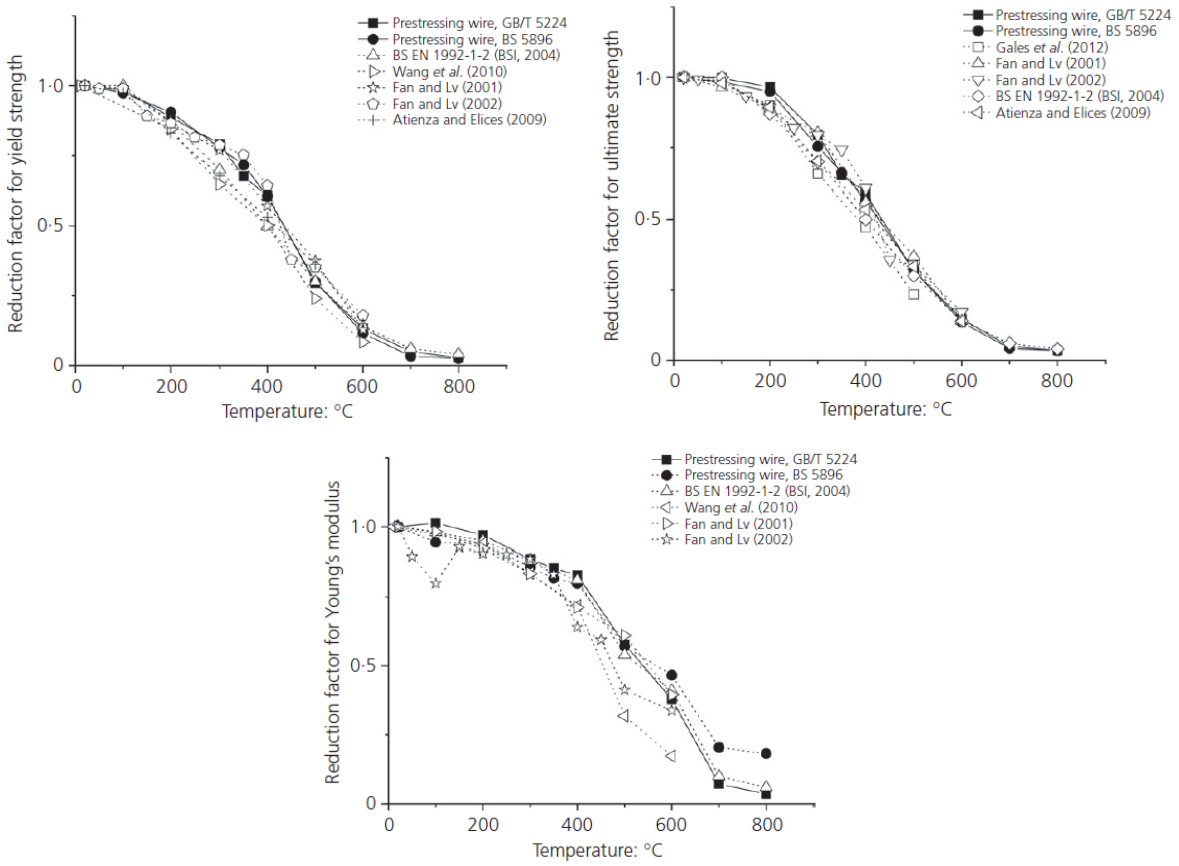

Figure 2.35: Comparison of reduction factors for yield strength of prestressing wires (top L); reduction factors for ultimate strength of prestressing wires (top R); reduction factors for elastic modulus of prestressing wires (bottom) at elevated temperatures

The properties of prestressing steel after cooling from elevated temperatures are discussed as follows. As noted previously, the post-fire condition of prestressing steel is of particular concern, as the residual strength losses for given temperatures are much greater than those for other types of steel. A 2014 study performed a meta-analysis on studies of the residual mechanical properties of prestressing steel after thermal exposure [32]. The types of steel used in the studies included a variety of as-drawn, stress-relieved, and low-relaxation strands and wires. Figure 2.36 shows the residual 0.1% proof stress of prestressing steel reported in the studies, along with the yield strengths of hot-rolled reinforcing steel and heat-treated /cold-worked reinforcing steel from the meta-analysis discussed in previous sections [5] for comparison. Proof stresses are often used as an arbitrary definition for the yield point of high-strength steel, and this particular study adopts a 0.1% proof stress definition as required by *Australian Standard AS 3600*.

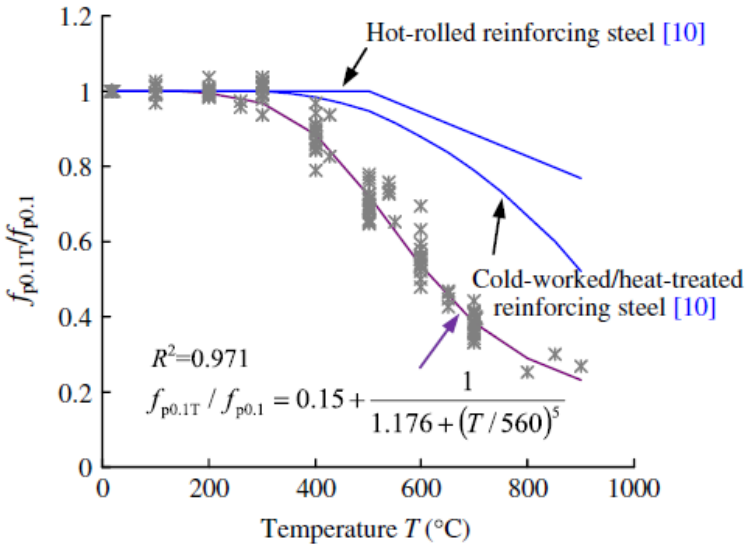

Figure 2.36: Residual 0.1% proof stress of prestressing steel and yield strengths of reinforcing and heat-treated/cold-worked steel

The residual yield strength (0.1% proof stress) is considerably lower for prestressing steel than hot-rolled or heat-treated/cold-worked reinforcing steel at any temperature above 200°C. Figure 2.37 [32] shows the residual ultimate strength of prestressing steel compared to the data for of hot-rolled reinforcing steel and heat-treated/cold-worked reinforcing steel from [5]. As with the residual yield strength, the relative residual ultimate strength of prestressing steel is far lower than that of hot-rolled reinforcing steel and heat-treated/cold-worked reinforcing steel. Comparing with the models for prestressing steel at elevated temperatures in Figure 2.35, it can be seen the prestressing steel also regains some of its strength upon cooling, as with the other types of steel, but to a lesser extent than the other types of steel.

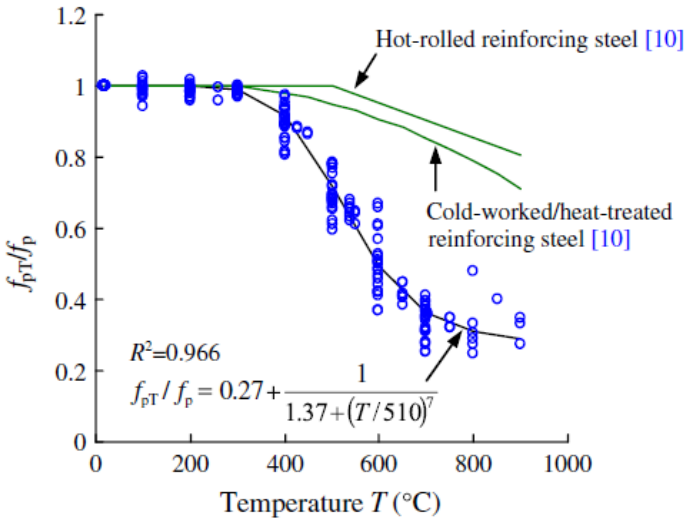

Figure 2.37: Residual ultimate strength of prestressing steel, reinforcing steel, and heat-treated/cold-worked reinforcing steel

In addition, while most of the studies included in the meta-analysis performed residual tests on specimens that were unstressed during heating, some studies did conduct residual tests in which the specimens had a working stress applied during heating, with the stress usually ranging from 40% to 70% of the ultimate strength of the steel. The effect of applying a working stress during heating was found to not have an effect on the residual strength, but several studies reported that rupture of the steel will occur above 300°C if the stress of the steel is held constant during the experiment. As a result, some researchers used strain relaxation tests in which the strain of the steel, rather than the stress, was held constant during the experiment, allowing them to perform stressed residual tests to temperatures greater than 300°C.

Another concern unique to prestressing steel is the possibility of loss of tension/prestressing force. Tension force/prestressing force in prestressing steel can be reduced by fire due to loss of elastic modulus in the concrete, relaxation due to creep, and unrecoverable extension of the steel. Not much data is available on this phenomenon, though some tests have been conducted to assess the relaxation of prestressing steel due to heat. Figure 2.38 shows the relaxation of prestressing steel over time at various temperatures up to 400°C. Increasing temperature increases the rate of relaxation, and for a given time duration will generally increase the amount of relative relaxation that occurs [10]. Each test is performed on the same type of wire, but the initial stress for each test is set to the proportional limit of the steel at that temperature.

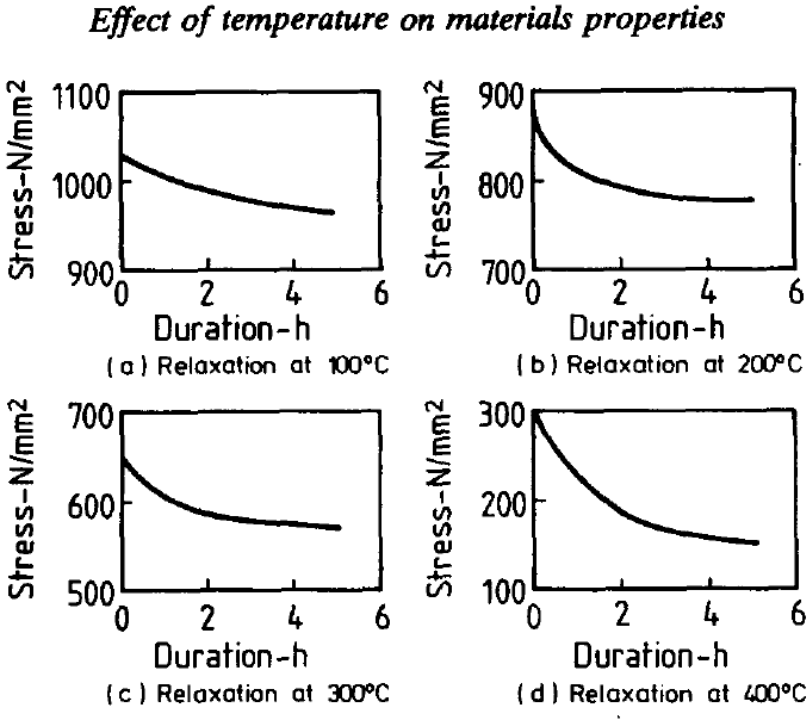

Figure 2.38: Relaxation of untreated cold-drawn prestressing wire due to thermal exposure

2.2.5. Summary of the Effects of Heat on Steel

The key findings of the previous section on steel and fire can be summarized as follows:

- All types of steel have a higher residual yield strength than yield strength at elevated temperature. In other words, steel regains much of the strength loss that occurs at high temperatures upon cooling.
- Different types of steel are affected more significantly by temperature exposure than others. For instance, after heating to 600°C and cooling, the residual yield strength of the four types of steels studied are as follows:
    - Hot-rolled structural steel: 90%–100% of original.
    - Hot-rolled reinforcing steel: 80%–100% of original.
    - Heat-treated/cold-worked steel: 70%–100% of original.
    - Prestressing steel: 40%–60% of original.
- Different types of steel are affected more significantly by temperature exposure than others. The residual yield strengths after cooling from a given temperature can be generally ordered as follows, from lowest to highest: prestressing steel, heat-treated/cold-worked steel, reinforcing steel, and structural steel.
- The condition of prestressing steel during and after a fire is the most critical of the four types of steel, as it can lose about 40%–60% of its residual strength after cooling from 600°C. Further compounding this issue is the potential loss of prestressing in the steel, which can decrease the residual capacity of the structural member even further.

2.3 Residual Bond between Concrete and Steel

In addition to deteriorating steel and concrete material alone, heat can also deteriorate the residual bond between concrete and steel in reinforced concrete and composite members [1,10]. Experimental studies have indicated that two types of bond failure can occur. Pullout failure can occur when the concrete cover is thick or the rebar is under a high degree of confinement. In this failure mode, concrete between the ribs of deformed rebar will gradually crush, eventually leading to a pullout failure. Alternatively, if the cover is thinner, splitting failure can occur due to cracks which propagate radially from the rebar [22,42]. The crushing and splitting of concrete due to interaction with rebar are depicted in Figure 2.39 [43].

To study the change in bond strength after heating and cooling, researchers typically perform either the pullout test or the beam test. For the pullout test, reinforcing steel is cast in the center, edge, or corner of cylindrical or cube-shaped concrete specimens. Specimens are then heated to a certain temperature, allowed to cool in air or water, and subsequently the force required to pull the reinforcing steel out of the concrete specimens is measured. The average bond stress can be calculated by dividing the pullout force by the surface area of the embedded portion of the bar. The pullout test for assessing bond strength should not be confused with the pull-out test method for measuring the compressive strength of concrete, which is presented in Section 4.2.2. The reason for varying the location of the rebar placement, such as the center versus the corner, is that reinforcing steel placed in the center

of a sufficiently thick specimen will typically experience bond failure during a pullout test, whereas reinforcing steel placed near an edge or corner is more likely to fail due to concrete splitting. For the beam test, rebar is cast into bottom of a concrete beam specimen, and the specimen is heated to a certain temperature and allowed to cool in air or water. Then, the specimen is subjected to a three-point bending test. The bond strength can be determined by the relative slip between the rebar and the concrete.

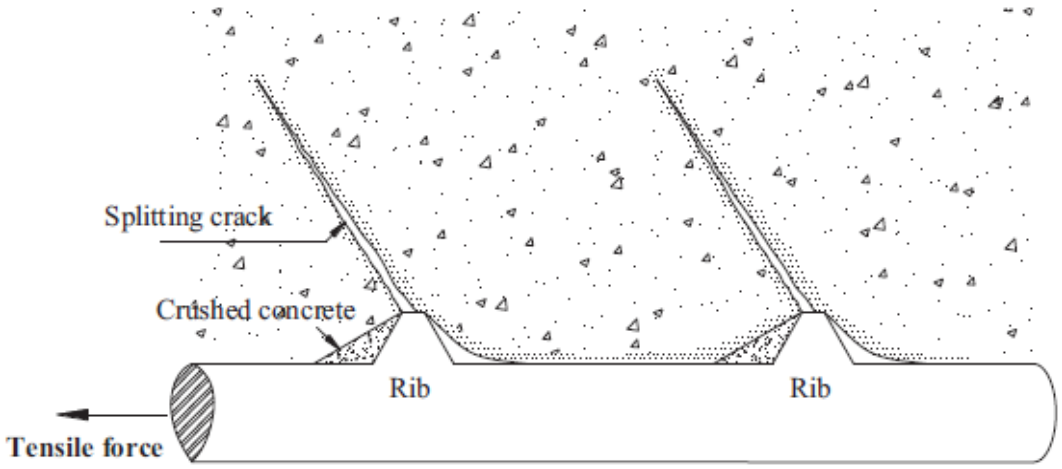

Figure 2.39: Schematic of the crushing and splitting of concrete with an embedded deformed rebar under tension

One study analyzed the effect of embedment length on residual bond strength of normal strength concretes and deformed (ribbed) rebar using the pullout test [44]. ϕ8 mm bars were cast into the center of concrete cylinders 100 mm in diameter and 200 mm in height, with embedment lengths of 6 cm, 10 cm, and 16 cm. Two different concrete strengths were used, C20 and C35 (minimum 28-day compressive strength of 20 MPa and 35 MPa, respectively). For reference, the required bond length for ϕ8 mm bars in tension per *ACI 318-19* is 37 cm for the C20 concrete, and 28 cm for the C35 concrete. The specimens were heated to various temperatures up to 700°C and held at the maximum temperature for three hours, to ensure the specimens were uniformly heated. Afterwards, they were cooled either in air or in water before the pullout tests were performed. Figure 2.40 shows the bond strength (pullout force) for the rebar cast into C20 concrete, and Figure 2.41 shows the bond strength (pullout force) for the rebar cast into C35 concrete [44].

In general, shorter bond lengths result in greater relative losses of bond strength after heat exposure. For instance, after being exposed heated to 700°C, the bond strength of rebar embedded 16 cm into the C35 concrete decreased by about 37% compared to its original bond strength, while the rebar embedded only 6 cm into the C35 concrete decreased by about 70% compared to its original bond strength. Another conclusion that can be drawn is that the bond strength increases as compressive strength of the concrete increases. The cooling method did not have a clearly discernible effect on the residual bond strengths.

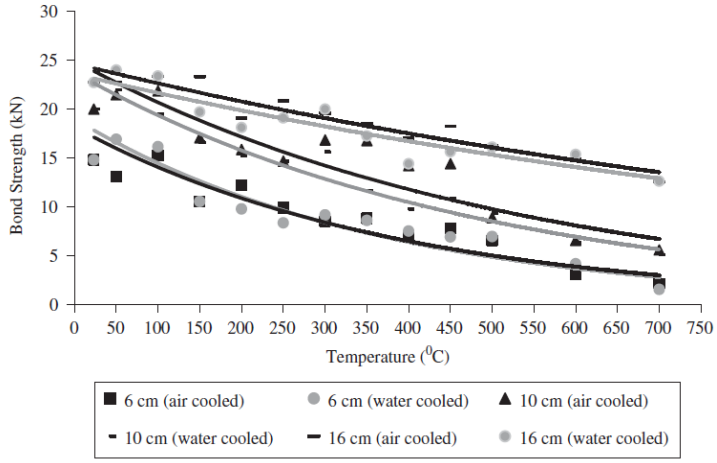

Figure 2.40: Residual bond strength of C20 (20 MPa) concrete

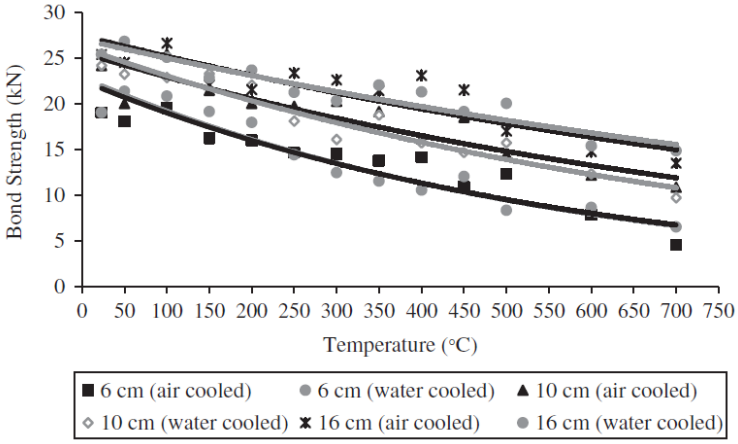

Figure 2.41: Residual bond strength of C35 (35 MPa) concrete

Another study sought to analyze the effect that position of the rebar in the concrete (i.e., center, edge, or corner) has on the residual bond strength after heating and cooling [42].

Deformed rebar was cast into the center, edge, and corner of cube-shaped concrete specimens as shown in Figure 2.42. The embedment length of each bar was the diameter of the bar multiplied by 8 (128 mm). The specimens were heated to various temperatures up to 700°C and held at the maximum temperature for 3 hours to ensure the specimens were uniformly heated. Afterwards, the specimens were cooled to room temperature in air before the pullout tests were performed. Figure 2.43 shows the average bond stress (pullout force divided by surface area of portion of bar embedded in concrete) of the rebar by the location in which it was cast into the concrete cube [42].

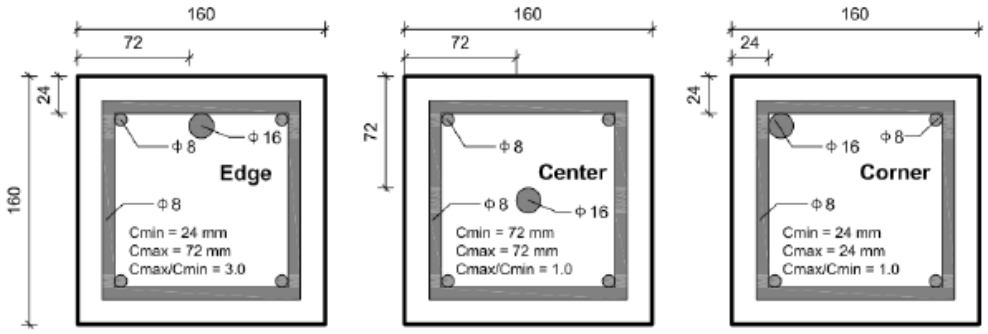

Figure 2.42: Three different locations of rebar specimen (φ16 bar) for pullout tests

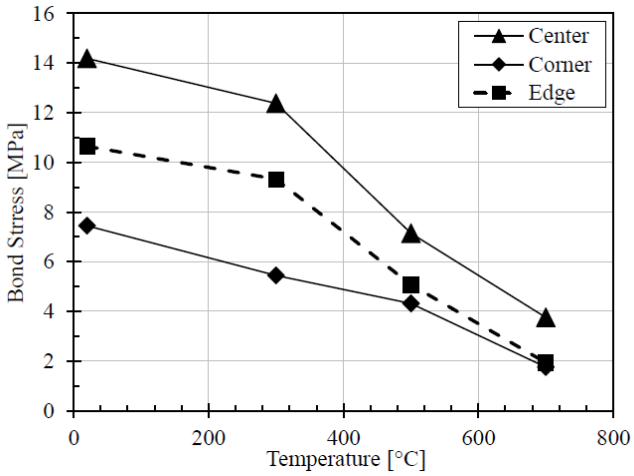

Figure 2.43: Residual bond stress for three locations of rebar

Rebar placed at the edge and corner of the cubes had a lower average bond strength overall and had slightly greater relative strength losses compared to rebar placed at the center for a given temperature, but the relative strength decreases were not vastly different among the different placement locations. Still, the reduction in residual bond strength was apparent even at 300°C, the lowest temperature tested.

Noting that many existing studies only analyzed the residual bond strength of normal-strength concrete, one study sought to analyze the residual bond behavior of high-strength concrete (80 MPa, 11,600 psi) and deformed rebar [45]. In contrast to the two studies previously shown that used pullout tests to determine residual bond strength, in this study the beam test was employed. A schematic of the beam specimen is shown in Figure 2.44 [45]. The notch in the bottom center of the beam allows the slip of the rebar to be measured at both the center (S1+ and S2+) and the end of the beam (S1 and S2).

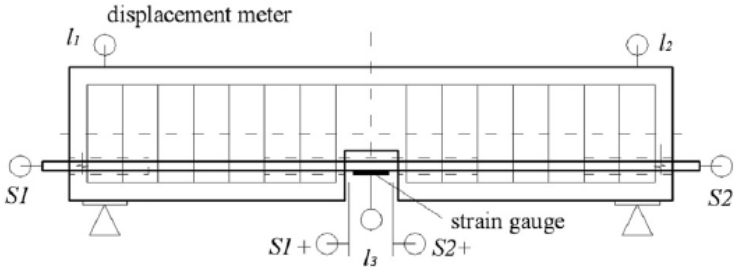

Figure 2.44: Beam test specimen for assessing residual bond strength

Beam specimens were heated to various temperatures up to 600°C and allowed to cool to room temperature in air. Afterwards, they were subjected to a three-point beam test. Figure 2.45 shows the degradation of the bond strengths as measured by the beam test and the degradation of the concrete strength measured by compression tests on separate specimens made of the same concrete mixture as the beams [45]. At and below 400°C, the compressive strength and bond strength degradation are nearly identical, but above 400°C, the bond strength decreases more than the concrete compressive strength. The results are also compared to bond strength obtained in a similar experiment previously performed by the researchers (labelled "Bond strength obtained by pullout test [9]") that used the pullout test rather than the beam test.

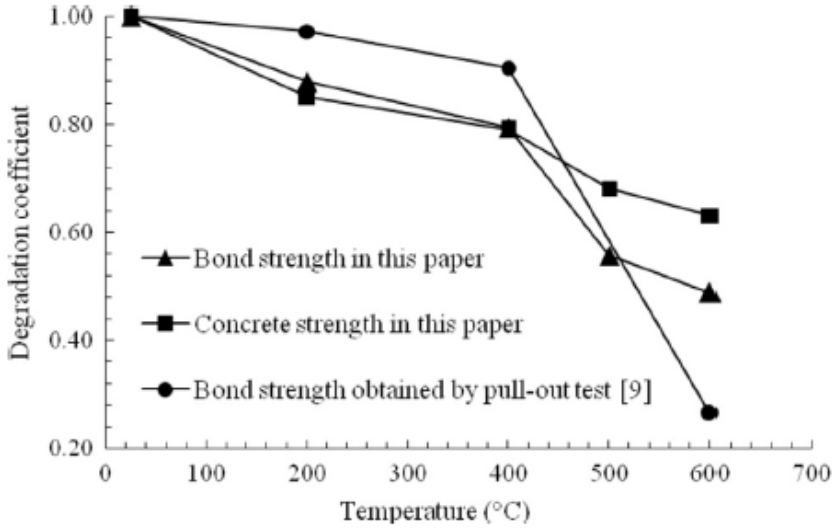

Figure 2.45: Degradation coefficients for bond strength measured by beam test, concrete compressive strength, and bond strength measured by pullout test on similar concrete

2.3.1. Summary of Effects of Heat on Residual Bond Strength between Concrete and Steel

The key findings of the previous section on steel and fire can be summarized as follows:

- The residual strength of the concrete/steel bond after heating and cooling from certain temperatures decreases to a similar or greater degree compared to the decrease in residual concrete compressive strength.
- Greater embedment length generally results in smaller decreases in residual bond strength.
- The residual bond strength is significantly affected by the thickness of the concrete cover. Rebar with a thinner cover generally has a lower residual bond strength than concrete with a thicker cover, due to transformation from a compression to a splitting failure mechanism.

This page left blank intentionally.

3.0 Effect of Fire on Structural Members

Although studies on the residual strength of concrete, steel, and the concrete/steel bond are valuable in understanding the residual behavior structural members, it is difficult to use these properties alone to fully predict the residual strength and stiffness of structural members. Therefore, many experimental studies on the residual strength and stiffness of structural members have been conducted [46–66].

Experimental tests to determine the residual strength of structural members are typically performed by exposing the member to a design fire in a furnace, either while loaded or unloaded, allowing the member to cool to room temperature, and testing the member to failure. One of the key differences between residual strength tests for concrete and steel versus structural members is that a non-uniform temperature distribution in the specimen is desired in the latter case, as this is more representative of the exposure conditions that a structural member would experience in a fire.

The following section summarizes five experimental studies on the residual strength of concrete members. Particular focus will be given to the construction/dimensions of the members, heat exposure conditions and temperature distributions within the members, and the ultimate strength reductions (if any) in the members.

3.1 Experimental Studies on Residual Strength of Structural Members

3.1.1. El-Hawary et al., 1996: Reinforced Concrete Beams in Flexure

El-Hawary et al. in 1996 conducted experimental studies on the residual strength of reinforced concrete beams after heating and cooling [46]. Four beam specimens were prepared for the study, each 200 mm in depth, 120 mm in width, and 1800 mm in length, with a concrete compressive strength of 25 MPa. Each beam was reinforced with two ϕ10 mm longitudinal bars with a minimum yield strength of 358.5 MPa, another two ϕ10 mm longitudinal bars with a minimum yield strength of 255 MPa, and ϕ8 mm stirrups with a minimum yield strength of 255 MPa spaced at 8 cm.

The four beams specimen were denoted B, B1, B2, and B3. B was not heated and was used as a control, while B1, B2, and B3 were exposed to 650°C heat for 30 minutes, 60 minutes, and 120 minutes, respectively, and were not subjected to any load during heating. The furnace used for heating and a curve showing the measured furnace air temperature over time are shown in Figure 3.1 [46]. After heating, the specimens were sprayed with water until cooled to room temperature and subjected to four-point bending tests.

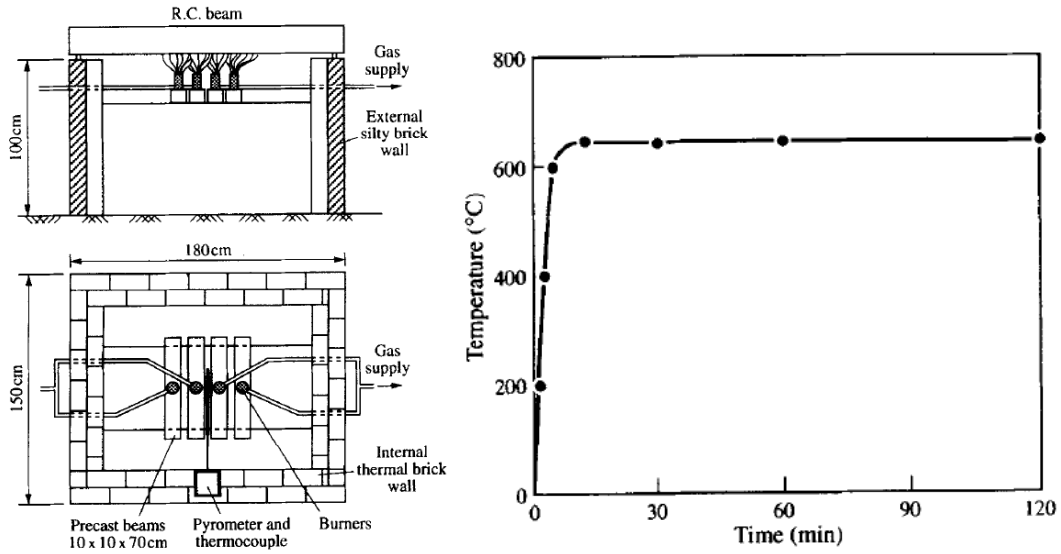

Figure 3.1: Schematic of furnace (L) and time-temperature curve of furnace (R)

The study did not report the visual condition of the beams, such as any potential spalling or exposed rebar, after heating; however, the authors did perform some non-destructive testing with a rebound hammer, a technique that is discussed in Section 4.2.1. Compared to the control beam, the beams exposed to heat experienced significant reductions in flexural strength and stiffness, and the magnitude of these reductions increased with increased exposure time. The ultimate strengths in flexure and the load-deflection plots for the beams are shown in Figure 3.2 [46]. Beams B1, B2, and B3 had 88.2%, 80.7%, and 61.3%, respectively, of the flexural strength of the control beam (B). Furthermore, the stiffness steadily decreased with increased exposure time, with B3 having a 76.3% greater midspan deflection at failure compared to the control beam.

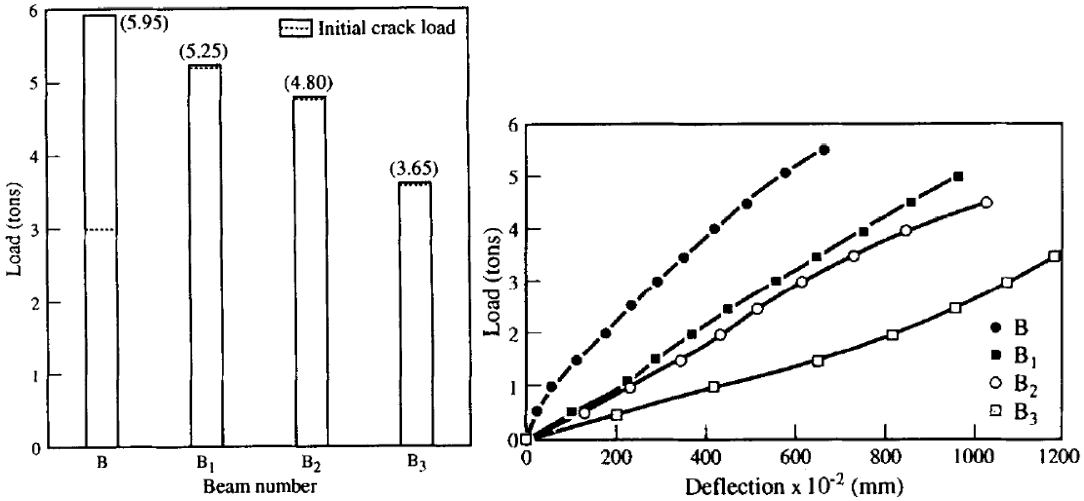

Figure 3.2: Ultimate load for each beam (L); load-deflection plots for each beam (R)

The results suggest that exposure time has a significant impact on the residual strength of reinforced concrete beams, as the three heated beams were exposed to the same temperature

(650°C) but for varying amounts of time. Moreover, as evidenced by the 11.8% strength loss in the beam heated for 30 minutes, even short heating times can reduce the residual flexural capacity of reinforced concrete beams.

3.1.2. Kodur et al., 2010: High-Strength Reinforced Concrete Beams in Flexure

Kodur et al. performed residual strength tests on reinforced concrete beams and compared the results of the tests with a simplified method for calculating the residual strength of reinforced concrete beams that the researchers developed [49]. The beams were each 406 mm deep, 254 mm wide, and 3960 mm long. One of the beams, denoted B1, was made with high-strength concrete (58.2 MPa), and the other two beams, denoted B2 and B3, were made with super-high-strength concrete (106 MPa). Each beam was reinforced with three ϕ19 mm longitudinal bottom bars, two ϕ13 mm longitudinal top bars, and ϕ6 mm shear stirrups spaced at 150 mm. The longitudinal bars had a yield strength of 420 MPa. Each beam was fitted with thermocouples at three cross-sections along the beam, as shown in Figure 3.3 [49].

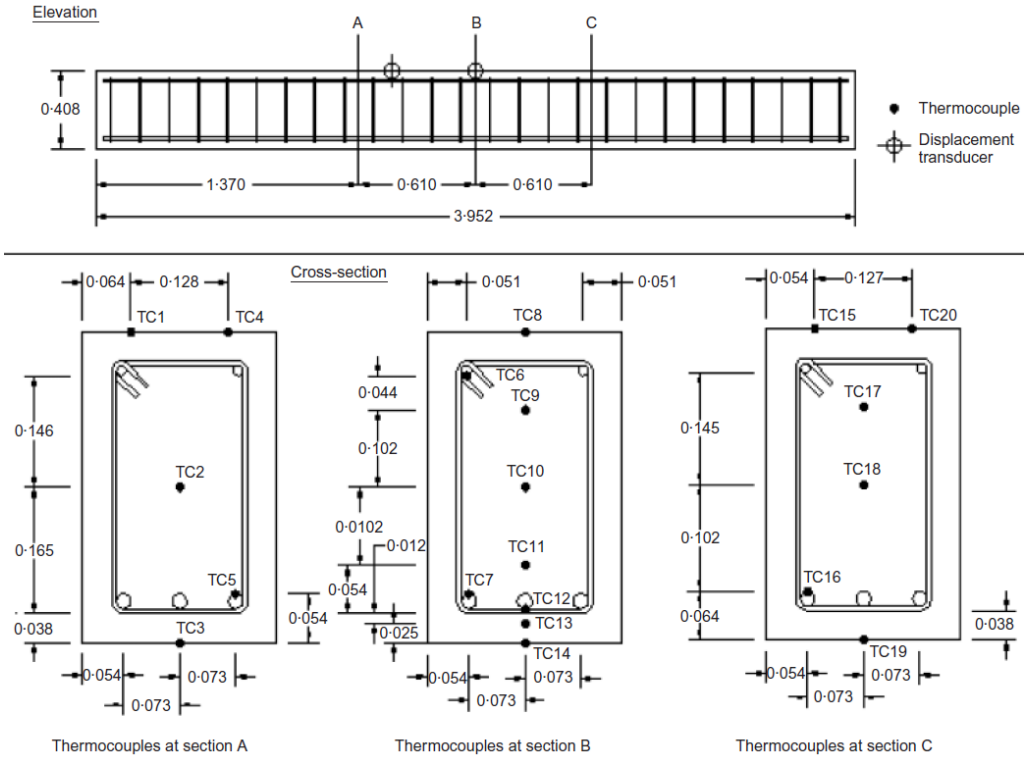

Figure note: TC = Thermocouple

Figure 3.3: Location of thermocouples in each beam

Two different time-temperature curves for the fire exposure were used: a short design fire (SF) and a long and severe design fire (LF), shown in Figure 3.4 [49]. B1 and B2 were subjected to the SF fire, while B3 was subjected to the LF fire. During the heat exposure, point loads were applied to each beam that loaded the beams to 55% of their flexural capacity, according to standard flexural equations from ACI 318.

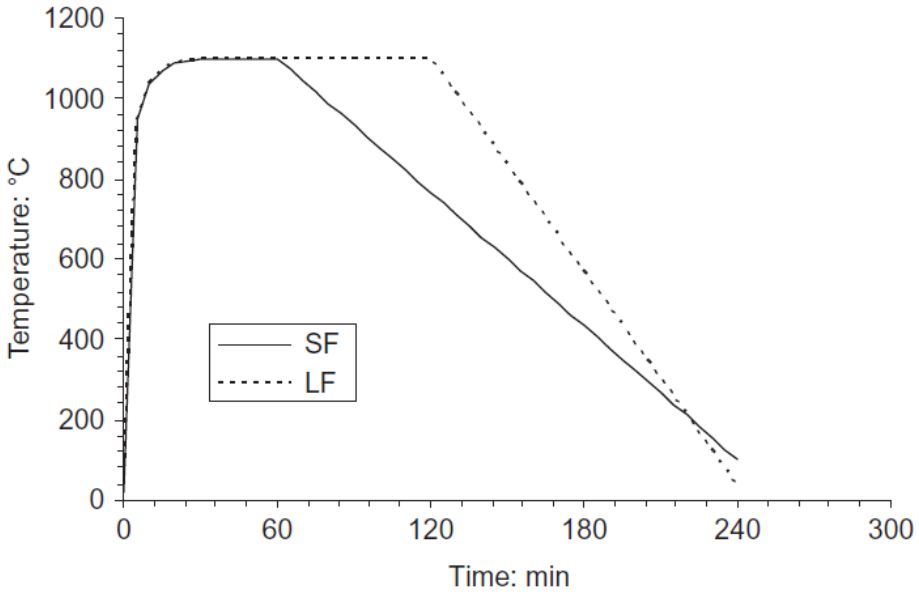

Figure 3.4: Two design fires used in experiment

The temperatures measured by the thermocouples during heating are shown in Figure 3.5, where SF is the average recorded furnace temperature during the SF fire, LF is the average recorded furnace temperature during the LF fire, and rebar B1, B2, and B3 are the recorded temperatures of the bottom rebar in each beam specimen [49]. It was noted that the temperatures of the bottom rebar would likely have the greatest impact on the residual strength of the beams, since the beams were heated from the bottom.

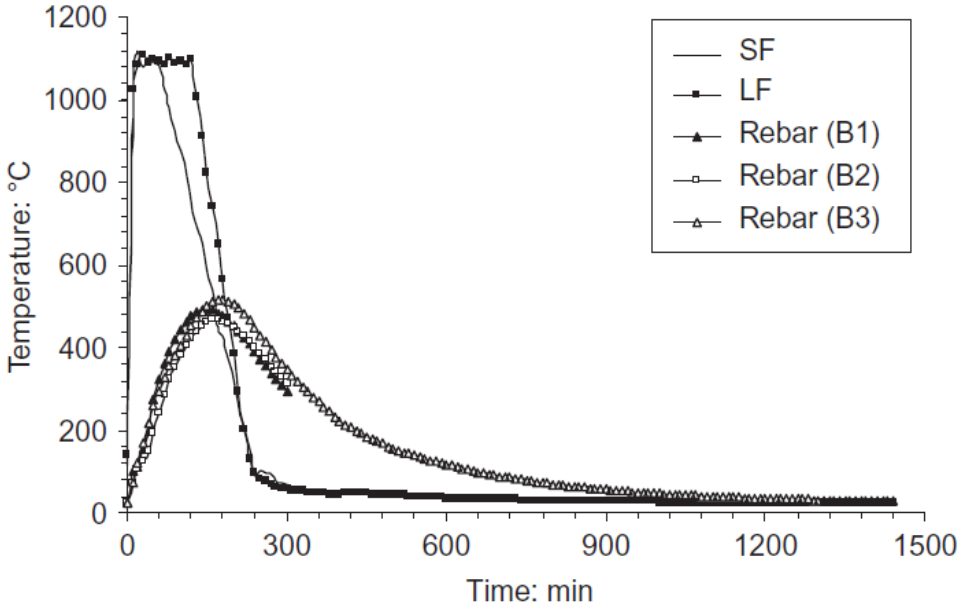

Figure 3.5: Bottom rebar temperatures during heating

After the beams had cooled, spalling was observed in B2 and B3, possibly due to the use of super-high strength concrete for these specimens. After cooling, the beams were loaded to failure, and the results of the tests are shown in Table 3.1 [49]. For the two super-high-strength concrete specimens, the beam subjected to a longer duration fire had 77% of the residual strength of the beam subjected to the shorter duration fire. Furthermore, the residual flexural capacity of all of the beams were greater than the capacity predicted by ACI 318 code equations (92.7 kN for B1, and 94.5 kN for B2 and B3).

Table 3.1: Details about beam specimens and results of load testing

Beam	Support condition*	Fire exposure	Concrete type	Maximum rebar temperature: °C	Initial deflection: mm	Measured residual load capacity: kN	Predicted residual load capacity: kN
B1	AR	SF	NSC	493	13·8	119·5	85·7
B2	SS	SF	HSC	466	28·0	129·7	87·4
B3	AR	LF	HSC	552	28·8	99·3	84·5

*AR, axially restrained; SS, simply supported

Table 3.1 also includes predictions of residual strength, using a simplified hand method developed by the researchers that is intended to allow one to estimate the residual strength of fire-damaged reinforced concrete beams without performing a finite element analysis. The method consisted of four steps:

1. Estimate the fire temperature and duration based on eyewitnesses or visual assessment of coloration in concrete.
2. Estimate the maximum temperature reached in the rebar based on a simplified empirical equation proposed by the researchers.
3. Estimate the residual strength of the rebar based on strength-temperature relationships for reinforcing steel.
4. Compute the residual capacity of the beam per ACI 318 equations for flexural strength at ambient temperatures, using the reduced strength of steel found in (3) and a reduction factor to account for the loss of concrete section.

The researchers proposed an equation for the temperature of the rebar:

$$T_{smax} = \lambda T_{fmax} \quad where, \quad \lambda = 1.45(t_h + \frac{t_c}{w})^{0.2}\left(0.4 + 0.03\frac{H}{B}\right) - 5a \qquad (4.1)$$

Where T_{smax} is the maximum rebar temperature, T_{fmax} is the maximum fire temperature, λ is a modification factor for the cross-section dimensions and fire exposure, t_h is the duration of the heating phase (in hours), t_c is the duration of the cooling phase (in hours), H is the section depth (m), B is the section width (m), and a is the axis distance (m). This empirical equation was developed based on the results of hundreds of finite element heat transfer analyses with 17 different design fires performed by the researchers. After the temperature of the rebar is estimated, the residual strength of the rebar can be estimated based on a residual strength-temperature relationship such as that used in the study, shown in Figure 3.6 (originally from Neves et al., 1996 [49]).

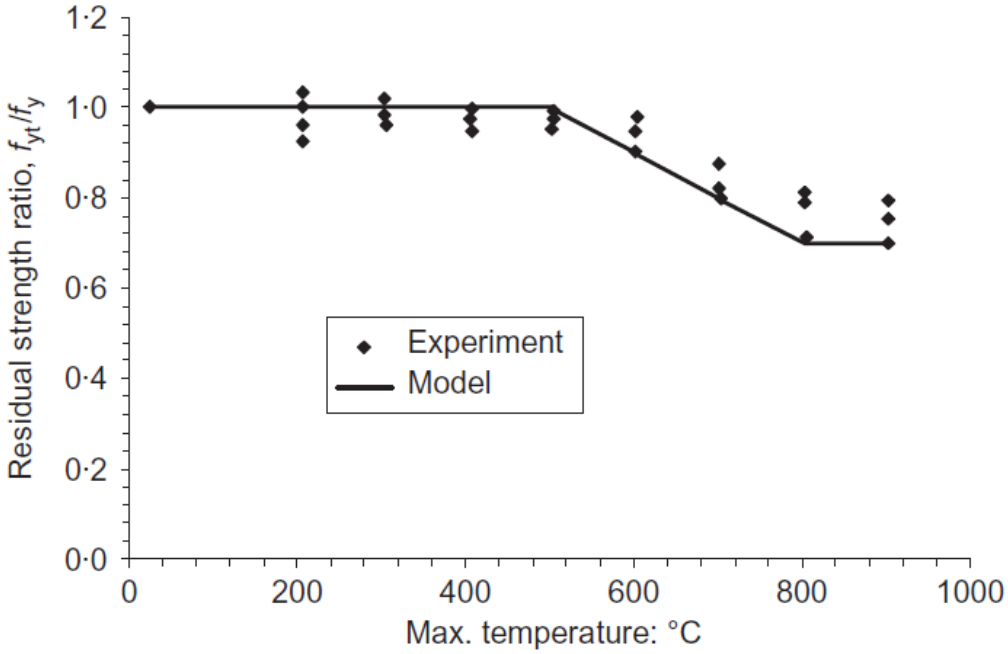

Figure 3.6: Residual strength of reinforcing steel

The residual strength of the section can then be estimated using the equation:

$$M_n = A_s f_{yT} (d^* - \frac{A_s f_{yT}}{1.7 b^* f_c'}) \quad (4.2)$$

Where A_s is the area of tension steel, f_{yT} is the residual strength of reinforcing steel, d* is the effective depth of the damaged concrete section, b* is the width of the damaged concrete section, f'_c is the initial compressive strength of the concrete. Observing that the experimentally determined ultimate loads were 17%–48% higher than the predicted ultimate loads using this method, the researchers noted that the method, as with the ACI 318 flexural strength equations for ambient temperatures, does not take strain hardening of steel into account.

Though this method presents an interesting addition to the arsenal of post-fire assessment tools, some of the parameters required may be very difficult to determine, such as the heating and cooling lengths of the fire. Furthermore, this method is only applicable to standard reinforced concrete beams.

3.1.3. – Federal Highway Administration (FHWA) 2007: Prestressed Concrete Box Beams in Flexure

Unlike the other studies presented in this section, in which the specimens were heated in laboratories and testing facilities under controlled conditions, a 2007 study by the FHWA analyzed the residual flexural strength of concrete box beams from a bridge that had been exposed to a fire in service [47]. On July 12, 2005, a gasoline tanker truck on a bridge near Ridgefield, Connecticut, overturned and caught fire. Burning fuel covered portions of the

deck and spilled into the Norwalk River beneath the bridge. Figure 3.7 shows the condition of the exterior of the bridge after the fire [47].

Figure 3.7: Fascia of Ridgefield, CT, bridge after the fire

After the fire, the Connecticut Department of Transportation (ConnDOT) elected to replace all the beams in the bridge, since it could not be determined if the fire had damaged the prestressing strands in the beams. It was then decided that four of the interior beams that were removed would be inspected and tested to see if they had lost significant flexural capacity.

The bridge, constructed in 1957, consisted of 15 adjacent prestressed box beams that spanned 14.6 m. A cross-section of a typical beam is shown in Figure 3.8 [47]. The reinforcement mostly consisted of 9.5 mm prestressing strands, though there were also two #4 rebars at the top. The concrete cover for the prestressing strands varied from 33 to 46 mm.

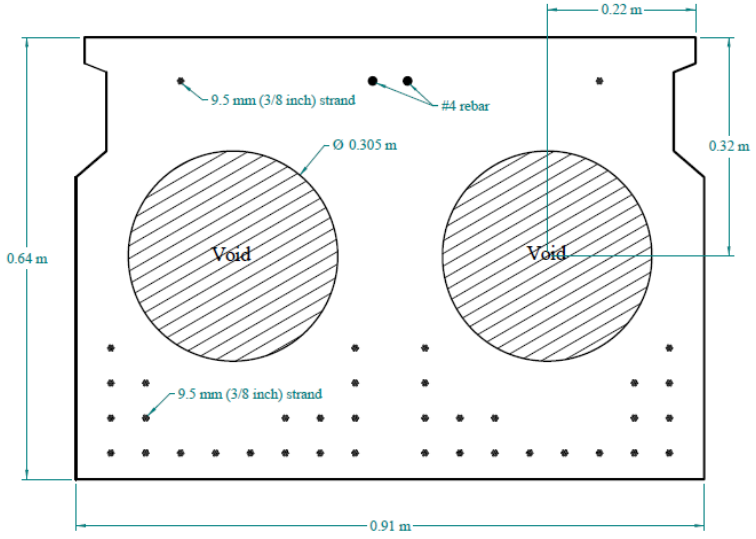

Figure 3.8: Cross-section of typical prestressed box beam in bridge

Before the load tests were performed, each beam was subjected to a visual inspection and petrographic analysis. The visual inspection revealed extensive concrete scaling on the bottom of the beams, shown in Figure 3.9 [47]. The average scaling depth was found to be 10 mm, but some areas had scaling up to 15 mm.

Figure 3.9: Visual condition of bottom of Beam 4, Ridgefield bridge

Furthermore, a petrographic analysis indicated that cracking in the concrete due to the fire extended approximately 25 mm from the exposed surface, for a total average damage depth in the concrete of 35 mm (scaling depth plus cracking depth).

After the visual inspection and petrographic examination, the beams were loaded to failure in a three-point bending test, and the ultimate loads and deflections were recorded. The experimental results were compared with the findings of a 1999 rating report of the bridge, which estimated the ultimate strength of a typical interior beam to be 1,407 kN-m. Table 3.2 provides a summary of the ultimate load and deflections determined experimentally for the four beams and a comparison of their ultimate strengths to the estimated strength of the interior beams per the 1999 rating report. The ultimate strengths include both the beam self-weight and the applied loading.

Table 3.2: Strength results from load testing of beams

Beam #	Measured Ultimate Deflection (mm)	Measured Ultimate Flexural Strength (kN-m)	Ratio of Measured Strength to Analytically Determined Strength
Beam 3	343	1,692	1.20
Beam 4	284	1,678	1.19
Beam 7	236	1,633	1.16
Beam 14	236	1,572	1.12

The measured ultimate flexural strength of each beam exceeded the flexural strength estimated in the 1999 rating report, suggesting that the beams had not lost significant strength due to the fire. Since all the beams from the bridge were damaged by the fire, it was not possible to have a control specimen for comparison. Although the flexural strength of the beams was not affected, it was noted that accelerated corrosion of the strands remained a long-term concern, as the depth of cracking due to the fire had extended to the bottom of the prestressing strands in some areas.

3.1.4. Agrawal & Kodur, 2019: Super-High-Strength Reinforced Concrete Beams in Flexure

Agrawal and Kodur investigated the residual strength of super-high strength concrete beams exposed to different fire scenarios [59]. Four beam specimens were prepared for the study, each with a depth of 406 mm, width of 254 mm, and length of 3960 mm, with three ϕ19 mm bottom longitudinal bars, two ϕ13 mm top longitudinal bars, and ϕ6 mm stirrups spaced at 150 mm, with the longitudinal bars having a yield strength of 420 MPa. The beams were denoted B1, B2, B3, and B4. B1 and B3 were tested 16 and 8 months after casting respectively, while B2 and B4 were tested 9 years after casting. The concrete of B1 and B3 had a compressive strength of 106 MPa, while the concrete in B2 and B4 had compressive strengths of 103 MPa and 106 MPa, respectively. To measure the temperature within the specimens during heating, each beam was fitted with several thermocouples. The cross-section of the beams and the locations of the thermocouples are shown in Figure 3.10 [59].

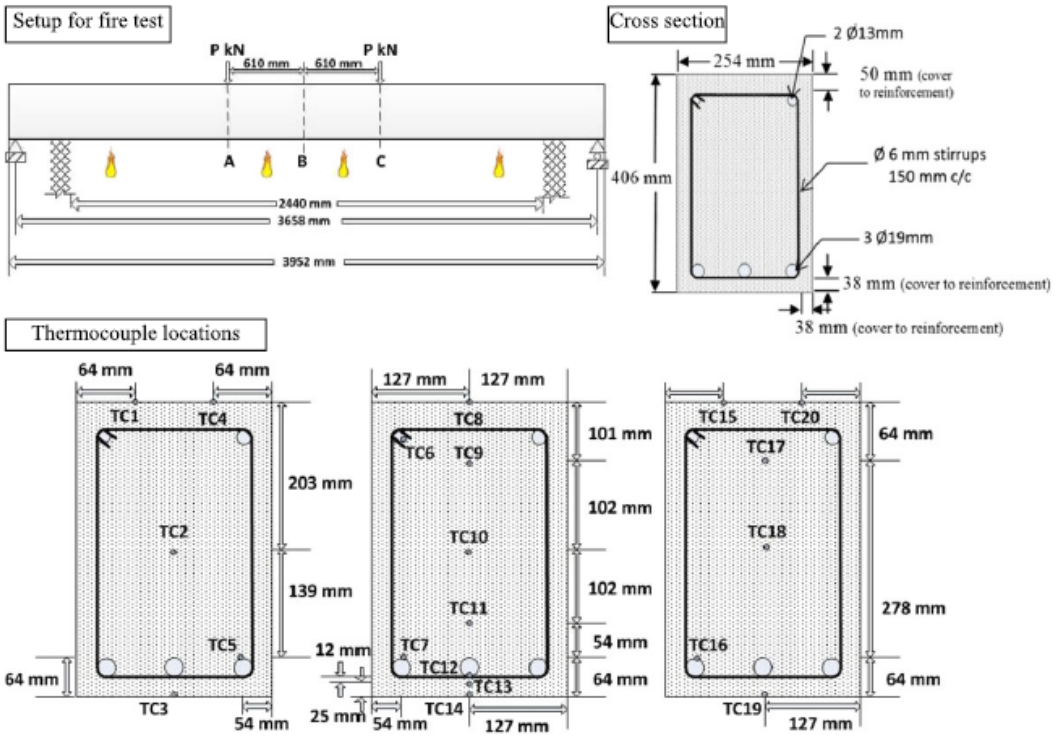

Figure 3.10: Beam cross-sections and locations of thermocouples (cross-section A, bottom L; cross-section B, bottom C; cross-section C, bottom R)

Each of the beam specimens was subjected to a different heating regime in a furnace. The measured air temperatures for each heating regime are shown in Figure 3.11 [59]. Two of the heating regimes were short design fires (SF), while the other two were long and severe design fires (LF). One of the SF fires (SF2) and one of the LF fires (LF2) had very fast cooling rates, which was intended to simulate a scenario in which the fire was put out quickly.

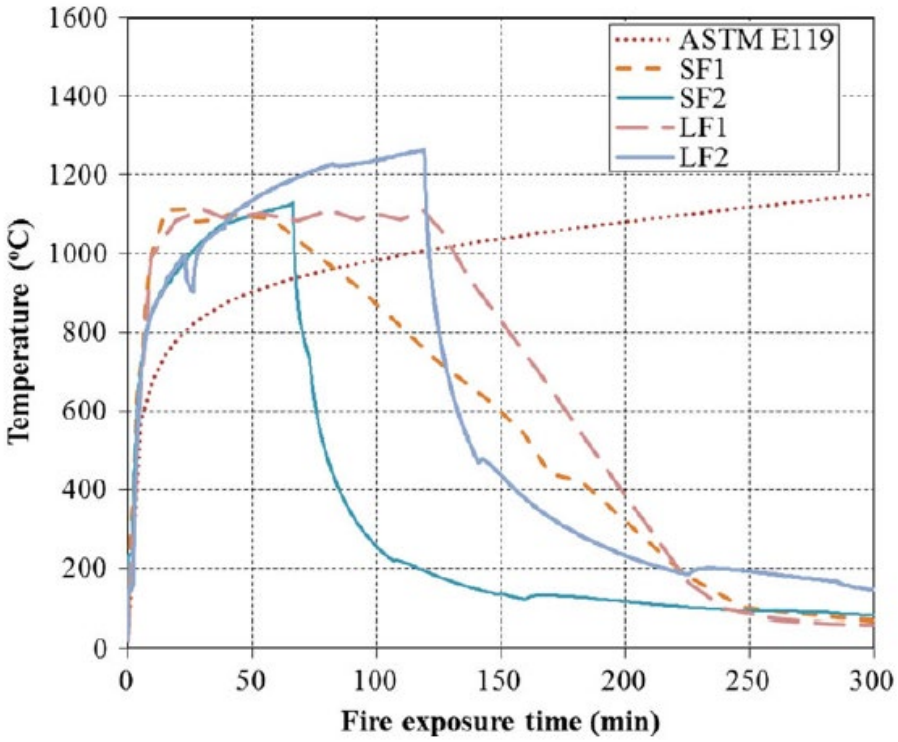

Figure notes: SF = short design fire; LF = long and severe design fire. *ASTM E119* curve shown for reference.

Figure 3.11: Air temperature inside furnace for each heating regime

During heating, B1, B2, and B3 were stressed to 53% of their flexural capacity per ACI 318, while B4 was stressed to 63% of its flexural capacity per ACI 318. B3 failed during heating due to excessive deflection, and therefore its residual strength capacity could not be tested. After heating, each beam was cooled in air to room temperature. For each residual strength test, the beam was loaded to failure in a four-point beam test. B1 was tested 24 hours after cooling, and B2 and B4 were tested a week after cooling. The results of the loading tests are shown in Table 3.3. Note that since no unheated control beam specimen was used, the original capacity of the beams before heating was determined using a finite element model. The original ultimate capacity of the beams was found to be 194 kN using the model. Furthermore, after heating, the researchers quantified the percentage of concrete lost due to spalling by comparing the final volume of the beam to the original volume of the beam.

Table 3.3: Details of beam specimens and results of experimental testing

Beam	Age of Beam at Testing (months)	f'_c (MPa)	Fire Exposure	Ultimate Residual Strength (kN)	Ratio of Residual Strength to Original Strength Determined by FEA	Spalled Volume Percentage
B1	16	106	SF1	129	.77	3.2
B2	107	103	SF2	112	.57	1.5
B3	8	106	LF1	-	-	7.0
B4	108	106	LF2	102	.43	3.3

All the beams were found to have a significantly reduced ultimate capacity, compared to their capacity before heating (as determined by the finite element model). The researchers suggested that the residual capacities of B2 and B4 were much lower than B1, because the beams were subjected to a rapid cooling phase during heating and were stored for a week after cooling. It is worth noting, however, that these beams were also much older than B1, and it is unclear if this could have affected the results. Although the ultimate capacities of all the beams were reduced, each still had a greater ultimate capacity than the capacity of the beams at room temperature predicted by the provisions of ACI 318, which was 94.5 kN.

3.1.5. Choi et al., 2013: Reinforced Concrete Beams in Flexure

A 2013 study by Choi et al. analyzed the residual flexural strength of reinforced concrete beams, focusing the on effects of spalling and temperature distribution within the members [54]. In total, 12 reinforced concrete beam specimens were prepared that were each 250 mm in width, 400 mm in depth, and 4700 mm in length. Two different concrete strengths (NSC and HSC), two different concrete cover amounts, and three different heating durations were used. Each beam was reinforced with three ϕ22 mm bars on the bottom and two ϕ22 mm bars on the top, with a tested ultimate strength of 439 MPa. Of the 12 beams, 4 were not heated and used as controls. The beams that were heated were subjected to a 40% service load during heating. Details about each specimen can be seen in Table 3.4 [54]. To measure the temperatures within the specimens during heating, each beam was outfitted with three thermocouples at the midspan, located at 50 mm, 200 mm, and 350 mm from the bottom of the beam, denoted as Low, Mid, and High, respectively. The locations of the thermocouples are shown in Figure 3.12 [54].

Eight of the beams were heated in a furnace according to the ISO 834 fire curve, while being subjected to a 40% service load. Only the bottom and the two sides of the beams were heated. The temperature distributions over time in the NSC beams with the two different cover thicknesses are shown in Figure 3.13 [54]. As would be expected, the NSC beams with the 40 mm cover experienced about 10% higher temperatures on average at the Low thermocouple than the NSC beams with 500 mm cover. The temperature at the Low thermocouples is significant, as it is near the longitudinal reinforcement, which could negatively affect the flexural capacity of the beam if heated to very high temperatures.

Table 3.4: Construction and heating details for each beam specimen

Specimen	Time period of furnace test (min)	Applied load (kN)	Strength of concrete (MPa)	Cover thickness (mm)
N[a]4[c]-0[e]	0	–	21	40
N4-1[f]	60	87.1	21	40
N4-2[g]	120	87.1	21	40
N5[d]-0	0	–	21	50
N5-1	60	87.1	21	50
N5-2	120	87.1	21	50
H[b]4-0	0	–	55	40
H4-1	60	96.3	55	40
H4-2	90	96.3	55	40
H5-0	0	–	55	50
H5-1	60	96.3	55	50
H5-2	90	96.3	55	50

[a]N: normal strength concrete; [b]H: high strength concrete; [c]4: cover thickness = 40 mm; [d]5: cover thickness = 50 mm; [e]0: no furnace test; [f]1: 60 min furnace test; [g]2: 90 or 120 min furnace test.

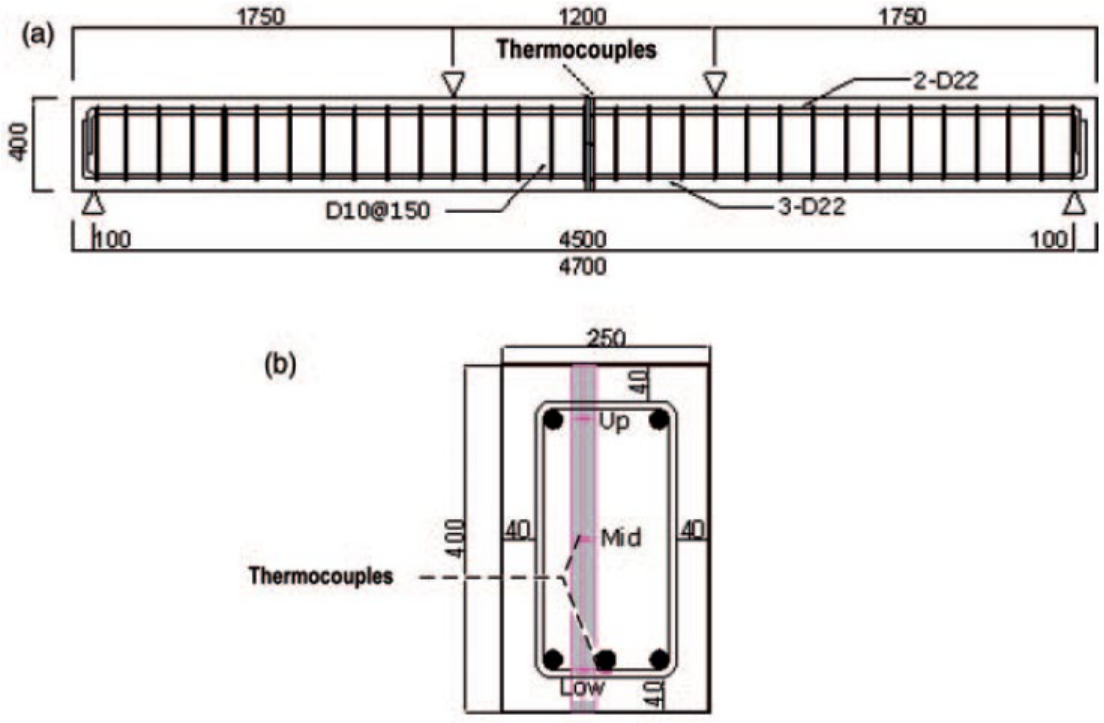

Figure 3.12: Specimen cross-sections and locations of thermocouples, for specimens with cover of 40 mm

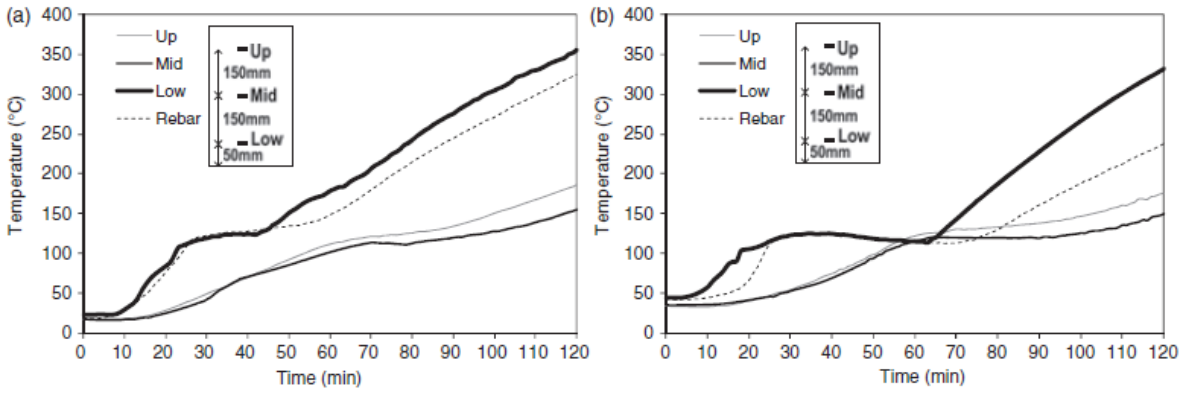

Figure 3.13: Temperature distribution in NSC beams with 40 mm cover (L); with 50 mm cover (R)

The temperature distributions for the HSC beams were also measured and are shown in Figure 3.14 [54]. For the HSC beams, the effect of the cover thickness on the temperatures at the Low thermocouple is not significant, since extensive spalling was reported in the HSC beams.

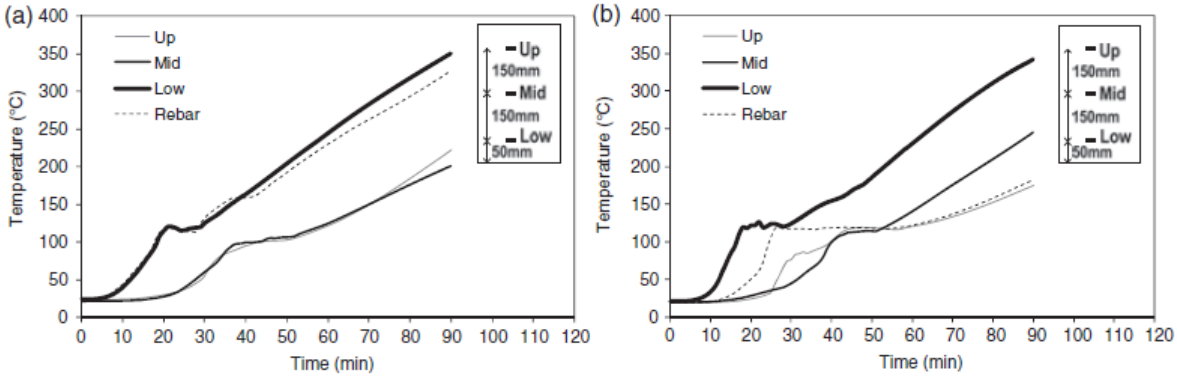

Figure 3.14: Temperature distribution in HSC beams with 40 mm cover (L); with 50 mm cover (R)

After heating and prior to the load testing, the beams were visually inspected. For the NSC beams, extensive cracking and loss of the concrete cover in some instances were noted, but significant spalling was not observed. On the other hand, the HSC beams experienced significant spalling, as shown in Figure 3.15 [54].

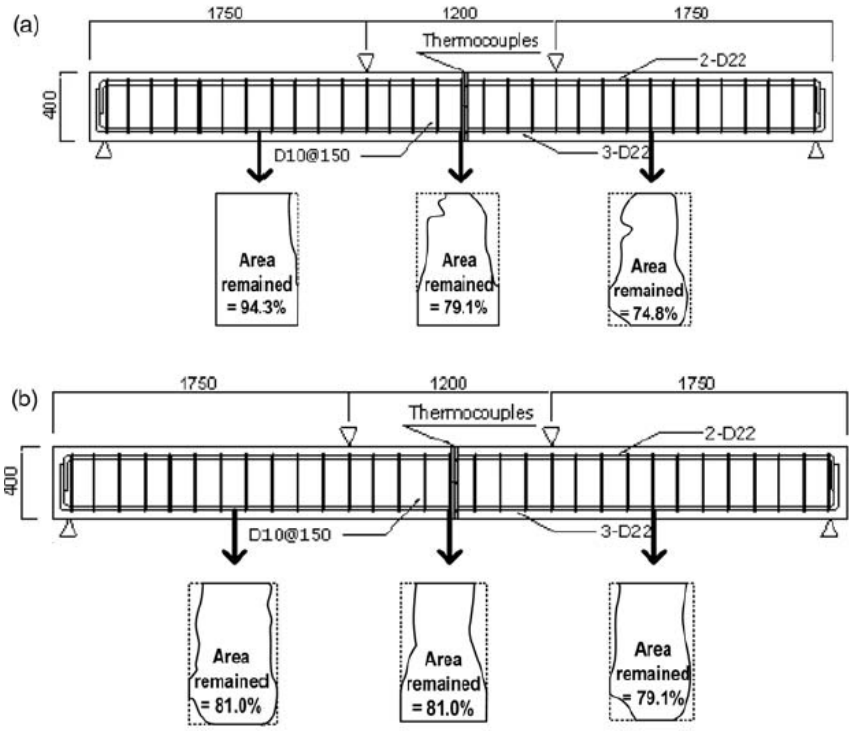

Figure 3.15: Spalling in HSC beams with 40 mm cover (top); with 50 mm cover (bottom)

After cooling, the beams were loaded to failure in a four-point bending test. The results of the tests are shown in Table 3.5 [54]. The ratio indicates the ultimate strength relative to the unheated control for each group of specimens. The most notable finding is that the HSC beams lost significantly more strength after heating than the NSC beams, possibly due the greater extent of spalling. None of the NSC beams lost more than 10% of their strength, whereas one of the HSC beams lost nearly 50% of its strength compared to the control. The NSC beams with 50 mm cover fared slightly better than the NSC beams with 40 mm cover, possibly due to the protection offered by the increased cover thickness. The HSC beams with the 50 mm cover performed worse than the HSC beams with 40 mm cover.

Table 3.5: Residual strength results of loading tests

Specimen	Maximum load (kN)	Ratio (%)	Specimen	Maximum load (kN)	Ratio (%)
N4-0	220.40	100	H4-0	265.05	100
N4-1	205.35	93	H4-1	231.75	87
N4-2	206.55	94	H4-2	227.10	86
N5-0	199.80	100	H5-0	257.40	100
N5-1	194.40	97	H5-1	202.05	79
N5-2	191.40	96	H5-2	139.20	54

Ultimately, the results suggest that spalling resulting in the reduction of concrete in the compression zone and exposure of tension reinforcement may have a significant effect on the residual strength of reinforced concrete members. Though the recorded temperatures near the longitudinal rebar were low enough that they likely did not experience any reduction in residual strength, the loss of concrete in compressive region of the HSC beams as shown in Figure 3.15 may have contributed to the significant loss of residual strength of the HSC beams.

3.1.6. Summary of Effects of Fire Exposure on Residual Strength of Structural Members

The key findings from the studies presented in the previous section can be summarized as follows.

- Unlike studies on concrete, steel, and bond strength, studies on the residual strength of members do not use standardized test specimens (such as concrete cylinders), making direct comparisons among studies difficult.
- Greater durations of exposure to heat generally result in greater residual strength losses after cooling.
- The residual strength reductions observed in the studies varied greatly. In some cases, ultimate strength losses of 5%–10% were observed, while in other cases residual strength losses up to nearly 60% were observed. Based on the wide variety of specimen dimensions and types, materials, and heating regimes used in the studies, it is difficult to draw conclusions about the specific factors that govern the residual strength loss, aside from the fact that greater lengths of exposure to heat generally result in greater residual strength losses.
- Spalling seems to result in greater strength losses compared to when spalling does not occur.
- Specimens with high-strength concrete are more likely to experience spalling.

This page left blank intentionally.

4.0 Existing Post-Fire Inspection Methods for Concrete Structures

The post-fire inspection of tunnels poses several challenges [67]. For one, the possibility of long fire durations and high temperatures means that the level of damage can range from minor surface damage to damage requiring extensive repairs. Furthermore, a wide variety of materials and structural elements may be present in tunnels, requiring the inspector to understand how fire may affect each component and material. Lastly, the inspector may be under pressure to decide if a tunnel is safe to be reopened as quickly as possible, due to the high economic and societal cost of traffic disruption.

There are several documents that describe existing techniques for the post-fire assessment of concrete structures [6,41,68,69]. Many of these techniques are aimed at evaluating the residual strength of structures after fire. From reviewing the literature, three main categories of inspection techniques emerge:

- Visual inspection methods
- Non-destructive testing methods
- Laboratory testing methods

Generally speaking, visual methods and non-destructive testing approaches are most suitable for a rapid inspection protocol, since laboratory methods may take weeks to perform. On the other hand, laboratory methods may give a more accurate and thorough assessment of the residual capacity of the structure. Since MassDOT's main interest is for the development of a rapid inspection protocol, this section will largely focus on the methods most suited for that purpose; however, other methods will be described as well in lesser detail, with relevant sources provided.

4.1 Visual Inspection Methods

While current visual methods are not suitable for directly determining the residual strength of structural components, they can give the inspector valuable information about the maximum temperatures reached in certain areas of the structure during the fire and a general sense of the severity of the damage.

4.1.1. Examination of Debris Materials

An important step in post-fire assessment of concrete structures is estimating the temperatures reached at certain areas of the structure, since the residual strength of steel and concrete largely depend on the maximum temperature to which they were exposed [4,5]. Examining the residual condition of debris and non-structural materials, such as melting of metals or charring of plastics, can reveal the upper and lower bounds of temperature

exposure in different areas of the structure [6,41]. Table 4.1 lists the visual condition of many common building materials after exposure to certain temperatures (reprinted from [41]).

Table 4.1: Degradation of selected materials at given temperatures

Table A6.1 Effect of temperature on selected substances

Approximate temperature (°C)	Substance	Typical examples	Condition [a]
100 150	Paint		Deteriorates Destroyed
120 120 – 140 150 – 180	Polystyrene	Thin-wall food containers, foam, light shades, handles, curtain hooks, radio casings	Collapse Softens Melts and flows
120 120 – 140	Polyethylene	Bags, films, bottles, buckets, pipes	Shrivels Softens and melts
130 – 200 250	Polymethyl methacrylate	Handles, covers, skylights, glazing	Softens Bubbles
100 150 200 400 – 500	PVC	Cables, pipes, ducts, linings, profiles, handles, knobs, houseware, toys, bottles	Degrades Fumes Browns Charring
200 – 300	Cellulose	Wood, paper, cotton	Darkens
240	Wood		Ignites
250 300 – 350 350 – 400	Solder Lead	Plumber joints Plumbing Sanitary installations, toys	Melts Melts, sharp edges rounded Drop formation
400 420	Zinc	Sanitary installations, gutters, downpipes	Drop formations Melts
400 600 650	Aluminium and alloys	Fixtures, casings, brackets, small mechanical parts	Softens Melts Drop formation
500 – 600 800	Glass	Glazing, bottles	Softens, sharp edges rounded Flowing easily, viscous
900 950	Silver	Jewellery, spoons, cutlery, etc.	Melts Drop formation
900 – 1000 950 – 1050	Brass	Locks, taps, door handles, clasps	Melts (particularly edges) Drop formation
900 900 – 1000	Bronze	Windows, fittings, doorbells, ornamentation	Edges rounded Drop formation
1000 – 1100	Copper	Wiring, cables, ornaments	Melts
1100 – 1200 1150 – 1250	Cast iron	Radiators, pipes	Melts Drop formation

Note

a Can be used to assess (maximum) temperature at the location of these materials. Examples are: wood char patterns; softening and melting (glass, brick, metals, plastics); aggregate, concrete and brick discolouration.

Researchers at the U.S. Nuclear Regulatory Commission employed this method after the 2007 Newhall Pass tunnel fire in California, to develop a map of the maximum and minimum temperatures reached along the length of the fire in the tunnel [70].

Figure 4.1: Picture taken during Newhall Pass fire event (L); post-fire condition of tunnel (R)

The researchers visually examined the condition of various metallic material samples from five burned vehicles in the tunnel, such as aluminum brackets and steel framing, and estimated the upper and lower temperature bounds by observing whether the samples were melted, partially melted, or not melted.

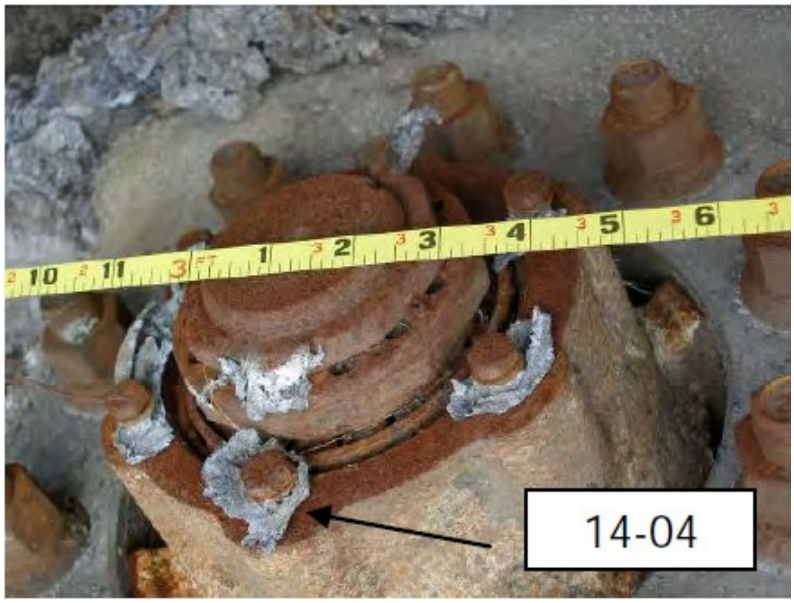

Figure 4.2: Melted aluminum alloy on wheel of truck

Differential scanning calorimetry (DSC) was used to precisely determine the melting points of the various samples, since the addition of alloying substances can alter the melting points of pure metals. However, the data provided in the study show that melting points determined using the DSC process were within +/-100°C of the melting points shown in Table 4.1. In addition to this method, the researchers also used hardness tests and microstructure analysis for some of the samples. Ultimately, a map of the temperature bounds at the physical location of each of the five burned vehicles was developed, based on the materials analysis.

4.1.2. Concrete Color Change Due to Heat

The color of concrete may change when exposed to high temperatures such as in a fire, due to physical and chemical processes that occur during heating. These processes can affect the color of both the aggregate and the cement matrix. It is generally agreed that concrete mixtures containing siliceous aggregates (quartz, flint) will develop a red/pink color in the range of 300°–600°C, due to the dehydration and oxidation of iron compounds in the aggregate. In addition, the cement matrix can change to a whitish-gray color in the range of 600°–900°C and a "buff" color in the range of 900°–1000°C [71,72]. The red/pink color change in concretes containing siliceous aggregates is quite useful, as concrete is generally said to have a marked reduction in residual compressive strength when heated to above 300°C [9]. Therefore, red/pink concrete present in a fire-damaged structure should be treated as being potentially damaged and investigated further. Some have recommended using a chisel or hand drill to determine the depth of red/pink concrete and taking the depth of red/pink concrete as the depth of the 300°C isotherm in the concrete, which indicates the depth of damaged concrete [68,72].

One study produced high-quality images of heated concrete, mortar, and cement paste at a series of temperatures ranging from 20° to 1000°C [71], which help show the progression of the color in concrete as it is heated to progressively higher temperatures. The study used both a normal-strength and a high-strength concrete containing CEM II/A-V 42,5 R cement, and natural riverbed aggregates. The color progression is shown in Figure 4.3.

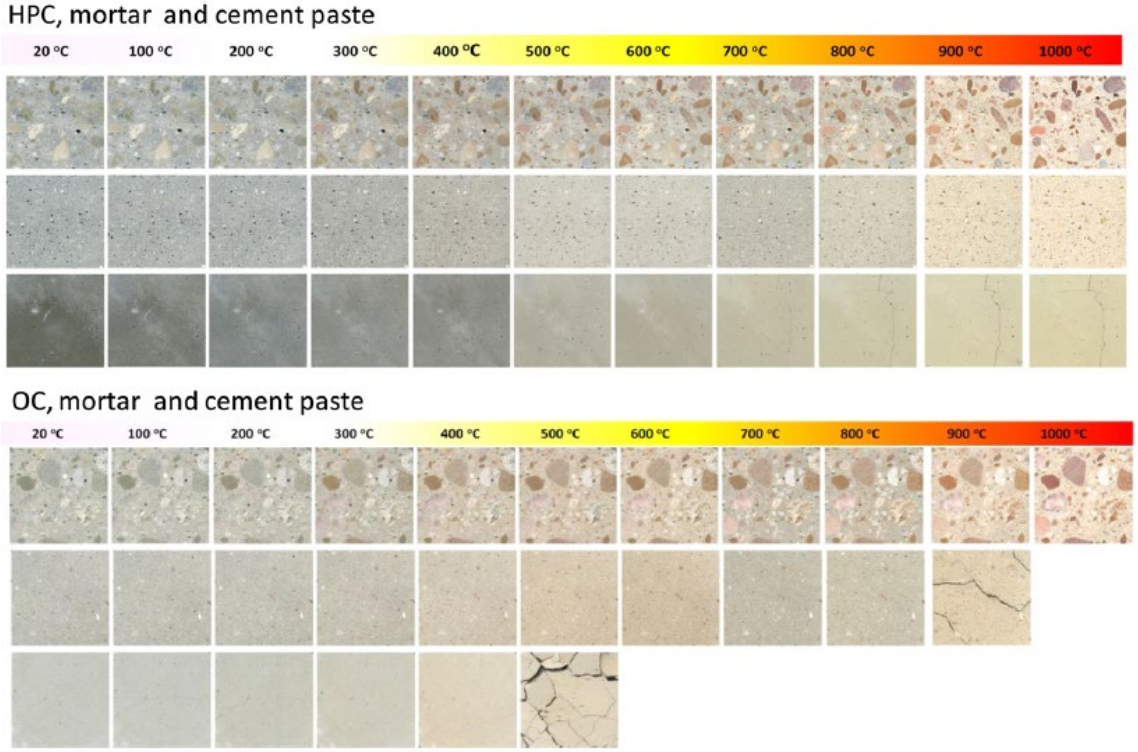

Figure 4.3: Color change of high performance and ordinary concrete, mortar, and cement paste heated to temperatures from 100°C to 1000°C

Another study tested four different concrete mixtures, each with a different type of aggregate: (i) siliceous gravel, (ii) crushed limestone, (iii) crushed granite, and (iv) Lytag, a proprietary lightweight aggregate [72]. It was found that the mixture with siliceous gravel had the greatest color change, while the color change in the mixtures with other aggregates was less noticeable. Furthermore, a transient heat analysis was conducted on some specimens, in which the specimens were heated only on one side. Figure 4.4 shows a cut and polished specimen subjected to this heating regime [72].

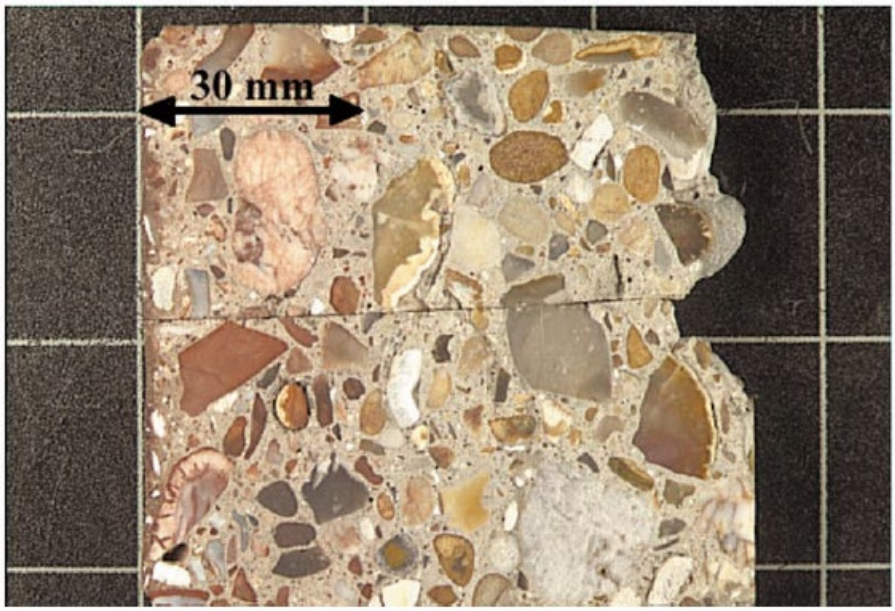

Figure 4.4: Concrete specimen heated on left face (transient heat analysis)

Several studies, including those mentioned previously, have attempted to systematically analyze the changes in color in concrete that occur due to heating [71–74]. This is typically done by digitally processing the images and quantifying changes using the red, blue, green (RGB) scale, or the hue, saturation, and intensity (HIS) scale. Unfortunately, processing the images can be a lengthy endeavor, and the lighting conditions can have a major impact on the results.

This approach comes with some important limitations. For one, while the red/pink color change in concretes with siliceous aggregates has been widely observed, studies of heated concretes with other aggregates such as limestone, granite, and Lytag have shown a much less significant color change [72]. In some cases, the color may not change at all. Furthermore, concrete can develop a red/pink color due to the natural process of carbonation, which occurs as the concrete ages. For this reason, it is important to compare concrete that is suspected of being damaged with concrete in parts of the structure that are known not to be affected, either visually or by using phenolphthalein to determine the carbonation depth, a technique which is described in Section 4.2.3 [68].

4.1.3. General Visual Damage Classification

Concrete and reinforced concrete members can experience many permanent, visible changes when exposed to high temperatures. Color changes, cracking, and spalling have been widely reported in fire-damaged concrete, and the extent and severity of these phenomena can be used to give a first indication of the residual condition of the concrete. A visual damage classification scheme for fire-damaged concrete is shown in Figure 4.5 [9].

Table 3. Simplified visual concrete fire damage classification[3]

Class of damage	Features observed					
	Finishes	*Colour*	*Crazing*	*Spalling*	*Reinforcement*	*Cracks/ deflection*
0 (Decoration required)	Unaffected	Normal	None	None	None exposed	None
1 (Superficial repair required)	Some peeling	Normal	Slight	Minor	None exposed	None
2 (General repair required)	Substantial loss	Pink/red *	Moderate	Localised	Up to 25% exposed	None
3 (Principal repair required)	Total loss	Pink/red * Whitish grey **	Extensive	Considerable	Up to 50% exposed	Minor/ None
4 (Major repair required)	Destroyed	Whitish grey **	Surface lost	Almost total	Up to 50% exposed	Major/ Distorted

Notes
* Pink/red discolouration is due to oxidation of ferric salts in aggregates and is not always present and seldom in calcareous aggregate.
** White-grey discolouration due to calcination of calcareous components of cement matrix and (where present) calcareous or flint aggregate.

Figure 4.5: Visual damage classification scheme for fire-damaged concrete

The general visual condition of the structure can also be used to assess its residual condition after a fire. An example of a visual damage classification chart for buildings is shown in Figure 4.6, from *Appraisal of Existing Structures* [41].

Class	Characterisation	Description
'0'	No discernible damage	Floor remote from fire Equipment remains in working order
1	Cosmetic damage, surface	Characterised by soot deposits and discolouration. Uneven distribution of soot deposits may occur Permanent discolouration on high-quality surfaces
2	Technical damage, surface	Characterised by damage to surface treatments and coatings Small extent only of concrete spalling or corrosion on uncovered metals Painted surfaces can be repaired. Plastic-coated surfaces need replacing or covering. Minor spalling may remain or can be replastered
3	Structural damage, surface	Characterised by some concrete cracking and spalling, lightly charred wood surfaces, some deformation of metal surfaces or moderate corrosion damage
4	Structural damage, cross-section (interior)	Characterised by major concrete cracking and spalling, deformed flanges and webs of steel beams, partly charred cross-sections of timber constructions, and degraded plastics. Damage can in many cases be repaired on the existing structure. Within the class are also deformations of structures so large that the load-bearing capacity is reduced, or dimensional alterations prevent proper fitting into building. This applies in particular to metal/steel constructions
5	Structural damage to members and components	Characterised by severely damaged structural members and components, impaired materials and large deformations. Concrete constructions are characterised by extensive spalling, exposed reinforcement and impaired compression zone. In steel structures extensive permanent deformations have arisen due to diminished load-bearing capacity caused by high-temperature conditions. Timber structures may have almost fully charred cross-sections. Changes in materials may occur after the fire, so they may display unfavourable properties

Figure 4.6: Damage classification scheme for post-fire inspections

It is typically recommended to verify that the classification schemes are appropriate for the structure being considered and that they are combined with other inspection techniques such as non-destructive testing or laboratory testing.

4.2 Onsite Non/Partially Destructive Testing Methods

While visual methods are useful for quickly assessing the general condition of a structure after fire event, it is sometimes necessary to estimate the residual strength of structural members more directly. There are a wide variety of non-destructive and partially destructive testing methods that have been used and recommended for the assessing the residual strength of concrete [6,10,67,68]. Figure 4.7 shows a list of common non-destructive and partially destructive techniques for assessing fire-damaged structures [9]. Figure 4.8 shows a more exhaustive list of non-destructive and partially destructive inspection tools, specifically for tunnel linings.

Table 1. Test method options for assessment of fire-damaged structures					
Test location	**Test type**	**Test method**	**Structural material**		
			Concrete	*Steel (including reinforcement)*	*Masonry*
On-site	Non-destructive	Visual inspection	✓	✓	✓
		Endoscope survey			✓
		Hammer soundings	✓	✓	✓
		Rebound hammer	✓		✓
		Ultrasonic testing	✓	✓	✓
		Magnetic particle imaging		✓	
	Partially destructive	Breakout/ drilling	✓		✓
		Load test	✓	✓	✓
Laboratory		Petrographic examination	✓		✓
		Metallography		✓	
		Hardness test		✓	
		Compressive strength	✓		✓
		Tensile strength		✓	

Figure 4.7: Common inspection methods for fire-damaged structures

(A) Average response of the concrete cover	(B) Point by point response of small samples	(C) Special interpretation techniques
Hammer tapping	Small scale mechanical testing	Sonic refraction
Hammer and chisel	While drilling tests	Impact-/pulse-echo
Schmidt rebound hammer	Dynamic Young's modulus	Impulse response
Windsor probe	Ultrasonic Pulse Velocity	Analysis of Surface Waves
Cut and Pull Out test	Porosimetry	Velocity and transmission
BRE internal fracture	Micro-crack density analysis	Spectral Analysis (SASW)
Ultrasonic Pulse	Air permeability	Modal Analysis (MASW)
Velocity (UPV)	Water absorption	Ground Penetr. Radar (GPR):
	Colorimetry	Wide Angle Reflection
	Petrographic examination	Refraction (WARR)
	Differential Thermal An. (DTA)	Common Middle Point (CMP)
	Thermo-Gravimetric An. (TGA)	Electric resistivity and capacity
	Dilatometry (TMA)	Quantitative impulse-thermography
	X ray diffraction (XRD)	
	Laser Induced Breakdown Spectroscopy (LIBS)	
	Thermoluminescence	
	Chemical analysis	

Figure 4.8: Extensive list of possible inspection methods for fire-damaged tunnel linings

This section will mostly focus on techniques suitable for a rapid inspection protocol; however, other common post-fire inspection techniques will be discussed as well.

4.2.1. Rebound Hammer

The rebound hammer is one of the most widely used non-destructive testing techniques for fire-damaged structures, owing to its low cost and ease of use [68]. Furthermore, several studies have investigated the use of the rebound hammer for assessing fire-damaged concrete [73–80]. Standard procedures for performing the rebound test are described in *ASTM C805-18* [81]. To operate the rebound hammer, the narrow end of the hammer, known as the plunger, is pressed into the concrete until a spring-loaded mass is released. The mass impacts the concrete and rebounds, and the rebound number is determined either by the ratio of the rebound travel distance of the mass to the initial travel distance of the mass, or the ratio of the rebound velocity to the initial velocity [82]. The amount of energy absorbed by the concrete on impact, which is expressed by the rebound number, is related to the strength and stiffness of the concrete. Generally, stronger, stiffer concrete will result in a higher rebound number, while weaker, less stiff concrete will result in a lower rebound number. In the case of non-fire-damaged concrete, the rebound hammer can be used to estimate compressive strength, provided that a correlation between the compressive strength and the rebound number for the particular concrete mix has been determined. It has been noted, however, that the rebound number is highly variable and can be affected by many factors. Moisture/water content, aggregate size, carbonation, and surface texture of the concrete are some of the most influential factors that can affect the rebound number [69]. The accuracy of the rebound hammer in measuring the in-place compressive strength of non-fire-damaged concrete has been estimated to range from +/-25% to 40%.

Due to the inherent unreliability of the rebound hammer and the fact that performing a calibration for the particular concrete mix in an existing structure is often impractical, it is generally recommended that the rebound hammer only be used to delineate damaged areas in a fire-damaged structure, rather than to estimate the compressive strength of fire-damaged concrete [6,68]. It has been suggested that the rebound hammer can be used to detect areas of concrete where 30%–50% of strength has been lost. The poor sensitivity of the rebound hammer to low levels of damage can be explained by the dehydration of the concrete that occurs when it is heated. Dryer concrete is known to register higher rebound numbers than concrete saturated with water. As a result, the decreasing value of the rebound number that might otherwise occur due to thermal damage is offset by the simultaneous dehydration of the concrete; hence, the rebound number will begin to diminish only after significant loss of compressive strength has occurred [6]. In spite of this limitation, an attempt has been made to create a curve that correlates the rebound number to the strength of fire-damaged concrete [76].

Several studies have quantified the decrease in rebound number that occurs based on maximum exposure temperature and decrease in compressive strength. In one study, rebound hammer tests were conducted on concrete cubes made with siliceous aggregates and ordinary Portland cement that had been heated and cooled [73]. The cubes were heated to a uniform temperature throughout, up to a maximum temperature of 600°C. Some of the cubes were tested immediately after cooling; others were stored in water or air for 28 days. All the cubes were then subjected to tests with the rebound hammer. The data are shown in Figure 4.9, where the curve labelled (RRI_0d) indicates the cubes tested immediately after cooling;

(RRI_28d_water) indicates the cubes tested after being stored in water for 28 days; (RR__28d_air) indicates the cubes tested after being stored in air for 28 days; and (fccub150_0d) indicates an additional set of cubes about which no further information was given.

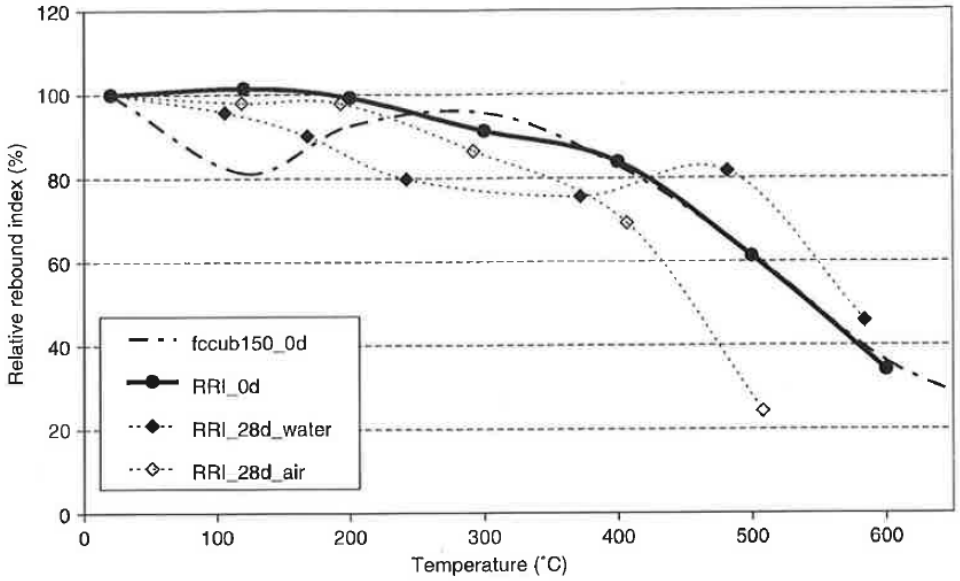

Figure 4.9: Ratio of rebound index after heating to rebound index before heating

From these data, the researchers proposed a criterion to help determine whether a region of concrete has been damaged based on the rebound number:

$RI_T / RI_{20°C} > 0.85$: concrete element is superficially damaged only

$0.85 \geq RI_T / RI_{20°C}$: concrete element should be further investigated

Though it was not described how this criterion was determined, a relative rebound ratio of 0.85 appears to coincide roughly with exposure to temperatures of 300°C (from Figure 4.9), which is generally stated as the temperature at which concrete begins to lose significant compressive strength [9].

In another study, two batches of concrete cubes were created: a normal-weight concrete made with siliceous aggregates, and a lightweight concrete made with expanded clay coarse aggregate and siliceous sand [74]. Some cubes were not heated to serve as a control, and the rest of the cubes were subjected to a slow heating and cooling cycle to achieve "uniform damage" throughout the cubes, to maximum temperatures of 200°C, 400°C, 600°C, and 800°C. After cooling, the rebound numbers measured from the cubes were recorded, and the cubes were subjected to compression tests to measure the corresponding compressive strengths. On the left, Figure 4.10 shows the ratio of the compressive strengths of the cubes at each temperature to the strength of the unheated cubes (the strength decay ratio). On the right, Figure 4.10 shows the ratio of the rebound index of the heated cubes to the rebound index of the unheated cubes plotted against strength decay of the concrete, which includes data from this study and data from another similar study at Aston University [72].

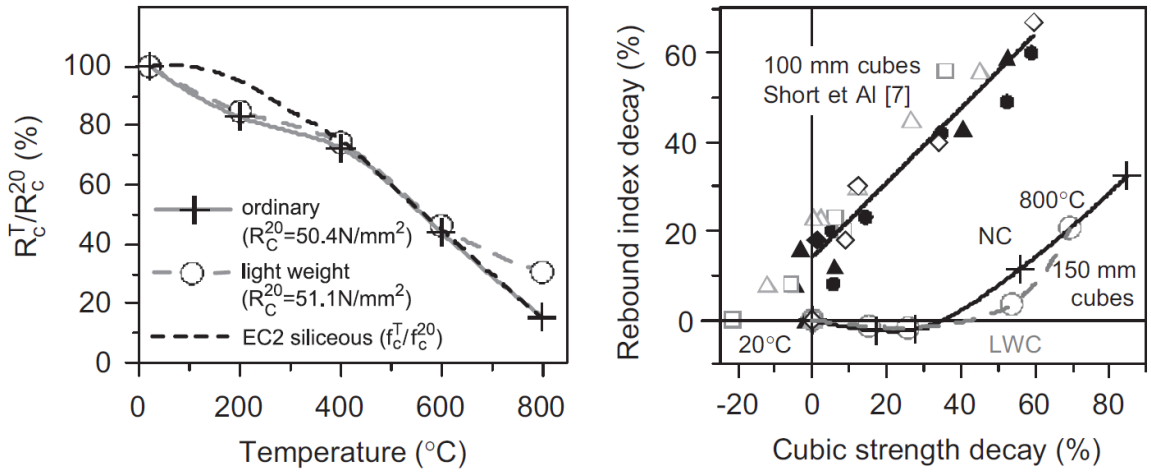

Figure 4.10: Relative residual strength of cubes from compression tests (L); relative rebound index of cubes plotted against compressive strength decay ratio (R)

This same study also demonstrated the ability of the rebound hammer to delineate areas damaged by fire with a separate experimental setup [74]. In this part of the study, a concrete wall partially protected by a concrete duct (at left in Figure 4.11) was subjected to 90 minutes of the ISO 834 fire curve. Since concrete has excellent thermal insulation properties [1], the duct would greatly reduce the temperature that the protected part of the wall experienced. After cooling, rebound tests were performed at various heights along the wall (lines A-E). The rebound index results are shown in Figure 4.11 at center. In addition, the temperatures recorded at lines A-E and the corresponding compressive strength decreases (f^T_c/f^{20}_c) are shown at right. The rebound numbers are significantly lower at the exposed parts of the wall as compared to the protected part of the wall, supporting the idea that the rebound hammer can delineate areas of concrete damaged by fire.

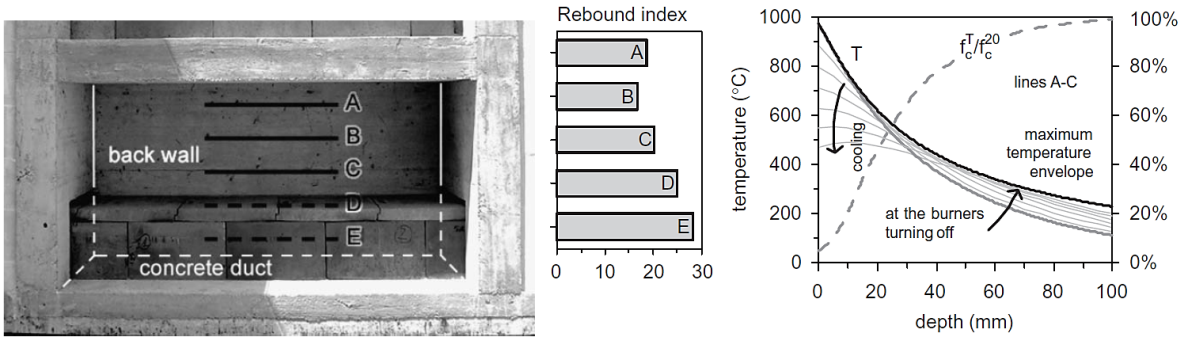

Figure 4.11: Concrete wall partially blocked by concrete duct (L); average rebound indices measured at each line (C); recorded temperature and corresponding compressive strength decay at lines A–C on wall (R)

Though the previously mentioned studies provide a lot of useful data on the relationship of fire exposure, loss of compressive strength, and change in the rebound number of concrete, all were conducted under controlled laboratory conditions that may not completely reflect the in-situ conditions of a structure after a real fire. In a case study of a six-story reinforced

concrete office building in Islamabad, Pakistan, that experienced a severe fire, several different NDT techniques, including the rebound hammer, were used to assess the condition of the concrete in the building [78]. The rebound hammer test was performed at several locations in the building, and at each test location, a concrete core was extracted to perform compressive strength tests (Figure 4.12). This allowed the researchers to correlate the rebound number to the measured compressive strength of the concrete.

Figure 4.12: Extraction of concrete cores for compressive strength tests

The rebound number data is shown in Figure 4.13. The red dashed line shows the rebound number and the corresponding measured compressive strength. The blue solid line ostensibly shows the compressive strength estimated by a typical correlation curve or perhaps the manufacturer's provided correlation curve, but the line is not fully described in the study [78].

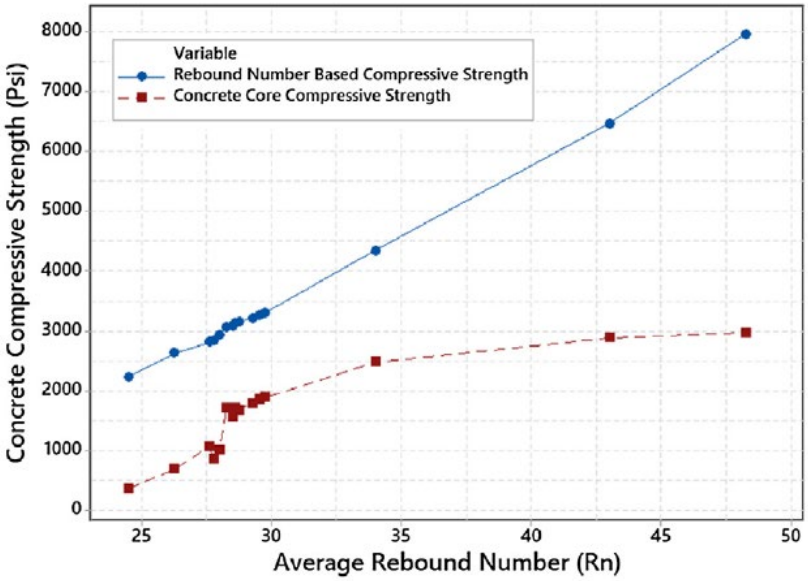

Figure 4.13: Measured core strength of concrete vs. rebound number and compressive strength estimated by rebound number

Overall, the rebound number clearly decreases as the measured compressive strength decreases, but in a nonlinear manner. The data indicate a high sensitivity to the initial decreases in strength, which contrasts with the findings of other researchers [74]. One notable limitation of this analysis method is that it is unclear how the non-uniform damage gradient along the concrete would affect the results of the compression tests.

4.2.2. Pullout Tests

The pullout test is another commonly used method for estimating the compressive strength of concrete; it has also been proposed to be used for the case of fire-damaged concrete [67,80,82]. Standard procedures for performing the pullout test are described in *ASTM C900-19* [83]. Two types of pullout tests exist: those that are cast into the concrete and those that are post-installed into hardened concrete. For post-fire inspection, post-installed tests are the only feasible type, such as the commercially available cut and pullout (CAPO) test. The post-installed test is conducted in four steps, as shown in Figure 4.14 [83].

1) a 45-mm-deep, 18.4-mm-diameter hole is drilled perpendicular to the surface of the concrete, and part of the hole is routed to 25 mm at a depth of 25 mm in the initial hole.
2) The metal expandable insert is inserted into the hole.
3) The bottom of the insert is expanded.
4) The bearing ring and hydraulic loading system are installed, and the insert is subjected to an increasing tensile force until failure of the concrete occurs, which extracts a cone-shaped piece of concrete. The maximum pullout force is recorded.

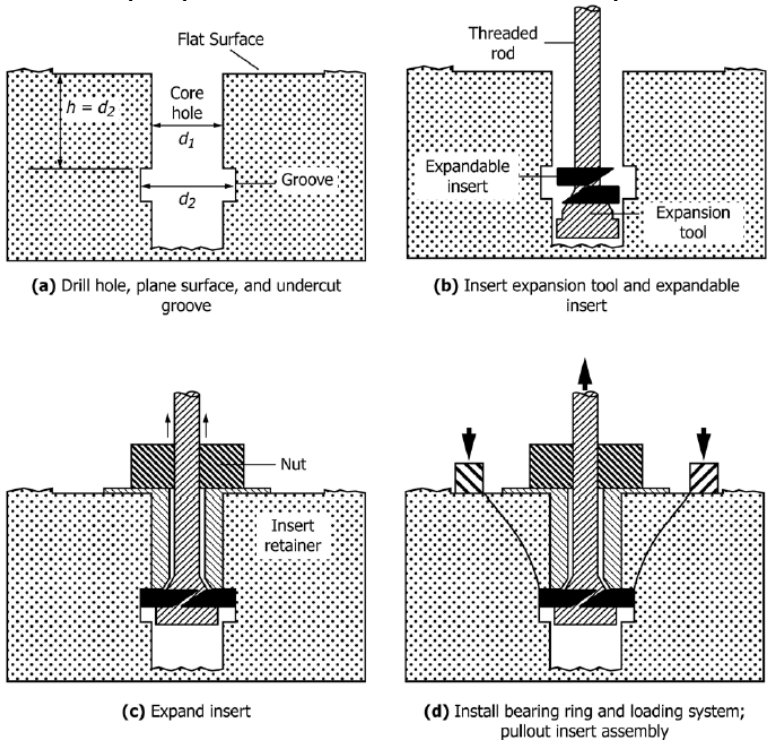

Figure 4.14: Schematic showing procedure of conducting post-installed pullout test

Though the specific failure mechanism governing the ultimate pullout force is debated [82], the pullout force has been shown to have an excellent correlation with compressive strength [69]. Though *ASTM C900-19* states that a calibration of the pullout force to the compressive strength must be performed for each new concrete mixture, the excellent correlation between pullout force and compressive strength in the literature has led many researchers to suggest that a single strength-pullout force correlation curve is applicable for all normal-density concrete mixtures, except for mixtures with a maximum aggregate size exceeding 40 mm [69]. Figure 4.15 (from Germann.org) shows the results from several studies on the relationship between cube, core, cylinder compressive strength, and pullout force. In Figure 4.15, the Lok Test is a commercial pullout test system in which the inserts are cast in place, whereas the CAPO test is a system that uses post-installed inserts. Cast in place and post-installed inserts have been shown to give comparable results [82].

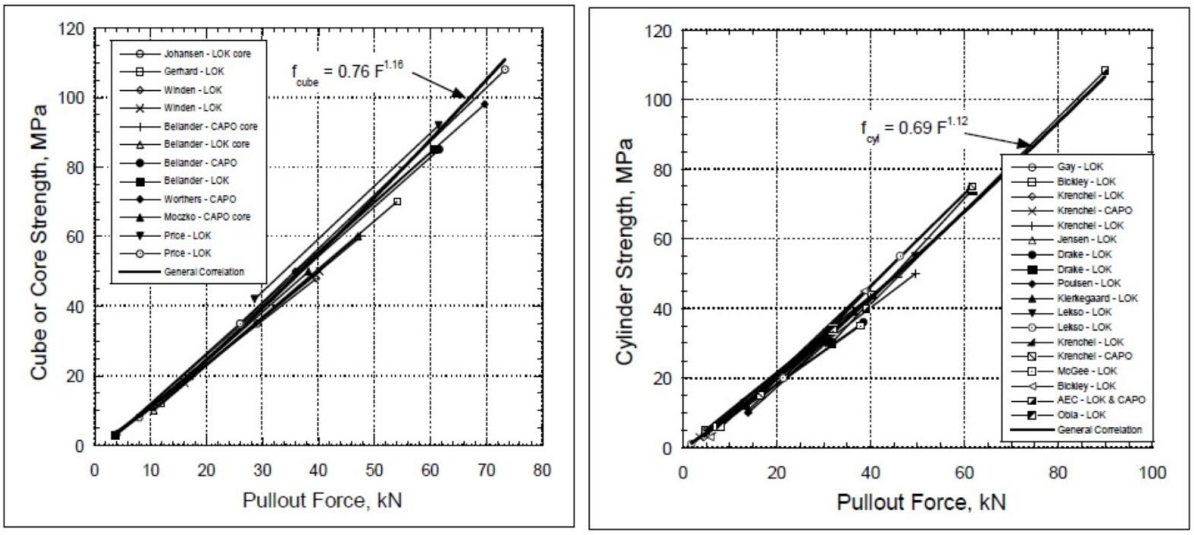

Figure 4.15: Compressive strength–pullout force correlations from several studies

One study assessed the efficacy of the pullout test, specifically the CAPO test, for estimating the compressive strength of fire-damaged concrete [84]. In the first part of the study, two sets of ordinary Portland cement concrete cubes, an "ordinary" set and lightweight set, were cast. The cubes were then subjected to a slow heating and cooling cycle to achieve uniform damage throughout the cubes, to maximum temperatures of 200°C, 400°C, 600°C, and 800°C. After cooling, CAPO tests were performed on the cubes to determine the change in pullout force due to heating. Additionally, compressive strength tests were performed on the cubes to measure the corresponding compressive strength decrease. The results are shown in Figure 4.16 [84].

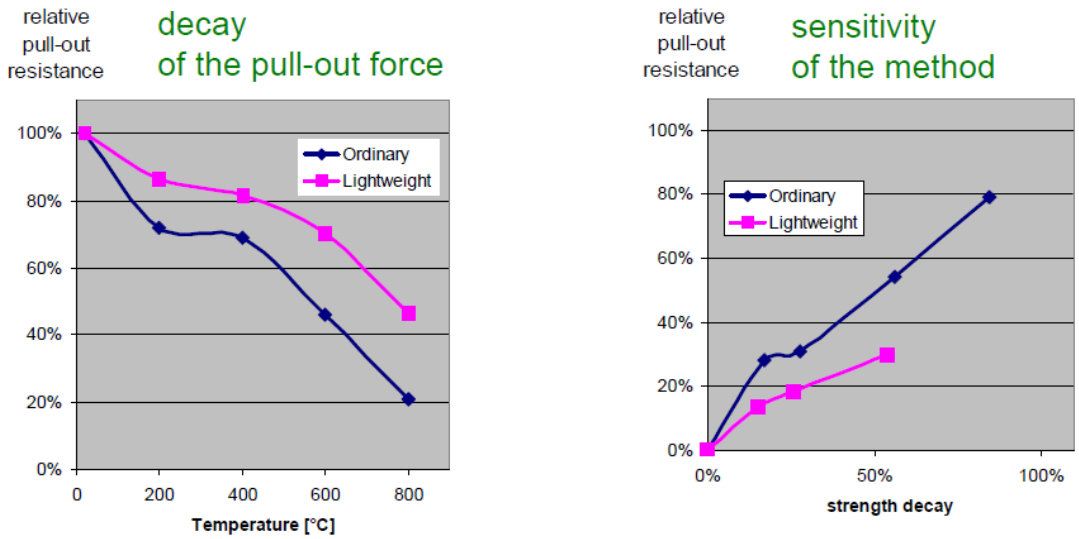

Figure 4.16: Measured pullout force vs. maximum temperature of concrete cube (L); pullout force vs. measured strength decay of the cubes (R)

Though the number of data points was limited, the method was shown to have a good sensitivity to the reduction in compressive strength caused by heat. Though this data is informative, concrete is rarely damaged in a uniform manner in real fire scenarios [1]; fire-damaged concrete usually has a damage gradient that can vary along the surface and depth of the concrete. To address this, two concrete panels (one with ordinary concrete and one with lightweight concrete) heated on only one side were also subjected to the CAPO test. The measured pullout forces for both panels are shown in Figure 4.17 [84]. Three CAPO tests were conducted on each panel, shown in blue, and the average of the three for each panel is shown in red. According to the researcher, the CAPO test results seem to give an indication of the condition of the concrete very near the surface (5–10 mm), based on the other pullout force results from the cube tests.

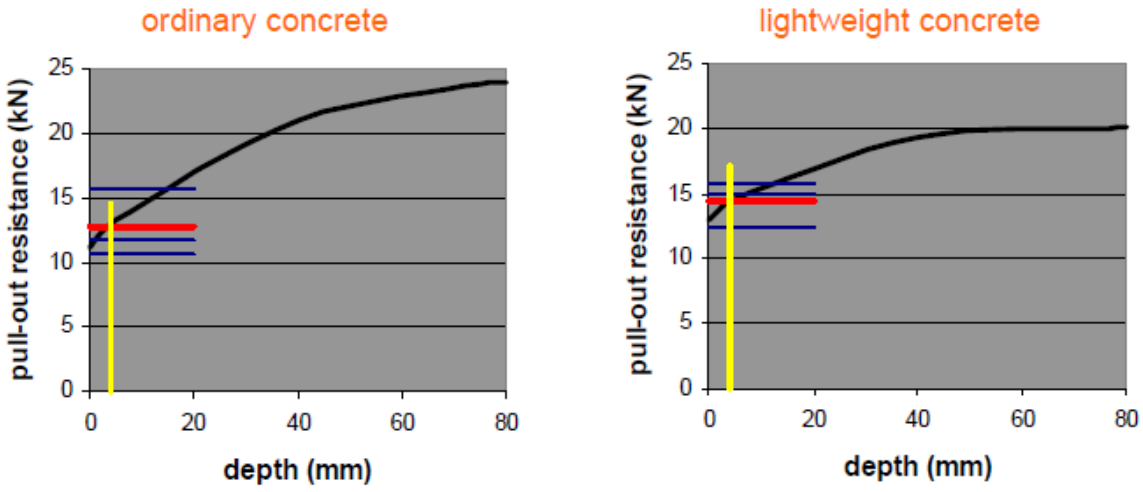

Figure 4.17: CAPO results for concrete panels heated on only one side

The CAPO test is somewhat time-consuming compared to other NDT techniques, taking about a half-hour per test, which may not be acceptable in certain circumstances.

4.2.3. Carbonation Tests

The carbonation test is a quick, simple test that can be used to approximate the depth of damage in a concrete member. As concrete is heated, several reversible and irreversible chemical reactions can occur, as shown in Table 2.1. In the range of 450°–500°C, portlandite (a.k.a. $Ca(OH)_2$, calcium hydroxide) will undergo dehydroxylation, meaning that the calcium hydroxide begins decomposing in this temperature range [9]. Since portlandite exists in saturated solution in concrete pores, the pH of concrete will decrease when exposed to temperatures above 450°–500°C. Therefore, assessing the pH along the depth of the concrete can indicate the depth of concrete that has been exposed to at least 450°–500°C. The depth of dehydroxylation of the portlandite is often referred to as the carbonation depth, as it will be referred to hereafter.

The pH indicator phenolphthalein is typically used to assess the pH of fire-damaged concrete in a process known as the carbonation test [6,75,85,86]. The color range of phenolphthalein is shown in Figure 4.18 (from Modernsoapmaking.com). A few methods have been used to apply phenolphthalein or pH indicators to fire-damaged concrete. Some have sprayed phenolphthalein solution directly onto the concrete in situ [10,85]. This may require chiseling a certain depth of the concrete to observe the depth of color change from colorless to pink. Others have applied phenolphthalein to concrete powder or concrete cores extracted from the structure [75,87]. The depth of carbonation is typically assumed to be the depth in the concrete at which the phenolphthalein indicator transitions from colorless to pink. One important note when conducting the carbonation test is that carbonation can occur in structures due to natural processes such as aging [68,87]. As a result, the carbonation depth of parts of the structure suspected to be damaged must be compared with parts of the structure known not to be damaged.

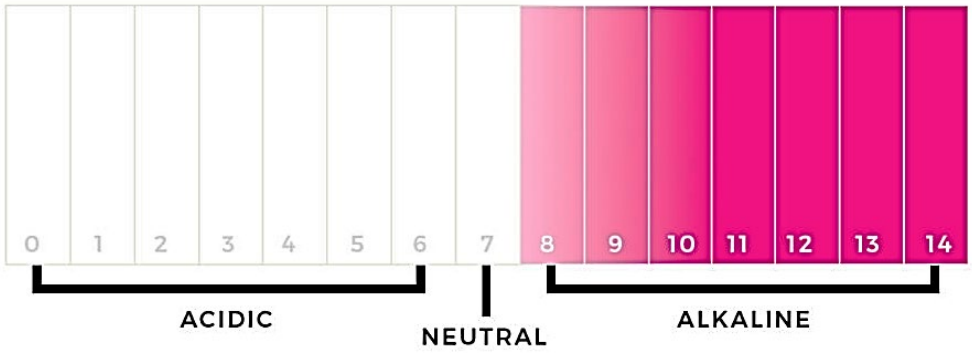

Figure 4.18: Color range of phenolphthalein

One study evaluated fire-damaged concrete using the Carbontest® kit, a commercially available kit that was developed and patented by the researcher [75]. The Carbontest® device, shown in Figure 4.19, collects the concrete powder that results from drilling with an ordinary hand drill and keeps the powder sorted in terms of the order of extraction. A separate study by the same author showed that the device was effective in keeping the powder sorted by order of extraction [87].

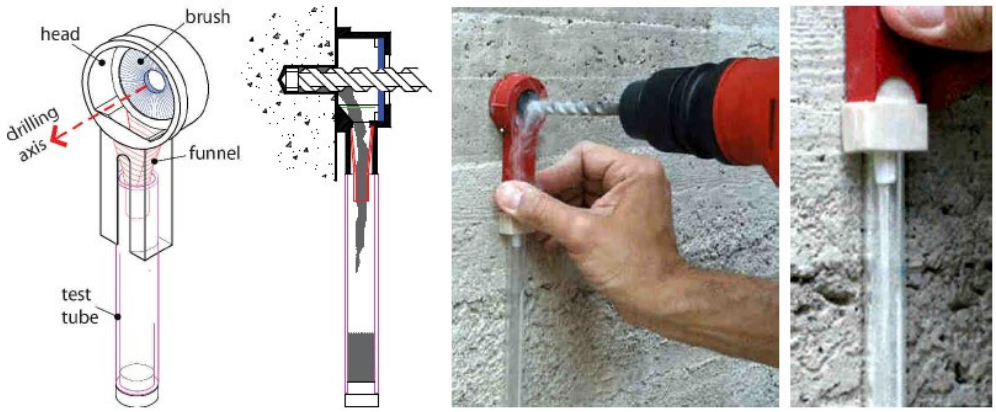

Figure 4.19: Schematic of Carbontest device (L) and Carbontest device in use (R)

In the study, a 135-mm-thick rectangular concrete panel was heated on only one side, up to a maximum surface temperature of 840°C on the heated side. The temperature profile within the panel during the test was estimated using three embedded thermocouples. After cooling, the five Carbontest tubes were filled with powder by drilling into the panel with a hand drill. The tubes were then filled with a phenolphthalein solution, as shown in Figure 4.20 [75].

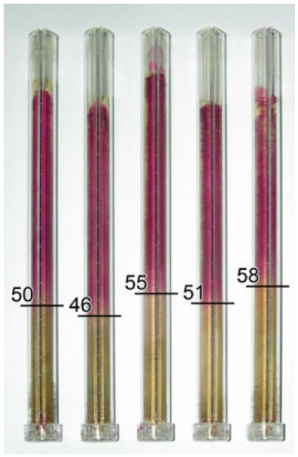

Figure note: Carbonation depth multiplied by 2 (depth of colorless solution) marked in cm.

Figure 4.20: Carbontest tubes with concrete powder after addition of phenolphthalein

From the depth of the colorless part of the concrete powder in the tubes, the carbonation depth of the panel was estimated to be 26 mm, considering that a scale factor of 2:1 between the length of the powder sample and the length of original hole must be applied for a 10-mm drill bit. This result is plotted along with the estimated temperature profile shown in Figure 4.21 (modified from [75]), which shows that the maximum depth of carbonation (the carbonation front) coincided with a maximum temperature of 450°C. These test results suggest that the carbonation test can be used to determine the approximate depth of the 450°C isotherm in the concrete. For reference, the residual strength of concrete that reaches temperature of 450°C is about 50%–60% of the original strength.

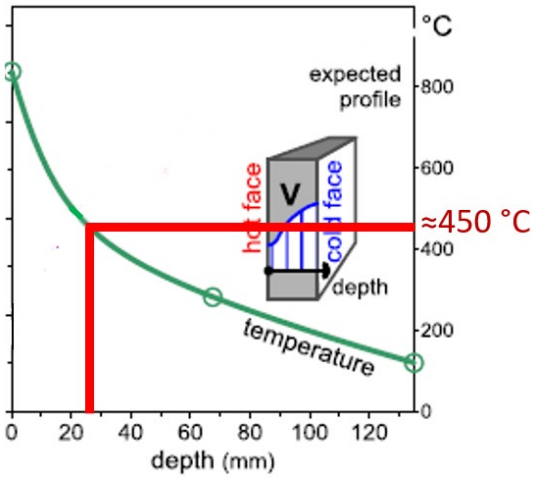

Figure 4.21: Estimated maximum temperature at carbonation front

Another study presented in [10] analyzed the carbonation depth in several buildings exposed to fire of different intensities. For each building, the fire damage was categorized as none, medium, or severe. The carbonation depths were determined by spraying the concrete with phenolphthalein and observing the depth into the concrete at which the phenolphthalein transitioned from colorless to pink. A plot of the measured carbonation depths is shown in Figure 4.22 [10].

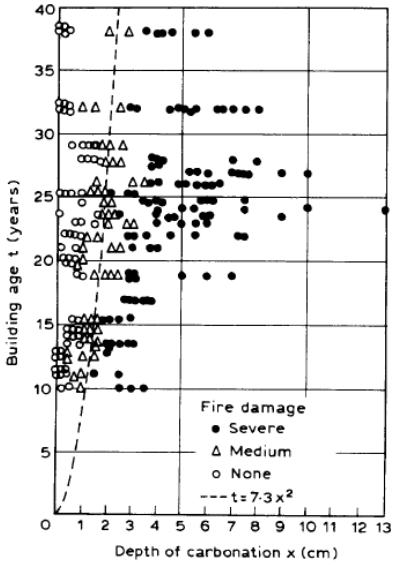

Figure 4.22: Carbonation depths in buildings exposed to fire, measured 3–4 years after fires

4.2.4. Penetration Resistance Tests

Another non-destructive testing method that has been suggested for use with fire-damaged concrete is the penetration resistance test, often known as the commercial testing system Windsor Probe, shown in Figure 4.23 (photo from Humboldtmfg.com) [6,67,68,82]. The test is performed by firing a metal probe into hardened concrete using a probe gun with a

standardized powder cartridge and measuring the depth of penetration of the probe or the length of the exposed probe (Figure 4.24). Like the rebound hammer, the penetration resistance test is a hardness tester, and while no theoretical relationship between penetration depth and compressive strength has been established, empirical relationships can be determined [82]. Generally, the penetration depth is inversely related to the compressive strength of the concrete.

Manufacturers typically provide calibration tables to relate the penetration depth to compressive strength, and the tables may include variables such as aggregate hardness to adjust the penetration depth/strength relationship. These tables may not give accurate results in all cases, and both *ASTM C803-18* and *ACI 228.1R* recommend developing a penetration depth/strength correlation for each concrete mixture and testing kit; however, penetration resistance tests can still be used to delineate zones of poor-quality concrete without using a calibration curve by comparing relative penetration depth values.

Figure 4.23: Windsor Probe testing kit (probe gun, probes, depth gauge)

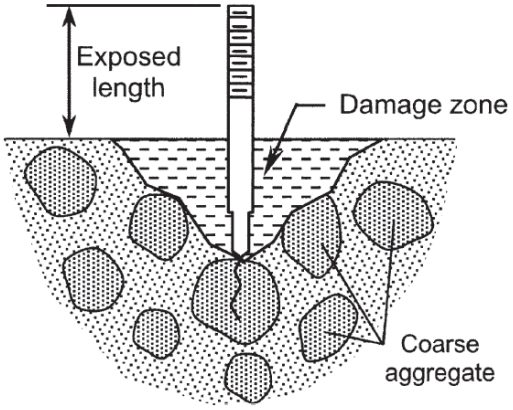

Figure 4.24: Area damaged by insertion of metal probe

To the knowledge of the researchers, no calibration curves for penetration resistance exist for fire-damaged concrete. It has been suggested that penetration resistance tests can be used to determine areas of concrete damaged by fire. Furthermore, *fib* suggests that the relative strength profile along the depth of the concrete could be established by performing the test on the surface of concrete cut/chiseled to various depths [6].

4.2.5. Ultrasonic Pulse Velocity (UPV)

The behavior of various types of waves (mechanical, acoustic, electromagnetic, etc.) as they travel through concrete mediums has been studied and used as a means of assessing the condition concrete in situ [69]. So-called ultrasonic methods are a popular choice for assessing the residual condition of concrete after fire events, as they can delineate areas of concrete damaged by fire. A wide variety of techniques fall under the category of ultrasonic methods; therefore, only the most common method, ultrasonic pulse velocity, will be described here. Ultrasonic pulse velocity tests are performed by monitoring the transmission of elastic waves through concrete. The parameters that can be observed are the velocity of the elastic waves, as well as the attenuation of the elastic waves, although this parameter is much more difficult to study [69].

The elastic waves are generated in the concrete by an emitter transducer, which vibrates at its resonant frequency when sent short pulses of high-voltage electricity. These pulses are detected by a receiver transducer placed nearby [82], and the time of transmission is determined by a device containing a timer that is connected to both transducers. From this, the pulse velocity, C, can be determined by the equation $C = L/t$, where L = distance travelled, and t is time. A generalized schematic of this system is shown in Figure 4.25.

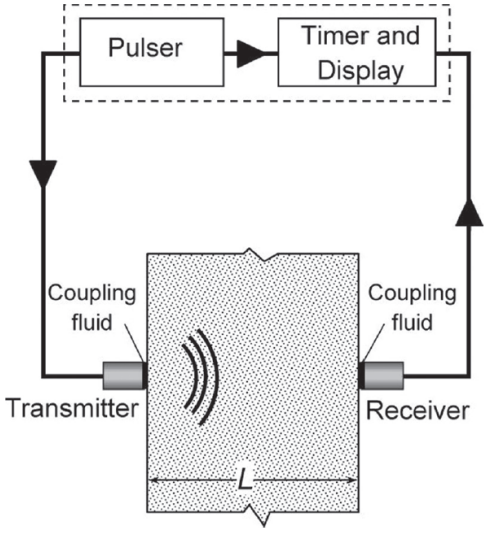

Figure 4.25: Diagram showing principle of ultrasonic pulse velocity test

Figure 4.25 shows the UPV technique applied by direct transmission through the concrete medium. Since this is not always possible depending on the geometry of the member and its location in the structure, it is also possible to use semi-direct transmission and indirect transmission. All three transmission types are shown in Figure 4.26 [69].

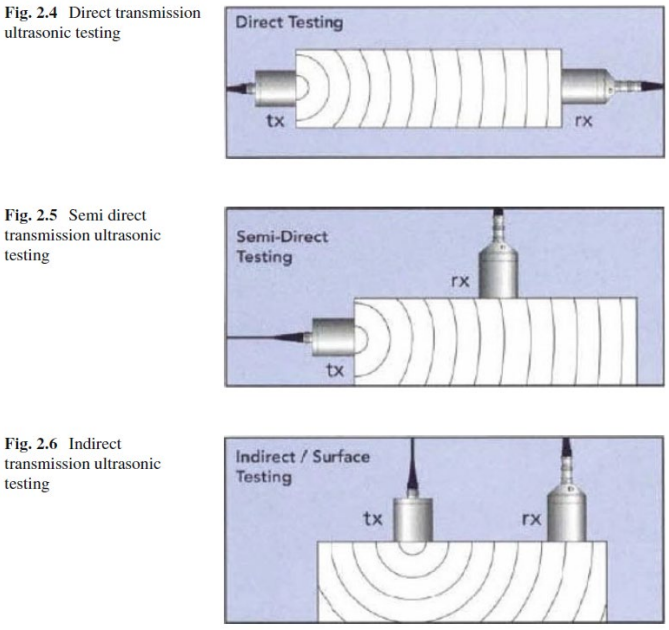

Figure 4.26: Transmission types used for ultrasonic pulse velocity test

The pulse velocity through concrete can be affected by many factors, including aggregate size and type, concrete mixture proportions, moisture content, concrete age, cracks or voids, and the amount and orientation of reinforcing steel, among other factors [69,82]. Owing to these complications and the requirement of special equipment for the tests, UPV tests must be performed by a qualified technician [69].

For example, one study sought to estimate the thickness of the damaged layer in a concrete wall that was heated only on one side according to the ISO 834 fire curve [74]. The concrete panel, shown in Figure 4.27, was 200 mm thick.

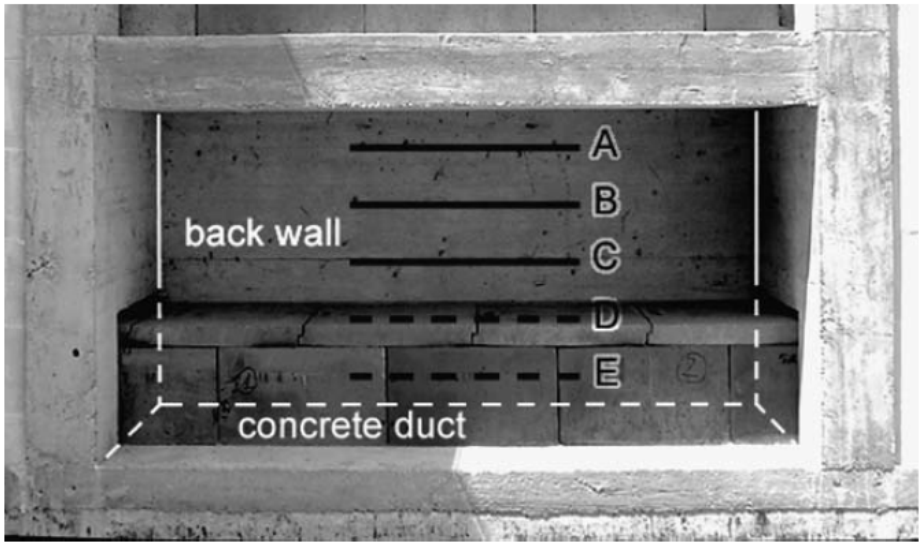

Figure 4.27: Concrete wall heated on only one side

After heating, UPV tests were performed along lines B and C, using the indirect method of transmission. The emitter transducer was held in the same location, while the receiver transducer was gradually moved farther away from emitter. The pulse velocity in concrete generally decreases with increasing damage. As a result, due to the damage gradient present in concrete after a fire, it can be assumed that the elastic wave speed will increase with increasing depth into the concrete, until an undamaged layer has been reached. When a pulse is sent, the path of the wave that arrives first will be the one that strikes the best compromise between the shorter travel distance of the surface layers, and the fast travel speeds of the deeper layers, as shown in Figure 4.28 [74]. When distance reaches a certain point, the velocity will converge on the asymptotic velocity value, which is the velocity of the pulses through undamaged concrete. The X-T plot shown in Figure 4.28 has also been used to analyze data in other studies [88].

An interpretation of the X-T graph produced indicated that the damage thickness was approximately 100 mm. Temperature measurements during heating of the panel indicated that the concrete at 100 mm depth reached a maximum temperature of 250°C, which is very close to the temperature at which concrete begins losing significant compressive strength (300°C) [9].

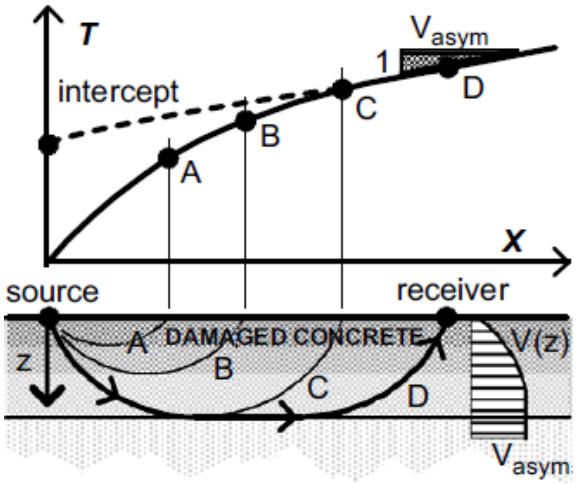

Figure note: X=distance between transducers; T = time of transmission.

Figure 4.28: Schematic of fastest path for pulse, with X-T curve

4.2.6. Other Non-Destructive Testing Methods

Several other non-destructive methods have been implemented in post-fire inspections of structures; however, these methods require a specialist to perform. Some of these methods were used for the structural inspections after the famous 1999 Mont Blanc tunnel fire. A summary of these specialty non-destructive testing methods is provided here.

The seismic refraction analysis method was used after the Mont Blanc tunnel fire to delineate damaged zones of the concrete. Similar to the ultrasonic pulse velocity (UPV) method, this technique uses the propagation of elastic waves to determine the subsurface conditions of the concrete. Unlike the UPV method, which generates the elastic waves by transducers, waves are generated by a steel ball hit against a steel anvil glued to the concrete surface. The

refraction patterns of the elastic waves can be measured be a seismograph and subsequently used to analyze the condition of the concrete [88].

Another method used after the Mont Blanc tunnel fire is the ground-penetrating radar technique. For this technique, the time of travel for electromagnetic impulses through concrete is measured. Since the waves are reflected at interfaces of materials with different properties, such as the layers of varying damage in concrete exposed to fire, the depth of damaged concrete can be determined [88].

Other techniques that been proposed in academic studies include crack pattern mapping, crack density measurements, and drilling resistance tests [67].

4.3 Laboratory Testing Techniques

In some cases, when visual inspections and non-destructive testing techniques are not sufficient, or a greater deal of confidence in the post-fire inspection is desired, laboratory testing methods are an excellent, proven option. Though the focus of this report is on rapid inspection of structures, for which laboratory testing methods are not suitable since they typically take days or weeks to complete, some of the most common methods will be summarized here.

Petrographic analysis is a widely used technique for the assessment of fire-damaged concrete structures. Standard procedures for performing petrographic analysis of concrete are described in *ASTM C856* [89]. To perform a petrographic analysis, cores of concrete must be extracted from the structure and sent to a laboratory with a qualified petrographer. The cores are first inspected with a low-power microscope to observe any changes in obvious changes in color or cracking. Afterwards, the cores are sliced into thin sections, which are then analyzed with a high-power microscope. Petrographic examination is generally used to determine the depth of damage in concrete exposed to fire [90].

Another well-known technique for assessing fire-damaged concrete is chemical analysis. For this technique, concrete must be chiseled along the damaged surface, producing samples for each “layer” of the concrete. The samples are then heated, evaporating the water, which allows the amount of combined water in the samples to be determined. Since the degree of dehydration of the cement paste is related to the temperature experienced, the temperature gradient in the concrete can be estimated [10].

Other methods, which are used mainly in academic research, include X-ray diffraction analysis, thermoluminescence tests, thermo-gravimetric analysis (TGA), differential thermal analysis (DTA), and derivative thermo-gravimetric analysis (TMA) [6,10,67].

4.4 Summary of Existing Inspection Methods for Fire-Damaged Structures

The key findings of the previous sections can be summarized as follows.

General

- Three main methods of inspection are available: visual, non-destructive, and laboratory methods. Visual methods are generally quickest but least accurate. Laboratory methods are generally the most time-consuming but the most accurate. Non-destructive techniques are of medium quickness and accuracy.

Visual Methods

- The condition of non-structural materials such as aluminum can be used to estimate the temperature history within certain areas of a structure.
- Concrete can change to a pink color in the range of 300°–600°C, which is useful since this temperature range coincides with onset of loss of residual strength.

Non-Destructive Testing Methods

- The rebound hammer is one of the most widely used non-destructive testing tools for post-fire inspections. It can be effectively used to delineate areas of concrete that have been damaged by fire, since damaged concrete will result in lower rebound numbers.
- The pullout test has been shown to give excellent predictions of compressive strength in non-fire-damaged concrete. Limited test data with fire-damaged concrete suggest that it is also effective in measuring the residual compressive strength of the near-surface layers of concrete exposed to fire.
- The penetration resistance test has also been shown to give good predictions of compressive strength in non-fire-damaged concrete. No studies could be found of its application with fire-damaged concrete.
- The carbonation test has been shown to be able to determine the 450°–500°C isotherm in fire-damaged concrete. Recently, a commercially available version of the test, Carbontest®, was developed.
- Ultrasonic pulse velocity is also a popular method for delineating areas of damaged concrete after a fire event but requires a trained technician to perform the test.
- The relative characteristics and efficacies of all the non-destructive testing techniques presented in the previous section, apart from the carbonation test, are shown in Figure 4.29 [69]. Note that these characteristics are presented for assessment of non-fire-damaged concrete but still give a good idea of the differences between the tests.

Test method	Cost	Speed of test	Damage	Representati-veness	Reliability of absolute strength correlations
General Applications					
Core	High	Slow	Moderate	Moderate	Good
Pull-out	Moderate	Fast	Moderate/ Minor	Near surface only	Moderate/Good
Penetration resistance	Moderate	Fast	Minor	Near surface only	Moderate
Pull-off	Moderate	Moderate/ Fast	Minor	Near surface only	Moderate/Good
Comparative Assessment					
Ultrasonic Pulse Velocity	Low	Fast	None	Good	Poor
Rebound	Very Low	Fast	Very minor	Surface only	Poor

Figure 4.29: Relative merits of different non-destructive testing techniques

Laboratory Testing Methods

Laboratory analysis methods are very accurate but may take days or weeks to complete. Petrographic examination is the most used laboratory technique for the assessment of fire-damaged concrete.

This page left blank intentionally

5.0 Repair Techniques for Fire-Damaged Concrete Structures

After the fire event and initial inspection, it must be determined if repairs to the affected structure are necessary. Due to concrete's excellent thermal insulation properties, even heavily damaged structures can usually be repaired [10]. Repair actions can range from aesthetic restoration to the replacement of damaged members. Several reports provide recommendations for the design and implementation of repairs in fire-damaged concrete structures [6,10,68]. In general, the following steps should be taken to repair a structure after a fire event:

1) Perform a detailed post-fire inspection and determine the extent and magnitude of damage.
2) Design repairs (if necessary).
3) Implement repairs (if necessary).

This section details the inspection process necessary to decide on the appropriate repairs and presents common repair methods and their implementation.

5.1 Evaluation/Classification of Damage

Although a quicker inspection will likely be performed immediately after a fire event to determine whether a structure poses any immediate safety hazards, a more detailed inspection should follow at a later time to decide what repairs, if any, are needed. The purpose of the detailed inspection is to determine the level of damage at various locations of the structure affected by fire, which will inform the repair actions needed for each area. The International Federation for Structural Concrete (*fib*) recommends the following steps for a detailed post-fire inspection [6]:

1) Collect data about the fire event and its effect on the structure.
2) Examine the damage due to the fire and the extinguishing efforts.
3) Classify the severity of the damage.
4) Identify and select repair methods.

Data collected about the fire event should include the time history of the fire and the location history of the fire. This could be ascertained from eyewitnesses such as first responders or from surveillance footage. Another option is to examine the visual condition of structural and non-structural materials such as steel or plastics in various areas of the structure. Materials that have melted, charred, or suffered other effects from heat exposure can indicate maximum temperature reached during the fire at certain locations in the structure. This technique was described in greater detail in Section 4.1.1. The classification of damage is usually performed by splitting up the affected area into zones and classifying the damage level in each zone using predetermined damage classes. *fib* suggests using the visual

classification chart shown in Figure 4.6 to classify damage levels, but classifications could also be based on the results of non-destructive tests or laboratory analysis of samples from the structure. The most common non-destructive testing methods for post-fire inspections are the rebound hammer and ultrasonic pulse velocity methods, as both can be quickly implemented over large areas. Non-destructive methods, however, are highly variable and often cannot directly measure residual mechanical properties of materials, such as the residual strength of concrete. If a more precise characterization of the condition of these materials is desired, samples of concrete and steel suspected to be damaged may be sent to a laboratory for more precise analysis such as petrographic examination, compression tests, or tensile tests. After the damage classification has been performed, the appropriate repair actions need to be determined for each location, which is described in the following section.

5.2 Common Repair Techniques

Once the damage has been thoroughly assessed, appropriate repairs should be designed and implemented. Common repair methods include [6,10]:

- Cleaning and aesthetic restoration.
- Repair of concrete surfaces with mortar or resins.
- Repair of concrete members and restoration of the original shape with sprayed concrete or flowable concrete.
- Strengthening of members by addition of reinforcing steel or fiber-reinforced polymers (FRP).
- Complete replacement of selected elements.

When designing a repair for a member, the cost of repair versus the cost of replacement should first be considered. Though fire-damaged elements can often be repaired, certain elements, such as those with prestressing steel, may be too difficult or too expensive to repair. In general, the objectives of a repair are to restore the load-bearing capacity and fire resistance of the member, restore the original shape of the member, and protect the reinforcement from corrosion over the remainder of its lifetime [10]. Sample calculations for assessing the strength of fire-damaged and repaired members can be found in Appendix B of *Assessment, Design, and Repair of Fire-damaged Structures* [68].

For reinforced concrete, the main steps in the repair process are to remove damaged concrete, replace the concrete to restore the member to its original size, and replace or supplement weakened reinforcement. It is generally recommended that all concrete that experienced temperatures above 300°C be removed. The 300°C isotherm in the concrete can sometimes be determined by observing the depth of pink discoloration in some concretes or can be determined by laboratory analysis on core samples collected from the structure [6,68]. In some cases, such as when buckling of reinforcement has occurred (Figure 5.1), additional concrete may need to be removed from behind the reinforcement to ensure that the concrete replacement material can fully surround the reinforcement. Damaged concrete can be removed by hammer and chisel, powered breaking tools, or high-pressure water jets.

Removal of concrete with a hammer and chisel is only practical when the damaged area is small. If extensive areas of concrete have been damaged, powered breaking tools or high-pressure water jets are more suitable [68].

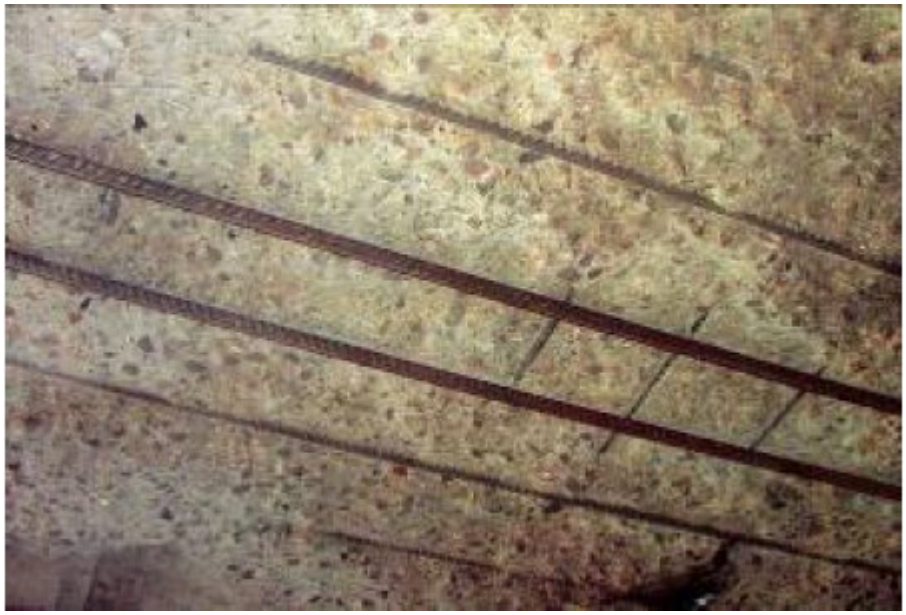

Figure 5.1: Buckled reinforcing bars in underside of slab

Sprayed concrete (e.g., shotcrete) or flowable concrete are both popular options for replacing concrete. Some of the advantages of sprayed concrete over flowable concrete are that no formwork is needed, and it can be much easier to apply in many circumstances. On the other hand, flowable concrete may be a better option where large amounts of concrete need to be replaced, or the reinforcement is very dense, which could result in air voids if sprayable concrete were used. The advantages and disadvantages of sprayed concrete compared to flowable concrete for concrete replacement are summarized in Figure 5.2 [68].

Advantages	Disadvantages
No formwork required Rapid placing Dense, homogeneous, high quality concrete Reduction in access requirements Good bond to substrate and between layers Reduced thermal stresses when placed in several layers Suitable for use of soffits where it may be difficult to get concrete to flow into a shutter	Specialists required for design and application Variable concrete quality (mainly with dry process) High material costs (pre-bagged materials, wastage) Poor encasement behind dense concentrations of reinforcement

Figure 5.2: Pros and cons of sprayed concrete for replacing fire-damaged concrete

For more minor damage, concrete can be replaced with mortar applied with a trowel. Unlike for sprayed or flowable concrete, bonding aids must be applied to the substrate before application of the mortar, to create a sufficient bond between the existing concrete and the

mortar. Resins have also been used to repair lightly damaged areas of concrete, though the performance of these materials under heat exposure is not well known [6,68].

After the replacement of the concrete with sprayable concrete, flowable concrete, mortars, or resins, the bond between the substrate and repair material should be assessed by a pull-off test [6]. The pull-off test is performed by attaching a circular disc to the repair material with an adhesive such as epoxy and pulling on the disc until failure. A typical pullout test setup is shown in Figure 5.3 [82].

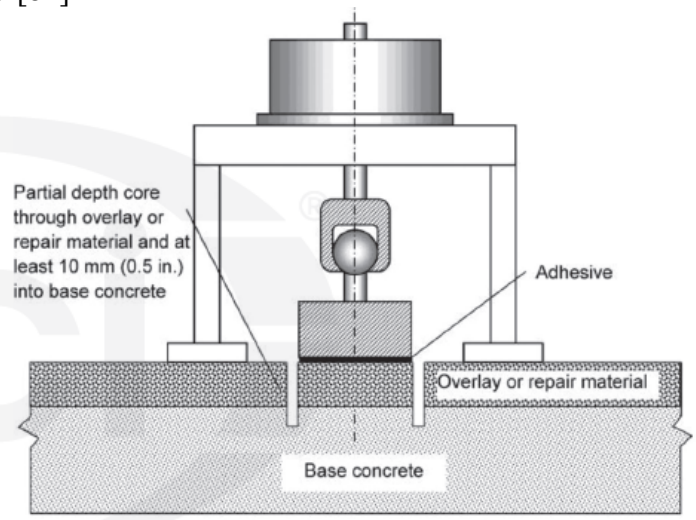

Figure 5.3: Pullout test setup

As shown in Figure 5.4, four different failure modes may occur during the pull-off test. As a result, only when failure between the repair material and substrate occurs should the pull-off load value be taken as the bond strength. Further details for application of the pull-off test for assessing bond between repair materials and existing concrete are described in *ASTM C1583-20* [82]. To ensure a sufficient bond, *fib* recommends a mean value of 1.5 N/mm^2 for a series of pull-off tests, and minimum value of 1.0 N/mm^2 for any one test in the series.

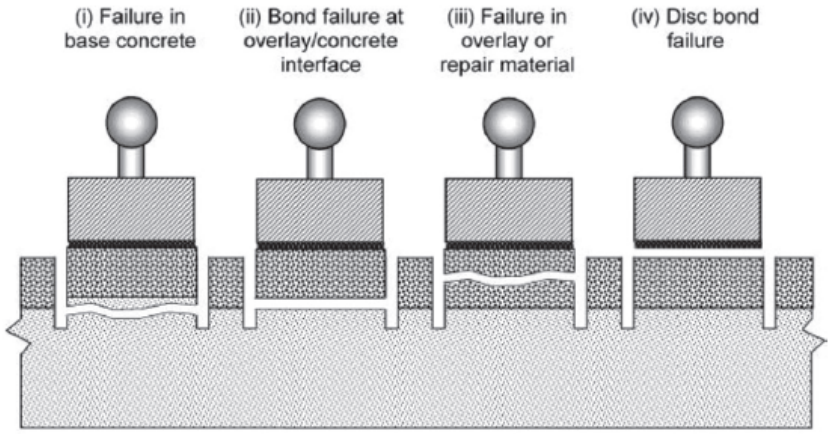

Figure 5.4: Possible failure modes during the pull-off test

In addition to concrete, reinforcing steel may also need to be replaced or supplemented after a fire if the residual strength of the steel has decreased. The residual strength of steel can be determined via tensile tests on specimens collected from the structure, or by in-situ hardness tests. Reinforcement can be added by lapping with the existing reinforcement, but it must be ensured that the required anchorage length is provided. Sleeve and wedge couplers can be used to attach bars in compression bars, while tension couplers can be used to attach bars in tension [6].

Another repair option for damaged members are fiber composite materials (FRPs), specifically carbon fiber reinforced polymers (CFRPs) and glass fiber reinforced polymers (GFRPs). FRP materials have a high-tensile strength, making them suitable for areas such as the positive flexure zones of beams and slabs. The FRP materials, such as FRP plates, are bonded to the damaged member with an adhesive to bolster the strength of the member. These types of repair materials must be applied to sound, undamaged concrete to ensure a good bond to the substrate (the existing concrete) [68,91].

5.3 Case Studies in Repair of Fire-Damaged Structures

In this section, two case studies of repairs of fire-damaged structures and members will be presented, which showcase some of the repair methods discussed in the previous section. The first case study details the repair process of the Tauern Tunnel after a 1999 fire, and the second describes the repair of a fire-damaged prestressed roof girder that was repaired and subjected to load testing to assess its residual strength after repair. Additional case studies can be found in Appendix A of *Assessment, Design, and Repair of Fire-Damaged Concrete Structures* [68].

5.3.1. Tauern Tunnel, Austria

A 2001 paper by Leitner [92] reviewed the repair of the Tauern Tunnel after a 1999 fire. The Tauern Tunnel, located in Salzburg, Austria, experienced a severe fire event on May 29, 1999, after a truck crashed into stopped vehicles and caught fire. Damage to the tunnel was extensive, and remedial work took three months to complete and cost about $6.5 million.

The cross-section of the tunnel originally consisted of an outer lining of shotcrete and bolts and an inner lining of unreinforced concrete. The tunnel also featured a transverse ventilation system separated from the roadway by a 150-mm-thick, cast-in-place reinforced concrete ceiling, which was partially supported by ceiling suspenders and partially supported by the sidewall. A cross-section of the tunnel is shown in Figure 5.5 [92].

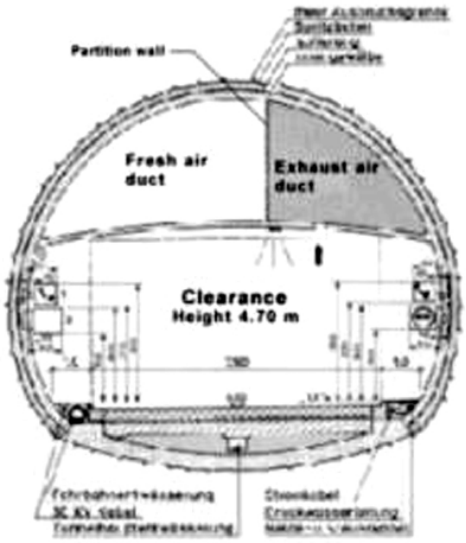

Figure 5.5: Cross-section of Tauern Tunnel before 1999 fire

The fire damage included extensive and deep (up to 400 mm) spalling of the sidewall, spalling and cracking of the ceiling concrete, damage to the ceiling reinforcement, and damage to the pavement and electrical housings.

The sidewall was repaired by removing the damaged concrete, adding rebar, and applying shotcrete. First, 50 mm of the sidewall concrete was removed with high-pressure water jets to remove damaged concrete and create a suitable surface for applying the shotcrete. Next, holes were drilled into the existing concrete, and rebar was inserted into the holes to help attach the existing concrete to the soon-to-be-applied shotcrete layer (Figure 5.6) [92]. Wire mesh was also installed along the sidewall. After the rebar and wire mesh were installed, shotcrete was applied to the sidewall. A cross-section presenting the details of the repairs to the sidewall is shown in Figure 5.7 [92].

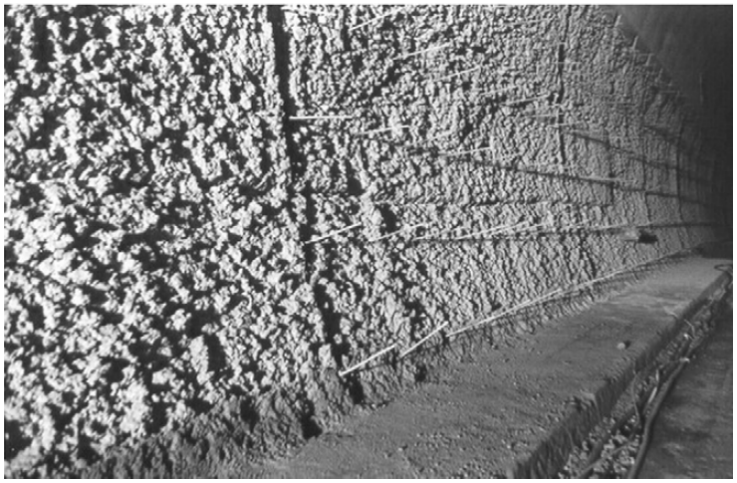

Figure 5.6: Rebar to connect existing concrete to shotcrete layer

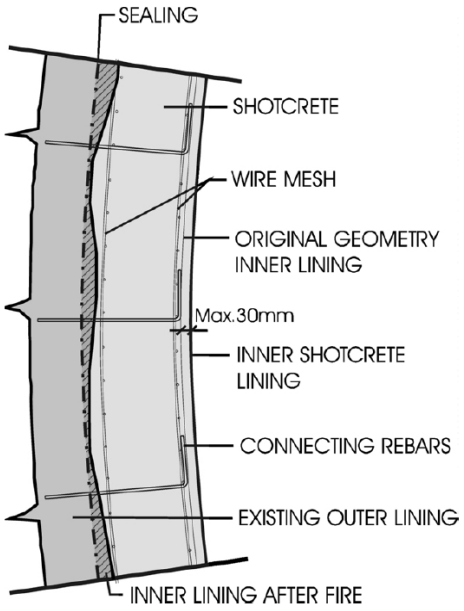

Figure 5.7: Schematic of repairs for sidewall

Due to the extensive damage to the ceiling, it was decided to replace 300 meters of the damaged cast-in-place ceiling with precast concrete panels, as shown in Figure 5.8. Furthermore, a rectangular concrete strip was added to the sidewall to support the ceiling. A schematic of the repairs is shown in Figure 5.9.

Figure 5.8: Installation of precast ceiling panels

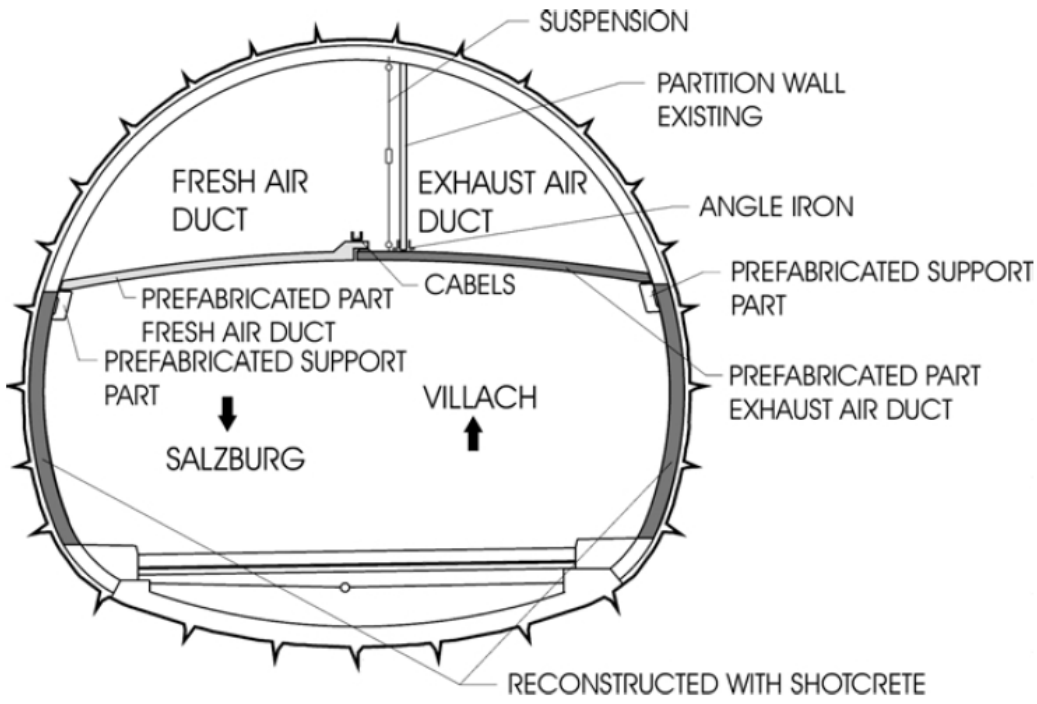

Figure 5.9: Repairs of sidewall and ceiling

5.3.2. Full-Scale Fire Test of an Industrial Precast Hall

A case study of a repair of a fire-damaged pretensioned roof girder was presented in *Fire Design of Concrete Structures – Structural Behavior and Assessment* [6]. In 1974, an industrial warehouse made with precast elements was constructed for use in a full-scale fire test. The warehouse was 12 m x 18 m in plan and consisted of three portal frames. Wood was used as a fuel, and the fire exposure of the building during the test was roughly equivalent to that of the ISO 834 fire curve.

After the fire test, one of the pretensioned roof girders was removed from the structure so that it could be repaired and subjected to a load test. The 18-meter-long roof girder had twelve 7-wire prestressing strands in the bottom flange, and two strands in the top flange, and the depth of the section varied along its span. As shown in Figure 5.10, the girder was badly damaged after the test. Extensive spalling exposed some of the shear stirrups and longitudinal rebar, and the concrete cover for the prestressing strands was missing in some areas [6].

To prepare the girder for the application of shotcrete, the surface of girder was cleaned, and damaged concrete was removed with a pneumatic hammer and a sandblaster. Shotcrete was then used to replace the damaged and spalled concrete, as shown in Figure 5.11. The midspan of the girder after the repairs is shown in Figure 5.12.

Figure 5.10: Cross-section of pretensioned roof girder (L), pretensioned roof girder after fire test (R)

Figure 5.11: Application of shotcrete to damaged girder

Figure 5.12: Midspan of girder after repair

After the repair, the beam was subjected to a load test to assess its residual capacity. Four-point loads were applied to the beam (Figure 5.13) and gradually increased until failure. The beam was able to carry 2.45 times the design service load of the beam before failure; moreover, the beam was found to have an ultimate capacity of 1629 kN-m compared to the expected capacity of 1616 kN-m. Overall, the test showed that the fire-damaged beam could be satisfactorily restored using common repair techniques.

Figure 5.13: Load testing setup for girder

5.4 Summary of Repair Methods for Fire-Damaged Concrete Structures

The key points from the previous sections on repair methods of fire-damaged concrete structures can be summarized as follows:

- Fire-damaged concrete structures and members can usually be repaired rather than replaced.
- The Tauern Tunnel in Austria was successfully repaired after a major tunnel fire event.
- The main steps in the repair process of reinforced concrete are to remove damaged concrete, replace the concrete to restore the member to its original size, and replace or supplement weakened reinforcement.
- Concrete material is usually replaced by sprayable concrete (e.g., shotcrete) or flowable concrete when larger volumes of concrete must be replaced.
- Strengthening fire-damaged members with fiber-reinforced polymers (FRPs) is becoming more common as the materials become commercially available.

This page left blank intentionally

6.0 Survey of Post-Fire Inspection Practices of Other State DOTs and Transit Authorities

In addition to the review of existing literature on fire and structures presented in the previous sections, a survey of post-fire inspection protocols, standard practices after a fire, and fire research efforts of other state DOTs and transportation organizations was conducted. The purpose of this survey was to evaluate the common practices for post-fire inspections of tunnels among organizations across the United States; gain an understanding of the concerns that other organizations have regarding fire; and gather additional literature and knowledge on the subject. To conduct this survey, engineering personnel in these organizations were contacted via email and asked if they would be willing to discuss their experience and knowledge of post-fire inspections with the UMass research team. This section describes the inquiry process, provides brief summaries of each discussion with officials at these organizations, and presents the key findings from correspondence and discussions with these organizations.

6.1 Reaching Out to State DOTs and Transit Authorities

In total, 49 state DOTs and 4 other transportation agencies were contacted via email (some states have other agencies aside from the state DOT that own tunnels, which is why they were included in the survey). Of those contacted, 31 state DOTs and 3 other transportation agencies replied, as shown in the map in Figure 6.1. Further details of the responses to the initial inquiry are presented in Figure 6.2. Though some organizations stated that they owned no or few tunnels, or had minimal concerns about fire, several of these replies led to video conferences and email discussions between members of the organizations and the UMass team. To facilitate the discussions with the members of these organizations, a questionnaire was developed and is included in Appendix A. The questions covered a wide range of subjects, including organizations' standard post-fire inspection practices, personal accounts of post-fire inspection by organization members, and research efforts related to post-fire inspection or assessment of structures. During video conferences, these questions were typically asked one by one, which helped field consistent responses. Email discussions were less structured, but the questionnaire was used as a guide. The next section will show summaries of the most important points from each email correspondence and video conference.

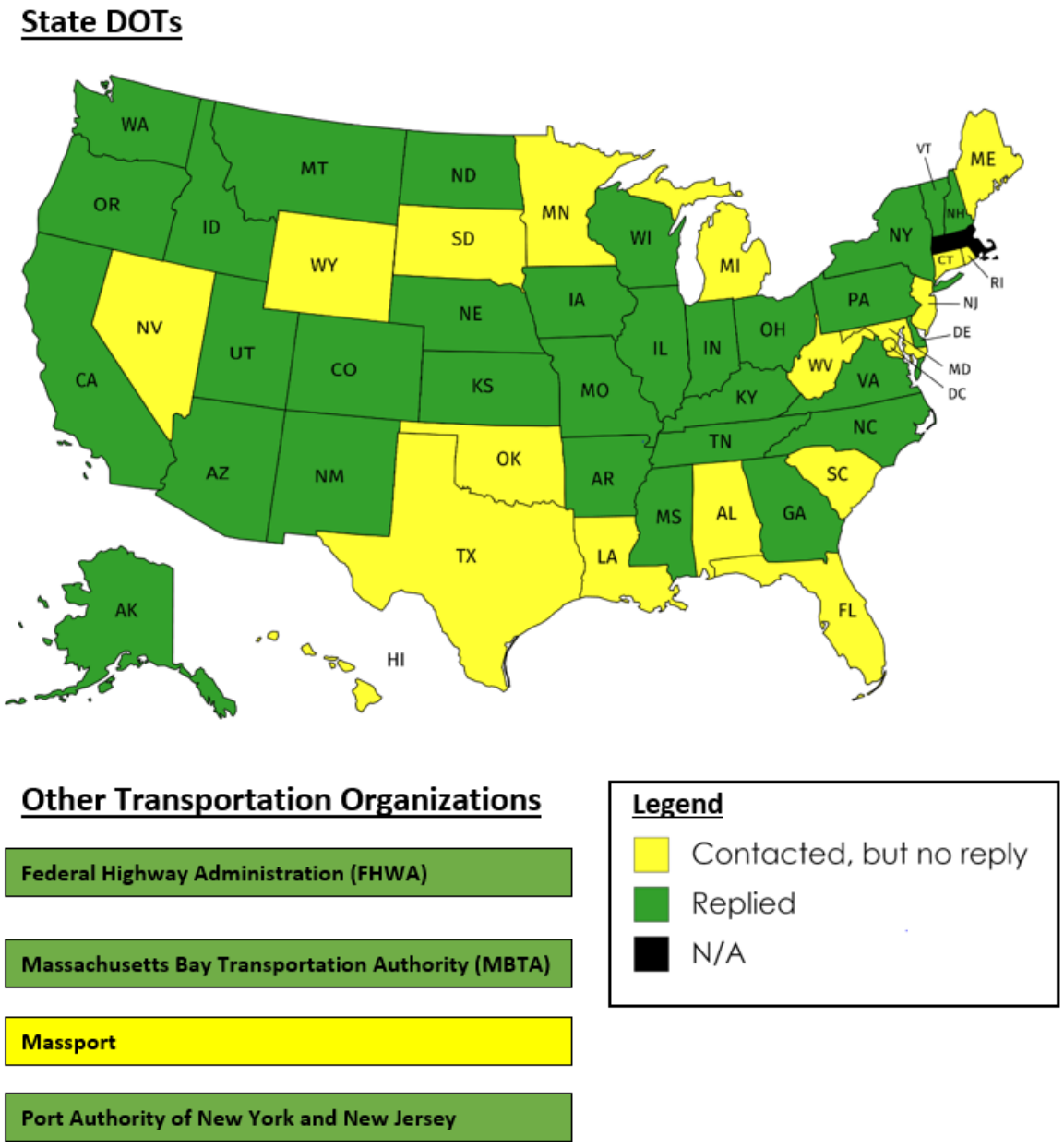

Figure 6.1: Summary of reach-outs and replies

Contacting DOTs and Other Transportation Authorities	
# Organizations Contacted by UMass	53
# Organizations That Replied to UMass	34

Response/Outcome of Those Who Replied	
Held Video Conference with UMass Team	**11**
Discussed via Email with UMass Team	**7**
Does Not Own Tunnels	**10**
Owns Few Tunnel/Minimal Concerns about Fire	**3**
Other	**3**

Figure 6.2: Summary of responses to inquiry

6.2 Summaries of Email Correspondence and Video Conferences with State DOTs and Transit Organizations

Some organizations were willing to discuss their experience with post-fire inspections in more detail via video conferences. These video conferences were held from May to June 2020 and were based around the questionnaire included in Appendix A. In some cases, organizations were interested in participating in the survey, but video conferences were not practical or were deemed unnecessary; therefore, some discussions were conducted by email. This section will summarize the key discussion points and insights from the video conferences and email correspondence with the organizations.

6.2.1. Summaries of Email Correspondence

Arkansas DOT (correspondence with Chad Adams, P.E., District Four Engineer)

- Arkansas DOT only owns one tunnel.
- The tunnel has not experienced any fires.
- Their post-fire protocol is the same inspection procedure as for their routine inspections, based on the *FHWA National Tunnel Inspection Standards* (NTIS).

Kentucky DOT (correspondence with Joshua Rogers, P.E., TE Branch Manager)

- Kentucky DOT owns 8 tunnels, one of which is complex with ventilation.
- They have had few fires in their tunnels.
- In the case of a fire, the post-fire inspection would be an element-level inspection in accordance with following documents: *FHWA Specifications for the National Tunnel Inventory* (SNTI), *FHWA Tunnel Operations, Inspection, and Evaluation Manual* (TOMIE), and an inspection manual specifically for Kentucky's tunnels.

Missouri DOT (correspondence with David Koenig, Bridge Management Engineer)

- Missouri DOT only operates one tunnel.

- David did not recall any recent fire incidents.

New York DOT (correspondence with James Flynn, P.E., Deputy Chief Engineer of Structures)

- New York DOT only owns 1 tunnel.
- The tunnel does not have any history of fires.

Ohio DOT (correspondence with Brandon Collet, P.E., Structures Planning Engineer)

- Ohio DOT owns 1 tunnel, which is a cast-in-place cut and cover tunnel.
- Brandon did not recall any significant fire events in the tunnel.

Port Authority of New York and New Jersey (correspondence with Steven Vecchione, P.E., Manager – Structural Integrity)

- The Port Authority owns 4 tunnels, which are all complex with ventilation systems.
- Frequently experience tunnel fires, but none in the last 13 years has resulted in structural damage.
- Port Authority employees conduct post-fire inspections.

Tennessee DOT (correspondence with Thomas Quinn, P.E., Assistant Director of Structures Division)

- Tennessee DOT owns 9 tunnels. One is bare rock cut, two are complex with ventilation, and six are concrete-lined bored tunnels.
- No fire incidents have occurred in the tunnels.
- In the case of a fire, the bridge inspection protocol would be used, which entails visual inspection, rock hammer soundings, and the extraction and analysis of cores, if needed.
- Tennessee DOT employees generally conduct the inspections, but private consultants are used in some cases.
- The inspection process is not standardized; instead, it is up to the discretion of the inspector.

6.2.2. Summaries of Video Conferences

Alaska DOT (discussion with Gordon Burton, Facilities Manager)

- Alaska DOT has 1 tunnel, which is a bored and rock-lined tunnel.
- Have experienced 2 locomotive fires, neither of which resulted in damage.
- In the case of a fire, the post-fire inspection protocol for bridges would be used for the tunnel.
- Use private consultants for detailed inspections after the fire.
- Main structural concerns for the tunnel after a fire are the condition of the rock liner and the geotechnical mesh over the rock.
- Inspection procedures are based on FHWA's TOMIE.

Caltrans (discussion with Vassil Simeonov, Ph.D., Supervising Bridge Engineer)

- Most notable tunnel fire event was the 1982 Caldecott Tunnel fire.
- No specific post-fire protocol is used, but the inspection would consist of looking for discolored concrete and testing the concrete with a rock hammer.
- Caltrans does not use private consultants for inspections, only state inspectors.
- Major structural concerns post-fire are plenum structures (hung ceiling slabs) and any equipment suspended above the traffic.
- Caltrans' Materials Engineering and Testing Services (METS) lab conducts all research for the organization.

Colorado DOT (discussion with Tyler Weldon, P.E., State Maintenance Engineer)

- Colorado tunnels have a wide variety of constructions: cast-in-place tunnels, rock and shotcrete-lined tunnels, and cut and cover tunnels.
- Two recent fires have occurred: a 2019 car fire and a 1998 RV fire, neither of which resulted in structural damage.
- For post-fire inspections, state inspectors follow the *FHWA National Tunnel Inspections Standards* (NTIS). Private consultants are also on call to perform an inspection after a fire event.
- Biggest structural concerns post-fire are the ceiling panels and any equipment suspended above traffic that could fall.
- Recommended looking at the NCHRP report on highway bridge fire hazard assessment.

FHWA (discussion with Stephen Bartha, P.E., Structural Engineer)

- Stephen used to work for MassDOT and has conducted several post-fire inspections for bridges.
- The post-fire inspection consisted of general inspection of concrete condition (spalling, cracking, etc.), and identifying any areas of pink/red concrete, which can indicate fire damage.
- Visual guides would be very helpful for an inspector during post-fire inspections.

Illinois DOT (discussion with Sarah Wilson, P.E., Bridge Maintenance Engineer)

- Illinois has 3 tunnels, 2 of which are exit/entrance ramps for another roadway.
- Illinois has not experienced any tunnel fires but has experienced bridge fires.
- No written protocols for the post-fire inspection are used. Visual inspection is focused on locating any possible distortion or warping in the steel members (Illinois' bridges are mostly constructed of steel).
- Main concerns after a fire are the condition of steel beams and any loose concrete that could injure motorists.

Massachusetts Bay Transportation Authority (discussion with Joe Guyder, P.E., Director of Civil Infrastructure, and Brian Mellen, P.E., Manager of Civil Engineering)

- Several minor debris fires have occurred, but no major fires.
- MBTA has a tunnel inspection guide, but it does not contain any information for post-fire inspections.
- Would use the post-fire inspection information in FWHA's TOMIE if a major fire occurred.

North Carolina DOT (discussion with Gichuru Muchane, P.E., Assistant State Structures Engineer)

- North Carolina has not experienced any tunnel fires.
- Bridge inspectors would conduct a post-fire inspection. No specific protocol for tunnel fires is in place, but inspectors are trained in accordance with the NBIS bridge inspection protocols.
- Most significant concern after a fire would be the condition of overhead lighting.
- North Carolina DOT conducted some research to determine the residual capacity of steel girders exposed to fire.

Nebraska DOT (discussion with Fouad Jaber, P.E., Assistant State Bridge Engineer)

- Nebraska does not have any tunnels.
- Have had 2 recent major bridge fires.
- The post-fire inspection of the bridges consisted of petrographic analysis of cores, and LIDAR to determine straightness of girders.

Oregon DOT (discussion with Albert Nako, P.E., Seismic Standards Engineer)

- Oregon has few tunnels, all of which are less than 1,100 feet in length.
- Albert did not recall any bridge or tunnel fires in the last 17 years.

Pennsylvania DOT (discussion with Lou Ruzzi, P.E., District Bridge Engineer, and Ben DeVore, P.E., Tunnel Maintenance Engineer)

- Frequently experience car fires in their tunnels. One fire in the early 2000s was quite large and resulted in damage to wall tiles.
- No specific post-fire inspection protocol exists; rather, the typical tunnel inspection protocol is followed.
- Major structural concerns after a fire include suspended ceiling panels and portals of the tunnel.

- Pennsylvania conducted research with Lehigh University to develop a visual inspection protocol for their bridges.

Virginia DOT (discussion with Prasad Nallapaneni, P.E., Assistant State Structure and Bridge Engineer)

- A tunnel fire in 2016 resulted in damage to the tunnel tiling.
- No post-fire inspection protocol is followed; inspection procedure is at the discretion of the inspector.

6.3 Findings of the Survey

This section presents the results of the survey of post-fire inspection practices of state DOTs and transit organizations. In total, of the 34 organizations that responded to the initial inquiry, 18 organizations took part in the survey via video conferences or email correspondence (Figure 6.2). Note that the FHWA does not own tunnels, and the discussion with FHWA was focused on understanding the federal guidelines for inspections. For reference, per the *FHWA National Tunnel Inventory* data as of June 2020, the number of tunnels owned by each DOT that participated in the survey is shown:

- California (Caltrans): 62 state-owned tunnels
- Massachusetts: 45 state-owned tunnels
- Colorado DOT: 20 state-owned tunnels
- Virginia DOT: 11 state-owned tunnels
- Oregon DOT: 9 state-owned tunnels
- Pennsylvania DOT: 8 state-owned tunnels
- Tennessee DOT: 7 state-owned tunnels
- Kentucky DOT: 4 state-owned tunnels
- North Carolina DOT: 4 state-owned tunnels
- Illinois DOT: 3 state-owned tunnels
- Alaska DOT: 2 state-owned tunnels
- New York DOT: 1 state-owned tunnel
- Ohio DOT: 1 state-owned tunnel
- Arkansas DOT: 1 state-owned tunnel
- Missouri DOT: 0 state-owned tunnels
- Nebraska DOT: 0 state-owned tunnels

Of the 12 states with the most state-owned tunnels in the United States, 6 participated in the survey (1 of the 12 is Massachusetts). Data about the number of tunnels owned by the MBTA and the Port Authority of New York and New Jersey were not readily available. Missouri DOT does not own any tunnels but does have jurisdiction of the maintenance of a tunnel in the state. Nebraska also does not have any tunnels, and as such the discussion with them focused on their experiences with bridge fires.

The survey was focused on identifying each organization's experiences with tunnel fires and their procedures for post-fire inspections. A summary of the organizations' responses to these questions is shown in Table 6.1. A wide variety of responses were received. For instance, of the 15 organizations with tunnels, 8 reported having experienced tunnel fires. Most of the reported fires were small and did not cause significant damage. It is also worth noting that most of the organizations that reported experiences with tunnel fires were those that owned the most tunnels.

Table 6.1: Summary of surveyed organizations' experiences with tunnel fires and their post-fire inspection procedures

Organization	Has experienced tunnel fires?	Has a written post-fire protocol for tunnels?	Uses private consultants for post-fire inspection of tunnels or bridges?
Arkansas DOT	No	Yes	Unknown
Colorado DOT	Yes	Yes	Yes
Kentucky DOT	No	Yes	Unknown
Missouri DOT	No tunnels	Unknown	Unknown
North Carolina DOT	No	No	Yes
Ohio DOT	No	Unknown	Unknown
Pennsylvania DOT	Yes	No	Yes
Port Authority of NY and NJ	Yes	Yes	Unknown
Tennessee DOT	No	No	Yes
Virginia DOT	Yes	No	Yes

Of the 15 organizations, 4 reported using a written document for their post-fire tunnel inspection procedures. All 4 of these organizations stated that they conduct their post-fire tunnel inspections in accordance with guidelines specified under the *National Tunnel Inspection Standards* (NTIS). Furthermore, Kentucky DOT stated that they referred to the FHWA document *Tunnel Operations, Maintenance, Inspection, and Evaluation Manual* (TOMIE) for their post-fire inspections. TOMIE contains a brief section on post-fire inspections, which explains how to assess damage based on visual techniques, including examining the condition of debris material (melting, charring, etc.) and identifying color changes in concrete that occur due to heat. None of the organizations surveyed indicated that they had any sort of custom post-fire protocol for their specific tunnels. The other organizations that did not use written protocols stated that inspection would be performed at the discretion of the inspectors. The organizations typically said that evaluations consisted of visual inspection and inspection of concrete with a rock hammer. Only a few reported experiences with non-destructive or laboratory testing, which was usually conducted by private consultants.

Of the organizations that did not use a post-fire protocol for their tunnels, several reported that if a major tunnel fire were to occur, they would use their protocols for assessing the condition of bridges after fire to assess their tunnels. Moreover, many organizations stated that they would call on their bridge inspectors to conduct a post-fire inspection of a tunnel. This is a significant point, as many states that did not report having tunnel fires reported numerous bridge fire incidents. The Colorado DOT noted that the National Cooperative Highway Research Program (NCHRP) *2013 Highway Bridge Fire Hazard Assessment* report contains information on the effect of fire on structural materials and contains information on post-fire assessment of bridges.

Most organizations reported using private consultants for the post-fire evaluations of their tunnels or bridges, including Stantec, Mott MacDonald, and Hardesty & Hanover. In most cases, consultants were called in after an initial inspection by personnel from the DOT or transportation agency to conduct a more thorough investigation. Some of these organizations stated that they have private consultants on call in case of the urgent need for a post-fire inspection.

Another question posed to several organizations assessed their main concerns for their tunnels after a fire, noting that tunnel constructions can vary widely. The organizations with complex tunnels all reported being concerned about the residual strength of ceiling and plenum panels, and about the condition of any overhead fixtures such as lighting or fans that could fall into traffic. Furthermore, many organizations expressed concerns about loose concrete falling onto the roadway, either from the ceiling panels or the liner.

Of the 15 organizations with tunnels, only Pennsylvania DOT reported conducting research related to the post-fire fire condition or evaluation of tunnels. A couple of states reported that they had conducted research on the post-fire condition of bridges.

6.4 Summary of the Findings of the Survey

The findings of the survey of the post-fire inspection practices and procedures from discussions with 18 respondents can be summarized as follows.

- Most surveyed organizations do not have a written protocol for post-fire tunnel inspection. Those who do rely on the guidelines in FHWA's *Tunnel Operations, Maintenance, Inspection, and Evaluation Manual* (TOMIE).
- Eight of the 15 surveyed organizations that owned tunnels reported experiencing tunnel fires, but most were not severe.
- Many organizations reported that in the event of tunnel fire, they would employ the same inspection principles used for post-fire evaluations of their bridges to inspect the tunnel.
- Many organizations have used private consultants to conduct post-fire evaluations of their bridges and tunnels.

- There is a general lack of research efforts related to the post-fire inspection of tunnels.

7.0 Preliminary Experimental Testing at UMass Amherst

This section describes the experimental testing conducted as part of this project. The scope included the purchase and setup of a heating system, procurement of sample specimens for testing, thermal and physical testing of specimens, and evaluation of results.

7.1 Purpose

The purpose of the experimental testing was to evaluate the feasibility and effectiveness of potential methods for assessing the damages to structural and non-structural tunnel elements due to heat exposure. This included obtaining and testing a heating system, conducting trial tests on representative samples, troubleshooting potential problems, and determining the feasibility and scope for Phase II testing. Specifically, the scope of work included the following tasks:

- Task 2.1. Procurement and setup of a high-temperature heat panel with control system for evaluation. The system will be capable of reaching temperatures in excess of 1000°C. Preliminary discussions with researchers have identified one viable system that is listed in the budget.

- Task 2.2. Working with the project's Technical Oversight Committee, critical components and materials of tunnels will be identified and prioritized for preliminary experimental testing. The purpose is to verify test methods for Phase II of the project. It is expected that concrete panels for walls or ceilings, supporting steel stringers, aluminum wire ways, or protective coatings (Chartek) would be considered.

- Task 2.3. Preliminary testing will determine the feasibility of test methods for material and component testing. Material testing would include subjecting samples to the heat system procured in Task 2.1 and photographing the surface of the specimen after being subjected to specific thermal loads to correspond to visual inspections. Some determination of thermal gradient through concrete with different levels of steel reinforcement will be completed, subject to budget limitations. Sample component testing is expected to include a concrete panel, either a newly fabricated specimen subjected to thermal damage or pieces damaged in actual events, if available, and tested to failure in the Brack Structural Testing Facility at UMass.

- Task 2.4. An effort will be made to find damaged components from past tunnel fires and deliver them to UMass for laboratory testing, to find their remaining capacity if time and budget permit or to be stored for testing in Phase II.

7.2 Heating Units and Setup

A review of potential heat systems was conducted. Watlow ceramic fiber heaters have the advantages of producing no open flame, reaching temperatures at the heating element up to 1100°C, and a history of successful test performance at Purdue University. The research team has been in contact with Dr. Amit Varma at Purdue University and determined that the experiences with this heating system (through informal personal communications and review of their research publications) indicate a high degree of certainty for the applicability and reliability of this type of heating system.

7.2.1. Heat Source

A system of three 16 in. by 12 in. Watlow ceramic 2030-style heaters with a high emissivity black surface coating were purchased, along with a Watlow F4T temperature controller with data logging capacity for six thermocouples. Six type K thermocouples, 1/8 in. diameter by 12 in. length, were used. One thermocouple was used to monitor each individual heater output, and the remaining three were used to monitor specimen temperatures.

The heaters were mounted on a custom-fabricated frame that could be easily attached to a portable wheel dolly for ease of heating of specimens (Figure 7.1). This allowed for the heating of several different types of specimens (e.g., aluminum, concrete blocks, beams, etc.) using different configurations, such as those shown in Figure 7.2.

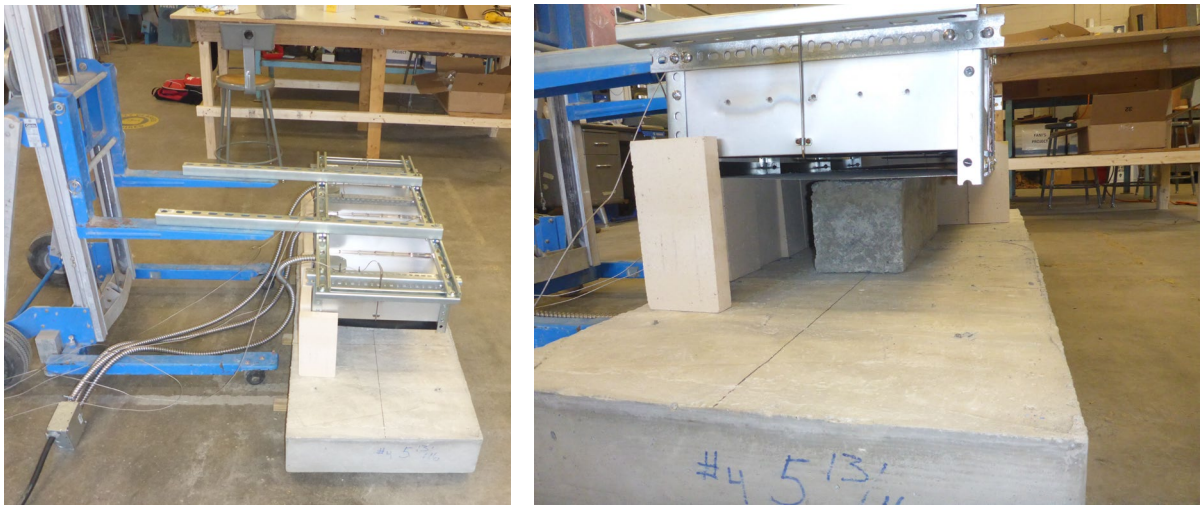

Figure 7.1: Heaters on wheel dolly assembly

Figure 7.2: Heating chamber configuration (top L and R); direct heating of specimen (center L and R); heating of smaller specimen between two throwaway slabs (bottom L and R)

To protect the heating elements from damage, a protective shield was recommended by manufacturers. Two types were custom fabricated and evaluated at UMass Amherst. The first was a solid sheet metal shield of thin gauge sheet metal, while the second was a flat expanded metal sheet (Figure 7.3).

Figure 7.3: Sheet metal shield (L); flat expanded metal shield (R)

Initial testing showed that the solid sheet metal shields were much less effective at transferring heat to the specimens, producing significant disparities between temperature at the heating element and at the specimen surface. The expanded metal sheets provided more consistent heat transfer to specimens, allowing for higher maximum temperatures at the surface of the specimens. A potential concern regarding the open shield configuration is damage to the heating elements should specimens exhibit explosive spalling. As discussed in Sections 7.5.4 and 7.5.5, two tests resulted in sudden spalling of beam specimens. The result was that the flat expanded metal sheet shield and thermocouple were pressed into the heating element. On both of these occasions, the heaters only experienced superficial damage, shown as the white areas where the coating has been damaged by the metal shield (Figure 7.4, left) and thermocouple (Figure 7.4, right), and the heating capabilities were not affected. Informal discussions with suppliers of Watlow heaters noted that damage to heaters has occurred using solid sheet metal shields during some heating and setup operations. The damage observed using the expanded metal sheet shield appears comparable. Based on these results, the flat expanded metal sheets are recommended for future testing.

As the heaters reached higher temperatures, both types of shield expanded and lost some stiffness, resulting in warping as shown in Figure 7.5. This did not affect any aspect of the heating regimen but would provide less protection against concrete spalling at extreme temperatures. Shields were intentionally connected such that deformations were outward to protect against contact with the heating elements.

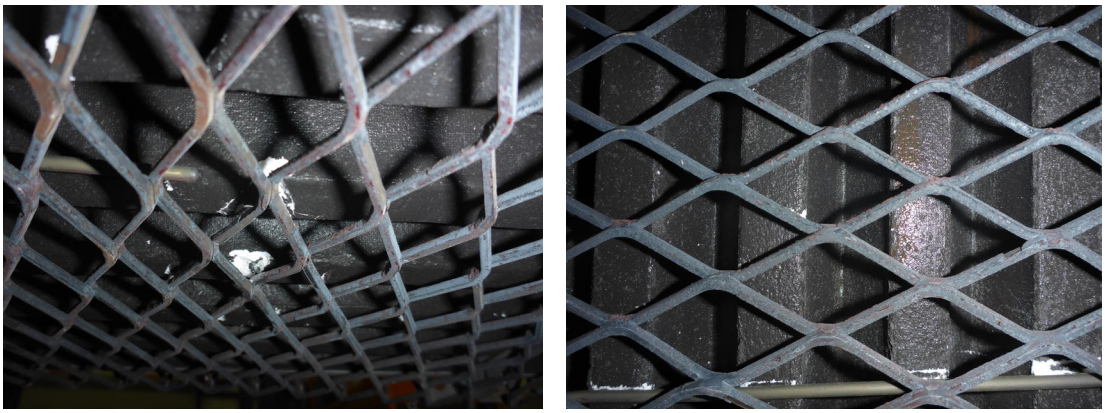

Figure 7.4: Damage to heater elements from shield (L); from thermocouple (R)

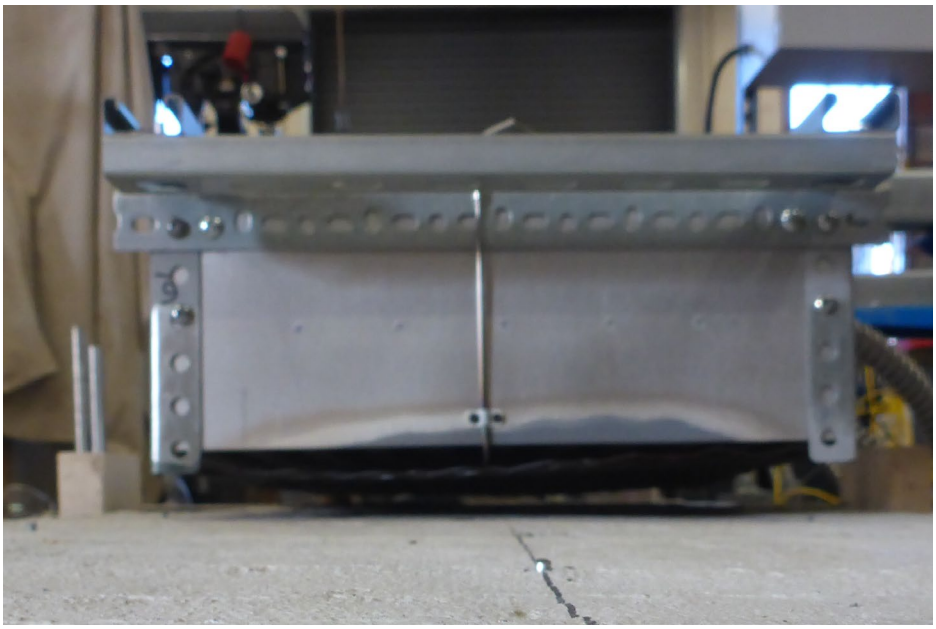

Figure 7.5: Deformation of shield

7.2.2. Insulation Requirements

Initial trials using the heaters showed that there was significant loss of heat between the heaters and the concrete surface when no further insulation was provided. Thermal firebrick, a 1-inch-thick insulation blanket, and a 2-inch-thick insulation blanket were obtained to improve insulation. A variety of setups were investigated to determine the impact on maximum attainable temperature and consistency in heating of specimens. It was determined that concrete specimen surface temperatures of up to 900°C could consistently be obtained by minimizing the volume of air being heated and the loss of heat due to drafts. The optimal setup for maximum temperatures was as follows: Specimens placed on or between concrete slabs with minimum distance between the heaters and the specimens, a layer of firebrick around the perimeter of the heaters, a 2-inch insulation blanket surrounding the firebrick and heaters, and the remaining gaps filled in with pieces of 1-inch insulation blanket. In order to position thermocouples, stands were provided on the outside of the insulation. This setup requires some openings in the insulation for the thermocouple body or wiring to enter the heated zone. The setup was varied for each test, depending on specimen size and temperature monitoring requirements. A typical setup is shown in Figure 7.6.

Figure 7.6: Typical Insulation setup. Heating setup before adding any insulation (top); firebrick around heaters (bottom L); insulation around firebrick (bottom R)

7.3 Thermocouple Monitoring

The thermocouple readings are critical to the thermal load being applied to the specimens. Initial testing noted that the load at the heating element source could vary significantly from the temperature of the air at the surface of the concrete, depending on the protective shield material used on the heater, robustness of the insulation, and other factors. The purpose of these tests is to determine the effects of temperature on the performance of materials such as wall and ceiling panels. This is independent of the heat source. For instance, a large fire farther away (closer to the ground for a ceiling panel or on the far side of the vehicle for a wall panel) may have a lesser effect than a moderate fire immediately adjacent to the panel. Of importance is determining the maximum temperature reached at the surface of the element and the resulting effects on damage and remaining capacity.

Varma (2020) (Time 23:44 to 26:14 of video of research findings posted at https://www.youtube.com/watch?v=EmAYfba6CKc) highlights this concept, comparing research using a similar heat system with steel surface temperatures in an ISO 834 fire test. However, as was noted in the Literature Review section, there are several fire curves that may be more severe than the ISO 834 test (such as the HC, HCM, RWS, and RABT/ZTW tests). These would similarly need surface temperature data to compare the test protocol to

the specific extreme events corresponding to specific fire curves. However, the intent of this research is not to model the behavior under these ultimate fire load conditions but rather to evaluate remaining capacity after a structure is subjected to an intermediate event.

The intent of this research program is to correlate visual aspects of fire damage to air surface temperatures and evaluate the residual condition of the specimens. This would allow confidence in post-fire inspection determinations of relative safety conditions.

Thermocouples were used to monitor the air temperature at specimen surfaces. Thermocouple readings are taken at the tip of the metal casing. Initially, there was some concern regarding the placement of these thermocouples to obtain an accurate reading of the concrete surface temperature. Figure 7.7 shows a test where one thermocouple was placed approximately 0.25 in. above the concrete surface, one was laid on the surface, and the third had the tip inserted directly against the edge of a drilled edge. All three thermocouples provided essentially identical readings, so thermocouples close to or touching the surface were used in all subsequent testing.

Additionally, some attempts were made to monitor internal concrete temperature by drilling from the side of the specimens and inserting the thermocouple. Side drilling may not be as effective, as insulating was difficult in the heating setup used, so heating of the metal casing outside the specimen could transfer heat into the hole to the tip of the thermocouple, providing erroneous results. A better method would be to drill from the bottom of the specimen, which would require bending of the thermocouples to fit the desired location. While this would be possible for future tests, the thermocouples cannot be bent multiple times, so to preserve the instrumentation available, this was not attempted. Readings taken in some preliminary tests indicated the feasibility of measuring internal concrete temperatures. However, for the tests where residual load capacity was to be assessed, the researchers were concerned about potential for weakening the specimen at the hole locations and thus only obtained surface temperature readings.

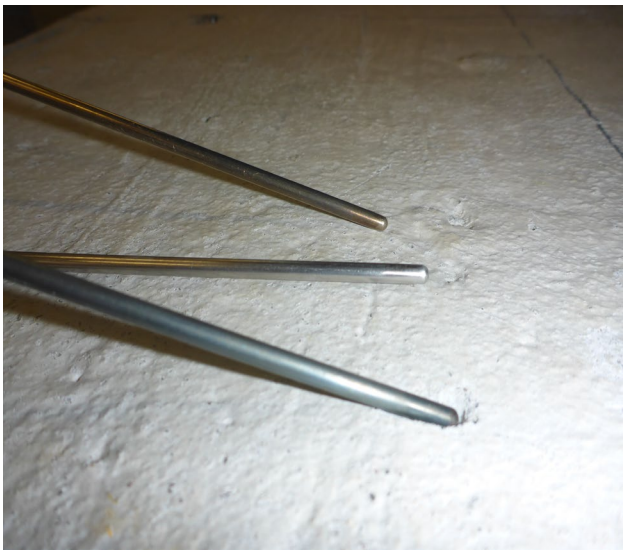

Figure 7.7: Thermocouple readings

7.4 Specimens for Testing

A single wall panel was provided to the laboratories at UMass Amherst for testing (Figure 7.8). The panel was removed from a MassDOT tunnel during maintenance and had been stored. Additional information was not available. This panel was compared to construction document drawing sets for ceiling panels, and it was found that similar details and overall dimensions were used, with the wall panels not including details such as recesses for lighting and openings for anchorage. The inside face of the panel had a tile covering, with the remaining sides plain concrete. The concrete had glassy, black, quartzlike coarse aggregate and darker paste area than typical DOT-specified concretes. Staining was prevalent on the back (non-tile) face of the specimens of reddish or whitish hues. The panel thickness is 4 inches, with a tiled surface of grouted 8-inch-square, 0.25-inch-thick clay tiles.

The research team took overall measurements and made estimates of expected reinforcement based on exposed reinforcement at damaged edges and inspection of inserts along the edges of the specimen. The expected reinforcement of these specimens from these evaluations is shown in Figure 7.9. These observations were used for initial recommendations for obtaining individual specimens from the panel, which were modified as needed during panel cutting. The intention of using individual specimens was to obtain three comparable specimens for flexural testing that would be comparable to overall ceiling or wall panel behavior, and any additional remainder specimens for testing.

Witch Enterprises Inc. was contracted to sawcut the panel into individual specimens. Initial cuts were made along the panel edges (approximately one tile from each edge and two tiles from the bottom of the wall panel, modified in the field to avoid reinforcement) to expose reinforcement. Inspection of the resulting exposed edges confirmed reinforcing bar and prestressing strand locations. The top and bottom strips were cut into small specimens, one or two tiles wide. Longitudinal cuts of 19-inch-wide sections were made, centered on the three interior prestressing strands. Additionally, two strips of 9.75 inches were made to include only welded wire mesh reinforcement, further cut in half to make four identical specimens with minimal reinforcement. The remainders from the panel were retained to use for preliminary testing. This resulted in the following specimens (shown in Figure 7.10).

- Three primary beam specimens (19 in. by 96 in.) with one prestressing strand and five longitudinal wires from the wire mesh reinforcement.
- Three beam specimens (9.75 in. by 48.25 in.) with wire mesh reinforcement only.
- Ten single tile dimension specimens (8 in. by 8 in.) (some damaged).
- Six 2-tile dimension specimens (16 in. by 8 in.) (some damaged).
- Nine miscellaneous remainders, often one of a kind or pairs, with one having significant spalling or inserts, some end sections with reinforcing steel and two prestressing strands, though these had preexisting edge damage when delivered and therefore had no companion specimens of similar properties.

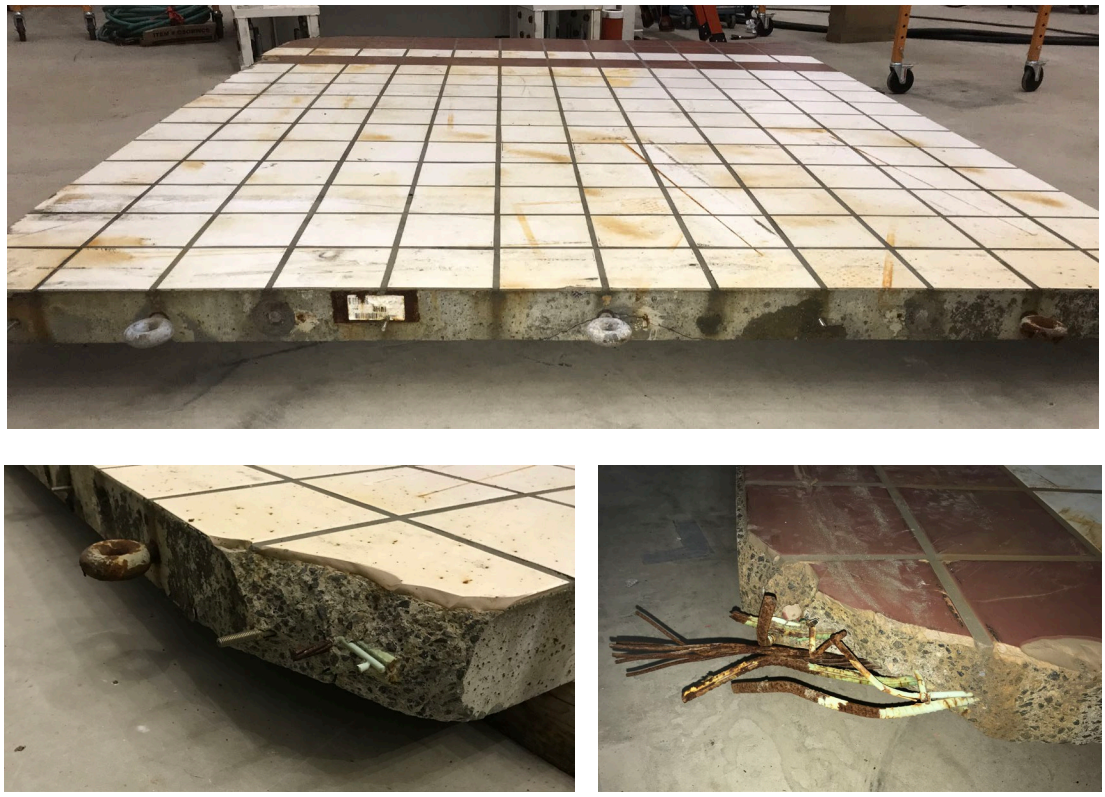

Figure 7.8: Panel as delivered

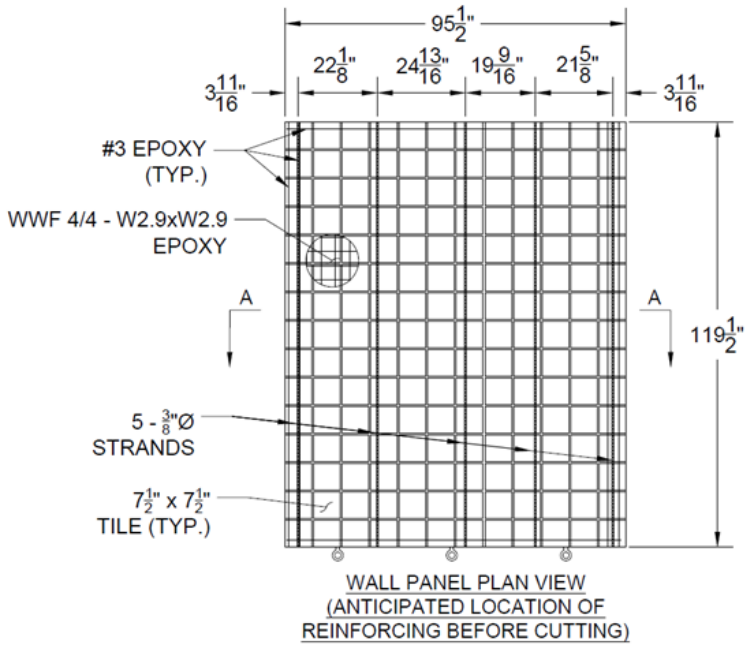

Figure 7.9: Panel dimensions and reinforcement

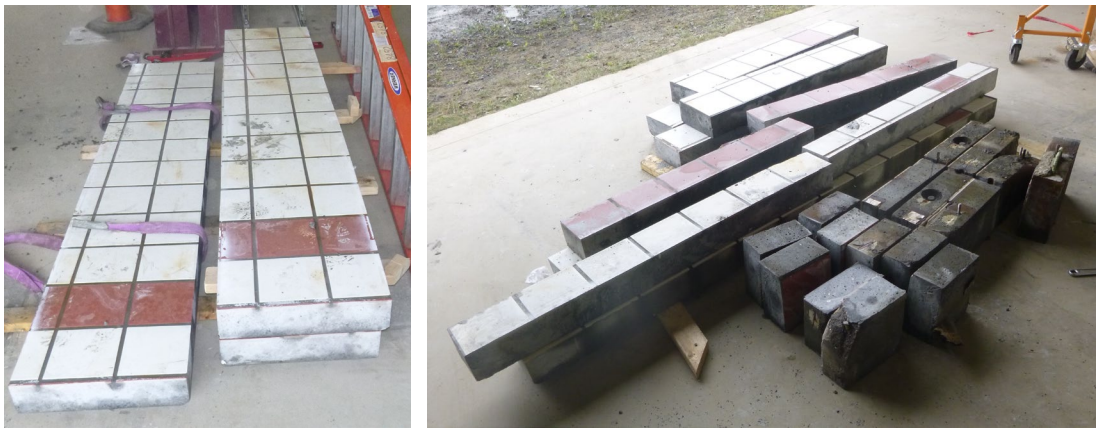

Figure 7.10: Specimens obtained from panel: three primary beams (L), blocks, smaller beams, and miscellaneous (R)

7.5 Initial Trials

For the initial testing, several different types of specimens were used: concrete specimens available in Gunness Laboratory (6 in. by 6 in. by 18 in. beam of undefined mixture properties and 22 in. by 34 in. by 6 in. slabs), individual block specimens from the wall panel (8 in. by 8 in. and 8 in. by 16 in.), an aluminum wireway provided by MassDOT, and beam specimens from the wall panel with only welded wire mesh reinforcement.

7.5.1. Heating of Small Plain Concrete Specimens

One specimen for previous concrete modulus of rupture testing was used as an initial specimen to evaluate the thermal load potential of the heaters. The concrete mixtures and strengths were unknown, aside from having f'_c<5ksi (from student laboratory results). This specimen was heated to a maximum surface temperature of 505°–560°C, with temperature reduced once maximum temperatures were reached (Figure 7.11). There was no observed spalling or deterioration in the specimen (Figure 7.12).

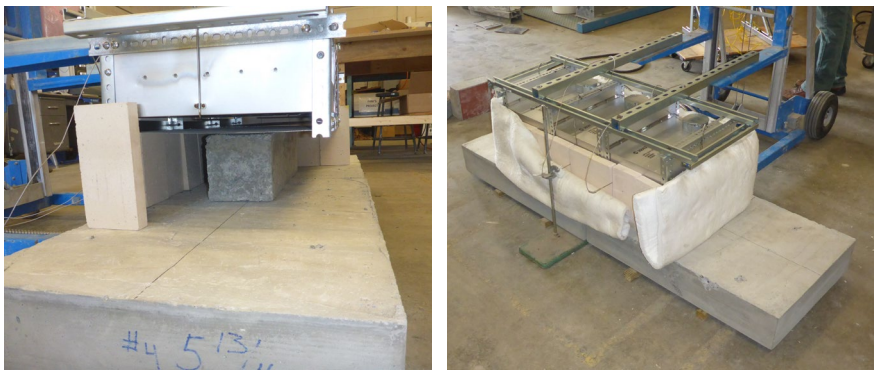

Figure 7.11: Sample test setup for heating plain concrete specimens

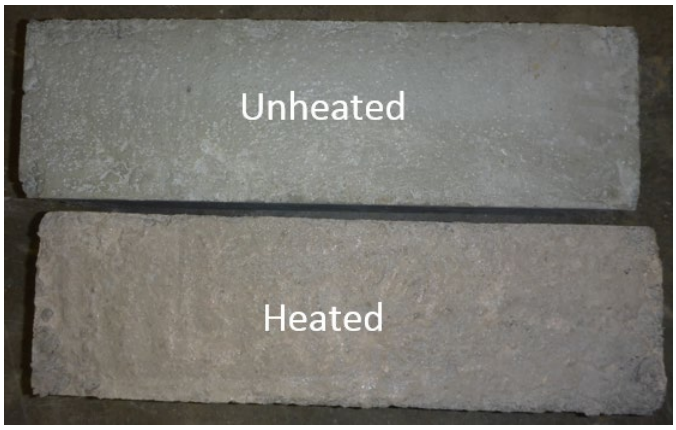

Figure 7.12 Plain concrete specimens: unheated (top); heated to surface temperatures up to 560°C (bottom)

7.5.2. Heating of Concrete Slabs

Smaller specimens being heated were set on or between slabs that had been used for previous Gunness Laboratory testing. These specimens were 22 in. by 34 in. by 6 in. and had two layers of 4/4 – W2.9xW2.9 reinforcement. The concrete was provided by a local ready-mix plant to meet 4 ksi requirements. The 28-day cylinders' strengths were f'_c= 4.8 ksi.

These slabs were used in all testing to support specimens and seal the insulated heated zone at the bottom, protecting the laboratory floor from the heat. Therefore, only a section of each slab was exposed to heat, with the remainder outside the insulation and at ambient temperatures. These slabs experienced surface temperatures that ranged from 300°C to 950°C for various time periods of thermal loading, and significant thermal gradients from within the insulated area to the ambient conditions outside. Two of the slabs were directly heated (Figure 7.13) and set aside after a known heat regimen and used to test the Carbontest® and rebound hammer test methods, reported in Section 7.7. No spalling occurred in any of the slab specimens.

Figure 7.13: Concrete slab heating setup

After heating to high temperatures, there was hairline map cracking on many of the slabs (Figure 7.14) and a distinctly lighter coloration of the concrete (Figure 7.15).

Figure 7.14: Typical map cracking pattern for slabs after heating up to 930°C

Figure 7.15: Slab before heating (L); whitening after heating to surface temperatures up to 930°C (R)

7.5.3. Heating of Panel Block Specimens and Aluminum Wireway

The first specimens investigated from the tunnel wall panel were some of the smaller block-shaped specimens that were one or two tiles wide. Initial testing was conducted to determine potential effects of heating the tile or concrete side and to investigate potential effects of heating on the panel concrete. The overall testing was shortened, due to complications with noxious odors in the tests. No spalling was observed in any specimens, with air temperatures at the concrete surface reaching up to 790°C.

Figure 7.16 shows a test where two specimens were heated simultaneously, one with the tile facing upward and the other with the tile on the bottom against the concrete slab. As the specimens reached approximately 470°C, the testing was halted due to a noxious chemical odor from the specimens that spread through the laboratory and adjacent hallway. After cooling, inspection of the specimen with the tiles facing upward toward the heater showed that a significant section of the grout between tiles and exposed on the edge had charred. This area of grout was easily sloughed off with a screwdriver (Figure 7.17). Subsequently, the researchers used a chipping hammer and hammer with chisel to break off the tile. When struck, the tiles in the vicinity of the charred grout broke off in small sections that separated near the grout line (Figure 7.18, bottom). In unheated specimens, the tiles and grout could not be separated from the concrete, instead breaking off in small sections that indicated no weak planes in the tile or grout (Figure 7.18, top).

Figure 7.16: Specimens with tile side up (near) and tile side down (far)

Figure 7.17: Charring of grout material

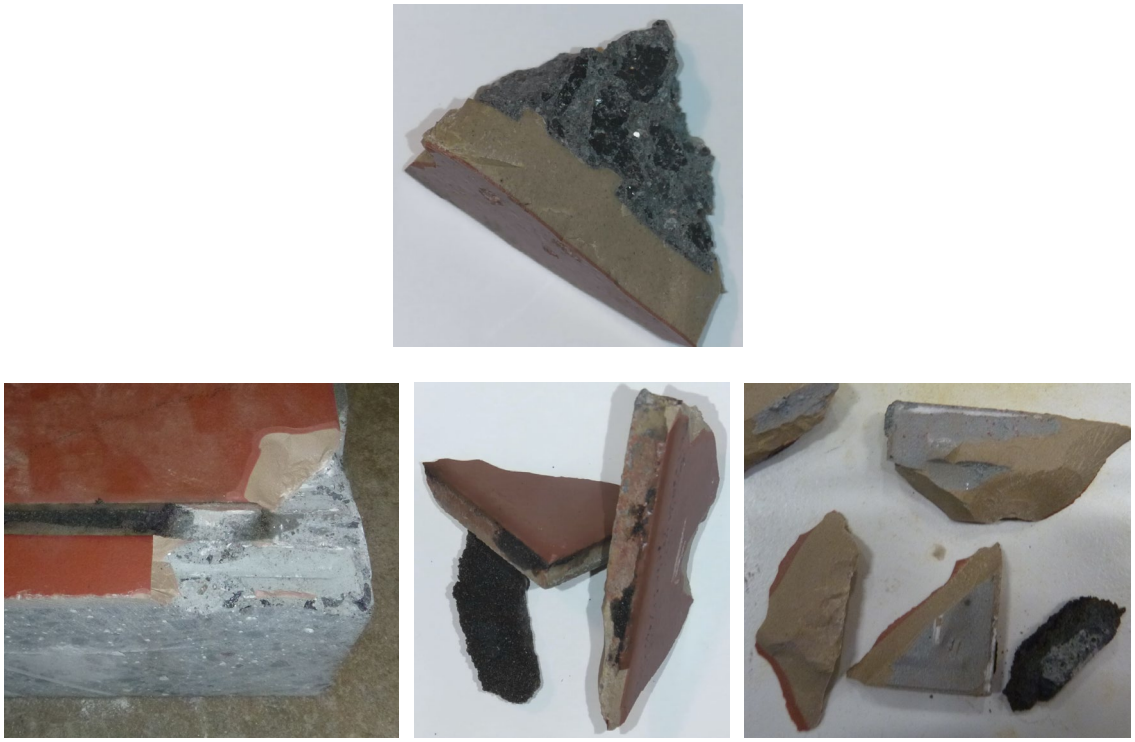

Figure 7.18: Tile and grout removal by chipping hammer and chisel. Unheated specimen (top); specimen heated to 470ºC with clean break at grout line (bottom)

In a subsequent test, a block-shaped specimen with the tile facing upward and a section of the aluminum wireway were heated to temperatures of 400°C, 550°C, and 750°C, and held at each of these temperatures for an hour. At a temperature of approximately 350°C, smoke began billowing out of the heating chamber, which was confirmed to be from the grout when the heaters were removed to take a picture of the condition after maintaining a 400°C temperature for an hour. This smoking continued for about an hour before subsiding. Figure 7.19 shows pictures of the wireway and tile after maintaining temperature for an hour at 400°C, 550°C, and 750°C, respectively. Note that while the wireway appears grayish in the 400°C photo, these was due to backlighting; the wireway in actuality still had a white appearance. At 400°C, minor peeling of the coating on the wireway was noted, and the grout had turned a dark grayish/black color. At 550°C, significant peeling of the wireway coating was noted, and the grout had turned a light whitish-gray color. At 750°C, the wireway had noticeably sagged, as shown in Figure 7.20, and the grout remained the same whitish-gray color as at 550°C. After the heaters were removed, a single hairline crack in the tile was observed, and additional smaller cracks could be seen forming during the first 5 minutes of cooling. The tile cracking pattern and aluminum wireway after heating and cooling are shown in Figure 7.21. After cooling, it was found that the grout had turned into a powder that could be scraped off easily with a screwdriver, as shown in Figure 7.22. Though attempts to pry the tile off the concrete were unsuccessful, it is postulated that the tiles can detach from the concrete during a fire due to the formation of cracks and the deterioration of the grout. Furthermore, it was noted that when water was poured on the hot tiles, the existing cracks

grew and new cracks formed, indicating that water from fire suppression efforts could also contribute to the detachment of tiles from concrete after a fire event.

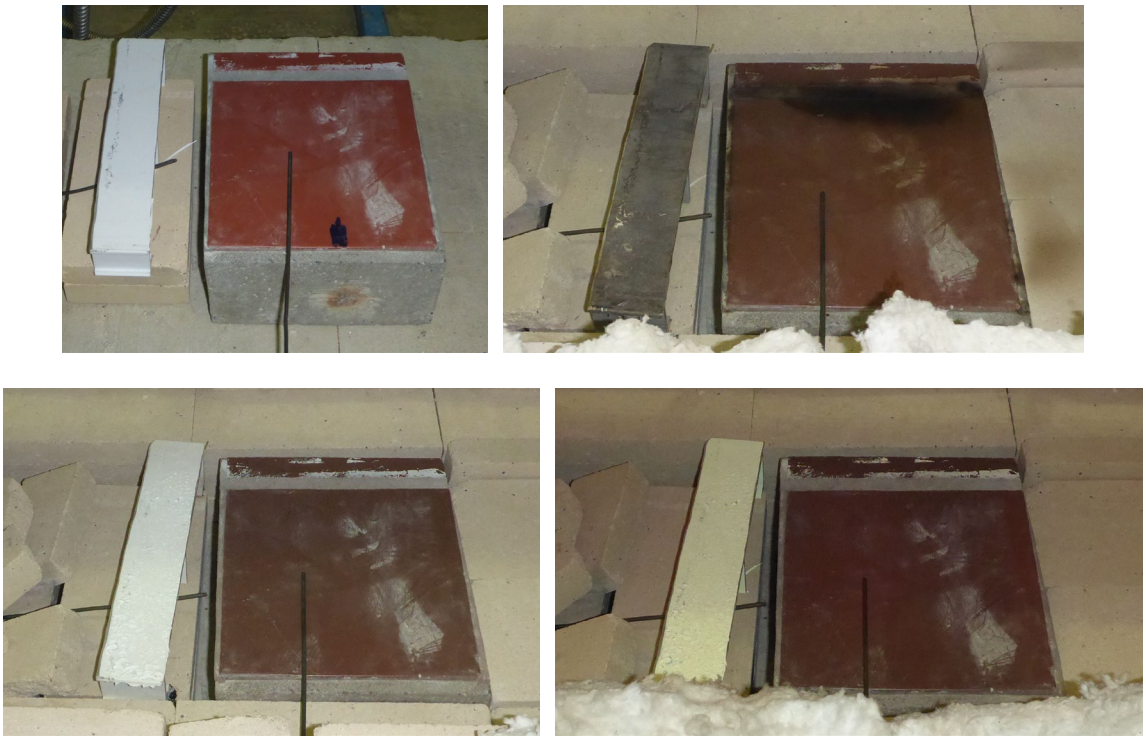

Figure 7.19: Appearance of aluminum wireway and wall panel tile: before heating (top L), and after one hour at: 400°C (top R); 550°C (bottom L); 750°C (bottom R)

Figure 7.20: Sagging of aluminum wireway after heating

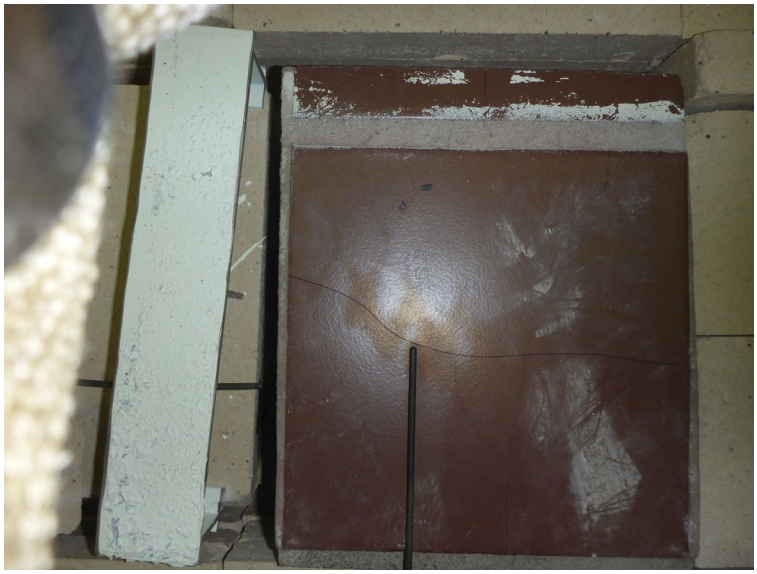

Figure 7.21: Closeup of tile and aluminum wireway after heating

Figure 7.22: Removal of grout with a screwdriver after heating

Another block-shaped wall panel specimen was tested in a configuration where most of the specimen sides were flush against the concrete slabs, with only the top surface and approximately 2 inches of the sides exposed to the maximum heat during the test. This test was halted due to noxious chemical odors and some smoke at 790°C. As seen in Figure 7.23, the epoxy coating around the exposed reinforcing bar had melted and dripped down the side of the specimen. This was not observed in other specimens with similar exposed reinforcement. Nonetheless, most future testing was completed with the sides of specimens below the protective slab surface.

Figure 7.23: Melting of epoxy reinforcement coating

7.5.4. Testing of Minimally Reinforced Beam Specimens

The purpose of these tests was twofold. First, these specimens were used to verify that the beam load testing setup was performing satisfactorily prior to the final beam tests. These tests would also provide data on the rupture capacity of heated specimens, though this has minimal design significance and would generally be applicable only to plain concrete members subject to flexure.

Three identical specimens were tested. One was not heated, to act as a comparison to the heated beams. The next was heated to 600°C. After 23 minutes at this temperature, the specimen suddenly spalled with significant loss of cross-section (Figure 7.24, left). The specimen was cooled to room temperature and removed from the heater setup (Figure 7.24, right). In moving the specimen, a final portion of the cross-section in the center of this photo became dislodged from the wire mesh, resulting in zero cross-section remaining over a large portion of the specimen. This specimen has no flexural capacity by inspection, so was not tested further. The final specimen was also heated to 600°C and maintained at this temperature for approximately 180 minutes. This specimen showed no signs of spalling (Figure 7.25), though slight map cracking was observed on the heated face of the specimen.

The heating curves for the two specimens are shown in Figure 7.26. These specimens also had holes drilled from the side of the specimens to monitor temperatures within the concrete at depths of approximately 2 inches from the heated surface (location of wire mesh) and 1 inch from the heated surface. The intent was for these to be fully isolated from the heat chamber, although further testing would be required to verify that this method accurately monitors concrete temperature and was not affected by hot air entering the drilled hole or heating the thermocouple casing. The monitored air temperature at the concrete surface at the center of the heated area was used to control the three heaters, while the control set point is the projected curve the heater output is intended to meet. For the intact specimen, the temperature drop occurred when insulating materials were removed to check for signs of spalling. The effects of cooling having less effect at depth can be seen clearly in the plot. The

plots do not indicate why one specimen spalled and the other did not. The two specimens were then load tested in flexure to failure. Figure 7.27 shows a schematic of the test setup.

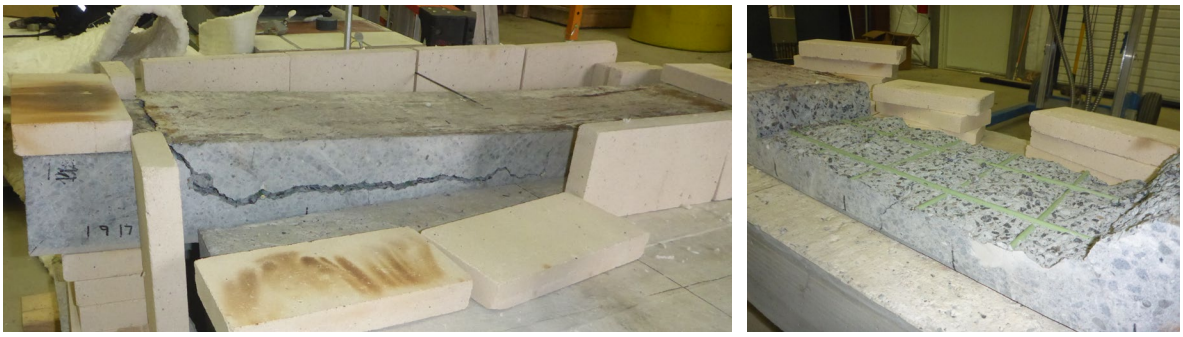

Figure 7.24: Spalled minimally reinforced beam specimen after heating (L); after removal from setup (R)

Figure 7.25: Intact minimally reinforced beam specimen after heating

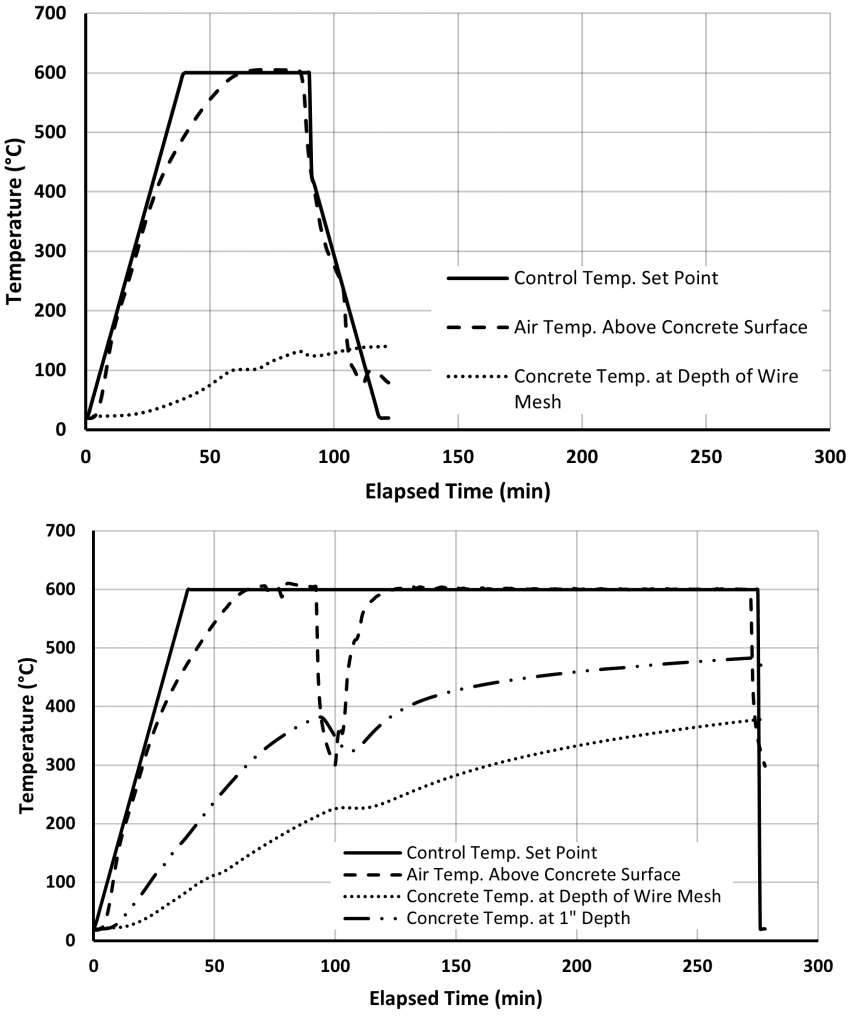

Figure 7.26: Heating curve temperature vs. time plots: spalled specimen (top); intact specimen (bottom)

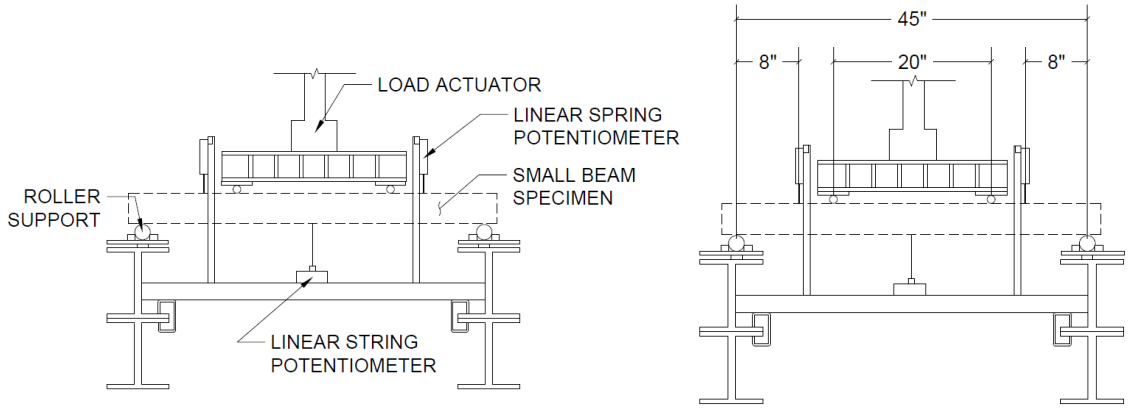

Figure 7.27: Schematic of test setup for minimally reinforced beams

The specimens were incrementally loaded until failure using manual control of load and displacement. This allowed for stopping at incremental load or displacement points to inspect the specimen and test apparatus.

Both specimens failed after propagation of a flexural crack in the constant moment region. Figure 7.28 presents photos of typical specimen failure. Figure 7.29 provides the applied load versus mid-span deflection plot for both specimens. For the control specimen, the maximum flexural capacity was reached at the cracking moment of the concrete tension fiber, though this would rarely be considered in design of members with reinforcement provided. After the cracking load was exceeded, the crack formed in the beam through approximately half of the depth and slowly progressed past the wire reinforcement and up to almost the tile prior to overall failure. The crack formed toward the left side of the specimen, and, therefore, deflections at the left reading were approximately twice the centerline deflection shown, with the right gauge reading smaller values.

Results from the heated specimen load test were virtually identical to the control specimen load test, with the exception of the cracking moment. A crack similarly formed toward the left side of the specimen and therefore deflections at the left reading were approximately 1.5 times the centerline deflection shown, with the right deflection gauge reading smaller values. The behavior of the load-deflection plot as well as maximum reinforced flexural capacity were nearly identical between the control and heated specimen. The only effect of heating on flexural capacity appeared to be to pre-crack the exposed face of the specimen with hairline cracks. This would not affect capacity if the concrete were heated in the tension region, and would only affect capacity if in the compression region by extending the zone of compression if the f'_c was lowered at the surface (resulting in a smaller moment arm between concrete in compression and steel in tension).

It is important to note that the force deflection curve past the initial concrete cracking (approximately 0.05 in.) would typically be considered for design of a reinforced member, as curing and aging will typically result in some cracking of concrete members, leading designers to neglect the concrete tensile strength. Therefore, the design capacity was not affected by the heating.

Post-failure inspection of the ruptured specimens indicated changed concrete characteristics. This is shown in Figure 7.30, compared to the control specimen. There was a lighter band of approximately 0.25 in. to 0.375 in. extending from the heated surface of the concrete, with a darker band of approximately 0.50 in. to 0.75 in. above that layer. The darker section had the appearance of moist concrete. The thermal curve at 1 in. depth indicates that these areas reached temperatures of 450°C to 600°C.

Figure 7.28: Photo of minimally reinforced beam specimens during load testing. Propagation of crack in control specimen during load application (top); after failure of heated specimen (bottom)

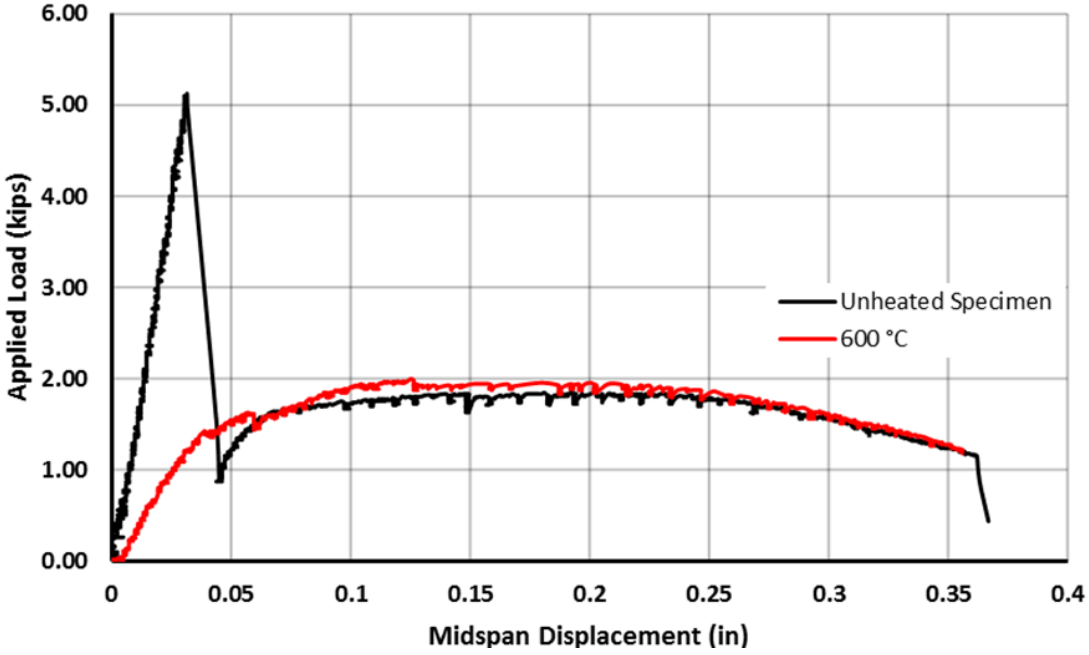

Figure 7.29: Load vs. deflection plot of minimally reinforced beam specimens

Figure 7.30: Interior visual inspection of heat effects of ruptured specimens: control specimen with consistent color through ruptured sections (L); specimen heated to 600°C specimen (C); closeup of specimen heated to 600°C (R)

7.6 Beam Tests

The purpose of these tests was to compare the residual flexural capacity of wall panel samples after being subjected to thermal load and determine the feasibility of this test plan for Phase II of the research program. Three specimens representative of ceiling and wall panels were tested. These included reinforcement of one prestressing strand and five longitudinal wires of the welded wire fabric, as shown in Figure 7.31.

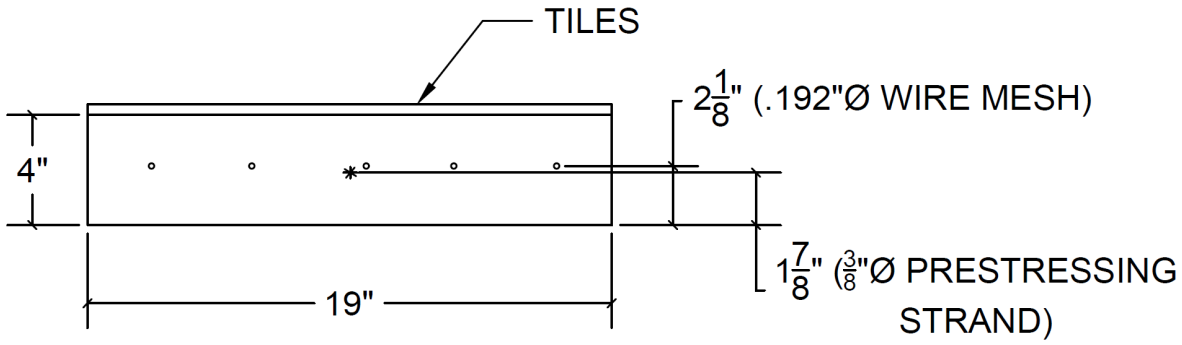

Figure 7.31: Beam cross section

Three identical specimens were tested. The first was tested in the as provided condition. The next was heated to 600°C. After 27 minutes at this temperature, the specimen suddenly spalled with significant loss of cross-section (Figure 7.32), and the heaters were removed. The final specimen was heated to 300°C and this temperature maintained for 240 minutes. This specimen showed no signs of deterioration.

Figure 7.32: Spalling of 600°C beam specimen prior to heating (L), post heating (R)

The heating curves for the two specimens are shown in Figure 7.33. These specimens included three thermocouples to monitor air temperature at the concrete surface, under the center heater, and near the left and right of the insulated area. The left thermocouple was near a seam in the insulation intermittently used to observe the specimen. The monitored air temperature at the concrete surface at the center of the heated area was used to control the three heaters, where the control set point is the projected curve the heater output is intended to meet. In both specimens, the temperature to the left is lower than the other temperatures, and additional insulation would be required to provide a more consistent applied heat through the entire insulated area. However, the center thermocouple is expected to be representative of most of the heated area, as there were few seams in the insulation.

The three specimens were then load tested in flexure to failure. A schematic and photo of the test setup are shown in Figure 7.34 and Figure 7.35, respectively. The specimens were incrementally loaded until failure using a manual control of load and displacement. This allowed for stopping at incremental load or displacement points to inspect the specimen and test apparatus. The expected nominal moment of the specimens is $M_n = 71.2$ kip-in., assuming $f'_c = 7$ ksi for the concrete, tile, and grout, $F_u = 90$ ksi for the welded wire ($A_{sw} = 0.029 in^2$) and $F_u = 270$ ksi for the prestressing strand ($A_{sp} = 0.085 in^2$). For the test setup, this would correspond to an ultimate applied load at failure of $P_u = 3.9$ kips.

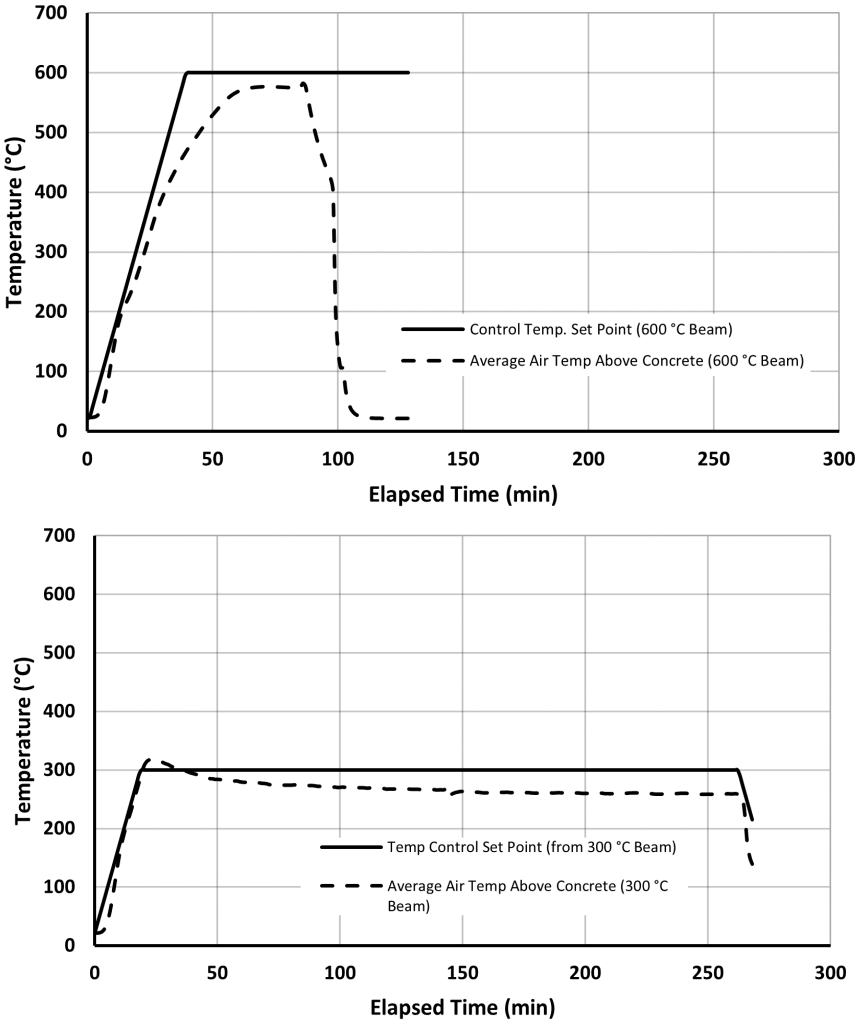

Figure 7.33: Heating curve temperature vs. time plots: spalled specimen (top); intact specimen (bottom)

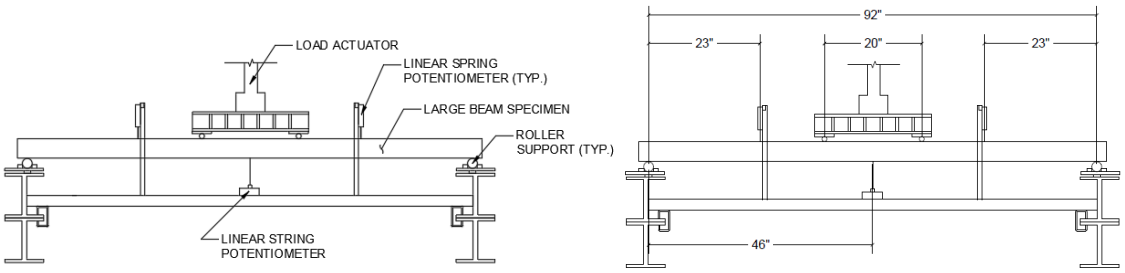

Figure 7.34: Test setup schematic for beam tests

Photos of the specimens during testing are presented in Figure 7.35, Figure 7.36, Figure 7.37, and Figure 7.38. The applied load versus mid-span deflection plot for all three specimens are presented in Figure 7.39.

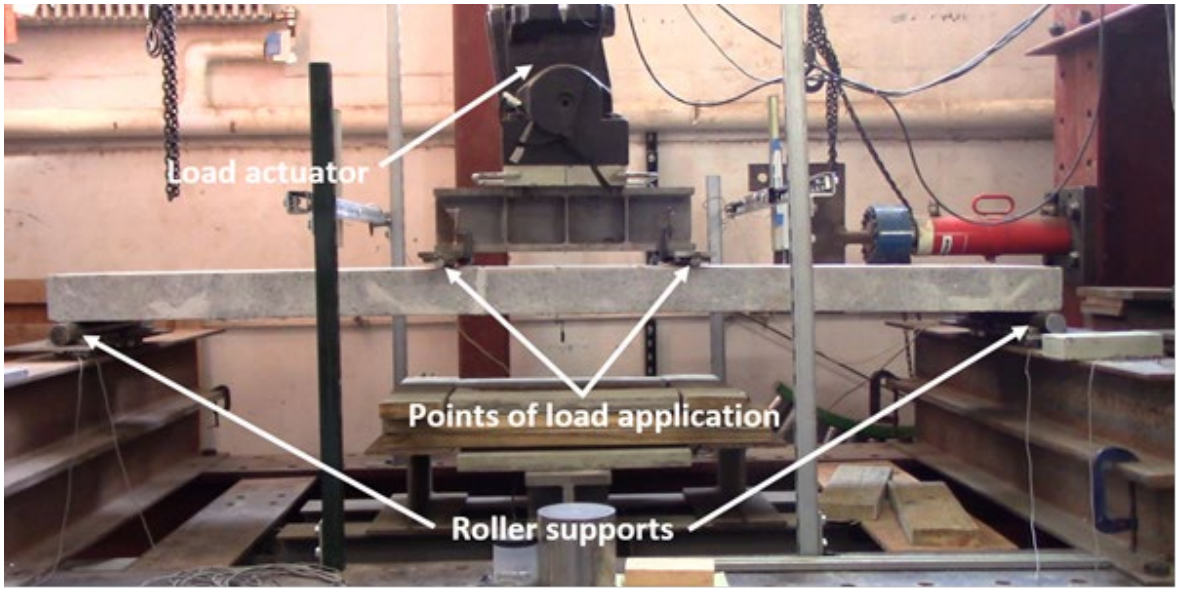

Figure 7.35: Test setup photo for beam tests

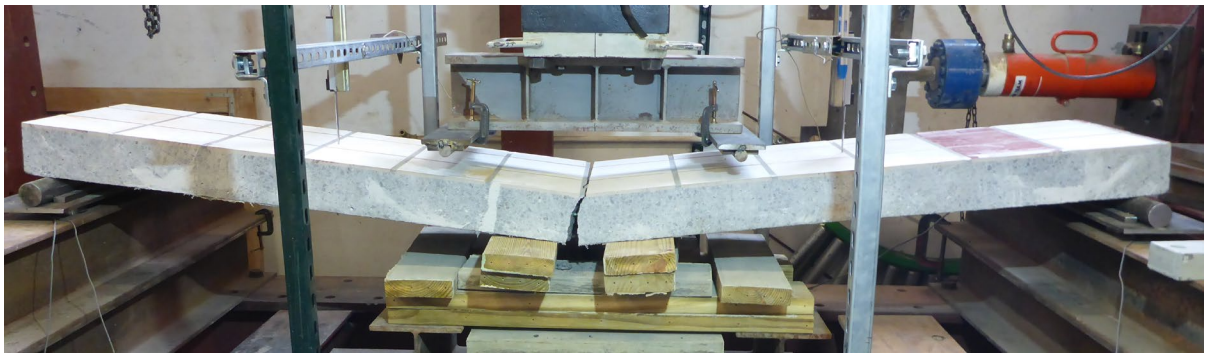

Figure 7.36: Photo of control specimen after failure

Figure 7.37: Photos of 300ºC intact specimen load testing. Multiple flexural cracks in constant moment region during load application (top and middle); after failure (bottom)

Figure 7.38: Photos of 600°C spalled specimen load testing. Prior to loading (top); propagation of crack during load application (center L and R); after failure (bottom)

The specimens all failed within the constant moment region. All tiles remained intact, and the final cracks were at or near grout lines. This indicates that the tile and grout were effective parts of the compression stress zone. Final cracks extended very close to the grout, further verifying the effectiveness of these components in compression. Load deflection plots (see Figure 7.39) showed no loss in strength in the heated specimens, but also an increase in ductility over the control, indicating that the heating process did not alter the internal steel properties (note that the spalled specimen temperature load was discontinued as soon as spalling occurred).

The control specimen exhibited a typical reinforced concrete beam response, though the moment to cause concrete cracking was higher than expected (as in the small minimally reinforced beam specimens), indicated by the initial peak on the plot. After first cracking, there was a load drop. The specimen load capacity then increased along a less stiff path

before reaching the peak load. The specimen heated to 300°C followed a similar initial path but had a gradual transition from the initial stiffness to the non-linear portion of the curve at a capacity slightly larger than the residual capacity of the control specimen after it cracked. It is conjectured that the heating induced some micro-cracking that slowly propagated with increasing moment, resulting in a smoother transition to the peak load capacity. The spalled specimen heated to 600°C showed immediate softening of the plot, as expected due to the significant damage and cracking in the concrete tension region. The specimen was able to continue loading to a peak load similar to the other two specimens.

It may not be intuitive that the highly damaged specimen had the most ductility and similar capacity. However, this specimen had an exposed length of prestress strand, whereas the other specimens confined all significant non-linear deformations of the reinforcement to a specific crack location. Yielding occurring over a longer length of reinforcement results in a larger total reinforcement lengthening (strain remaining constant prior to necking). This would result in larger deformation of this damage beam during loading. Differences in total load capacity of all specimens are minimal and in good agreement with the expected beam capacity.

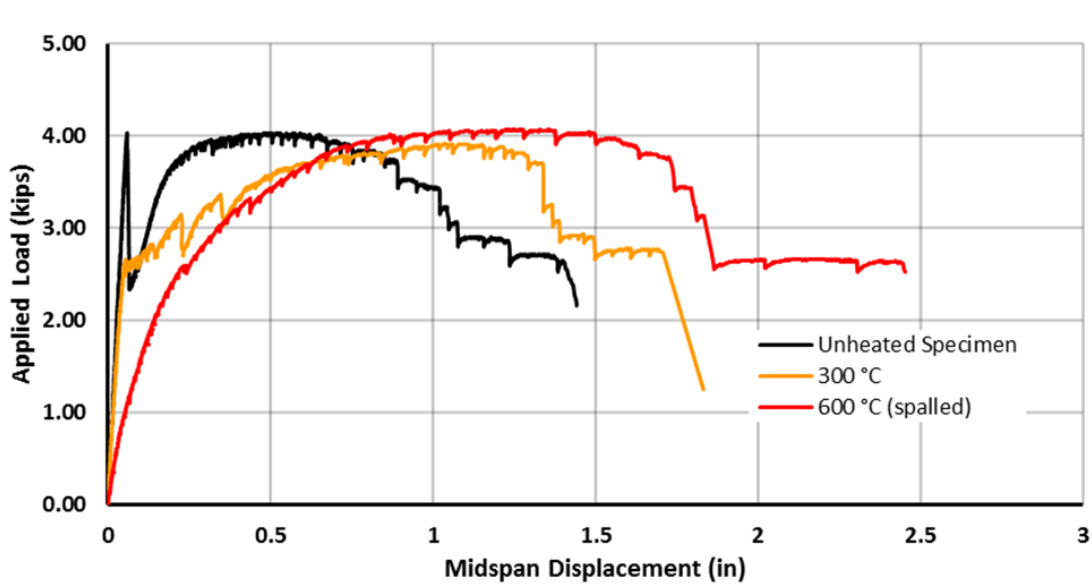

Figure 7.39: Load vs. deflection of tested specimens

Post-failure inspection of the specimen rupture planes showed no visible difference between the control and beam heated to 300°C (Figure 7.40).

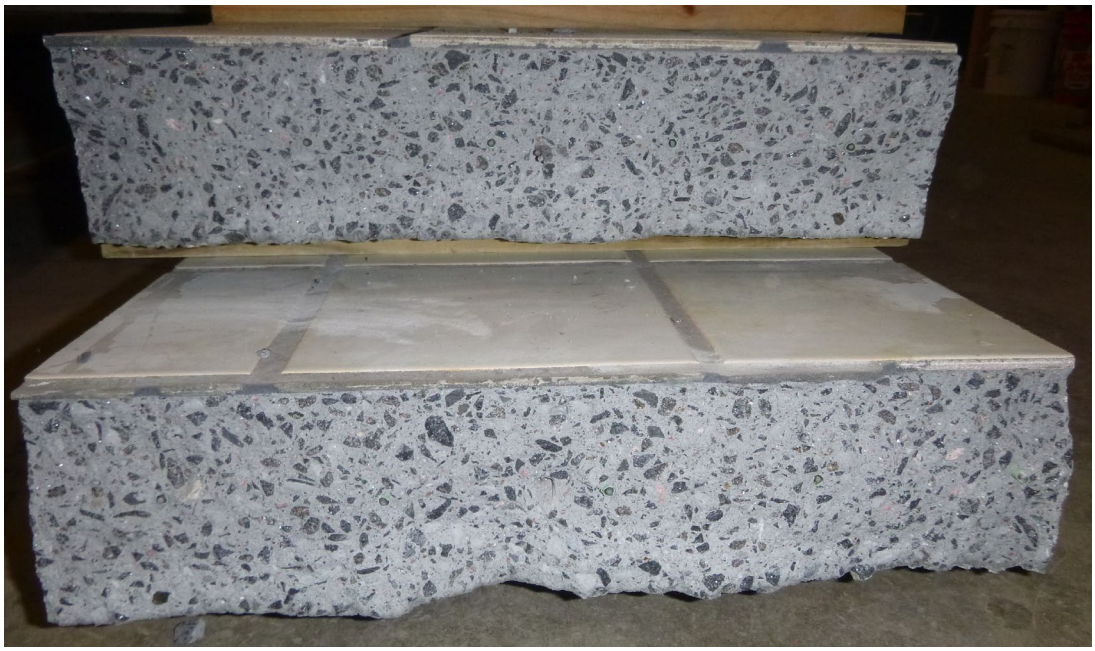

Figure 7.40: Ruptured surface of 300ºC heated specimen

7.7 Supplemental test data

Carbontest® and rebound hammer tests were performed before and after heating in order to determine their effectiveness in post-fire inspection. These tests were initially completed on slab specimens in the initial heating tests and on some of the beam specimens.

7.7.1. Carbontest®

The Carbontest was completed on one of the slab tests subjected to temperatures up to 900°C. Carbontest was completed in the center of the heated zone and in the non-heated zone. At least two samples were collected from each region.

Results for the slab specimen are shown in Figure 7.41. According to the Carbontest manual, concrete that remains colorless when a phenolphthalein solution is applied has been carbonated, while concrete that turns pink has not been carbonated. Carbonation can occur for several reasons, including heat exposure. With the heated powder being at the bottom of the tube, a minor difference in coloration was observed for the Carbontest performed in the heated zone versus the unheated zone. The test performed in the heated zone shows a lighter pink color at the bottom of the tube than the test performed in the unheated zone, which had a uniform pink color. There was not a distinct depth in the tube separating pink from colorless material. This preliminary test was therefore not conclusive, and further testing should be conducted to assess the viability of this method for determining the depth of carbonation in heated concrete.

Figure 7.41: Photo of slab Carbontest tubes from: center of heated zone (L), unheated zone (R)

7.7.2. Rebound Hammer Results

After heating, data was collected using the rebound hammer to determine the effectiveness of this tool in post-fire inspection. These tests were completed on slab specimens in the initial heating tests. Data was also collected prior to heating, and after failure, for the beam specimens.

Figure 7.42 presents slab specimen results. Results showed significantly lower readings (26–28) in the area of the slab that had been heated (area also visually appeared lighter in color) and consistent readings throughout the rest of the slab (38–44).

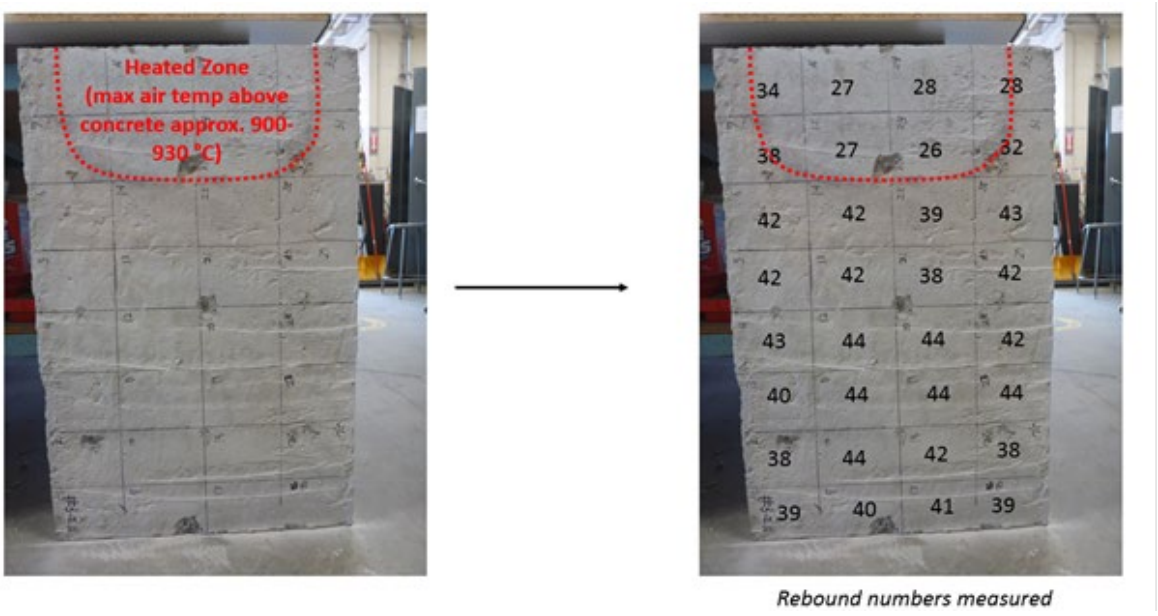

Figure 7.42: Photo of 900ºC slab rebound hammer and sample locations

Figure 7.43, Figure 7.44, and Figure 7.45 show results from the final beam tests for the control, 300°C, and spalled 600°C specimens, respectively. Note that the heaters were centered on squares 12 and 13. For all specimens in their original condition, the rebound numbers ranged from 25 to 57. This wide range can be attributed to debris that could not be removed, such as an unknown melted material staining the surface of the beams, and the presence of aggregate on the surface of the beams, which was noted to result in highly inconsistent readings. Readings on the 300°C specimen were also collected after the specimen had cooled. As shown, there were no noticeable differences, with some numbers

decreasing and others increasing by similar amounts, all within the range of scatter in the control and pre-heated specimens. Readings could not be taken post cooling on the spalled section of the 600°C heated specimen, but values outside the spalled area were relatively unchanged. Overall, the rebound hammer was not effective on the wall panel concrete, due to initial variability in readings in the as-delivered condition.

This beam was not heated

1 **40**	2 **45**	3 **35**	4 **50**	5 **33**	6 **50**	7 **42**	8 **44**
9 **41**	10 **48**	11 **32**	12 **49**	13 **50**	14 **28**	15 **44**	16 **50**
17 **53**	18 **40**	19 **25**	20 **53**	21 **44**	22 **38**	23 **50**	24 **47**

Figure 7.43: Unheated beam rebound hammer results

Before Heating

1 **56**	2 **48**	3 **50**	4 **40**	5 **48**	6 **32**	7 **34**	8 **53**
9 **57**	10 **50**	11 **28**	12 **38**	13 **30**	14 **40**	15 **38**	16 **38**
17 **46**	18 **37**	19 **35**	20 **33**	21 **51**	22 **48**	23 **33**	24 **44**

After Heating

1 **44**	2 **53**	3 **32**	4 **38**	5 **50**	6 **46**	7 **25**	8 **54**
9 **48**	10 **37**	11 **45**	12 **40**	13 **44**	14 **34**	15 **34**	16 **50**
17 **53**	18 **43**	19 **43**	20 **50**	21 **51**	22 **43**	23 **48**	24 **52**

Figure 7.44: 300°C beam rebound hammer results

Before Heating

1 **35**	2 **51**	3 **51**	4 **52**	5 **37**	6 **49**	7 **51**	8 **49**
9 **39**	10 **55**	11 **48**	12 **43**	13 **38**	14 **55**	15 **53**	16 **53**
17 **45**	18 **40**	19 **54**	20 **52**	21 **53**	22 **48**	23 **51**	24 **53**

After Heating

1 **30**	2 **52**	3 **x**	4 **x**	5 **x**	6 **x**	7 **48**	8 **50**
9 **48**	10 **53**	11 **50**	12 **x**	13 **x**	14 **x**	15 **55**	16 **52**
17 **51**	18 **49**	19 **45**	20 **x**	21 **x**	22 **50**	23 **55**	24 **52**

Figure 7.45: 600°C spalled beam rebound hammer results

7.8 Conclusions

The initial experimental results reported in this section provide several valuable conclusions.

- The heating system tested is an efficient way to perform the intended experiments. The setup will be able to perform the tests expected for Phase II of this research project.
- The heating system is capable of providing air temperature load at the surface of the concrete in excess of 900°C for ideal conditions. Higher temperatures may be possible with additional heaters.
- Temperature of the air at the surface of the concrete is effectively measured by the thermocouple. Literature has shown that this temperature is significantly less than the heat source temperature referenced in a typical ISO 834 fire test. Further literature review is required to determine if data is comparable to other fire test curves.
- Readily available materials such as firebrick and insulation blankets are sufficient for insulating the areas tested.
- Expanded metal sheet shield is sufficient to protect the heating elements from explosive concrete spalling.

- At 350°–470°C, tile grout on the wall panel gave off a noxious odor and became charred in appearance and brittle to the touch. At 550°–750°C, the tile grout became whitish-gray in appearance and had powdery consistency.
- At a temperature between 500°–790°C, exposed epoxy reinforcement coating at a cut face of a wall panel melted, producing a noxious odor. Other specimens with cut epoxy-coated wire mesh were heated to similar temperatures without any signs of melting.
- A tent system may be required to purify the air and avoid noxious fumes prior to further testing of specimens where significant grout, epoxy coatings, or other polymer-based components could produce significant off-gassing.
- Carbontest® tubes test equipment was straightforward to use on vertical surfaces, though readings did not provide a distinct depth of carbonation on initial specimens. Further testing is required to determine the viability of this method.
- Rebound hammer readings showed distinctly lower values on sections heated to 900°C on a typical concrete slab. However, the rebound hammer was ineffective on the wall panel concrete due to high variability of readings in the as-delivered condition, thought to be caused by the rough, uneven surface of the concrete.
- A specimen heated to 600°C showed visual indication of the depth of concrete property changes on the ruptured internal surface. These showed a light and dark band of approximate depths of 0.5 in. and 1.0 in., respectively.
- Concrete slabs heated to 900°C showed significant map cracking in the heated region. This deterioration was also noted through rebound hammer results on typical concrete and the lack of reaching a rupture capacity of the tension face of the wall panel concrete in small beam testing with minimal reinforcement.
- Spalling of wall panel concrete occurred in two specimens heated to 600°C within 30 minutes of reaching and maintaining this temperature. A third specimen heated to the same temperature showed no sign of spalling, though the concrete tensile strength at the surface was reduced. This indicates crack formation due to heating, and possibly less compression strength at the heated surface.
- Flexural load tests on three beams with wire mesh and prestressing strand reinforcement showed no change in the peak moment capacity due to heating. One specimen was heated to 300°C for four hours, while the other was heated to 600°C for less than 30 minutes, at which point it experienced significant spalling. The spalled specimen still maintained the peak load of the other specimens and experienced more ductility but had less elastic stiffness.

The last conclusion is the focus of the initial specimen load capacity testing. For a typical prestressed and reinforced section tested in flexure, there was no loss in flexural capacity due to thermal load, even when thermal load caused significant spalling.

The test setup developed in this study is proposed for use during Phase II of the research.

Discussions are ongoing with the project's Technical Oversight Committee regarding Phase II specimens. Possible sources of specimens have been identified and contacted. In case new specimens are required to be fabricated, quotes have been obtained from a regional

precasting company and can be budgeted for test specimens in Phase II. MassDOT has acquired a wireway support section and light fixtures for further testing.

8.0 Recommendations for Phase II Experimental Program

In this section, recommendations for Phase II testing will be discussed, based on the needs identified from Tasks 1 and 2 (the literature review and preliminary experimental testing). Though experimental testing was conducted as part of this first phase of the project, the main purpose of the testing was not to collect data on the effect of heat on structural and non-structural tunnel components, but rather to verify the feasibility of the proposed heating and load testing equipment and to determine the most useful avenues of experimental investigation going forward.

The main purposes of the future Phase II experimental investigation are to further understand the effects of heat on structural and non-structural tunnel components, and to identify and develop methods that help inspectors determine the safety of a tunnel structure after a fire. These methods may include visual methods, such as noting melting and deformation of common tunnel components, or non-destructive testing methods, such as the rebound hammer. In general, the condition of structural components is the main concern in a post-fire inspection; however, the condition of non-structural tunnel components could be used to infer the structural damage sustained during a fire. Since the degradation in the mechanical properties of concrete and steel, which are the main concerns after a tunnel fire, are largely dictated by the temperatures reached and duration of the fire, methods to identify maximum temperature exposure and duration would be very helpful to inspectors. For Phase II, the recommended testing plan includes heating structural elements, with a focus on ceiling panels, to given temperatures for given durations and performing residual strength tests afterward to determine the extent of strength loss, heating non-structural components to given temperatures to observe and document their visual condition, and investigating the use of non-destructive testing tools for post-fire inspection. From the literature review, it was found that while post-fire inspection methods do exist, the researchers were not able to find a concise post-fire inspection checklist or procedure. Based on this, and several discussions with MassDOT officials, the researchers recommend the following for Phase II.

- Conduct residual strength tests of ceiling panel components (heating components to a given temperature for a given duration, allowing the component to cool, then testing to failure).
- Heat non-structural components to given temperatures to observe any visual effects such as charring, melting, discoloration, etc.
- Further investigate the efficacy of non-destructive testing techniques such as the rebound hammer and Carbontest® for post-fire inspections.
- Develop a post-fire inspection checklist that can help inspectors quickly evaluate the safety of a tunnel structure after a fire (a draft of this checklist is shown in Section 11.2, Appendix B).
- Expand the capabilities of the existing radiant heating system by adding additional heaters and additional thermocouples for temperature monitoring.

Each of these points is discussed in greater detail as follows.

Residual Strength Tests (Ceiling Panels)

Residual strength tests are an excellent way not only to understand and quantify the potential strength and stiffness losses of structural components after a known heat exposure, but also to observe the correlating visual condition and non-destructive testing values of these components. For Phase II, it is recommended to use the radiant heating system presented in Section 7 and to heat and hold structural elements at steady temperatures for given durations. In meetings between the researchers and MassDOT officials, several tunnel components related to ceiling panels were identified as being priorities of further investigation, including:

- Precast, prestressed ceiling panels
- Ceiling panel hanger rods
- Ceiling panel angle supports
- Mechanical concrete anchors

Attempts to find existing precast ceiling panels from actual MassDOT tunnels were unsuccessful. Instead, it is proposed to have analogous panels constructed by a precaster be used for testing. To obtain a greater number of specimens for testing within budget constraints, the researchers proposed using versions of the panels that were modified in size as compared to the actual panels used in MassDOT tunnels. Shop drawings of a typical precast ceiling panel from the actual tunnel are shown in Figure 8.1, and the proposed analogous panels to be constructed by a precaster are shown in Figure 8.2.

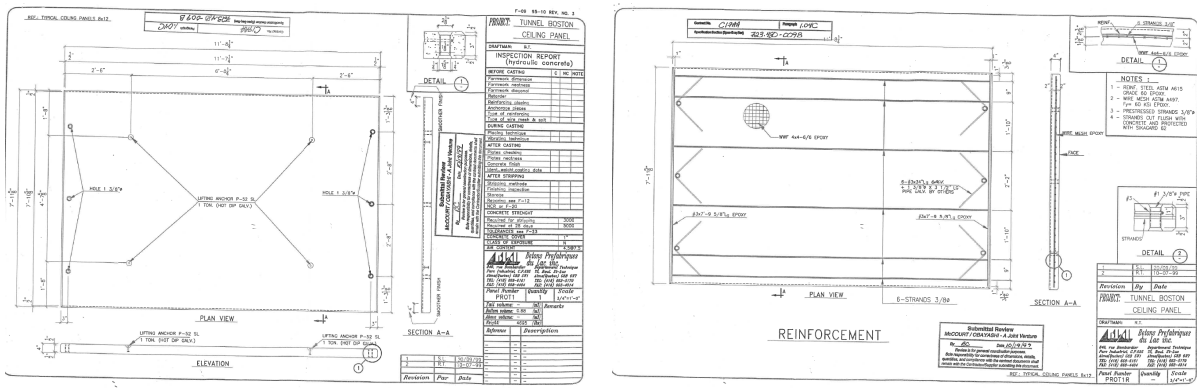

Figure 8.1: Shop drawings of typical precast, prestressed ceiling panel present in MassDOT tunnels: plan view (L); reinforcement view (R)

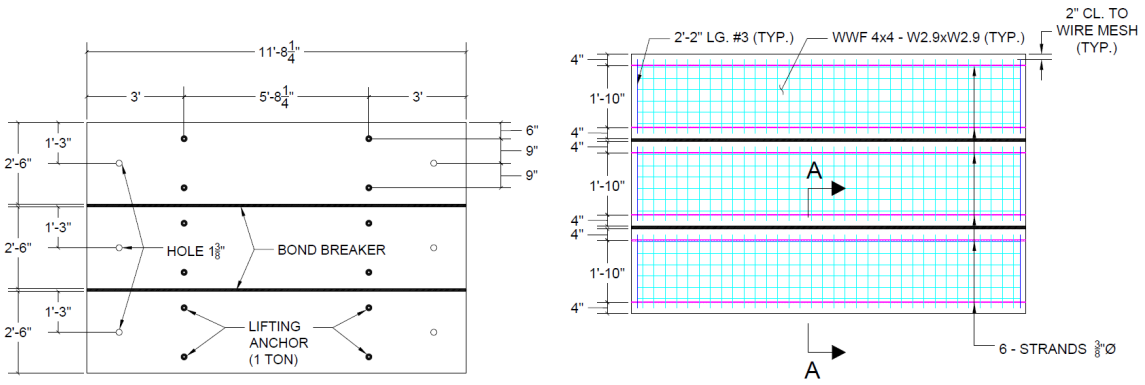

Figure 8.2: Proposed panels analogous to existing MassDOT precast, prestressing ceiling panels: plan view (L); reinforcement view (R)

The analogous panels are the same length as the original panels to maintain the appropriate bond length, but are subdivided into three similar panels within the width of the original panels, with the same types of reinforcement and a similar reinforcement ratio to the original panels. Relative strength values can be compared with each other before and after heating, to estimate the actual relative strength reductions of the original panels due to heat exposure. These plans were sent to a regional precaster, and the following quote was obtained from the precaster:

- Two panels (six strips) as shown.
- Two panels (six strips) as shown, without any lifting inserts or holes.
- Two panels (six strips) without any inserts or holes, and with epoxy-coated welded-wire-fabric.
- **Total price for all 6 panels (18 strips total): $28,000**

Subdividing each panel into three specimens will allow for testing the effects of a greater number of temperature and duration exposures and for a greater certainty in the results, noting that other researchers have found the strength losses in residual strength tests to be highly variable, even when the specimen dimensions, reinforcement, and heating regime are kept constant. The rationale for omitting the metal lifting inserts for some of the panels is to test whether these inserts could cause cracking in the concrete due to expansion of the metal during heating.

The researchers recommend a testing program using the following temperatures and heating durations:

- One strip of each type loaded to failure without being heated beforehand, to determine the original strength of each type of panel.
- Two strips of each type heated to 400°C and held at this temperature for 2–4 hours, cooled to room temperature, and loaded to failure.
- Two strips of each type heated to 600°C and held at this temperature for 2–4 hours, cooled to room temperature, and loaded to failure.
- One strip of each type heated to 800°C and held at this temperature for 2–4 hours, cooled to room temperature, and loaded to failure.

The lower bound of 400°C was chosen by noting that the peak residual moment capacity of the beams presented in Section 7.6 was unaffected after being heated for 4 hours and that the visual condition of the beam after heating was unchanged. 800°C is an upper bound used in several residual strength tests by other researchers and is representative of a relatively high intensity fire.

Residual Strength Tests (Ceiling Panel Components)

In addition to the ceiling panels, the ceiling panel hanger rods and angle supports were identified as points of potential structural concern after a fire. Depending on the number of components that can be obtained for testing, it is recommended to heat the hanger rods and angles to various temperatures up to 900°C and observe their visual condition. Subsequently, residual tension strength testing of the hanger rods and strength testing of the angle flanges could be conducted to determine any potential residual strength loss.

Heating of Non-Structural Components

In discussions with MassDOT officials, a couple of non-structural tunnel components have been acquired for heating tests, including the aluminum wireway for supporting light wiring and the phenolic light fixtures that will soon be installed in some of the tunnels. Heating these components to a variety of temperatures in the range of 300°–900°C and observing the resultant visual condition can give valuable data that can help inspectors identify the maximum and minimum temperatures reached in certain areas of the tunnel structure.

Evaluation of Non-Destructive Testing Techniques

Non-destructive testing performed after the fire can be used to estimate the extent and severity of the damage to structural elements. As part of the Phase I experimental testing, a limited number of rebound hammer and Carbontests were performed before and after heating to help understand how heat changes these values. Due to the small data set and the heterogeneity of the concrete, these tests were inconclusive. Further tests should be conducted in Phase II to determine the efficacy of these methods.

Post-Fire Inspection Checklist

The ultimate purpose of this research is to give inspectors tools and methods that can be used to assess the condition of a tunnel structure after a fire. As part of Phase I, a draft inspection checklist was proposed, as shown in Section 11.2, Appendix B. This draft is based on findings from the literature review, the preliminary experimental tests, and the previous experiences of MassDOT tunnel inspectors in post-fire inspection scenarios. The checklist is still in draft form, and criteria presented therein, including temperature cutoffs and visual condition photos, still need to be verified by the additional testing planned for Phase II.

Expansion of Radiant Heating System

The radiant heating system used for Phase I was devised with the understanding that expansion of the heating system may be required or desired for Phase II. The current system has 3 heaters and 6 thermocouples and could be expanded to 6 heaters and 12 thermocouples.

9.0 Conclusions

This report presented a literature review on the post-fire inspection of tunnels, and the findings from preliminary experimental testing. The purpose of the literature review was to gain an understanding of the effects of fire on the residual strength of tunnel structures and tunnel members and to search for existing inspection methods and protocols for fire-damaged tunnels. The purpose of the experimental testing was to verify the feasibility of a proposed heating system for Phase II experimental testing and to determine the most valuable avenues of investigation for experimental testing in Phase II. The key findings of this report are summarized as follows.

Effect of Fire on the Residual Mechanical Properties of Concrete, Steel, and the Concrete/Steel Bond (from review of literature)

A review of structural codes, standards, technical reports, and academic studies on the post-fire mechanical properties of concrete, steel, and the concrete/steel bond was conducted. This review focused on the residual strength and stiffness of concrete and steel after fire, as these properties can be related to the residual strength and stiffness of tunnel structures and structural members. The most significant findings can be summarized as follows.

- **Concrete**
  - The residual strength and stiffness of concrete after a fire are mainly dependent on the maximum temperature the concrete reaches during the fire.
  - The residual strength and stiffness of concrete after heating and cooling begins to be negatively affected after experiencing temperatures of 200°–300°C. After experiencing temperatures of 500°C, the residual strength is usually 40%–60% of its original value.
  - Concrete has excellent thermal insulation properties, meaning that typically only the regions of concrete near the exposed surface will be heated and damaged during a fire, while the inner regions of the concrete will be mostly unaffected.
  - Thermal spalling can occur during heating, cooling, and after cooling, and can expose rebar and reduce the effective cross-sectional area of structural members.
- **Steel**
  - All types of steel lose a significant amount of strength and stiffness when at elevated temperatures (in the "hot" state) but regain some of that strength and stiffness loss upon cooling.
  - Different types of steel are affected more significantly by temperature exposure than others. After heating to 600°C and cooling, the residual yield strength of the four types of steels studied are as follows:
    - Hot-rolled structural steel: 90%–100% of original.
    - Hot-rolled reinforcing steel: 80%–100% of original.
    - Heat-treated/cold-worked steel: 70%–100% of original.
    - Prestressing steel: 40%–60% of original.

    - Of the four types of steel studied, the post-fire condition of prestressing steel is most concerning, as it experiences the greatest strength losses and can experience loss of prestressing force.
- **Concrete and Steel Bond**
    - The residual strength of the concrete/steel bond after heating and cooling from certain temperatures decreases to a similar or greater degree compared to the decrease in residual concrete compressive strength.
    - The residual bond strength is significantly affected by the thickness of the concrete cover. Rebar with a thinner cover generally has a lower residual bond strength than concrete with a thicker cover.

Existing Experimental Studies on the Residual Strength of Reinforced Concrete Members (from review of literature)

Five existing experimental studies on the residual strength of reinforced concrete members after fire exposure were presented. In each study, the members were heated, cooled, and loaded until failure. The most significant findings can be summarized as follows.

- Unlike studies on concrete, steel, and bond strength, studies on the residual strength of members do not use standardized test specimens (such as concrete cylinders), making direct comparisons among studies difficult.
- Greater lengths of exposure to heat generally result in greater residual strength losses after cooling.
- The residual strength reductions observed in the studies varied greatly. In some cases, ultimate strength reductions of 5%–10% were observed, while in other cases residual strength reductions up to nearly 60% were observed. Based on the wide variety of specimen dimensions and types, materials, and heating regimes used in the studies, it is difficult to draw conclusions about the specific factors that govern the residual strength loss, aside from the fact that greater lengths of exposure to heat generally result in greater residual strength losses.
- Spalling seems to result in greater strength losses compared to when spalling does not occur.
- Specimens with high-strength concrete are more likely to experience spalling.

Existing Inspection Methods for Fire-Damaged Concrete Structures (from review of literature)

A review of visual, non-destructive, and laboratory testing methods for the assessment of fire-damaged structures was conducted, with a focus on methods that could be performed quickly and easily. The most significant findings can be summarized as follows.

General

- Of the three main methods of inspection available, visual methods and non-destructive testing methods are most practical for a rapid inspection protocol.

Visual Methods

- The condition of non-structural materials such as aluminum can be used to estimate the temperature history within certain areas of a structure.

- Concrete can change to a pink color in the range of 300°–600°C, which is useful since this temperature range coincides with onset of loss of residual compressive strength of concrete.

Non-Destructive Testing Methods

- From the review, the rebound hammer, Windsor probe, pullout test, and carbonation test emerged as the best-suited NDT methods for assessing fire-damaged concrete.
- The rebound hammer is one of the most widely used non-destructive testing tools for post-fire inspections. It can be effectively used to delineate areas of concrete that have been damaged by fire.
- The pullout test has been shown to give excellent predictions of compressive strength in non-fire-damaged concrete. Limited test data with fire-damaged concrete suggests that it is also effective in measuring the residual compressive strength of the near-surface layers of concrete exposed to fire.
- The penetration resistance test (Windsor probe) has also been shown to give good predictions of compressive strength in non-fire-damaged concrete. No studies could be found of its application to fire-damaged concrete.
- The carbonation test has been shown to be able to determine the 450°–500°C isotherm in fire-damaged concrete. Recently, a commercially available version of the test, Carbontest, was developed.

Laboratory Testing Methods

- Laboratory analysis methods are very accurate but may take days or weeks to complete.

Repair Methods for Fire-Damaged Concrete Structures (from review of literature)

A review of technical reports and case studies was conducted to determine the feasibility of repairing fire-damaged concrete structures and structural members. The most significant findings can be summarized as follows.

- Fire-damaged concrete structures and members can usually be repaired rather than replaced.
- The main steps in the repair process of reinforced concrete are to remove damaged concrete, replace the concrete to restore the member to its original size, and replace or supplement weakened reinforcement.
- Concrete material is usually replaced by sprayable concrete (e.g., shotcrete) or flowable concrete in the case of significant damage.

Survey of Post-Fire Inspection Practices across State DOTs and Other Transportation Agencies

A survey of post-fire inspection protocols, standard practices after a fire, and fire research efforts of other state DOTs and transportation organizations was conducted by contacting engineering personnel at these organizations and having discussions via video conference or email. The most significant findings of the survey are as follows.

- Most surveyed organizations do not have a written protocol for post-fire tunnel inspection. Those who do rely on the guidelines in FHWA's *Tunnel Operations, Maintenance, Inspection, and Evaluation Manual* (TOMIE).
- Eight of the 15 surveyed organizations that owned tunnels reported experiencing tunnel fires, but most were not severe.
- Many organizations reported that, in the event of a tunnel fire, they would employ the same inspection principles used for post-fire evaluations of their bridges to inspect the tunnel.
- Many organizations have used private consultants to conduct post-fire evaluations of their tunnels and bridges.
- There is a general lack of research efforts related to the post-fire inspection of tunnels.

Experimental Testing at UMass Amherst

Preliminary experimental testing was performed to evaluate the feasibility and effectiveness of potential methods for assessing the damages to structural and non-structural tunnel elements due to heat exposure. This included obtaining and testing a heat system, conducting trial tests on representative samples, troubleshooting potential problems, and determining the feasibility and scope for Phase II testing.

- The heating system tested is an efficient way to perform the intended experiments. The setup will be able to perform the tests expected for Phase II of this research project.
- The heating system can provide air temperature load at the surface of the concrete in excess of 900°C for ideal conditions. Higher temperatures may be possible with additional heaters.
- In the preliminary tests, several visually apparent deleterious effects of heat exposure were noted in the heated specimens that could be used in a post-fire inspection. This included cracking of tiling and deterioration of grout, melting of reinforcement epoxy coating, spalling of concrete, red/white discoloration of concrete, map cracking of concrete, and distortion of an aluminum wireway. Further investigation is needed to verify the temperature at which these effects occur, and the level of structural damage they may indicate.
- Results from the NDT inspection methods investigated, Carbontest and rebound hammer, were inconclusive; further investigation is needed to verify the feasibility and efficacy of these methods for use in a post-fire inspection.
- Spalling of wall panel concrete occurred in two specimens heated to 600°C within 30 minutes of reaching and maintaining this temperature. A third specimen heated to the same temperature showed no sign of spalling.
- Beam tests with typical reinforcement and heated at the tensile face showed no change in the peak moment capacity. One specimen was heated to 300°C for four hours, while the other was heated to 600°C for less than 30 minutes, at which point it experienced significant spalling. The spalled specimen still maintained the peak load of the other specimens and experienced more ductility but had less elastic stiffness.

Recommendations for Phase II Experimental Testing

The final part of the first phase of this research project was to identify needs based on the literature review and preliminary experimental testing and provide corresponding recommendations for Phase II experimental testing. The recommendations are as follows.

- Conduct residual strength tests of structural ceiling panel components (heating components to a given temperature for a given duration, allowing the component to cool, then testing to failure).
- Heat non-structural components to given temperatures to observe any visual effects such a charring, melting, discoloration, etc.
- Further investigate the efficacy of non-destructive testing techniques such as the rebound hammer and Carbontest for post-fire inspections.
- Develop a post-fire inspection checklist that can help inspectors quickly evaluate the safety of a tunnel structure after a fire (a draft of this checklist is shown in Section 11.2, Appendix B).
- Expand the capabilities of the existing radiant heating system by adding additional heaters, and additional thermocouples for temperature monitoring.

This page left blank intentionally

10.0 References

[1] Khoury, G. A. Effect of Fire on Concrete and Concrete Structures. *Progress in Structural Engineering and Materials,* Vol. 2, No. 4, 2000, pp. 429–447.

[2] Maraveas, C., and A. A. Vrakas. Design of Concrete Tunnel Linings for Fire Safety. *Structural Engineering International*, Vol. 24, No. 3,2014, pp. 1–11.

[3] Fletcher, I. A., S. Welch, J. L. Torero, R. O. Carvel, and A. Usmani. The Behavior of Concrete Structures in Fire. *Thermal Science,* Vol. 11, No. 2, 2007, pp. 37–52.

[4] Knaack, A. M., Y. C. Kurama, and D. J. Kirkner. Compressive Strength Relationships for Concrete under Elevated Temperatures. *ACI Materials Journal,* Vol. 107, No. 2, 2010, pp. 164–175.

[5] Tao, Z., X.-Q. Wang, and B. Uy. Stress-strain Curves of Structural and Reinforcing Steels after Exposure to Elevated Temperatures. *Journal of Materials in Civil Engineering,* Vol. 25, No. 9, 2013, pp. 1306–1316.

[6] International Federation for Structural Concrete (*fib*). *Fire Design of Concrete Structures—Structural Behavior and Assessment.* Bulletin 46, Lausanne, Switzerland, 2008.

[7] Ulm, F. J., P. Acker, and M. Levy. The "Chunnel" Fire II: Analysis of Concrete Damage. *Journal of Engineering Mechanics,* Vol. 125, No. 3, 1999, pp. 283–289.

[8] Ulm, F. J., O. Coussy, and Z. P. Bazant. The "Chunnel" Fire I: Chemoplastic Softening in Rapidly Heated Concrete. *Journal of Engineering Mechanics,* Vol. 125, No. 3, 1999, pp. 272–282.

[9] Ingham, J. Forensic Engineering of Fire-damaged Structures, in *Civil Engineering*, 2009.

[10] Schneider, U., and D. Drysdale. Repairability of Fire-damaged Structures. *Fire Safety Journal,* Vol. 16, 1990, pp. 251–336.

[11] Naus, D. J. *The Effect of Elevated Temperature on Concrete Materials and Structures*. U.S. Nuclear Regulatory Commission, Washington, D.C., 2006.

[12] Kodur, V. Properties of Concrete at Elevated Temperatures. *ISRN Civil Engineering,* 2014.

[13] Phan, L. T. *Fire Performance of High-Strength Concrete: A Report of the State-of-the-Art. National Institute of Standards and Technology*. Gaithersburg, MD, 1996.

[14] Felicetti, R., and P. G. Gambarova. Effects of High Temperature on the Residual Compressive Strength of High-strength Siliceous Concrete. *ACI Materials Journal,* Vol. 95, No. 4, 1998.

[15] Chiang, C. H., and C. C. Yang. Artificial Neural Networks in Prediction of Concrete Strength Reduction Due to High Temperature. *ACI Materials Journal,* Vol. 102, No. 2, 2005.

[16] Özbay, E., and M. Lachemi. Relative Compressive Strength of Concretes under Elevated Temperatures. *ACI Materials Journal,* Vol. 109, No. 2, 2012.

[17] Elsanadedy,H. M. Residual Compressive Strength of High-strength Concrete Exposed

to Elevated Temperatures. *Advances in Materials Science and Engineering,* Vol. 2019, No. 4, 2019, pp. 1–22.

[18] European Committee for Standardization. *Eurocode 2: Design of Concrete Structures, Part 1-2: General Rules—Structural Fire Design*. 2004.

[19] European Committee for Standardization. *Eurocode 4: Design of Composite Steel and Concrete Structures, Part 1-2: General Rules—Structural Fire Design*. 2005.

[20] American Concrete Institute. *Code Requirements for Determining Fire Resistance of Concrete and Masonry Construction Assemblies.* American Concrete Institute, Farmington Hills, MI, 2014.

[21] *Building Code Requirements for Structural Concrete,* American Concrete Institute, 2019.

[22] Khalaf, J., Z. Huang, and M. Fan. Analysis of Bond-slip between Concrete and Steel Bar in Fire. *Computers and Structures,* Vol. 162, 2016, pp. 1–15.

[23] Hertz, K. D. Limits of Spalling of Fire-exposed Concrete. *Fire Safety Journal,* Vol. 38, No. 2, 2003, pp. 103–116.

[24] Bostrom, L., and C. Larsen. Concrete Tunnel Linings Exposed to Severe Fire Exposure. *Fire Technology,* Vol. 42, 2006, pp. 351–362.

[25] Msaad, Y., and G. Bonnet. Analyses of Heated Concrete Spalling Due to Restrained Thermal Dilation: Application to the "Chunnel" fire. *Journal of Engineering Mechanics,* Vol. 132, No. 10, 2006, pp. 1124–1132.

[26] Zeiml, M., R. Lackner, and H. A. Mang.Experimental Insight into Spalling Behavior of Concrete Tunnel Linings under Fire Loading. *Acta Geotechnica,* Vol. 3, 2008, pp. 295–308.

[27] Jansson, R. *Fire Spalling of Concrete*. KTH Royal Institute of Technology, Stockholm, Sweden, 2013.

[28] Klingsch, E. W. *Explosive Spalling of Concrete in Fire*. Institut für Baustatik und Konstruktion der ETH Zurich, 2014.

[29] Hedayati, M, M.. Sofi, P. A. Mendis, and T. Ngo. A Comprehensive Review of Spalling and Fire Performance of Concrete Members. *Electronic Journal of Structural Engineering,* Vol. 15, No. 1, 2015.

[30] Liu, J. C., K. H. Tan and Y. Yao. A New Perspective on Nature of Fire-induced Spalling in Concrete. *Construction and Building Materials,* Vol. 184, 2018, pp. 581–590.

[31] Khoury, G. A., and Y. Anderberg. Concrete Spalling Review. *Fire Safety Design*, 2000.

[32] Tao, Z. Mechanical Properties of Prestressing Steel after Fire Exposure. *Materials and Structures,* Vol. 48, 2015, pp. 3037–3047.

[33] Outinen, J., and P. Makelainen. Mechanical Properties of Structural Steel at Elevated Temperatures and after Cooling Down. *Fire and Materials,* Vol. 28, 2004, pp. 237–251.

[34] Jinwoo, L., M. D. Engelhardt, and E. M. Taleff. Mechanical Properties of ASTM A992 Steel After Fire. *Engineering Journal,* Vol. 49, 2012, pp. 33-44.

[35] Crook, R. N. *The Elevated Temperature Properties of Reinforced Concrete*. University of Aston in Birmingham, Birmingham, England, 1980.

[36] Crook, R. N., *The Elevated Temperature Properties of Reinforced Concrete*. University of Aston in Birmingham, Birmingham, England, 1980.

[37] Neves, I. C., J. P. C. Rodrigues, and A. D. P. Loureiro. Mechanical Properties of Reinforcing and Prestressing Steels After Heating. *Journal of Civil Engineering Materials,* Vol. 8, No. 4, 1996, pp. 189–194.

[38] Ahmad, M. S. Effect of Sustained Elevated Temperature on Mechanical Behavior of Reinforcing Bar. *Procedia Engineering,* Vol. 173, 2017, pp. 905–909.

[39] Felicetti, R., P. G. Gambarova, and A. Meda. Residual Behavior of Steel Rebars and R/C Sections after a Fire. *Construction and Building Materials,* Vol. 23, No. 12, 2009, pp. 3546–3555.

[40] Zhang, L., F. T. K. Au, Y. Wei, and J. Li. Mechanical Properties of Prestressing Steel in and after Fire. *Magazine of Concrete Research,* Vol. 69, No. 8, 2017, pp. 379–388.

[41] The Institution of Structural Engineers. *Appraisal of Existing Structures*. The Institution of Structural Engineers, London, England, 2010.

[42] Bosnjak, J., A. Sharma, and S. Bessert. Bond Performance of Reinforcement in Concrete after Exposure to Elevated Temperatures. In *3rd International Symposium on Connections between Steel and Concrete*, Stuttgart, Germany, 2017.

[43] Lin, H., Y. Zhao, J. Ozbolt, P. Feng, C. Jiang, and R. Eligehausen. Analytical Model for the Bond Stress-slip Relationship of Deformed Bars in Normal Strength Concrete. *Construction and Building Materials,* Vol. 198, 2019, pp. 570–586.

[44] Bingol, A. F., and R. Gul. Residual Bond Strength between Steel Bars and Concrete after Elevated Temperatures. *Fire Safety Journal,* Vol. 44, No. 6, 2009, pp. 854–859.

[45] Xiao, J., Y. Hou, and Z. Huang. Beam Test on Bond Behavior between High-grade Rebar and High-strength Concrete after Elevated Temperatures. *Fire Safety Journal,* Vol. 69, 2014, pp. 23–35.

[46] El-Hawary, M. M., A. M. Ragab, A. A. El-Azim, and S. Elibiari. Effect of Fire on Flexural Behaviour of RC Beams. *Construction and Building Materials,* Vol. 10, No. 2, 1996, pp. 147–150.

[47] Graybeal, B. A. Flexural Capacity of Fire-damaged Prestressed Concrete Box Beams. Federal Highway Administration, Fairfax, VA, 2007.

[48] Chowdhury, E. U., L. A. Bisby, M. F. Green and V. K. R. Kodur. Residual Behavior of Fire-exposed Reinforced Concrete Beams Prestrengthened in Flexure with Fiber-reinforced Polymer Sheets. *Journal of Composites for Construction,* Vol. 12, No. 1, 2008, pp. 61–68.

[49] Kodur, V., M. B. Dwaikat, and R. S. Fike. An Approach for Evaluating the Residual Strength of Fire-exposed RC Beams. *Magazine of Concrete Research,* Vol. 62, No. 7, 2010, pp. 479–488.

[50] Abdelrahman, A. A., N. M. Nofel, A. H. Ghallab, T. H. El-Afandy, and A. Mahmoud. Behavior of Prestressed Concrete Beams Subjected to Fire. *HBRC Journal,* Vol. 7, No. 2, 2011, pp. 38–55.

[51] Jiangtao, Y., L. Zhaoudao, and X. Kai. Experimental Study on the Performance of RC

Continuous Members in Bending after Exposure to Fire. *Procedia Engineering,* Vol. 14, 2011, pp. 821–829.

[52] Chung, C. H., C. R. Im, and J. Park. Structural Test and Analysis of RC Slab after Fire Loading. *Nuclear Engineering and Technology,* Vol. 45, No. 2, 2013, pp. 223–236.

[53] Xu, Y., B. Wu, M. Jiang, and X. Huang. Experimental Study on the Residual Flexural Behavior of Reinforced Concrete Beams after Exposure to Fire. *Advanced Materials Research,* Vol. 457–458, 2012, pp. 183–187.

[54] Choi, E. G., Y.-S. Shin, and H. S. Kim. Structural Damage Evaluation of Reinforced Concrete Beams Exposed to High Temperatures. *Journal of Fire Protection Engineering,* Vol. 23, No. 2, 2013, pp. 135–151.

[55] Kadhum, M. M. Fire Resistance of Reinforced Concrete Rigid Beams. *Journal of Civil Engineering and Construction Technology,* Vol. 4, No. 4, 2014.

[56] Raouffard, M. M., and M. Nishiyama. Residual Load Bearing Capacity of Reinforced Concrete Frames after Fire. *Journal of Advanced Concrete Technology,* Vol. 14, 2016, pp. 625–633.

[57] Wang, W. Y., G. S. Huang, G. Q. Li, and M. D. Engelhardt. Behavior of Steel-concrete Partially Composite Beams Subjected to Fire, Part 1: Experimental study. *Fire Technology,* Vol. 53, 2017, pp. 1039–1058.

[58] Kodur, V., D. Hibner, and A. Agrawal. Residual Response of Reinforced Concrete Columns Exposed to Design Fires. *Procedia Engineering,* Vol. 210, 2010, pp. 574–581.

[59] Kodur, V., and A. Agrawal. Residual Response of Fire-damaged High-strength Concrete Beams. *Fire and Materials,* Vol. 43, 2019, pp. 310–322.

[60] Beneberu, E., and N. Yazdani. Residual Strength of CFRP Strengthened Prestressed Concrete Bridge Girders after Hydrocarbon Fire Exposure. *Engineering Structures,* Vol. 184, 2019, pp. 1–14.

[61] Alcaíno, P., H. Santa-María, C. Magna-Verdugo, and L. López. Experimental Fast-assessment of Post-fire Residual Strength of Reinforced Concrete Frame Buildings Based on Non-destructive Tests. *Construction and Building Materials,* Vol. 234, 2020.

[62] Meda, A., P. G. Gambarova, and M. Bonomi. High-performance Concrete in Fire-exposed Reinforced Concrete Sections. *ACI Structural Journal,* Vol. 99, No. 3, 2002, pp. 277–282.

[63] Hsu, J. H., and C. S. Lin. Effect of Fire on the Residual Mechanical Properties and Structural Performance of Reinforced Concrete Beams. *Journal of Fire Protection Engineering,* Vol. 18, 2008, pp. 245–273.

[64] Kalaba, N., P. Bamonte, and R. Felicetti. Prestressed Members under Natural fire: A preliminary study on the residual behavior. In *Applications of Structural Fire Engineering*, Dubrovnik, Croatia, 2015.

[65] Kodur, V. K. R., and A. Agrawal. An Approach for Evaluating Residual Capacity of Reinforced Concrete Beams Exposed to Fire. *Engineering Structures,* Vol. 110, 2016, pp. 293–306.

[66] Kodur, V. K. R., and A. Agrawal. Critical Factors Governing the Residual Response of Reinforced Concrete Beams Exposed to Fire. *Fire Technology,* Vol. 52, 2016, pp. 967–

993.

[67] Felicetti, R. Assessment Methods of Fire Damages in Concrete Tunnel Linings. *Fire Technology,* Vol. 49, 2013, pp. 509–529.

[68] Concrete Society. *Assessment, Design, and Repair of Fire-damaged Concrete Structures.* Concrete Society, 2008.

[69] Non-destructive Assessment of Concrete Structures: Reliability and limits of single and combined techniques. RILEM, 2012.

[70] Axler, K., T. Mintz, K. Das, and J. Huczek. Structural Materials Analysis of the Newhall Pass Tunnel Fire, 2007. United States Nuclear Regulatory Commission, San Antonio, TX, 2011.

[71] Hager, I. Colour Change in Heated Concrete. *Fire Technology,* Vol. 50, 2014, pp. 945–958.

[72] Short, N., J. Purkiss, and S. Guise. Assessment of Fire Damaged Concrete Using Colour Image Analysis. *Construction and Building Materials,* Vol. 15, No. 1, 2001, pp. 9–15.

[73] Annerel, E. V., and L. R. Taerwe. Assessment Techniques for the Evaluation of Concrete Structures after Fire. *Journal of Structural Fire Engineering,* Vol. 4, No. 2, 2013, pp. 123–129.

[74] Colombo, M., and R. Felicetti. New NDT Techniques for the Assessment of Fire-damaged Concrete Structures. *Fire Safety Journal,* Vol. 42, No. 6–7, 2007, pp. 461–472.

[75] Felicetti, R. Assessment of Fire Damage in Concrete Structures: New inspection tools and combined interpretation of results. In *8th International Conference on Structures in Fire*, Shanghai, China, 2014.

[76] Brodzovsky, J., and L. Bodnarova. Contribution to the Issue of Evaluating the Compressive Strength of Concrete Exposed to High Temperatures Using the Schmidt Rebound Hammer. *Russian Journal of Nondestructive Testing,* Vol. 52, No. 1, 2016, pp. 44–52.

[77] Dolinar, U., G. Trtnik, and T. Hozjan. Determination of Mechanical Properties of Normal Strength Limestone Concrete after Exposure to Elevated Temperatures. In *3rd European Symposium on Fire Safety Science*, 2018.

[78] Aseem, A., W. L. Baloch, R. A. Khushnood, and A. Mushtaq. Structural Health Assessment of Fire Damaged Building Using Non-destructive Testing and Micro-graphical Forensic Analysis: A case study. *Case Studies in Construction Materials,* Vol. 11, 2019.

[79] Alcaino, P., H. Santa-Maria, C. Magna-Verduro, and L. Lopez. Experimental Fast-assessment of Post-fire Residual Strength of Reinforced Concrete Frame Buildings Based on Non-destructive Tests. *Construction and Building Materials,* Vol. 234, 2020.

[80] Albrektsson, J., M. Flansbjer, J. E. Lindqvist, and R. Jansson. Assessment of Concrete Structures after Fire. SP Technical Institute of Sweden, 2011.

[81] *Standard Test Method for Rebound Number of Hardened Concrete.* ASTM C805, 2018.

[82] ACI Committee 228. Report on Methods for Estimating in-place Concrete Strength.

American Concrete Institute, Farmington Hills, MI, 2019.

[83] *Standard Test Method for Pullout Strength of Hardened Concrete.* ASTM C900-19, 2019.

[84] Felicetti, R. New NDT Techniques for the Assessment of Fire Damaged RC Structures. 2005.

[85] Du, S., Y. Zhang, Q. Sun, W. Gong, J. Geng, and K. Zhang. Experimental Study on Color Change and Compression Strength of Concrete Tunnel Lining in a Fire. *Tunnelling and Underground Space Technology,* Vol. 71, 2018, pp. 106–114.

[86] Chang, C. F., and J.-W. Chen. The Experimental Investigation of Concrete Carbonation Depth. *Cement and Concrete Research,* Vol. 36, No. 9, 2006, pp. 1760–1767.

[87] Felicetti, R. Assessment of Deteriorated Concrete Cover by Combined While-drilling Techniques. *Journal of Infrastructure Systems,* Vol. 18, No. 1, 2012, pp. 25–33.

[88] Abraham, O., and X. Derobert. Non-destructive Testing of Fired Tunnel Walls: The Mont-Blanc Tunnel case study. *NDT & E International,* Vol. 36, No. 6, 2003, pp. 411–418.

[89] *Standard Practice for Petrographic Examination of Hardened Concrete.* ASTM C856-20, 2020.

[90] Ingham, J. P. Application of Petrographic Examination Techniques to the Assessment of Fire-damaged Concrete and Masonry Structures. *Materials Characterization,* Vol. 60, No. 7, 2009, pp. 700–709.

[91] Zahid, M. M., B. A. Bakar, F. Nazri, M. Ahmad, and K. Muhamad. Review of Repair Materials for Fire-damaged Reinforced Concrete Structures. *Materials Science and Engineering,* Vol. 318, 2018.

[92] Leitner, A. The Fire Catastrophe in the Tauern Tunnel: Experience and conclusions for the Austrian guidelines. *Tunnelling and Underground Space Technology,* Vol. 16, 2001, pp. 217–223.

[93] Phan, L. T. High-Strength Concrete at High Temperature—An Overview.

[94] Chiew, S. P., M. S. Zhao, and C. K. Lee. Mechanical Properties of Heat-treated High Strength Steel under Fire/Post-fire Conditions. *Journal of Constructional Steel Research,* Vol. 98, 2014, pp. 12–19.

[95] Lubloy, E., and G. L. Balazs. Temperature Effects on the Bond between Concrete and Reinforcing Steel. *Journal of Faculty of Civil Engineering,* Vol. 26, 2014, pp. 27–35.

[96] Cooke, G. M. E. An Introduction to the Mechanical Properties of Structural Steel at Elevated Temperatures. *Fire Safety Journal,* Vol. 13, 1988, pp. 45–54.

11.0 Appendices

11.1 Appendix A: Questions for the Survey of Post-Fire Inspection Practices

- Has your organization experienced any notable tunnel fire events?
- Does your organization currently have a post-fire tunnel inspection protocol, or post-fire inspection protocol for other types of structures?
    - If yes, what does this protocol entail (e.g., non-destructive testing, visual inspection, etc.)
    - If yes, what is the basis these protocols (e.g., experimental testing, published standards, etc.)?
- Does your organization use private consultants to assess the condition of tunnels after fire events?
- Are there any particular post-fire structural concerns that your organization has in regard to the particular construction(s) of your tunnels?
- Has your organization conducted any fire tests on structural materials, members, or structures?
    - If yes, would your organization be willing to share the testing results or the scope of these tests?
- Are you aware of any other research efforts or projects regarding post-fire tunnel inspections?
- Are you aware of any literature or documents on the subject?
- Are there any codes (regional, state, federal) regarding this issue?
- Have you personally conducted an inspection after a fire or seen a tunnel right after a fire?
- Do you have any contacts in other states or neighboring states?
- Do you know any other DOTs that may be interested in this sort of research?

11.2 Appendix B: Draft Post-Inspection Checklist

DRAFT RAPID POST-FIRE TUNNEL INSPECTION CHECKLIST

GENERAL INFORMATION

INSPECTOR(S): _____ DATE/TIME: _____

TUNNEL NAME: _____ TUNNEL STATION: _____

AIR TEMPERATURE: _____ FIRE EXTING. METHOD: _____

AIR FLOW: _____

SURFACE TEMPERATURE MEASUREMENTS (NR IF NOT RECORDED)

LEFT WALL _____(meas. or est. max) (°C or °F)

RIGHT WALL _____(meas. or est. max) (°C or °F)

INVERT _____(meas. or est. max) (°C or °F)

ROOF _____(meas. or est. max) (°C or °F)

PLENUM WALL _____(meas. or est. max) (°C or °F)

SUB-CEILING _____(meas. or est. max) (°C or °F)

STEEL STRINGERS, HANGERS, OR BEAMS _____(meas. or est. max) (°C or °F)

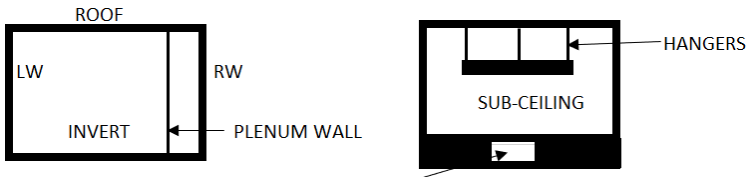

CROSS-SECTION LOOKING UP-STATION

CROSS-SECTION LOOKING UP-STATION

SOUND & RECORD OBSERVED DAMAGE LIMITS

	TOTAL	REMOVED CONC.	C.S.	NOTES (SPALLING, CRACKING, COLOR, ETC., & RELATIVE DISTANCE ALONG MEMBER)
LEFT WALL	____ x ____(FT x FT)	____ x ____(FT x FT)	____	_____
RIGHT WALL	____ x ____(FT x FT)	____ x ____(FT x FT)	____	_____
INVERT	____ x ____(FT x FT)	____ x ____(FT x FT)	____	_____
ROOF	____ x ____(FT x FT)	____ x ____(FT x FT)	____	_____
PLENUM WALL	____ x ____(FT x FT)	____ x ____(FT x FT)	____	_____
SUB-CEILING	____ x ____(FT x FT)	____ x ____(FT x FT)	____	_____

OTHER NOTES (DEFLECTIONS, DEFORMATIONS, ETC.)

_____

_____

_____

_____

ITEMIZED CHECKLIST

CONCRETE CEILING PANEL

PINK/RED/WHITENED CONCRETE	YES ☐	NO ☐
DROP IN REBOUND HAMMER READINGS VERSUS UNDAMAGED CONCRETE	YES ☐	NO ☐
CRACKS WIDTHS ≥ 0.025" OVER PANEL	YES ☐	NO ☐
REINFORCING STEEL DAMAGE (MELTED EPOXY, DISTORTION, ETC)	YES ☐	NO ☐
NOTICEABLE MIDSPAN DEFLECTION	YES ☐	NO ☐

STEEL HANGER RODS

DISTORTION/PEELING OF PAINT OR GALV./DISCOLORATION	YES ☐	NO ☐

STEEL SUPPORT BEAMS/ANGLES

DISTORTION/ PEELING OF PAINT OR GALV. /DISCOLORATION/BUCKLING	YES ☐	NO ☐

SUPPORT ANCHORS

CREEP OR EXCESSIVE GAP	YES ☐	NO ☐

WALL PANEL

TILE LOSS	YES ☐	NO ☐
DAMAGE TO SUPPORTS/INSTABILTIY	YES ☐	NO ☐

LIGHT FIXTURES

MELTING OF LIGHT FIXTURE	YES ☐	NO ☐
MELTING/DEFORMATION OF ALUMINUM WIREWAY	YES ☐	NO ☐
UN-SOUND CONCRETE AROUND ANCHOR OR INSTABILITY	YES ☐	NO ☐

ROADWAY SURFACE

SLICK ROADWAY OR POTHOLES/SPALLS THAT IMPACT RIDING SURFACE	YES ☐	NO ☐

RECOMMENDED ACTION BASED ON VISUAL OBSERVATIONS AND RECORDED DATA

NOTE: FLOWCHART IS INTENDED TO SERVE AS A GUIDE TO A POST-FIRE TUNNEL INSPECTION. HOWEVER, PROFESSIONAL JUDGMENT SHOULD BE USED IN AN ACTUAL INSPECTION

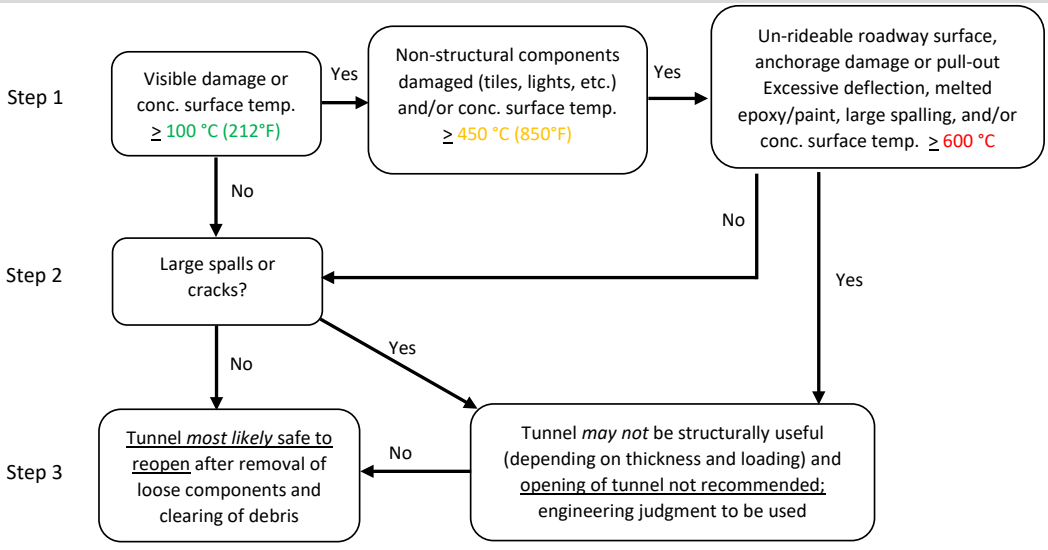

*to assist estimating max. concrete temperature experienced, use attached reference guide

REFERENCE GUIDE

Disclaimer: Many factors are to be considered in concrete strength reduction that should be considered as part of post-inspection review

Notes: Surface temperatures may not always correlate with structural damage (such as explosive spalling from rapid/short-term temp. rises or the result of blast impact), however, large/deep cracking and structural damage could occur. Engineering judgment should be used

CONCRETE CONDITION STATE

Rating	Description
1	No damage/soot clearance only
2	Damaged tiles/small pop-outs, crack widths < 0.012”
3	Spalling with no exposed rebar, crack widths ≤ 0.025”
4	Exposed rebar, deep/wide cracking > 0.025”

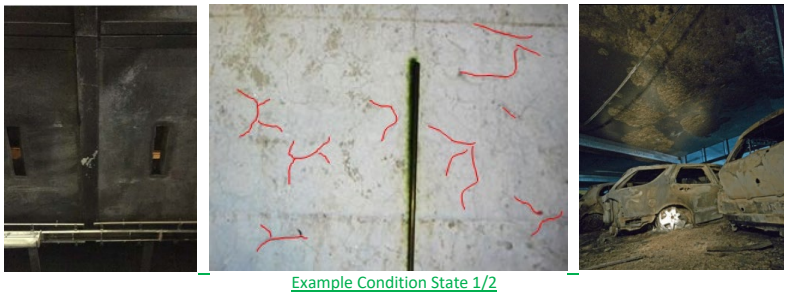

Example Condition State 1/2
Map cracking; crack widths < 0.012”
(likely safe to open; monitor condition)

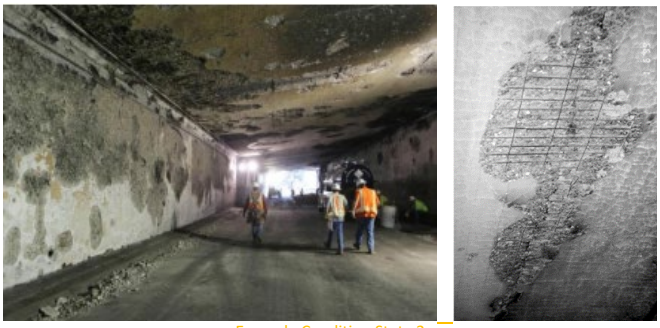

Example Condition State 3
Shallow spalls & crack widths ≤ 0.025”
(potential tunnel closure w/future repair)

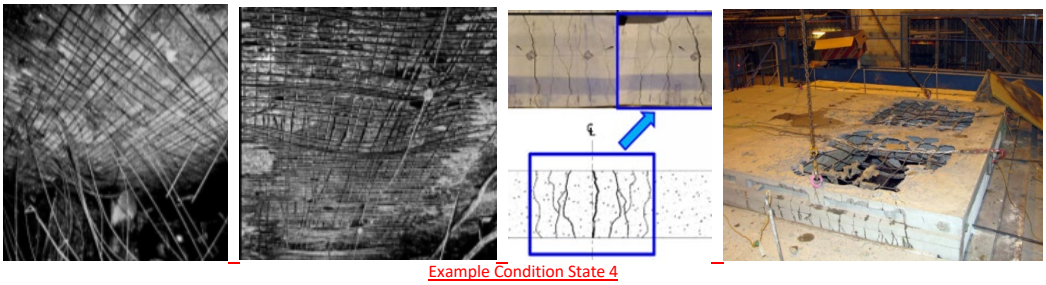

Example Condition State 4
Deep spalls & full-depth cracks or crack widths > 0.025”
(recommended tunnel closure)

CONCRETE VS TEMPERATURE VISUAL GUIDE

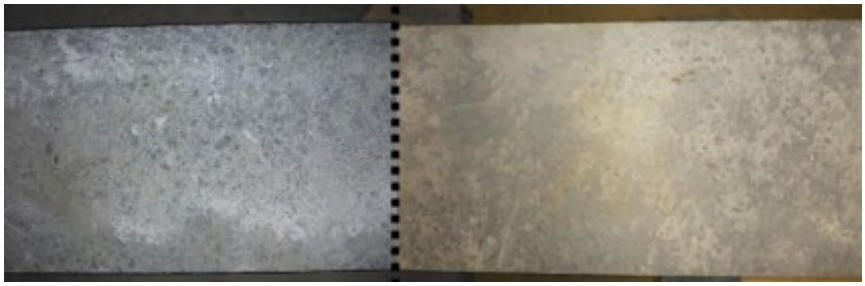

Concrete discoloration at 600°C (1,112°F)

Concrete discoloration at 1000°C (1,832°F)

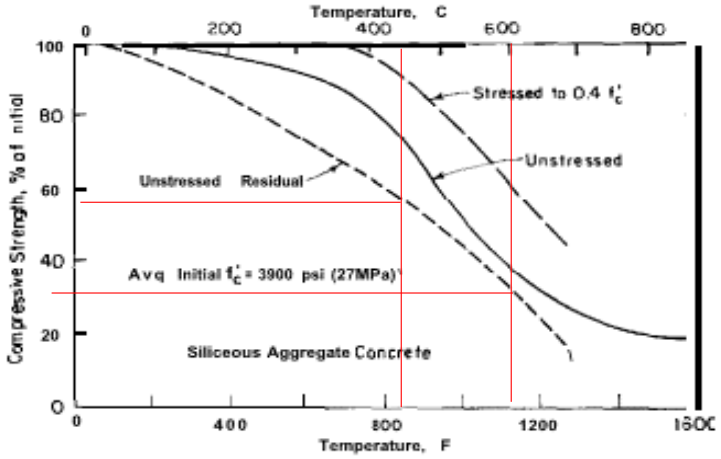

ACI 216.1-14 – Concrete strength vs. temperature

STEEL COATING VS TEMP. VISUAL GUIDE

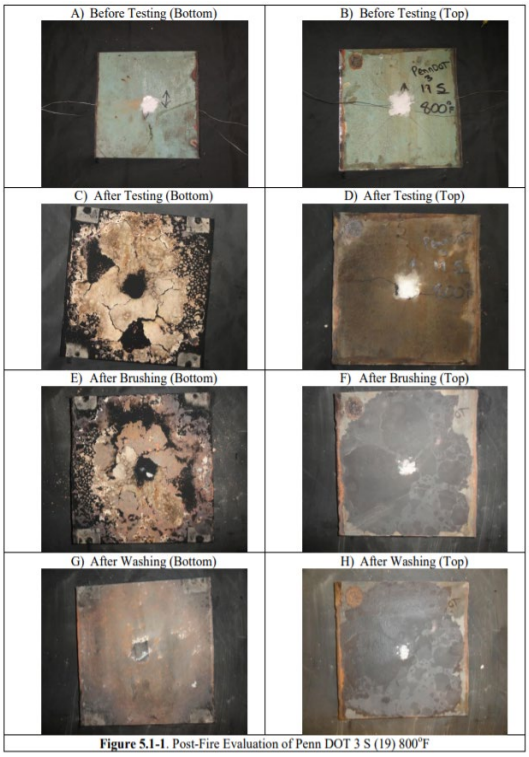

Figure 5.1-1. Post-Fire Evaluation of Penn DOT 3 S (19) 800°F

Ref. (PennDOT Effects of Fire Damage on the Structural Properties of Steel Bridge Elements)

MISC. COMPONENTS VISUAL GUIDE

Wall tiles & lights
(Temp. ≥ 450°C (842°F))

Aluminum wireway damage
(Deformation at 450°C (842°F))
(Melts at 600°C (1,112°F))